MCEER

EARTHQUAKE ENGINEERING TO EXTREME EVENTS

ISSN 1520-295X

Seismic Behavior of Bidirectional-Resistant Ductile End Diaphragms with Unbonded Braces in Straight or Skewed Steel Bridges

by

Oguz C. Celik and Michel Bruneau

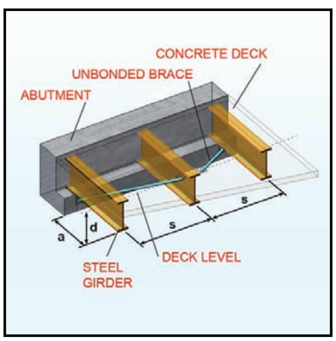

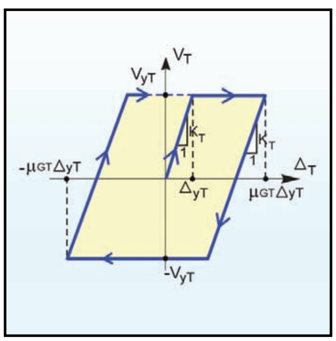

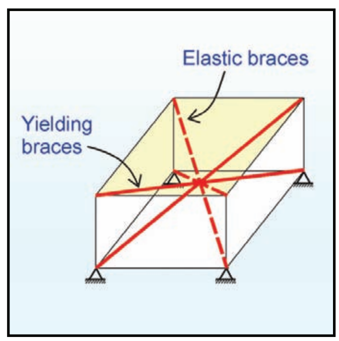

Technical Report MCEER-07-0003

April 11, 2007

This research was conducted at the he University at Buffalo, State University at New York and was supported by the Federal Highway Administration under contract number DTFH61-98-C-00094.

MCEER
EARTHQUAKE ENGINEERING TO EXTREME EVENTS

Seismic Behavior of Bidirectional-Resistant Ductile End Diaphragms with Unbonded Braces in Straight or Skewed Steel Bridges

by

Oguz C. Celik[1] and Michel Bruneau[2]

Publication Date: April 11, 2007
Submittal Date: February 20, 2007

Technical Report MCEER-07-0003

Task Number 094-C-3.2

FHWA Contract Number DTFH61-98-C-00094

1 Visiting Professor, Department of Civil, Structural and Environmental Engineering, University at Buffalo, State University of New York; Associate Professor, Faculty of Architecture, Division of Theory of Structures, Istanbul Technical University
2 Professor, Department of Civil, Structural and Environmental Engineering, University at Buffalo, State University of New York

MCEER
University at Buffalo, The State University of New York
Red Jacket Quadrangle, Buffalo, NY 14261
Phone: (716) 645-3391; Fax (716) 645-3399
E-mail: *mceer@buffalo.edu*; WWW Site: *http://mceer.buffalo.edu*

DISCLAIMER

❖ This document has been reproduced from the best copy furnished by the sponsoring agency.

Preface

The Multidisciplinary Center for Earthquake Engineering Research (MCEER) is a national center of excellence in advanced technology applications that is dedicated to the reduction of earthquake losses nationwide. Headquartered at the University at Buffalo, State University of New York, the Center was originally established by the National Science Foundation in 1986, as the National Center for Earthquake Engineering Research (NCEER).

Comprising a consortium of researchers from numerous disciplines and institutions throughout the United States, the Center's mission is to reduce earthquake losses through research and the application of advanced technologies that improve engineering, pre-earthquake planning and post-earthquake recovery strategies. Toward this end, the Center coordinates a nationwide program of multidisciplinary team research, education and outreach activities.

MCEER's research is conducted under the sponsorship of two major federal agencies, the National Science Foundation (NSF) and the Federal Highway Administration (FHWA), and the State of New York. Significant support is also derived from the Federal Emergency Management Agency (FEMA), other state governments, academic institutions, foreign governments and private industry.

The Center's Highway Project develops improved seismic design, evaluation, and retrofit methodologies and strategies for new and existing bridges and other highway structures, and for assessing the seismic performance of highway systems. The FHWA has sponsored three major contracts with MCEER under the Highway Project, two of which were initiated in 1992 and the third in 1998.

Of the two 1992 studies, one performed a series of tasks intended to improve seismic design practices for new highway bridges, tunnels, and retaining structures (MCEER Project 112). The other study focused on methodologies and approaches for assessing and improving the seismic performance of existing "typical" highway bridges and other highway system components including tunnels, retaining structures, slopes, culverts, and pavements (MCEER Project 106). These studies were conducted to:

- assess the seismic vulnerability of highway systems, structures, and components;
- develop concepts for retrofitting vulnerable highway structures and components;
- develop improved design and analysis methodologies for bridges, tunnels, and retaining structures, which include consideration of soil-structure interaction mechanisms and their influence on structural response; and
- develop, update, and recommend improved seismic design and performance criteria for new highway systems and structures.

The 1998 study, "Seismic Vulnerability of the Highway System" (FHWA Contract DTFH61-98-C-00094; known as MCEER Project 094), was initiated with the objective of performing studies to improve the seismic performance of bridge types not covered under Projects 106 or 112, and to provide extensions to system performance assessments for highway systems. Specific subjects covered under Project 094 include:

- development of formal loss estimation technologies and methodologies for highway systems;
- analysis, design, detailing, and retrofitting technologies for special bridges, including those with flexible superstructures (e.g., trusses), those supported by steel tower substructures, and cable-supported bridges (e.g., suspension and cable-stayed bridges);
- seismic response modification device technologies (e.g., hysteretic dampers, isolation bearings); and
- soil behavior, foundation behavior, and ground motion studies for large bridges.

In addition, Project 094 includes a series of special studies, addressing topics that range from non-destructive assessment of retrofitted bridge components to supporting studies intended to assist in educating the bridge engineering profession on the implementation of new seismic design and retrofitting strategies.

This research aims to extend the ductile end diaphragm concept used on steel bridges to make it applicable for bidirectional earthquake excitations, using unbonded braces as ductile fuses. Irregular (i.e. skewed) bridge superstructures are also covered to determine if the ductile diaphragm concept could be used in skewed bridges. Two retrofit schemes are investigated in detail to determine the best geometrical layout (to maximize the dissipated hysteretic energy) of the ductile diaphragms with unbonded brace end diaphragms. Closed form solutions are sought for practical design purposes. Behavioral characteristics of the proposed retrofit schemes are quantified with an emphasis on hysteretic energy dissipation. Results from numerical examples show that the bidirectional loading, loading ratio (or the assumed combination rule), and skew angle have a pronounced effect on the end diaphragm's inelastic behavior. Based on volumetric hysteretic energy dissipation, the effectiveness of the proposed retrofit schemes are compared under several loading cases for both non-skewed and skewed bridge superstructures.

ABSTRACT

Since end diaphragms of many bridges in North America were built without seismic design considerations, they may suffer damage in future earthquakes. Recent earthquake reconnaissance investigations have reported damage in bridge end diaphragms due to earthquake effects. To reduce the seismic demands in steel bridges, one approach (among many such as base isolators of any kind) is to provide bridge superstructures with special ductile diaphragms as “seismic fuses” as an appropriate retrofit solution. Although the behavior of metallic fuses in the bridge transverse direction has been investigated both analytically and experimentally under unidirectional loading, no guidance exists to help the engineer determine the seismic behavior under bidirectional loading. Furthermore, to date, the ductile diaphragm concepts were limited in recommended applications to the retrofit of regular (i.e. non-skewed) bridges and this solution thus has to be combined with another retrofit solution for resistance to earthquakes exciting bridges in their longitudinal direction.

This research mainly aims to extend the known ductile end diaphragm concept to make it applicable for bidirectional earthquake excitation, using unbonded braces as the ductile fuses. Irregular (i.e. skewed) bridge superstructures are also covered to determine if the ductile diaphragm concept could be used in skewed bridges. Two retrofit schemes (Retrofit Scheme-1 and Retrofit Scheme-2) are investigated in detail to search the best geometrical layout (to maximize the dissipated hysteretic energy) of the ductile diaphragms with unbonded brace end diaphragms. Closed form solutions are sought for practical design purposes.

Behavioral characteristics of the proposed retrofit schemes for end diaphragms are quantified with an emphasis on hysteretic energy dissipation. Results from many numerical examples show that, the bidirectional loading, the loading ratio (or the assumed combination rule), and the skew angle have pronounced effect on the end diaphragm’s inelastic behavior. Based on volumetric hysteretic energy dissipation, the effectivenesses of the proposed retrofit schemes are compared under several loading cases for both non-skewed and skewed bridge superstructures. These comparisons indicate that, in most cases, Retrofit Scheme-1 is superior over Retrofit Scheme-2 and may exhibit better seismic response.

ACKNOWLEDGEMENTS

This research was conducted by the State University of New York (SUNY) at Buffalo and was supported by the Federal Highway Administration (FHWA) under contract number DTFH61-98-C-00094 to the Multidisciplinary Center for Earthquake Engineering Research (MCEER).

Assoc. Prof. Stuart S. Chen of the Department of Civil, Structural & Environmental Engineering at University at Buffalo kindly opened his steel bridge archive for obtaining average values of bridges geometric properties used in diagrams in Sections 4 and 5. This help is greatly acknowledged.

However, any opinions, findings, conclusions, and recommendations presented in this report are those of the authors and do not necessarily reflect the views of the sponsors.

TABLE OF CONTENTS

TABLE OF CONTENTS (continued)

LIST OF ILLUSTRATIONS

LIST OF ILLUSTRATIONS (continued)

LIST OF ILLUSTRATIONS (continued)

LIST OF ILLUSTRATIONS (continued)

LIST OF ILLUSTRATIONS (continued)

LIST OF ILLUSTRATIONS (continued)

LIST OF ILLUSTRATIONS (continued)

LIST OF TABLES

NOTATIONS

a	length to internal diaphragm anchor point
A, A_g	cross-sectional area of an unbonded brace
a_{max}	expected maximum ground acceleration
C_L	compression in longitudinal unbonded braces in Retrofit Scheme-1
	compression in long unbonded braces in Retrofit Scheme-2
C_S	compression in short unbonded braces in Retrofit Scheme-2
C_T	compression in skew unbonded braces in Retrofit Scheme-1
d	end diaphragm depth
E	modulus of elasticity of unbonded braces
Eff. Ratio	ratio of hysteretic energy dissipation per volume to maximum one
E_H	hysteretic energy dissipation during a complete cycle
E_H/Vol.	hysteretic energy per total unbonded braces volume
$E_{H1....H3}$	hysteretic energy dissipation in each hysteretic region
$E_{H, 1/4}$	approximate hysteretic energy dissipation for ¼ cycle
g	acceleration of gravity
h	normal girder spacing
K_E	initial stiffness
K_L	initial stiffness of system in longitudinal direction
K_T	initial stiffness of system in transverse direction
K_1	initial stiffness of short unbonded braces
K_2	initial stiffness of long unbonded braces
L_B	length of unbonded braces
LL	long brace length in Retrofit Scheme-2
LS	short brace length in Retrofit Scheme-2
m	total mass of bridge superstructure
n_L	number of unbonded braces in longitudinal direction in Retrofit Scheme-1
n_T	number of unbonded braces in skew direction in Retrofit Scheme-1

P_1	loading in longitudinal direction of bridge
P_2	loading in transverse direction of bridge
P_1/P_2	bidirectional loading ratio (longitudinal to transverse)
P_2/P_1	bidirectional loading ratio (transverse to longitudinal)
PGA	peak ground acceleration
P_y	axial yield strength of unbonded brace both in tension and compression
s	skew girder spacing
S1,…,S9	selected end diaphragm systems in Example 1
S_d	maximum displacement demand in end diaphragm system
s_L	longitudinal brace length in Retrofit Scheme-1
s_T	skew brace length in Retrofit Scheme-1
T	fundamental period of end diaphragm system
T_L	tension in longitudinal unbonded braces in Retrofit Scheme-1
	tension in long unbonded braces in Retrofit Scheme-2
T_S	tension in short unbonded braces in Retrofit Scheme-2
T_T	tension in transverse or skew unbonded braces in Retrofit Scheme-1
u,v,w	displacement components of bridge bearings in x, y, and z directions
V_B	base shear strength
V_L	total base shear in bridge longitudinal direction
Vol.	total volume of unbonded braces used
V_T	total base shear in bridge transverse direction
V_{yL}	longitudinal base shear at yield
V_{yT}	transverse base shear at yield
V_{y1}	transverse base shear when short unbonded braces yield
V_{y2}	transverse base shear when long unbonded braces yield
W	total weight of bridge superstructure
X	loading in X direction
X+Y	loading in both directions
Y	loading in Y direction
α_1, α_2	projection angles in idealized system

β	angle between vertical axis and long unbonded brace in Retrofit Scheme-2
γ	angle between vertical axis and short unbonded brace in Retrofit Scheme-2
δ_y	axial yield displacement of unbonded brace in tension and compression
Δ_L	longitudinal displacement
Δ_{max}	maximum displacement
Δ_{maxL}	maximum longitudinal displacement
Δ_{maxT}	maximum transverse displacement
Δ_T	transverse displacement
Δ_y	yield displacement
Δ_{yL}	longitudinal yield displacement
Δ_{y1}	yield displacement in system when short unbonded braces yield
Δ_{y2}	yield displacement in system when long unbonded braces yield
Δ_{yL}/d	yield drift in longitudinal direction
Δ_{yT}	transverse yield displacement
Δ_{yT}/d	yield drift in transverse direction
ε	bidirectional loading ratio (P_1/P_2, longitudinal to transverse)
θ_1	angle between longitudinal brace and bridge longitudinal axis in Retrofit Scheme-1
θ_2	angle between skew brace and bridge skew axis in Retrofit Scheme-1
μ	target axial displacement ductility of each unbonded brace both in tension and compression
μ_G	global ductility demand
μ_{GL}	system global ductility in longitudinal direction
μ_{GT}	system global ductility in transverse direction
φ	skew angle
ω	fundamental frequency of end diaphragm system
Ω_1, Ω_2	projection angles in idealized system
Φ_x,Φ_y,Φ_z	rotation components of bridge bearings around x, y, and z axes

ABBREVIATIONS

AASHTO	American Association of State Highway and Transportation Officials
AISI	American Iron and Steel Institute
ATC	Applied Technology Council
EBF	Eccentrically Braced End Diaphragms
FHWA	Federal Highway Administration
JRA	Japan Road Association
MCEER	Multidisciplinary Center for Earthquake Engineering Research
SA	Same Brace Area
SBS	Same Base Shear
SDOF	Single Degree of Freedom
SIS	Same Initial Stiffness
SPS	Shear Panel Systems
SUNY	State University of New York
TADAS	Steel Triangular Plate Added Damping and Stiffness Devices
VSL	Vertical Shear Link

SECTION 1
INTRODUCTION

1.1 Overview

Many slab-on-girder steel and deck truss bridges in North America are located in seismic regions. Since most of them were built without seismic-design considerations, they may suffer damage in future earthquakes. The end diaphragms in these bridges generally do not have ductile details (members and connections). Recent earthquake reconnaissance investigations have reported damage in bridge end diaphragms due to transverse earthquake effects. Currently, seismic evaluation and retrofit research activities throughout North America are looking for cost effective solutions to this problem. To reduce the seismic demands in steel bridges, several retrofitting systems have been proposed. One approach (Zahrai and Bruneau 1999a; 1999b; Bruneau et al. 2002) suggests that special ductile diaphragms could provide an appropriate retrofit solution. This concept requires replacing existing end diaphragms with specially detailed diaphragms that can act as "seismic fuses", i.e. which could yield prior to other sub and superstructure elements. This concept has been experimentally verified using specially designed ductile end diaphragms having either shear panel systems (SPS), steel triangular plate added damping and stiffness devices (TADAS), or eccentrically braced end diaphragms (EBF). In the time since those tests, the effectiveness of unbonded braces[1] has been recognized, and it appears that unbonded braces could be used to provide an effective ductile end diaphragms concept. However, in all cases considered to date, the ductile diaphragm concepts was limited in recommended applications to the retrofit of regular (i.e. non-skewed) bridges against earthquake excitation in the bridge transverse direction. This solution thus has to be combined with another retrofit solution for resistance to earthquakes exciting bridges in their longitudinal direction.

The research presented here essentially aims to extend the ductile end diaphragm concept to make it applicable for bidirectional earthquake excitation, using unbonded braces as the ductile fuses. A first question arises as to the best geometrical layout of the ductile diaphragms to be

[1] Unbonded braces are also known as "Buckling Restrained Braces". This latter terminology has become more widely adopted following the publication of the 2005 Seismic Provisions of the American Institute of Steel Construction. "Unbonded braces" is used here, as this study preceded the publication of the AISC document.

used for this purpose. Answering this question can also help establish if the ductile diaphragm concept could be used in skewed bridges. This is to be investigated analytically. Closed form solutions are sought for practical design purposes. This work is also conducted to define the parameters for a future experimental study on bridge end diaphragms with unbonded braces to validate the proposed concepts.

1.2 Research Approach

The use of various bracing layout for the ductile diaphragms is considered analytically, using simple hand calculation models and SAP2000 for verification. Braces are assumed to be unbonded braces with idealized elastic-plastic bilinear force-displacement relationships. This inelastic model is a reasonable first approximation given that such braces exhibit stable, unpinched, and full hysteretic behavior under axial force (both in compression and tension).

A design objective of maximum hysteretic energy dissipation at a prescribed ductility level has been set to compare the efficiency of various geometries. However, using closed form derivations allow the consideration of alternative objectives (e.g. maximum stiffness, minimum drift, etc.)

Constraints imposed on the ductile end diaphragm concept by previous studies are to be eliminated by this study accounting for the generic bridge dimensions (including the skewness), bidirectional earthquake effects, and the implementation of unbonded braces instead of VSL, EBF, and TADAS devices. Two bracing configurations are first considered, and their effect on structural behavior is analyzed. Since inelastic deformations concentrate in the end diaphragms (Zahrai and Bruneau 1999a), as a first approximation, the entire seismic inelastic behavior of the bridge and its end diaphragms can be expressed by a simplified model. All deformations in that simplified model are taken by the end diaphragm system, i.e. by the unbonded end braces. Both straight and skewed bridges are analyzed to explore the effect of skew on the bridge behavior.

1.3 Outline

In Section 2, previous theoretical and experimental research on the seismic behavior of steel bridges end diaphragms is reviewed.

In Section 3, hysteretic modeling of bridge unbonded brace end diaphragms is described. Simplified cyclic elastic-plastic model is suggested for the hysteretic behavior of unbonded braces.

In Section 4, for the proposed Retrofit Scheme-1, generalized closed form formulas are derived for skew bridges with end diaphragms subjected to bidirectional earthquake effects. Factors affecting the bridge end diaphragm behavior are discussed.

In Section 5, for the proposed Retrofit Scheme-2, generalized closed form formulas are derived for skewed bridges with end diaphragms subjected to bidirectional earthquake effects. Factors affecting the bridge end diaphragm behavior are discussed.

In Section 6, design examples are given to show the practical use of the derived formulas.

In Section 7, general conclusions from this research and recommendations for future work on this subject are given.

SECTION 2
LITERATURE REVIEW

2.1 General

Limited amount of studies have focused on the behavior of bridges having supplemental passive seismic energy dissipation systems in their end diaphragms to protect bridge sub and superstructures from excessive seismic demands. Since this study is somewhat an extension of the studies on bridge ductile end diaphragm concept, the previous work on this topic is first presented in Section 2.2 to clarify the main contribution of this work.

2.2 Previous Research on Bridge End Diaphragms for Seismic Retrofit

This section first reviews past theoretical and experimental studies on the seismic response of bridge end diaphragms.

Bruneau et al. (1996) reviewed past and current Japanese bridge design requirements, followed by an overview of the observed damage to steel bridges during the 1995 Hyogo-ken Nanbu (Kobe) earthquake. Seismic performance of steel bridges was generally found to be better than concrete bridges of similar vintage. But, that steel bridges can still be vulnerable to earthquakes in a number of ways. Seismic deficiencies, severe damage, and collapse were observed in steel highway and railroad bridges, from short span to long span bridges. Bridge damage due to diaphragm connection failure has occurred.

Zahrai and Bruneau (1998) quantitatively investigated the impact of diaphragms on the seismic response of straight slab-on-girder steel bridges. Typical 20 to 60-m span bridges with and without diaphragms were considered and studied through elastic and inelastic pushover analyses. Hand calculation formulas were developed to evaluate their period, elastic response, and pseudo spectral acceleration at first yielding. The analysis results indicated that the presence of intermediate diaphragms did not significantly influence the seismic performance of these types of bridges in either elastic or the inelastic range.

Zahrai and Bruneau (1999a) studied the adequacy of a seismic retrofit strategy that relies on ductile end diaphragms inserted in steel bridges superstructures. The objective of the study was to calibrate these diaphragms to yield before the strength of the substructure is reached. Simplified models for slab-on-girder steel bridges of the type found in North America were developed and nonlinear inelastic analyses were performed. The effectiveness of the VSL, EBF, and TADAS devices as selected ductile retrofitting alternatives was discussed. Only bridges on stiff substructure (or a range of substructure stiffness) were considered, and further studies on bridges on flexible substructure were recommended to verify the validity of this retrofit strategy.

Zahrai and Bruneau (1999b) presented the results of cyclic tests on full-size bridge girder specimens with the SPS (shear panel system), EBF, and TADAS devices in their end diaphragms. Experimentally obtained hysteresis curves demonstrated that the specimens had adequate initial elastic stiffness, strength, and capacity to dissipate hysteretic energy. The specimens developed 0.2 rad. rotational capacity in TADAS specimen, 0.08 to 0.11 rad. link distortion angles in EBF and SPS systems. Images from TADAS plates under 2% drift and the deformation of the vertical link (SPS) at 1.5% drift are shown in Figure 2.1a and 2.1b respectively.

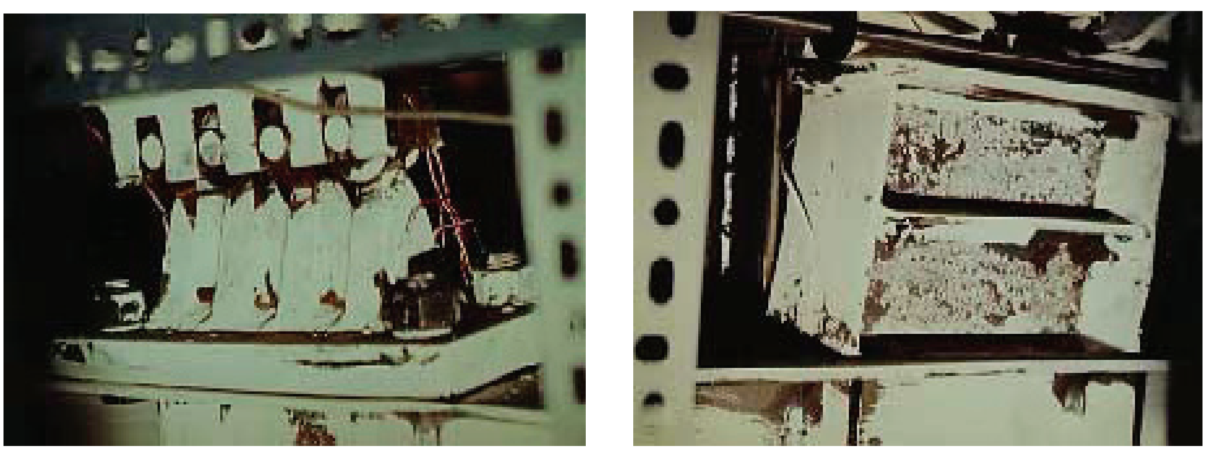

(a) **(b)**

FIGURE 2-1 Deformation of Energy Dissipating Devices in End Diaphragms : (a) TADAS at 2% Drift; (b) SPS at 1.5% Drift (Adapted from Zahrai and Bruneau, 1999b)

Ductile end diaphragms having bolted connections suffered slippage, and resulted in pinched hysteretic loops. Welded specimens improved the cyclic behavior of the specimens, and led to fuller hysteretic loops. Also specimens with nominal channel diaphragms and specimens without any diaphragm dissipated less hysteretic energy, suffered bolt rupture, buckling of web stiffeners, and fracture of the stiffness at large drifts.

Sarraf and Bruneau (1998a) proposed a similar seismic retrofit solution for deck-truss bridges, converting the deck-slab into a composite slab and replacing the end cross-frames and the lower lateral braced panels adjacent to the supports by special ductile cross-frames (i.e. diaphragms). These ductile fuses were designed to dissipate energy by yielding, and to limit the seismic demands in the remaining superstructure and substructure members. An analytical procedure based on the governing transverse seismic response of retrofitted deck-trusses was recommended to determine overall stiffness and strength of such ductile panels. As a numerical example, an 80-m span deck-truss bridge was analyzed. Computer simulations of the dynamic behavior of the retrofitted deck-truss subjected to 0.6g El Centro earthquake ground motion showed satisfactory performance and validated the analytical procedure. In a companion paper, Sarraf and Bruneau (1998b) presented performance based design procedures accompanied by graphical approaches for the seismic response analyses of deck-truss bridges retrofitted using EBF, VSL, or TADAS systems. TADAS systems were found to be subjected to less constraints than the EBF and VSL systems and were relatively simpler to design. To test the proposed innovative retrofit strategy for existing deck-truss steel bridges, a 27 feet (8229.6 mm)-long deck-truss bridge model was constructed (Figure 2-2a), and pseudo-dynamically tested in its as-built as well as retrofitted conditions (Sarraf and Bruneau, 2002,2004). EBF (Figure 2-2b) and vertical shear links (VSL, Figure 2-2c) were used as ductile retrofit techniques, and both performed well. These ductile retrofit devices exhibited a robust hysteretic behavior, dissipated the seismic induced energy and prevented damage in other structural members of the model bridge under the scaled El Centro earthquake. The devices exhibited considerable cyclic ductility. It was noted that possible substantial overstrength of the devices be further investigated and taken into account in the retrofit design.

(a)

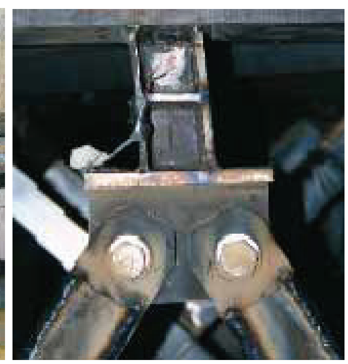

(b) (c)

FIGURE 2-2 Pseudo-Dynamic Testing of 27-Foot Long Deck-Truss Model : (a) Test Set-Up; (b) Inelastic Deformation in EBF; (c) Inelastic Deformation in VSL (Adapted from Sarraf and Bruneau, 2002, 2004)

Alfawakhiri and Bruneau (2000) addressed the elastic dynamic response of simply supported bridges to ground motion in their transverse direction. The interaction between superstructure and support flexibilities was studied for symmetric spans. The bridges were modeled as beams with uniformly distributed mass and elasticity, simply supported at the ends by elastic springs. A stiffness index was then defined based on the stiffnesses of bridge sub and superstructures. It was found that span/support stiffness index completely defines the modal shapes. Closed form expressions based on approximate shape functions were derived for the dynamic parameters of the first mode. Numerical case studies were included in the study to illustrate and assess the use of equations proposed for the seismic analysis of bridges. It was noted that neglecting support flexibility leads to an artificially stiff bridge, resulting in a shorter fundamental period, which in turn may cause a significant error in the evaluation of seismic loads, especially when design spectra exhibit sharp variations of spectral acceleration with period.

Alfawakhiri and Bruneau (2001) further investigated the inelastic dynamic response of simply supported bridges to ground motion in their transverse direction. The effect of relative substructure-superstructure flexibility on the inelastic response of bridges was studied for symmetric spans. The bridges were modeled as elastic beams with distributed mass, simply supported at the ends by elastic-plastic springs. Closed form expressions that capture interaction of local and global ductility demands were derived and used to show how substructure flexibility increases the ductility demand in ductile end diaphragm systems. Also shown was how span-to-substructure relative flexibility could significantly increase ductility demand in bridge supports/substructure.

Bruneau et al. (2002) overviewed the ductile end diaphragm concept in bridge superstructures for seismic retrofit purposes of seismically vulnerable slab-on-girder and steel truss-deck bridges. Design equations were given for the retrofit systems having SPS, EBF, and TADAS devices. A flow chart was proposed as a guide to design ductile diaphragm. Limitations pertaining to the procedure (such as stiffnesses of the sub and superstructures, application in short and long-span bridges etc.) were discussed. It was emphasized that other types of ductile diaphragms could be implemented provided that they possess a yield strength that could be accurately assessed, and could sustain repeated cycles of inelastic deformations in a ductile manner without significant strength degradation.

Itani et al. (2004) conducted experimental and analytical investigations on steel plate girder bridges and their components. Behavior of steel plate girder bridges under lateral loading was evaluated considering lateral load path and modeling issues. Results showed the importance of shear connectors in distributing and transferring lateral forces to the end and intermediate cross frames. Seismic performance of steel bridges during recent earthquakes was also reviewed. Observed damage was grouped in categories such as end cross frame failures, reinforced concrete substructure failures, steel pier failures, seismic restrainer failures, bearing failures, and bridge girder failures. Special emphasis was given to the ductile end diaphragm concept and on the latest information on specifications and guidelines for the seismic design of steel plate girder bridges in the United States.

Carden et al. (2003) transversely tested a 2/5-scale straight bridge model to study the seismic response of a typical steel slab-on-girder superstructure. Earthquake loads were simulated by pseudostatically applying forces at the deck level using twin actuators. The impact of composite action between the deck and steel superstructure, end cross frames, web stiffeners and bearings on the overall behavior was discussed. The end cross frames were found to transfer the majority of the transverse earthquake forces into the substructure, thus supporting the conceptual feasibility of the ductile end cross frames. Stresses in the superstructure were small due to longitudinal earthquake loading. Carden et al. (2006a,b) investigated the cyclic inelastic and pseudo-dynamic seismic performance of bridge having either single angle X braces with good connection details or ductile unbonded braces in their end diaphragms (Figure 2-3).

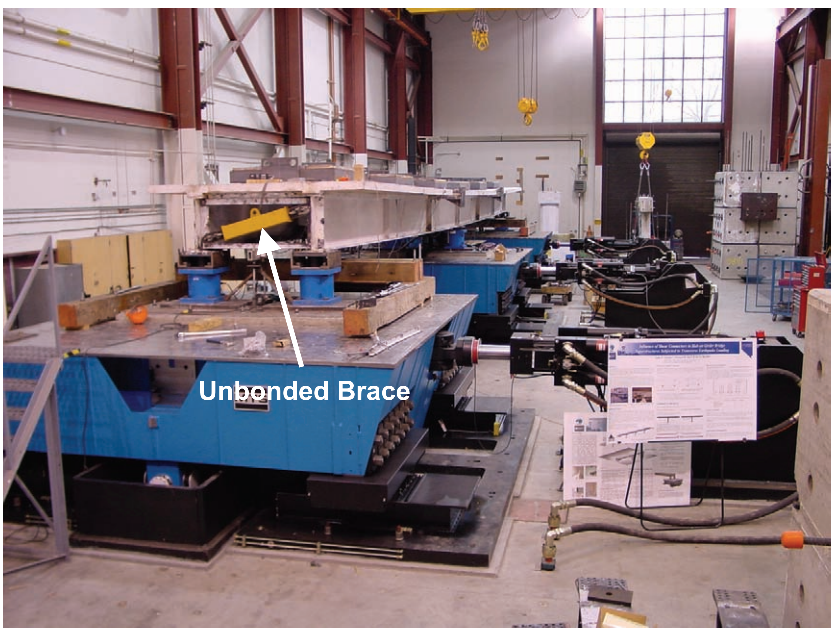

FIGURE 2-3 Testing of Slab-on-Girder Bridge Model with Unbonded Brace End Diaphragm (Adapted from Itani, 2003)

These experimental studies showed that both types of end diaphragms could exhibit satisfactorily ductile seismic performance. Maximum drifts of 5.3% and 6.6% were respectively obtained for those systems, but the unbonded braces were noted as less likely to need replacement following an earthquake. This experimental study was limited to a straight two-girder bridge, without skew, subject to transverse earthquake excitation.

2.3 Implementation of Unbonded Braces

Unbonded braces have recently been implemented in buildings as energy dissipation members, mostly in Japan and in the United States. Because of their stable, repetitive, and unpinched hysteretic characteristics and ease of design, the rate of implementation in building applications is increasing. However, at the time the research presented in this report was initiated, to the knowledge of the authors, unbonded braces had not been implemented in bridge structures as ductile end diaphragms. In the time since, unbonded braces have been used to retrofit the Minato bridge in Japan (Kanaji et al. 2003; Kanaji et al. 2005), the world's third longest truss bridge (Figure 2-4a,b, 2-5a,b), using a concept similar to the one developed by Sarraf and Bruneau (1998a; 1998b).

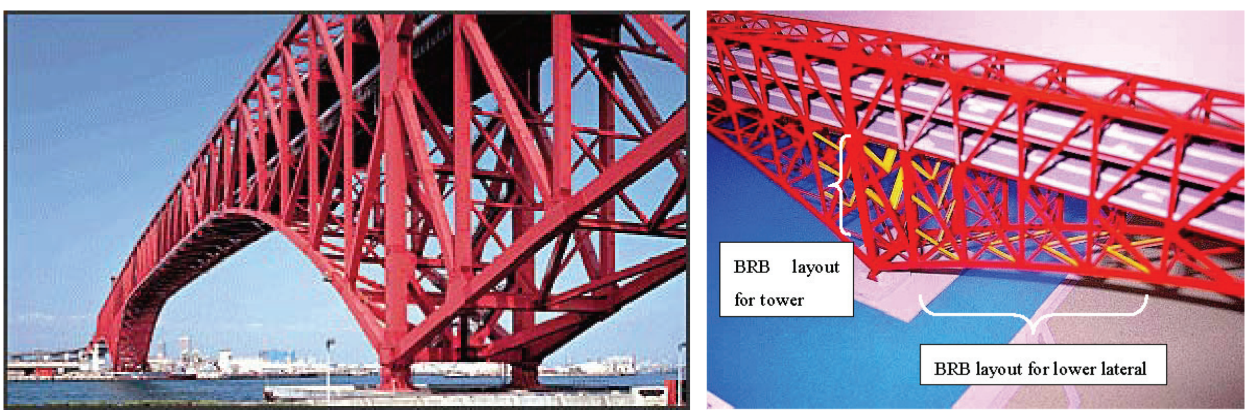

(a) **(b)**

FIGURE 2-4 The Minato Bridge in Osaka, Japan : (a) Overall View; (b) Optimal Layout of Unbonded Braces (Adapted from Kanaji et al, 2003, 2005)

Figure 2-5 shows the failure patterns and a sample hysteresis curve from the test results given in Kanaji et al. (2005). For each 1/6-scale unbonded brace specimen considered, the impact of cross sectional configuration on the hysteretic behavior was investigated. Using these experimental hystereses, equivalent damping ratios were calculated to vary between 37% and 50%.

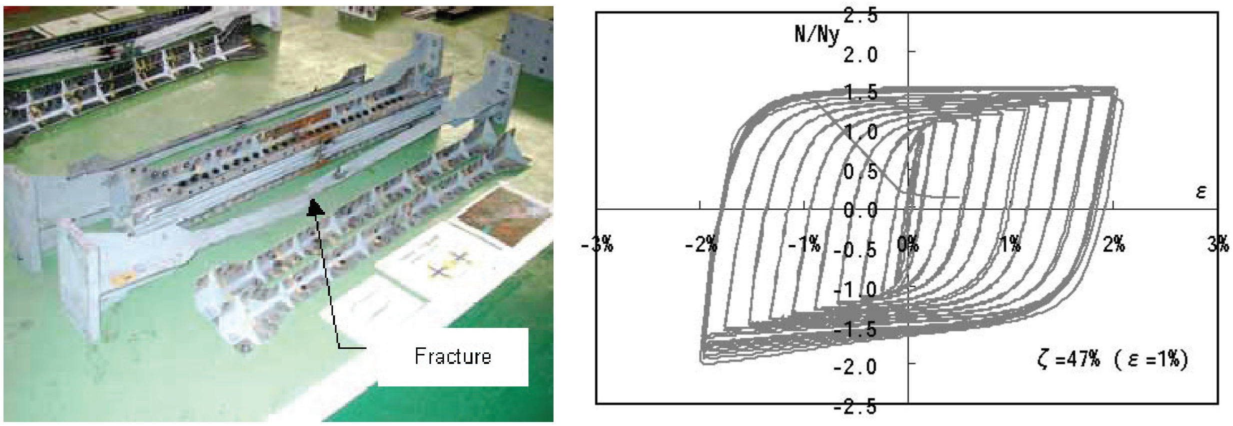

(a) **(b)**

FIGURE 2-5 Cyclic Testing of Several Unbonded Braces: (a) Failure Patterns; (b) Stable Hysteretic Behavior and Equivalent Damping Ratio (Adapted from Kanaji et al, 2005)

In light of the superior hysteretic behavior of unbonded braces over “traditional” braces and other energy dissipation devices which were shown to be effective in bridge diaphragm to improve seismic response in the transverse direction, this report extends the ductile end diaphragm concept using unbonded braces to resist bidirectional earthquake effects.

SECTION 3
HYSTERETIC MODELING OF BRIDGE END DIAPHRAMS WITH UNBONDED BRACE END DIAPHRAGMS

3.1 General

Unlike conventional braces that exhibit complex, unsymmetrical hysteretic loops under tension and compression forces, and significant strength deterioration in cyclic compression strength in the inelastic range, unbonded braces have predictable hysteretic behavior with cyclic hysteretic symmetric loops in the elastic and inelastic ranges and substantial energy dissipation capacities (Figure 3-1).

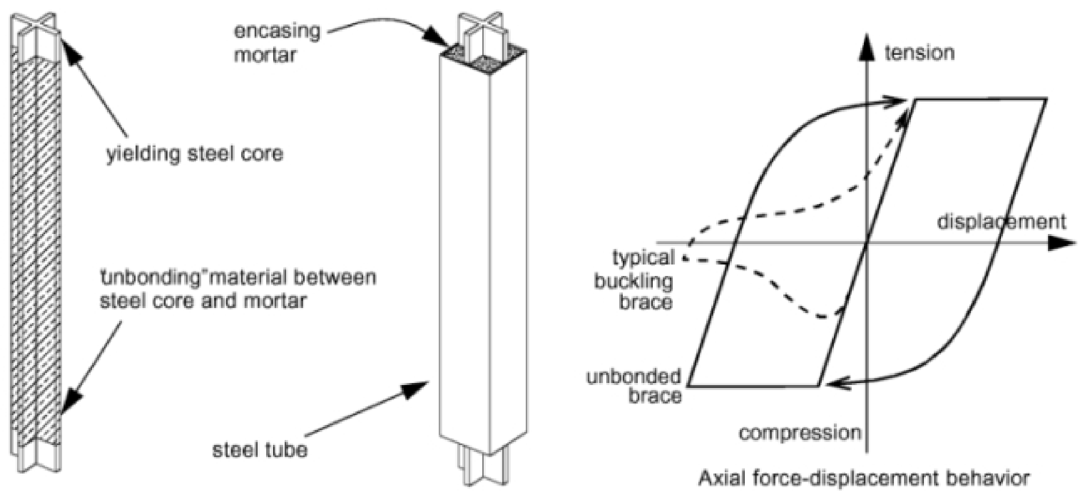

FIGURE 3-1 Unbonded Braces Components and Hysteretic Behavior of Unbonded Braces (Adapted from Clark et al. 1999)

Based on a large-scale experimental study, Black et al. (2002) characterized the hysteretic behavior of unbonded braces using the Bouc-Wen model. They also calibrated the model using the experimentally obtained values. With appropriately selected quantities that control the shape of the hysteretic loop, the Bouc-Wen model approaches the bilinear hysteretic model. Analyses results suggested that the bilinear approximation could be used with confidence, since a good agreement in seismic response was observed between results obtained by the Bouc-Wen and the bilinear models for a set of earthquake data. Moreover, Sabelli et al. (2003) modeled unbonded braces as simple truss elements having ideal bilinear hysteretic behavior, exhibiting no stiffness or strength degradation.

A bilinear hysteretic model for unbonded braces is therefore assumed in this study. Although some studies suggest that unbonded braces may have up to 10% greater compressive strength than tensile strength, this effect is neglected. Additionally, post-yield stiffness of braces is set to zero, assuming an elastic-perfectly plastic axial force-displacement relationship. Since closed form expressions are sought for practical design purposes, these approximations help to reduce the complexity of these expressions. The bilinear hysteretic model used is illustrated in Figure 3-2.

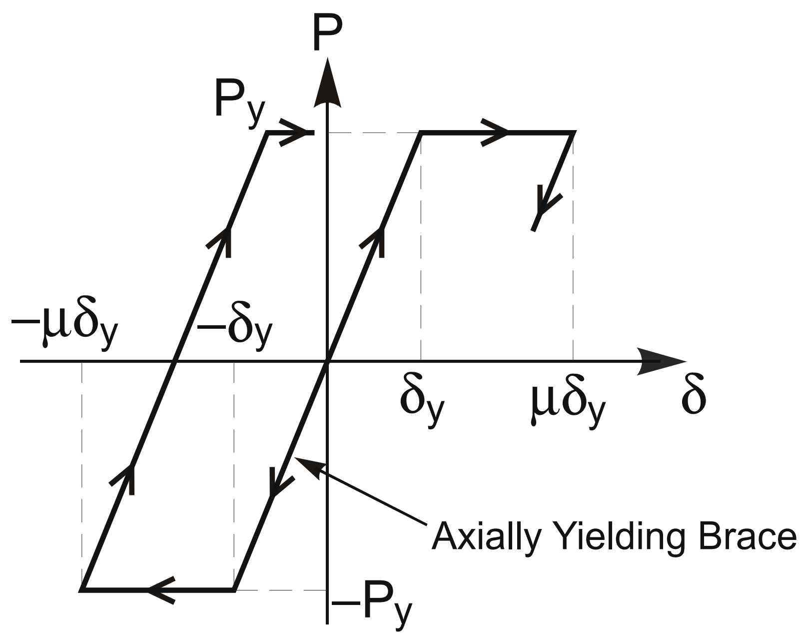

FIGURE 3-2 Bilinear Hysteretic Model for Unbonded Braces

On that figure, P_y, δ_y, and μ indicate the unbonded brace axial yield strength (symmetric in tension and compression), axial yield displacement (symmetric in tension and compression), and target axial displacement ductility respectively.

3.2 Modeling Bridge End Diaphragms

3.2.1 Proposed Retrofit Schemes

In this work, for seismic retrofit purposes, two types of bracing configurations acting as ductile fuses in bridge end diaphragms are considered:

- *Retrofit Scheme-1* (2D) : Using two pair of unbonded braces at each end of a span, in a configuration that coincides with the skew and longitudinal directions (Figure 3-3). In other words, one pair of unbonded braces are oriented parallel to the longitudinal axis of the bridge, connecting the abutment to the underside of the bridge deck (or other component of the bridge if preferred), and another pair is in the conventional diaphragm configuration, parallel to the skew if skew is present, and thus perpendicularly to the axis of the bridge in absence of skew.
- *Retrofit Scheme-2* (3D) : A single pair of unbonded braces at each end of a span, in a configuration that does not coincide with the bridge longitudinal and skew directions (Figure 3-4), but rather connect the abutment to the underside of the bridge deck at a certain distance from the abutment, at an angle making it possible for the single pair of braces used in this case to resist lateral loads applied in all horizontal directions.

Note that in Retrofit Scheme-1 (in Figure 3-3), the bottom connection of the pair of braces oriented along the skew angle can be accomplished either to the abutment, or between web stiffeners of the bridge girders, this latter condition being the usual one done in steel bridges. The pair of longitudinal braces are a new concept, and would need to be connected at the abutment, either at the bearing level (on the horizontal side) or on the vertical side. As discussed later, detailing decisions depend on the existing boundary conditions of the girders. For the deck level connection, specially designed cross beams would be required to elastically resist forces from the unbonded brace, unless connection to the existing interior cross frames or girders can be developed without damaging any internal component (capacity design).

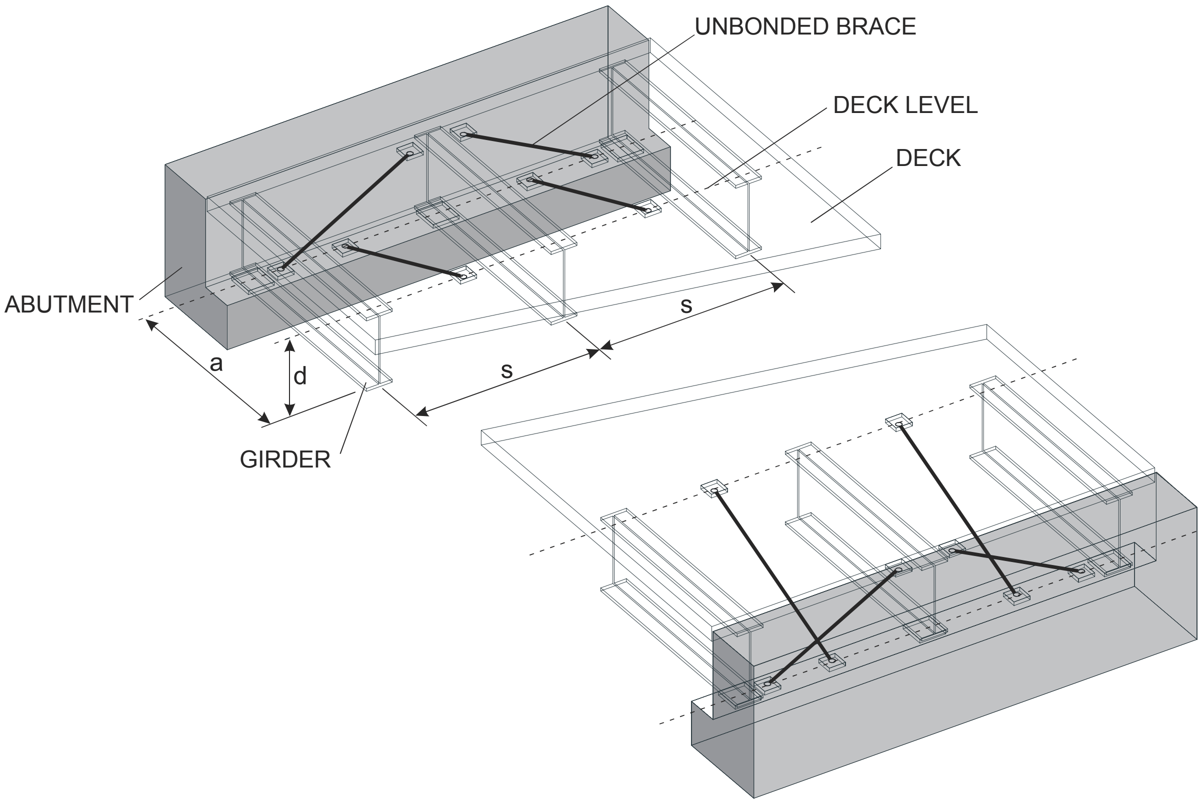

FIGURE 3-3 Retrofit Scheme-1

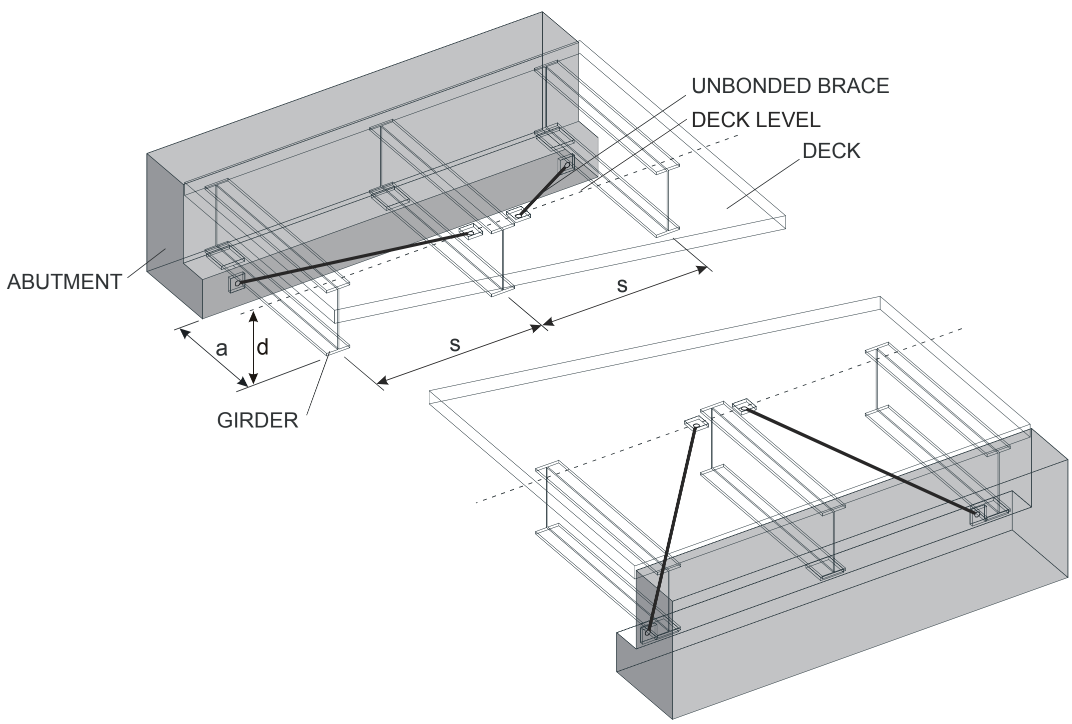

FIGURE 3-4 Retrofit Scheme-2

3.2.2 Bearings

Modeling issues need to be resolved to address the various boundary conditions likely to be encountered in bridges of the type considered here (e.g., superstructure on neoprene bearings free to move in all direction, superstructure span with fixed bearings at pier/abutment location restraining longitudinally movement, etc.). Shown in Figure 3-5 are the possible bridge bearing displacements and rotations expressed in terms of translational and rotational parameters. Some frequently encountered displacement and rotation boundary conditions encountered for bearings in slab-on-girder and deck-truss bridges are shown on the same figure. These notations and plan illustrations are used throughout this report.

Figure 3-6 is useful in demonstrating the potential boundary conditions in plan for a skewed bridge having two girders resting on abutments. Neoprene bearings, bidirectional sliding bearing, and other bearings having negligible strength to horizontal deformations (and to some degree even damaged bearings damaged by an earthquake but that could slide in a stable manner) are simulated as shown in Figure 3-6a.

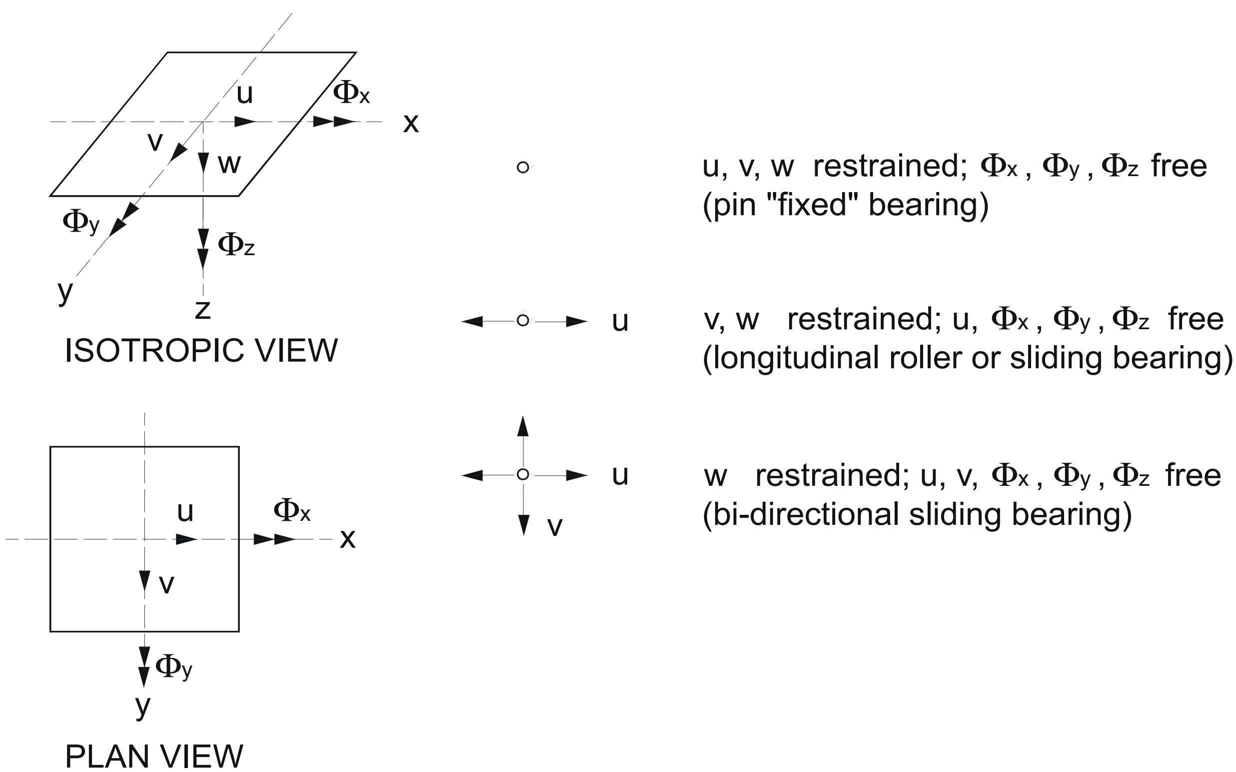

FIGURE 3-5 Displacement and Rotation Components for Bridge Bearings

This case is further called the “floating span” in this work. Floating span type bridges have no resistance to lateral earthquake loading, and therefore need to be restrained laterally by devices to limit their horizontal displacements. In this study, the unbonded braces serve this purpose. Most commonly used type of bridges would be the one shown in Figure 3-6b (with the equivalent of pin bearings at one end, and rollers at the other), which may provide stable seismic behavior if end diaphragms are present and response remains elastic. The bearings at the right abutment in this case can be rocker bearing, elastomeric bearing or sliding bearing. Figure 3-6c shows other possible combination of bearing types.

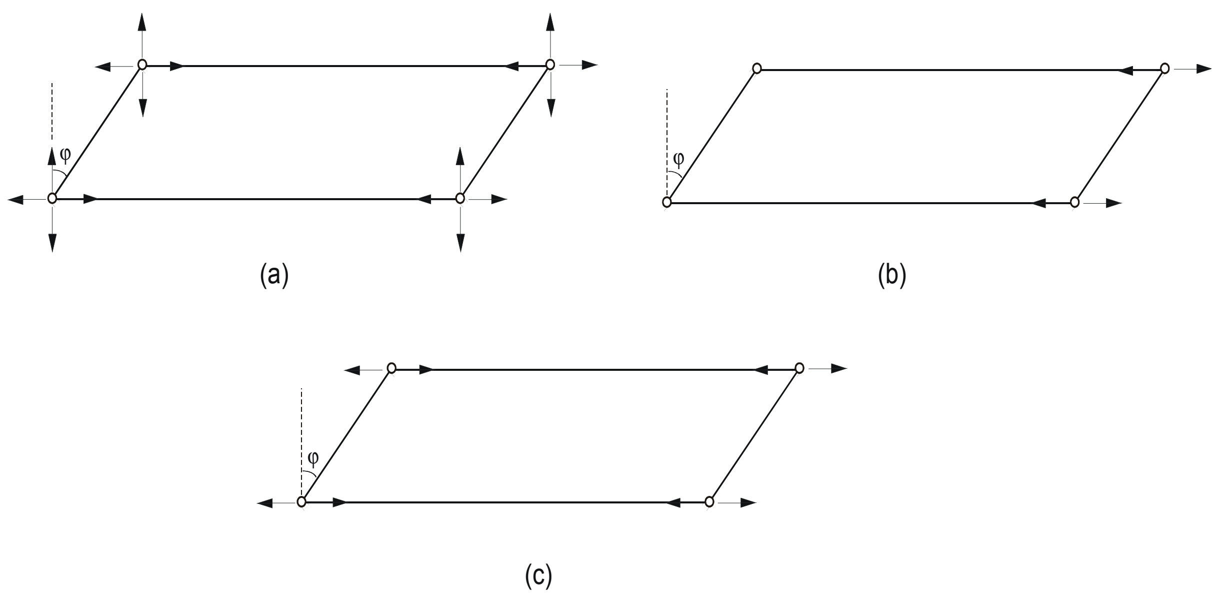

FIGURE 3-6 Example Boundary Conditions (Skewed Bridge Plan Layouts): (a) Floating Bridge (No Restraint in Two Orthogonal Horizontal Directions); (b) Left Pin Bearing, Right Rolled Bearing (Restrained in Transverse Direction); (c) Left and Right Roller Bearings (Restrained in Transverse Direction)

Since the previous research on the behavior of steel slab-on-girder bridges suggests that seismic demand could concentrate at end diaphragms (Zahrai and Bruneau, 1998), for lateral load analysis, the impact of intermediate cross braces on the overall behavior of these bridges can be neglected. This leads to the development of a simplified structural model to simulate the system behavior. For each seismic retrofit scheme, the steps followed to idealize a skewed bridge having end diaphragms into a simpler model are given in Figures 3-7 and 3-8.

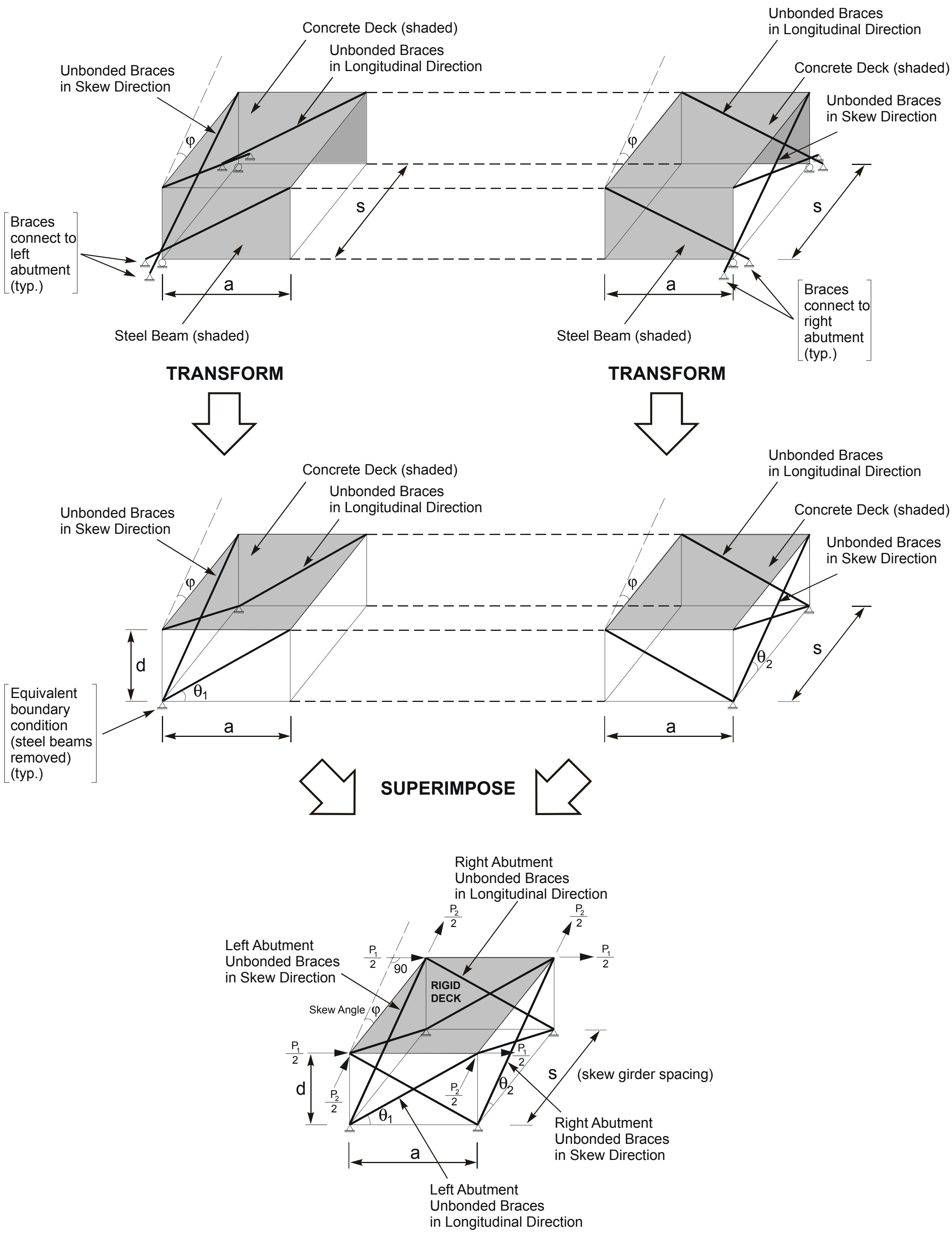

FIGURE 3-7 System Idealization Steps for Retrofit Scheme-1

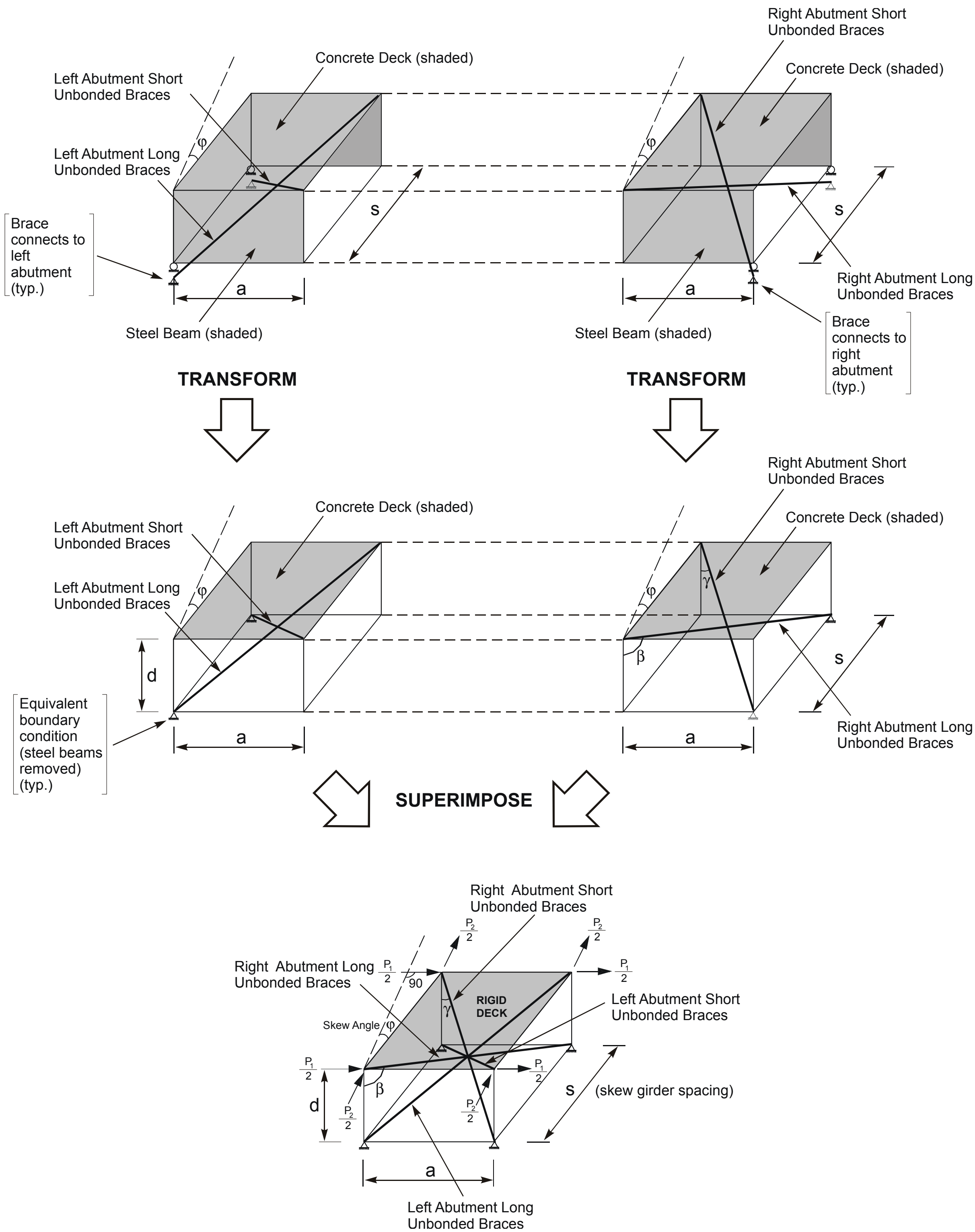

FIGURE 3-8 System Idealization Steps for Retrofit Scheme-2

As a first step, the left and right segments of the bridge over which the special end diaphragms would be inserted are considered. The actual boundary conditions that would exist are recognized – typically, in this study, all unbonded braces are considered to be connected to the abutments (note that in some conditions, the results presented in this report can be interpreted as valid for other boundary conditions – for example, for forces applied in the bridge transverse direction of a non-skewed bridge having bearing restrained in this transverse direction, similar results could be obtained for the end-diaphragms perpendicular to the bridge axis if these were connected in the conventional manner between the stiffeners of the steel girders).

The steel girders and concrete deck are considered rigid in their own plane. The concrete deck and the steel girders are continuously connected, but assumed fully flexible about their connection axis (parallel to the bridge axis), i.e. the angle between the plane of the concrete deck and the plane of the steel beam can change without developing out-of-plane flexural moments.

Second, by removing the steel girders, the only restraint of the concrete deck against horizontal lateral loads applied to it are provided by the unbonded braces. The boundary conditions can therefore be modeled as fixed pin support to which the unbounded braces can connect.

Finally, the interior segment of the bridge is eliminated and the two end-segments of the bridge are brought together. Furthermore, since the deck is rigid, it is in fact possible to superimpose the two segments on top of each other, as shown at the bottom of Figures 3.7 and 3.8.

These assumptions, along with the assumed pinned end connections for unbonded braces, lead to an idealized and relatively simple system model which is actually a three dimensional truss supporting a rigid deck. This simplified model captures the actual behavior of slab-of-girder bridges having the various configurations of unbonded brace diaphragms considered when subjected to lateral loading applied at deck level.

In Sections 4 and 5, closed form solutions are obtained for bidirectional earthquake excitations (for bridges with and without skew) for the two different diaphragm bracing configurations considered. These formulas can be used to investigate load-displacement behavior for the proposed retrofit systems. The analytical models account for general system geometric dimensions, such as the skew angle (φ), skew girder spacing (s), end diaphragm depth (d) and length to internal diaphragm anchor point (a), as well as bidirectional earthquake effects. Cross-sectional areas of unbonded braces and skew angles are taken to be the same for each of the two end diaphragms used in each specific bridge.

The generalized equations derived can then be simplified for simpler cases of non-skewed bridges, or unidirectional seismic excitation. Static pushover analyses are also carried out on a set of selected end diaphragm configurations using SAP 2000 to validate the analytical equations formulated, and to help understand the impact of system parameters on the inelastic response of bridges with bidirectionally acting end diaphragms. As stated in Section 5, boundary conditions of the bridge girders also have an effect on the inelastic response of these end diaphragms.

Analytical results of interest (and presented in Sections 4 and 5) include base shear forces at yield, yield displacements, member versus global (system) ductility relationships, initial stiffness of the retrofit system (needed for response spectrum analysis), total and volumetric hysteretic energy dissipations, in both orthogonal bridge directions (as applicable). Results from this study will serve as the basis to assess the effectiveness of various configurations of ductile diaphragms in skewed bridges.

SECTION 4
CLOSED-FORM HYSTERETIC MODEL FOR RETROFIT SCHEME-1 UNDER BIDIRECTIONAL EARTHQUAKE EFFECTS

4.1 General

Static pushover analysis help trace the monotonic response of structures up to collapse. Currently, many structural analysis softwares (including SAP2000) enable users to perform static pushover analysis. Plastic hinge properties implemented in those programs are usually based on the ones proposed by structural codes or design guidelines. However, in some circumstances, especially when the system is complex, data generation may be cumbersome, and numerical results obtained from a software usually need to be checked using simple models for reliability purposes. Thus, analytical closed form solutions can be powerful tools in simplified analysis and for preliminary design purposes.

Previous work on seismic behavior of steel bridges and the modeling approaches described in Section 3 show how it is possible to transform slab-on-girder steel bridges into equivalent simplified systems for the purpose of lateral load analysis. Furthermore, since the inelastic behavior of unbonded braces can be modeled by simple elastic-plastic elements as discussed in Section 3, closed form solutions can be derived, and would be convenient in determining the hysteretic response of slab-on-girder steel bridges having unbonded brace end diaphragms.

Section 4.2 describes the geometric properties, assumptions, method of analysis, and the derivation of formulas for Retrofit Scheme-1. A similar approach is followed for Retrofit Scheme-2 in Section 5.2. These two retrofit schemes are described in Section 3.2.

For each case (i.e. Retrofit Scheme-1 and Retrofit Scheme-2), formulas are derived for the distinctive boundary condition of "floating span" (or floating deck). In addition, in Retrofit Scheme-2, the "simple span" (or longitudinally restrained deck) model is also analyzed to evaluate the effect of boundary conditions on the hysteretic response of end diaphragms. These two boundary conditions should cover the majority of cases encountered in practice for which ductile end diaphragms are desirable.

4.2 Bidirectional Pushover Analysis of Retrofit Scheme-1 (Floating Deck)

4.2.1 Brace Axial Forces (Elastic Behavior)

Figure 4-1 (as explained previously) shows the selected configuration of unbonded braces for Retrofit Scheme-1.

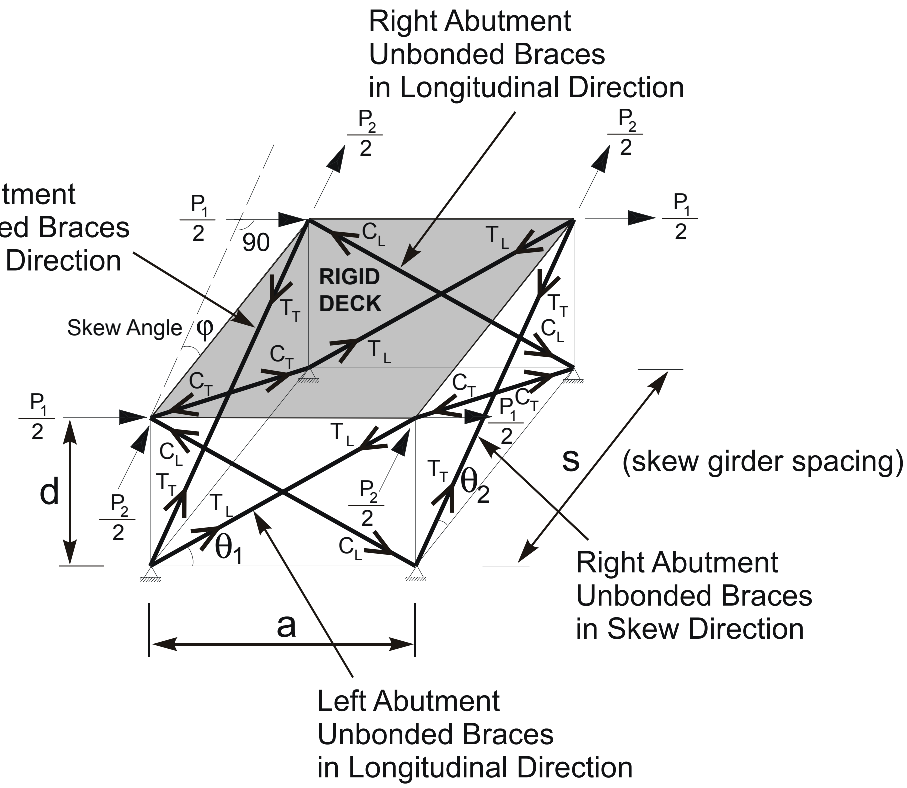

FIGURE 4-1 Configurations of Unbonded Braces in Bridge End Diaphragms and Geometric Properties for Retrofit Scheme-1

Left and right abutment side unbonded braces, bridge deck, girders of a skewed bridge are modeled by a three dimensional idealized truss system, as explained before, having rigid deck and unbonded braces with equal cross sectional area, A, and elastic modulus, E. The model has two limitations, namely the equal area braces and the equal skew angles, φ, at each end. However, the number of braces can be different from each other in each direction as discussed later. Other dimensions are the girder skew spacing (i.e. skewed distance between girders), s, end diaphragm depth, d, which is approximately equal to the girder depth, and the value of “a” which is the horizontal longitudinal distance between connections of the unbonded braces at deck level and the abutment. Note that the skewed distance between girders, s, is equal to the girder spacing divided by cosφ, as shown in Figure 4-1. Of all of these values, the spacing of girders and the girder depth are already known if the bridge is an existing structure. The value of "a" could be eventually chosen to be a function of the girder spacing and would be selected based on engineering judgment (the outcome of this study could help in selecting an optimal value for this parameter). As shown in Figure 4-1, θ_1 and θ_2 are the horizontal angles between the unbonded braces and the horizontal plane for the longitudinal and skew braces respectively.

In that model, all braces and other members representing the existing bridge elements are assumed to be pin connected. Bridge deck is idealized by truss elements with infinite axial stiffnesses. Equal proportions of the total lateral load in a given direction are applied at each corner of the deck. P_1 and P_2 are the lateral earthquake loads acting at the deck level on one diaphragm in the longitudinal and transverse directions respectively. The ratio of P_1/P_2 (or P_2/P_1) is typically set constant in pushover analyses. Additionally, the unbonded braces do not resist gravity load from the bridge superstructure; in other words, they are assumed to be active only under earthquake loading.

The following summarizes the structural characteristics of the idealized system as functions of system geometrical properties.

With reference to the three-dimensional idealized truss system given in Figure 4-1, brace lengths in the longitudinal (s_L) and skew (s_T) directions are

$$s_L = \sqrt{a^2 + d^2} = a / \cos\theta_1 \qquad (4\text{-}1a)$$

$$s_T = \sqrt{s^2 + d^2} = s / \cos\theta_2 \qquad (4\text{-}1b)$$

Total base shear forces in the elastic range are equal to V_L=$2P_1$ and V_T=$2P_2$, since there are two end diaphragms considered in this model. Static equilibrium gives the following brace axial forces under bidirectional loading. Brace axial forces, in the skew and longitudinal directions, are obtained as follows (as shown in Figure 4-1):

$$T_T = -C_T = \frac{s_T}{2s\cos\varphi} P_2 \tag{4-2}$$

$$T_L = -C_L = \frac{s_L}{2a}(P_1 - P_2 \tan\varphi) \tag{4-3}$$

where T_T, C_T and T_L, C_L show tension and compression forces in the skew and longitudinal braces respectively. After defining $\varepsilon = P_1/P_2$, n_T and n_L to be the ratio of bidirectional loads, and the number of braces in the skew and longitudinal directions resisting the seismic loads P_1 and P_2 at an abutment respectively, Eq. (4-2) and (4-3) take the following forms:

$$T_T = -C_T = \frac{s_T}{n_T s\cos\varphi} P_2 \tag{4-4}$$

$$T_L = -C_L = \frac{s_L(\varepsilon - \tan\varphi)}{n_L a} P_2 \tag{4-5}$$

There are two possible collapse mechanisms for this system. The first collapse mechanism occurs when the skew braces yield. The second mechanism is reached when the longitudinal braces yield. Actually, as a special case, it is also possible for both mechanisms to occur simultaneously when all braces yield at the same time. However, as discussed later, this happens only at a certain skew angle or for a specific loading ratio.

Furthermore, since the bridge behavior is bidirectional due to both bidirectional loading and the bridge skew for each collapse mechanism, both transverse and longitudinal responses are investigated separately.

4.2.2 Behavior when Skew Braces Yield

Yielding in the skew braces occur when the absolute value of axial forces for braces in the skew direction is greater than for braces in the longitudinal direction. As seen from the above formulas, axial forces produced in a brace vary depending on the system geometric dimensions.

To determine which collapse mechanism governs and assess behavior, knowledge of the value given by the ratio between the axial forces can be helpful. This ratio is calculated as

$$\frac{C_T}{C_L} = \frac{T_T}{T_L} = \frac{n_L s_T a}{n_T s_L s(\varepsilon \cos\varphi - \sin\varphi)} \tag{4-6}$$

The possible limits of this ratio and the corresponding meaning are further described below:

If	$\frac{C_T}{C_L} = \frac{T_T}{T_L} > 1$	then	transverse braces yield first
If	$\frac{C_T}{C_L} = \frac{T_T}{T_L} < 1$	then	longitudinal braces yield first
If	$\frac{C_T}{C_L} = \frac{T_T}{T_L} = 1$	then	all braces yield at the same time

Note that the sign of the denominator of Eq. (4-6) can be negative or positive, depending on skew angle and the ratio of seismic lateral loads. Also, the variation of this ratio with respect to the skew angle can be characterized for a selected bridge geometry (for example, for predetermined d/s and d/a ratios). This is further discussed in Section 4.2.4.

Response in the Transverse Direction

Figure 4-2 shows the typical hysteretic curve of the system in the transverse direction. Base shear component in the transverse direction (V_{yT}) can be calculated by substituting $\pm P_y$ (the axial yield strength of unbonded braces) for C_T and T_T (axial forces in the yielding braces), and using equilibrium in the transverse direction:

$$V_{yT} = 2n_T P_y \frac{s}{s_T} \cos\varphi \tag{4-7a}$$

or substituting $P_y = F_y A$

$$V_{yT} = \frac{2n_T s \cos\varphi}{s_T}(F_y A) \tag{4-7b}$$

where F_y and A are the yield stress and cross sectional area of each brace. Note that only the skew braces contribute to base shear strength in the transverse direction.

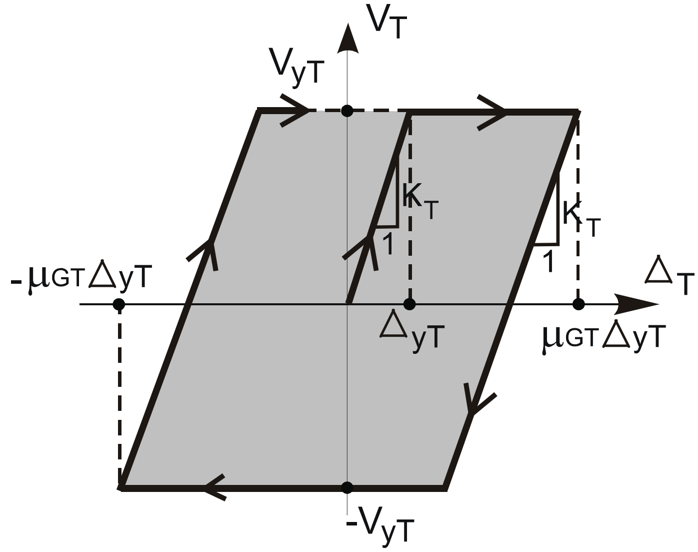

FIGURE 4-2 Transverse Base Shear versus Displacement Hysteretic Curve for Retrofit Scheme-1

Lateral displacements of the system at yield (i.e. the yield displacement) can be determined using the method of virtual work. This procedure requires the application of external virtual unit loads to each of the four deck corners in the transverse direction of the system. For this unit loading, axial forces in the braces are then found, and the desired displacement is obtained. Knowing the yield displacement also allows to evaluate the initial stiffness as well as the fundamental period for response in both orthogonal directions.

To evaluate the impact of member ductility on the overall system ductility, the displacement ductility μ can also be incorporated into the formulation. Eq. (4-8a) gives the displacement in the transverse direction.

$$\Delta_T = \frac{n_T s_T^3 a^2 \mu - n_L s_L^3 s^2 \sin\varphi(\varepsilon\cos\varphi - \sin\varphi)}{2 s_T a^2 s \cos\varphi}\left(\frac{F_y}{E}\right) \tag{4-8a}$$

and substituting μ=1 yields the transverse displacement at yielding of the skew braces as follows:

$$\Delta_{yT} = \frac{n_T s_T^3 a^2 - n_L s_L^3 s^2 \sin\varphi(\varepsilon\cos\varphi - \sin\varphi)}{2 s_T a^2 s \cos\varphi}\left(\frac{F_y}{E}\right) \tag{4-8b}$$

These equations account for the contributions of both the yielding and elastic (i.e. not yielding) braces. The ratio of maximum displacement to the yield displacement in the transverse direction (i.e. the system global ductility, μ_{GT}) can be obtained by the ratio of the displacements that correspond to μ=μ and μ=1. Hence,

$$\mu_{GT} = \frac{n_T s_T^3 a^2 \mu - n_L s_L^3 s^2 \sin\varphi(\varepsilon\cos\varphi - \sin\varphi)}{n_T s_T^3 a^2 - n_L s_L^3 s^2 \sin\varphi(\varepsilon\cos\varphi - \sin\varphi)} \tag{4-9}$$

Dividing Eq. (4-7b) by Eq. (4-8b) gives the initial stiffness (K_T) of the system in the transverse direction. This yields:

$$K_T = \frac{4 n_T a^2 s^2 \cos\varphi}{n_T s_T^3 a^2 - n_L s_L^3 s^2 \sin\varphi(\varepsilon\cos\varphi - \sin\varphi)}(EA) \tag{4-10}$$

which enables to evaluate the initial stiffness in terms of axial stiffness (EA) of the unbonded brace.

Hysteretic energy dissipation (E_H) during a complete cycle is given by the shaded area in Figure 4-2, or equivalently, the same hysteresis can be calculated from the sum of the hysteretic energy for all individual members. Performing this calculation gives:

$$E_H = 4(\mu_{GT} - 1)V_{yT}\Delta_{yT} = 8n_T(\mu - 1)s_T A\left(\frac{F_y^2}{E}\right) \tag{4-11}$$

The corresponding hysteretic energy per total brace volume (Vol.) is:

$$\frac{E_H}{Vol.} = \frac{4(\mu - 1)n_T s_T}{n_T s_T + n_L s_L}\left(\frac{F_y^2}{E}\right) \tag{4-12}$$

This equation could also be rewritten in terms of containing the global system ductility, μ_{GT}. However, to keep the formulas simple, throughout this report, hysteretic energy is formulated in terms of the member ductility, μ.

Response in the Longitudinal Direction

In a similar manner, base shear, yield displacement, and initial stiffness can be calculated for response in the longitudinal direction.

Again, from the equations of equilibrium, the longitudinal component of base shear (V_{yL}) when the skew braces yield is equal to the following:

$$V_{yL} = \frac{2s\left[n_T \sin\varphi + n_L(\varepsilon\cos\varphi - \sin\varphi)\right]}{s_T}(F_y A) \tag{4-13}$$

To evaluate the longitudinal displacement, external unit virtual loads are applied to the truss joints in the longitudinal direction. The longitudinal displacement at yielding of skew braces can then be expressed as

$$\Delta_L = \frac{n_L s_L^3 s(\varepsilon\cos\varphi - \sin\varphi)}{2s_T a^2}\left(\frac{F_y}{E}\right) \tag{4-14}$$

Note that Eq. (4-14) does not include the member ductility term, revealing that there is no energy dissipation in the longitudinal direction braces. Therefore, during reversed cyclic loading, only elastic recovery takes place, and after yielding, displacement in the longitudinal direction remains unchanged while the displacement in the other direction increases.

Initial stiffness in the longitudinal direction can be obtained using Eq. (4-13) and (4-14). After simplifications, the following formula for the initial stiffness is reached:

$$K_L = \frac{4a^2\left[n_T \sin\varphi + n_L(\varepsilon\cos\varphi - \sin\varphi)\right]}{n_L s_L^3(\varepsilon\cos\varphi - \sin\varphi)}(EA) \qquad (4\text{-}15)$$

4.2.3 Behavior when Longitudinal Braces Yield

Depending on the axial force ratios of the braces defined by Eq. (4-6) when the ratio is lesser than 1.0, the longitudinal braces yield first. In this case, new formulas are needed to characterize the system inelastic behavior. Setting tension (T_L) and compression forces (C_L) of the longitudinal braces equal to P_y and $-P_y$ respectively, axial forces in the transverse braces are:

$$C_T = -T_T = \frac{s_T a}{s_L s(\varepsilon\cos\varphi - \sin\varphi)}P_y \qquad (4\text{-}16)$$

As done in the previous section, and for the same reasons, two potential collapse mechanisms are separately investigated here, namely, response in the transverse and longitudinal directions.

Response in the Transverse Direction

Yielding braces do not contribute to base shear strength in the transverse direction, since they are in the other orthogonal direction. Therefore, only unyielding braces should be considered for the transverse base shear strength. Using this fact leads to the equation below:

$$V_{yT} = \frac{2n_T a\cos\varphi}{s_L(\varepsilon\cos\varphi - \sin\varphi)}(F_y A) \qquad (4\text{-}17)$$

The transverse displacement can be calculated as before, using the method of virtual work. The resulting equation is

$$\Delta_T = \frac{-n_L s_L^3 s^2 \sin\varphi(\varepsilon\cos\varphi - \sin\varphi)\mu + n_T s_T^3 a^2}{2as_L s^2 \cos\varphi(\varepsilon\cos\varphi - \sin\varphi)}\left(\frac{F_y}{E}\right) \tag{4-18a}$$

Again, the yield displacement is found by substituting $\mu=1$ in Eq. (4-18a).

$$\Delta_{yT} = \frac{-n_L s_L^3 s^2 \sin\varphi(\varepsilon\cos\varphi - \sin\varphi) + n_T s_T^3 a^2}{2as_L s^2 \cos\varphi(\varepsilon\cos\varphi - \sin\varphi)}\left(\frac{F_y}{E}\right) \tag{4-18b}$$

Base shear strength given in Eq. (4-17) and the yield displacement given in Eq. (4-18b) are sufficient to obtain the hysteretic curve of the system, shown in Figure 4-2.

Following the same procedure as before, the global system ductility, μ_{GT}, can be calculated by the ratio of the maximum displacement (displacement that correspond to $\mu=\mu$) and yield displacement (at $\mu=1$). This gives:

$$\mu_{GT} = \frac{-n_L s_L^3 s^2 \sin\varphi(\varepsilon\cos\varphi - \sin\varphi)\mu + n_T s_T^3 a^2}{-n_L s_L^3 s^2 \sin\varphi(\varepsilon\cos\varphi - \sin\varphi) + n_T s_T^3 a^2} \tag{4-19}$$

The initial stiffness is given by $V_{yT}/\Delta_{yT}(\mu=1)$, which results in:

$$K_T = \frac{4n_T a^2 s^2 \cos^2\varphi}{-n_L s_L^3 s^2 \sin\varphi(\varepsilon\cos\varphi - \sin\varphi) + n_T s_T^3 a^2}(EA) \tag{4-20}$$

The hysteretic energy dissipation during a single full cycle can be written as:

$$E_H == 4(\mu_{GL} - 1)V_{yL}\Delta_{yL} = 8n_L(\mu - 1)s_L A\left(\frac{F_y^2}{E}\right) \tag{4-21}$$

and the corresponding hysteretic energy per total brace volume (Vol.) is:

$$\frac{E_H}{Vol.} = \frac{4(\mu - 1)n_L s_L}{n_T s_T + n_L s_L}\left(\frac{F_y^2}{E}\right) \tag{4-22}$$

Response in the Longitudinal Direction

Base shear in the longitudinal direction can be expressed as

$$V_{yL} = \frac{2a\left[n_L(\varepsilon\cos\varphi - \sin\varphi) + n_T\sin\varphi\right]}{s_L(\varepsilon\cos\varphi - \sin\varphi)}(F_y A) \tag{4-23}$$

Eq. (4-24) gives the longitudinal displacement in terms of member ductility and system geometric properties:

$$\Delta_L = \frac{n_L s_L^2 \mu}{2a}\left(\frac{F_y}{E}\right) \tag{4-24a}$$

and the displacement at brace yielding takes the following form:

$$\Delta_{yL} = \frac{n_L s_L^2}{2a}\left(\frac{F_y}{E}\right) \tag{4-24b}$$

Skew braces do not contribute to the displacement in the longitudinal direction. Figure 4-3 illustrates the hysteretic behavior in the longitudinal direction.

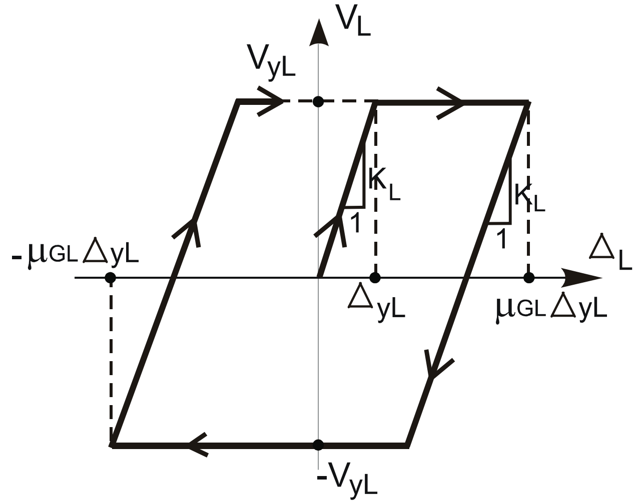

FIGURE 4-3 Longitudinal Base Shear versus Displacement Hysteretic Curve for Retrofit Scheme-1

By dividing Eq. (4-24a) by Eq. (4-24b), the global displacement ductility is obtained for this case, and is equal to the member ductility, as given below.

$$\mu_{GL} = \frac{\Delta_L}{\Delta_{yL}} = \mu \tag{4-25}$$

Dividing Eq. (4-23) by Eq. (4-24b) gives the initial stiffness of the system in the longitudinal direction:

$$K_L = \frac{4a^2\left[n_L(\varepsilon\cos\varphi - \sin\varphi) + n_T \sin\varphi\right]}{n_L s_L^3 (\varepsilon\cos\varphi - \sin\varphi)}(EA) \tag{4-26}$$

4.2.4 Special Cases

Although the general equations derived above are complex, due to the large number of geometric parameters they take into account, they take simpler forms in special cases. For example, assuming that the number of braces in the transverse and longitudinal directions is equal (i.e. n_T=n_L), a few of these special cases are presented below. Also, to illustrate the implications from above formulas, diagrams are also developed using some typical practical numerical values for bridges.

4.2.4.1 Special Case 1- Non-Skewed Bridges ($\varphi=0^o$)

For non-skewed bridges, the following formulas are obtained by substituting $\varphi=0^o$ in the relevant equations.

From Eqs. (4-4) and (4-5), and substituting the brace lengths in terms of the end diaphragm geometric relations as per Eqs. (4-1a) and (4-1b), brace axial forces become:

$$T_T = -C_T = \frac{\sqrt{1+(d/s)^2}}{n_T} P_2 \tag{4-27}$$

$$T_L = -C_L = \frac{\varepsilon\sqrt{1+(d/a)^2}}{n_L} P_2 \tag{4-28}$$

Since it is assumed that $n_T=n_L$, using Eq. (4-6) for the ratio of brace axial forces simplifies to:

$$\frac{C_T}{C_L} = \frac{T_T}{T_L} = \frac{1}{\varepsilon}\sqrt{\frac{1+(d/s)^2}{1+(d/a)^2}} \tag{4-29}$$

Variation of brace axial forces ratio with respect to end diaphragm geometric relations are given in Figure 4-4. Since many bridge standards and regulations basically rely on two simplified combination rules to account for bidirectional earthquake effects in seismic design, the 30% rule as per AASHTO (1996) and the 40% rule as per ATC-32 (1996) are selected in this Figure to show the impact of this value on the brace forces ratio.

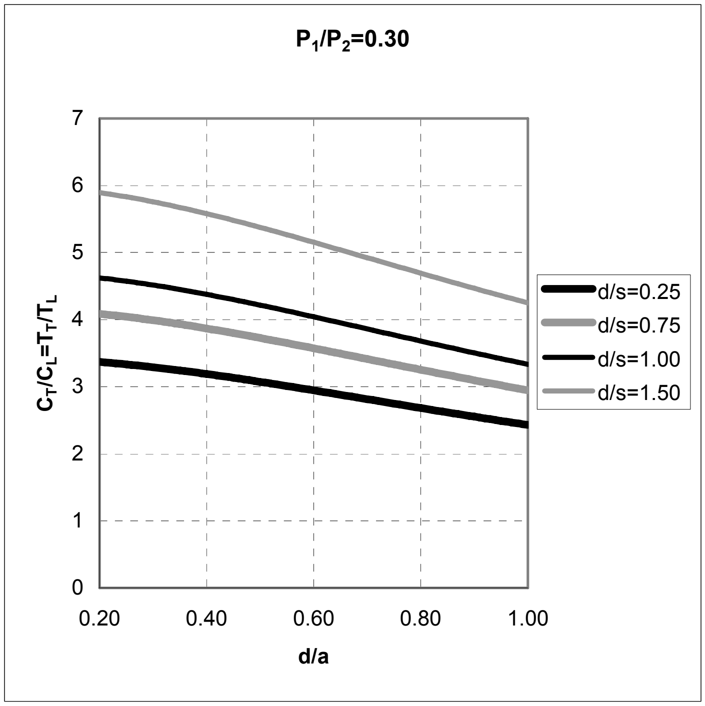

(a)

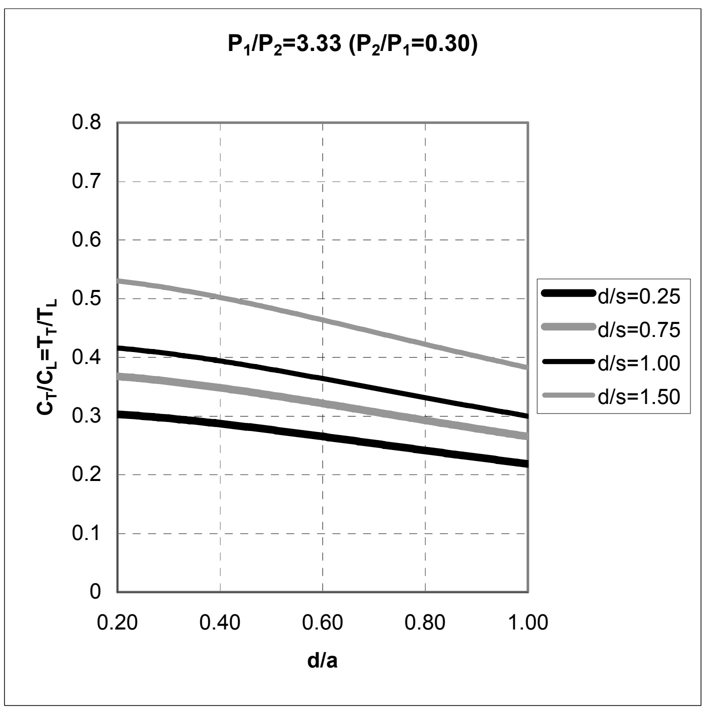

(b)

FIGURE 4-4 Variation of Brace Axial Forces Ratio with Bridge Geometric Relations: (a) For P_1/P_2=0.30; (b) For P_1/P_2=3.33

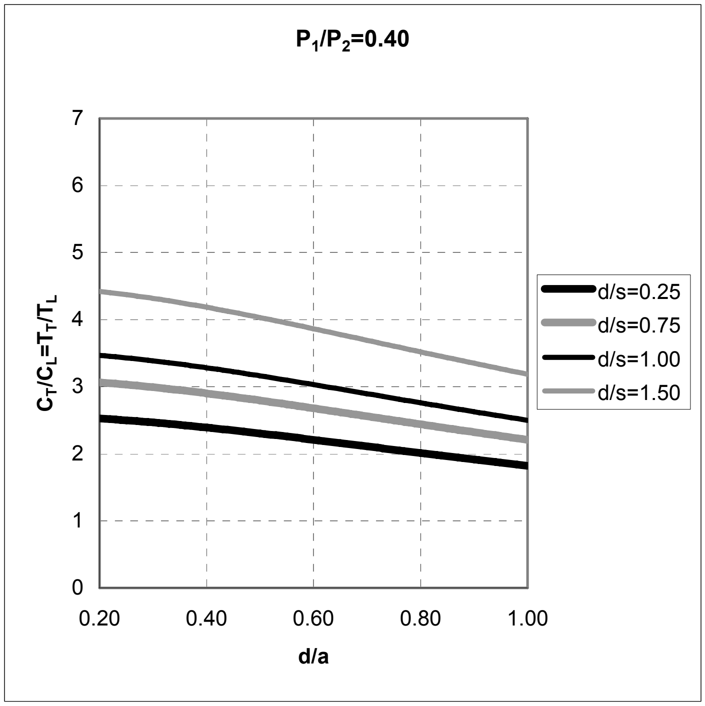

(c)

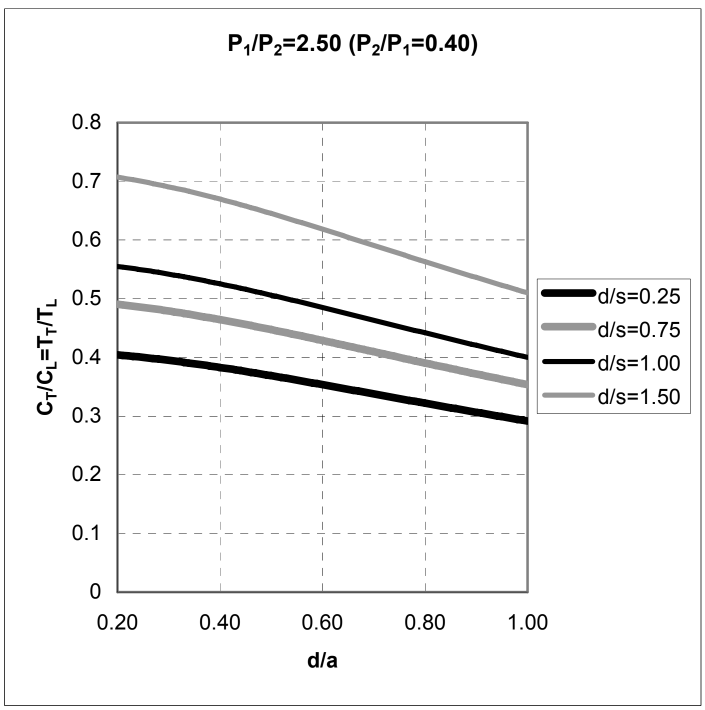

(d)

FIGURE 4-4 Variation of Brace Axial Forces Ratio with Bridge Geometric Relations (continued): (c) For P_1/P_2=0.40; (d) For P_1/P_2=2.50

4.2.4.1.1 Transverse Braces Yield

4.2.4.1.1.1 Transverse Response

When $C_T,T_T > C_L,T_L$, the transverse braces yield only, and base shear strength (V_{yT}), yield displacement (Δ_{yT}) and corresponding drift (Δ_{yT}/d) at yield, global ductility (μ_{GT}), and the stiffness of the system (K_T) in the transverse direction are obtained using Eqs. (4-7b), (4-8b), (4-9), and (4-10) respectively, as follows:

$$V_{yT} = \frac{2n_T}{\sqrt{1+(d/s)^2}}(F_y A) \tag{4-30}$$

$$\Delta_{yT} = \frac{n_T(s^2+d^2)}{2s}\left(\frac{F_y}{E}\right) \tag{4-31a}$$

$$\frac{\Delta_{yT}}{d} = \frac{1+(d/s)^2}{2(d/s)}\left(\frac{n_T F_y}{E}\right) \tag{4-31b}$$

$$\mu_{GT} = \mu \tag{4-32}$$

$$K_T = \frac{4s^2}{(s^2+d^2)^{3/2}}(EA) \tag{4-33a}$$

$$K_T = \frac{4(d/s)}{\left[1+(d/s)^2\right]^{3/2}}\left(\frac{EA}{d}\right) \tag{4-33b}$$

Nondimensional expressions have also been generated to generalize these equations, yet, for a single specific value of the yield strength, F_y. Recent investigations and implementations in buildings on unbonded braces suggest that unbonded steel core material grade ranging from low yield strength (235 MPa) up to high yield strength 415 MPa (60 ksi) could be used successfully. For bridge retrofit design purposes, a 345MPa (50 ksi) grade steel with E=200000 MPa (29000 ksi) is assumed for the results presented in Figures 4-6 and 4-9a to 4-9d.

Figure 4-5 shows nondimensional transverse base shear strength (V_{yT}) versus d/s curves resulting from Eq. (4-30). The base shear strength is observed to decrease as the d/s ratio increases. Transverse drift (Δ_{yT}/d) at yield versus the d/s ratio is illustrated in Figure 4-6 per Eq. (4-31b). Note that transverse drift takes its minimum value at d/s=1 (incidentally, this is independent of the material yield strength used). Also, the reduction in drift is relatively less after d/s=0.5.

Similarly, the variation of nondimensional transverse stiffness (K_T) with the d/s ratio is given in Figure 4-7. It is observed from that figure that the nondimensional transverse stiffness is maximum at d/s=0.707. From Figures 4-6 and 4-7, for this retrofit scheme, it seems that an optimal value for d/s value should be selected between 0.5 and 1.0 if the intent is to limit transverse displacements.

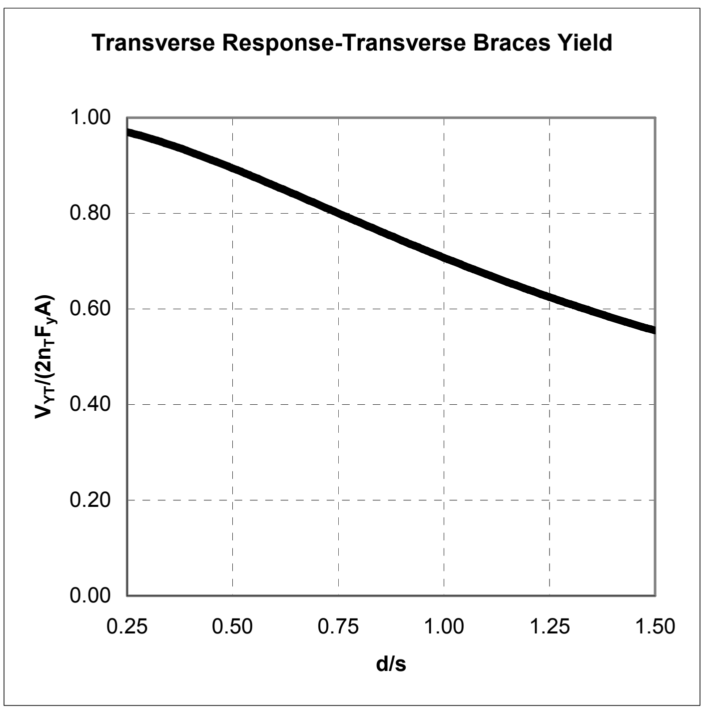

FIGURE 4-5 Nondimensional Transverse Base Shear Strength versus d/s Ratio When Transverse Braces Yield

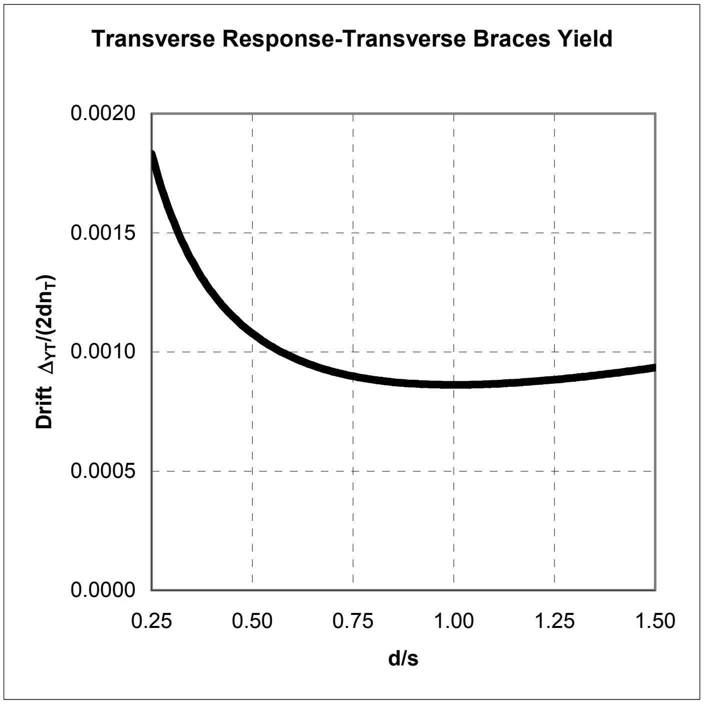

FIGURE 4-6 Transverse Drift versus d/s Ratio When Transverse Braces Yield

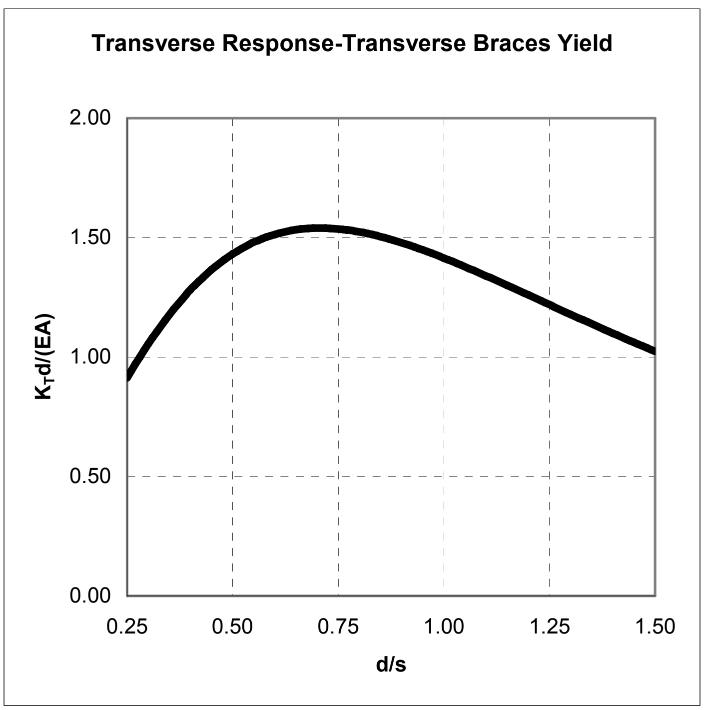

FIGURE 4-7 Nondimensional Transverse Stiffness versus d/s Ratio When Transverse Braces Yield

4.2.4.1.1.2 Longitudinal Response

Since the behavior is bidirectional, the response in the longitudinal direction is also investigated. Since yielding only occurs longitudinally and φ=0° (no skew) for this Retrofit Scheme-1, members in the longitudinal direction remain elastic. Using Eqs. (4-13), (4-14), and (4-15), it is also possible to obtain simplified equations for the elastic behavior in the longitudinal direction.

$$V_L = \frac{2n_L\varepsilon}{\sqrt{1+(d/s)^2}}(F_yA) \tag{4-34}$$

The longitudinal displacement when transverse braces yield is:

$$\Delta_L = \frac{n_L s\varepsilon(a^2+d^2)^{3/2}}{2a^2\sqrt{s^2+d^2}}\left(\frac{F_y}{E}\right) \tag{4-35a}$$

and the corresponding drift is:

$$\frac{\Delta_{yL}}{d} = \frac{\varepsilon\left[1+(d/a)^2\right]^{3/2}}{2(d/a)\sqrt{1+(d/s)^2}}\left(\frac{n_LF_y}{E}\right) \tag{4-35b}$$

The longitudinal stiffness is:

$$K_L = \frac{4a^2}{(a^2+d^2)^{3/2}}(EA) \tag{4-36a}$$

and in terms of nondimensional geometric ratios, the following is found:

$$K_L = \frac{4(d/a)}{\left[1+(d/a)^2\right]^{3/2}}\left(\frac{EA}{d}\right) \tag{4-36b}$$

Figures 4-8 to 4-10 are obtained for the longitudinal response characteristics of the system.

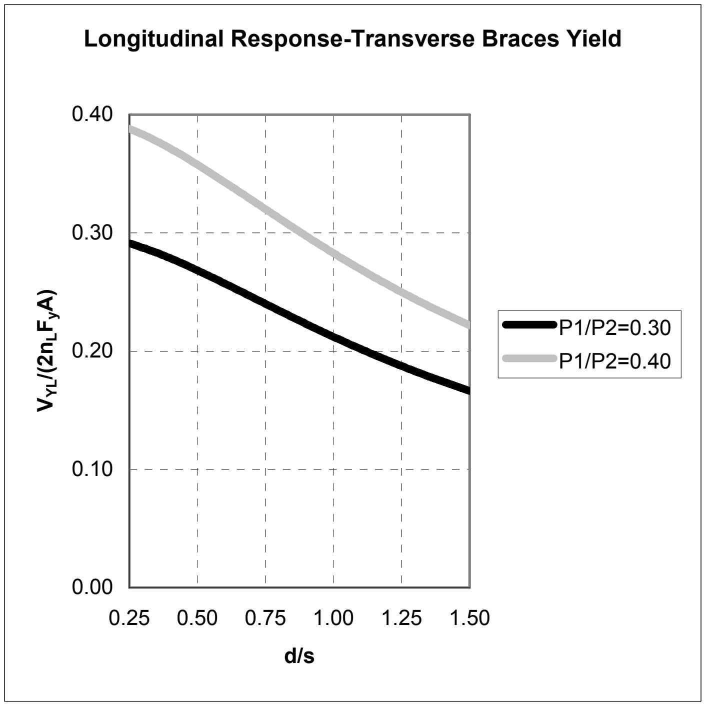

(a)

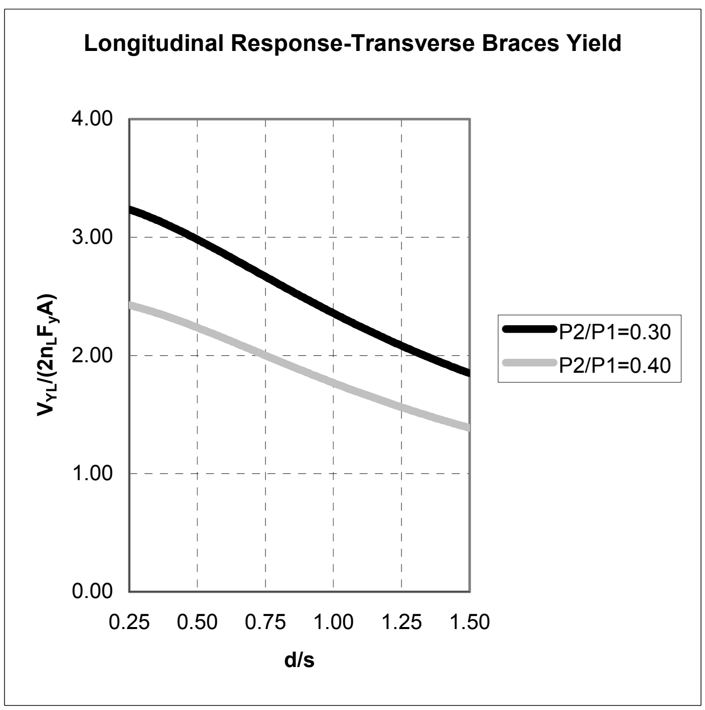

(b)

FIGURE 4-8 Nondimensional Longitudinal Base Shear versus d/s Ratio When Transverse Braces Yield: (a) For P_1/P_2=0.30 and 0.40; (b) For P_2/P_1=0.30 and 0.40

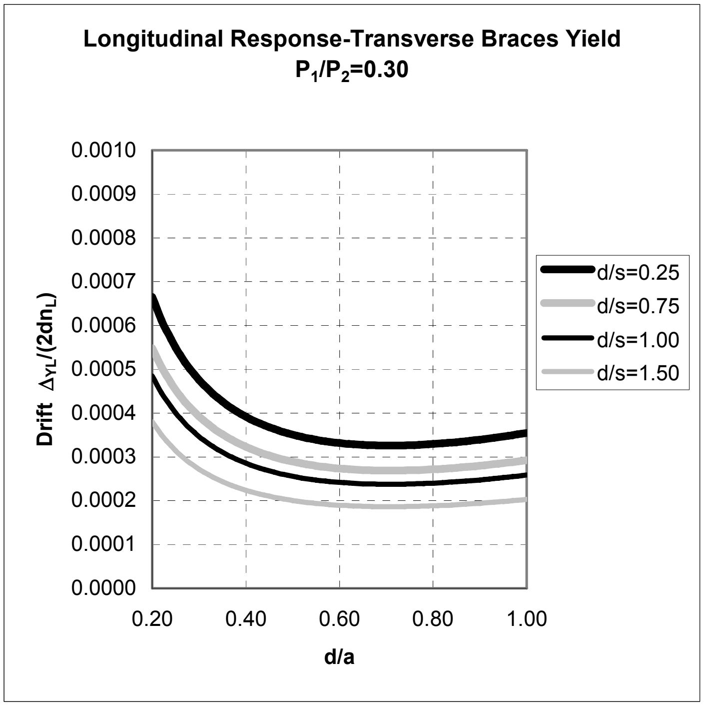

(a)

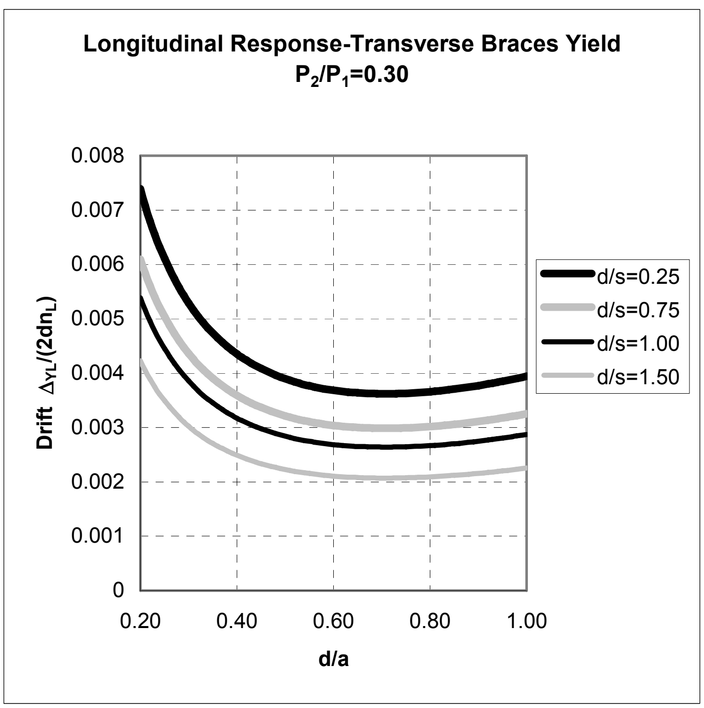

(b)

FIGURE 4-9 Longitudinal Drift versus d/a Ratio When Transverse Braces Yield: (a) For P_1/P_2=0.30; (b) For P_2/P_1=0.30

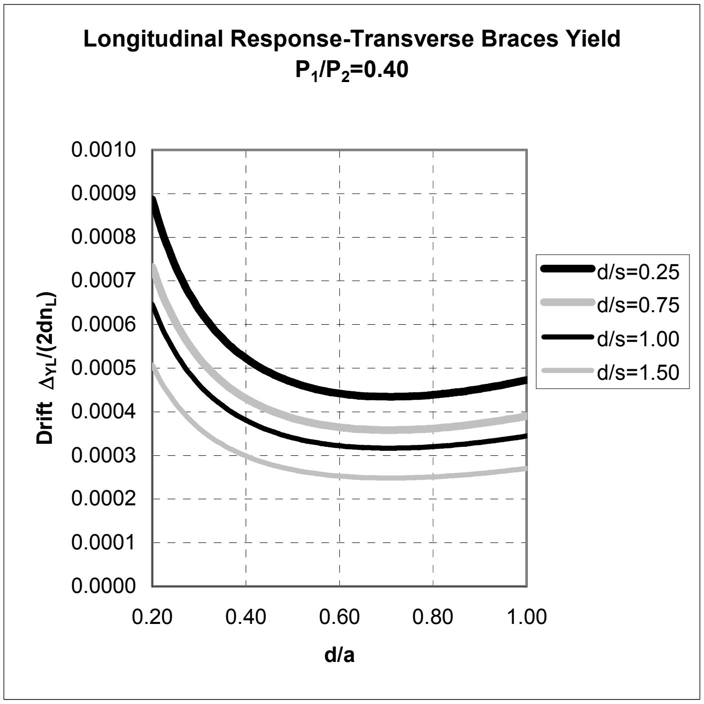

(c)

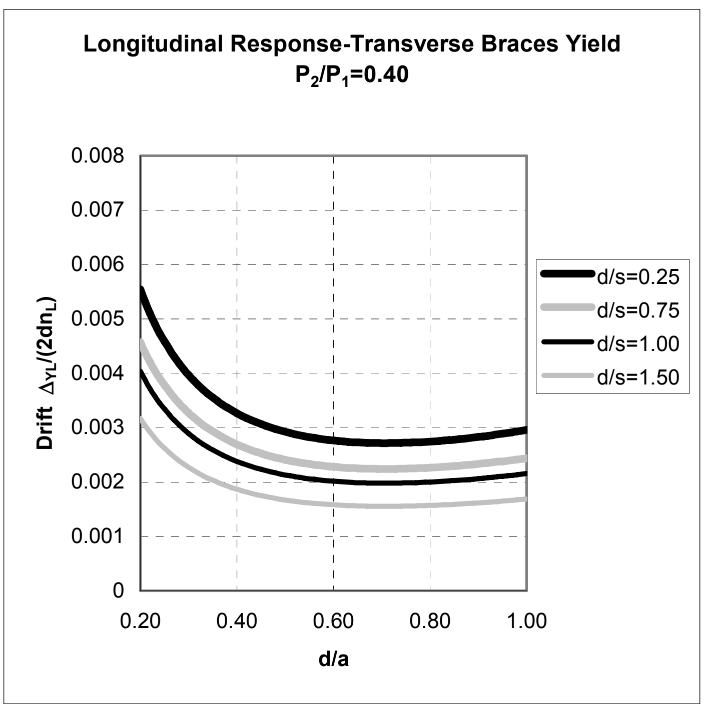

(d)

FIGURE 4-9 Longitudinal Drift versus d/a Ratio When Transverse Braces Yield (continued): (c) For P_1/P_2=0.40; (d) For P_2/P_1=0.40

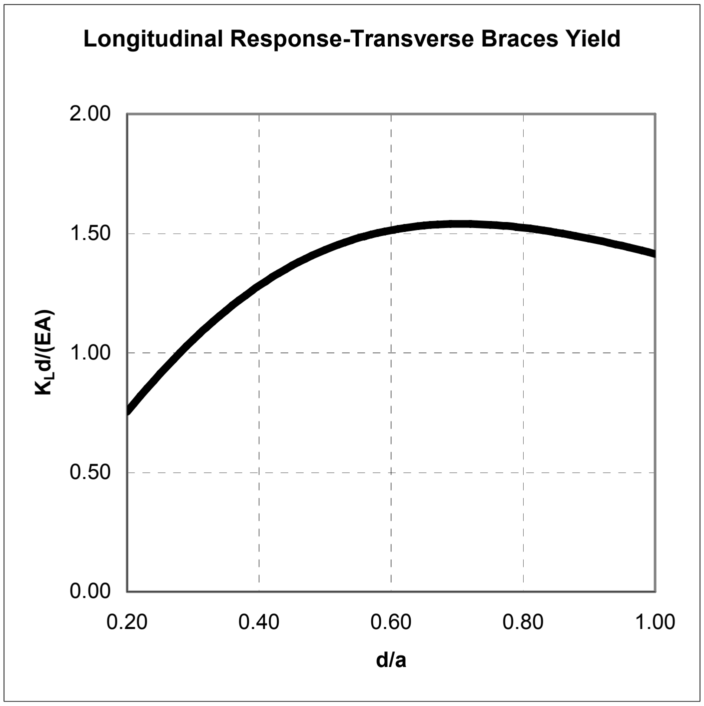

FIGURE 4-10 Nondimensional Longitudinal Stiffness versus d/a Ratio When Transverse Braces Yield

Nondimensional base shear and drift also dependen on the previously defined bidirectional load ratio (P_1/P_2 or P_2/P_1). Consistently to what has been done before, two code defined values of P_1/P_2 (or P_2/P_1) are assumed here, namely 0.30 and 0.40, to explore the impact of combination rules on the system behavior. Figure 4-8 shows the variation of nondimensional base shear in the longitudinal direction as a function of end diaphragm geometric ratios when transverse braces yield. There is a decrease in this value as the d/s ratio increases.

The variation of longitudinal drift as a function of end diaphragm geometric ratios and the P_1/P_2 (or P_2/P_1) values are shown in Figures 4-9a through 4-9d. For a constant d/s, these curves reveals that longitudinal drift becomes minimum at d/a=0.707. However, as seen on the same figures, the variation in drift after d/a=0.5 is relatively insignificant, which suggests that optimal d/a ratios can be selected between 0.5 and 1.0, if the intent is to minimize drfit. Again, Figure 4-10 shows that maximum nondimensional longitudinal stiffness is reached at d/a=0.707.

Generally, the total hysteretic energy dissipated in one cycle is the sum of the areas under the global hysteretic curves in both directions (i.e. summation of the areas under Figures 4-2 and 4-3), or simply equal to the energy dissipated by the yielding braces. Both are equivalent (per the conservation of energy principle), but the former gives the energy dissipation in terms of global ductility reached, while the latter gives results in terms of the member ductility, which seems more convenient to obtain simpler formulas. From Eq. (4-12), the following expression gives the volumetric energy dissipation for the system considered:

$$\frac{E_H}{\text{Vol.}} = \frac{4(\mu - 1)}{1 + \sqrt{\dfrac{a^2 + d^2}{s^2 + d^2}}} \left(\frac{F_y^2}{E} \right) \tag{4-37a}$$

$$\frac{E_H}{\text{Vol.}} = \frac{4(\mu - 1)}{1 + \dfrac{(d/s)}{(d/a)} \sqrt{\dfrac{1 + (d/a)^2}{1 + (d/s)^2}}} \left(\frac{F_y^2}{E} \right) \tag{4-37b}$$

Note that recent experimental investigations on unbonded braces suggest that these braces can exhibit stable and ductile hysteretic behavior up to member axial displacement ductilities of 20 or more. To investigate the possible hysteretic energy dissipation in bridge end diaphragms using unbonded braces, member ductility ratio is also considered as a parameter here, and the variation of hysteretic energy dissipation per brace volume is plotted against different values of μ between 5 through 20. Figures 4-11a through 4-11d illustrate that nondimensional dissipated hysteretic energy increases as d/a increases for constant values of d/s, but decreases as d/s increases for constant values of d/a. However, as observed on the relavent diagrams, the decrease in energy dissipation is relatively less for larger values of d/s. Apparently, there is no an optimum hysteretic energy dissipation within the assumed geometric range in this special case. Hysteretic energy increases (logically) as member ductility increases. Note that since longitudinal response is elastic, all hysteretic energy is dissipated by the transverse braces. In other words, displacement in the longitudinal direction remains unchanged upon yielding of the transverse braces. During cyclic loading, only elastic loading/unloading develops in the longitudinal braces.

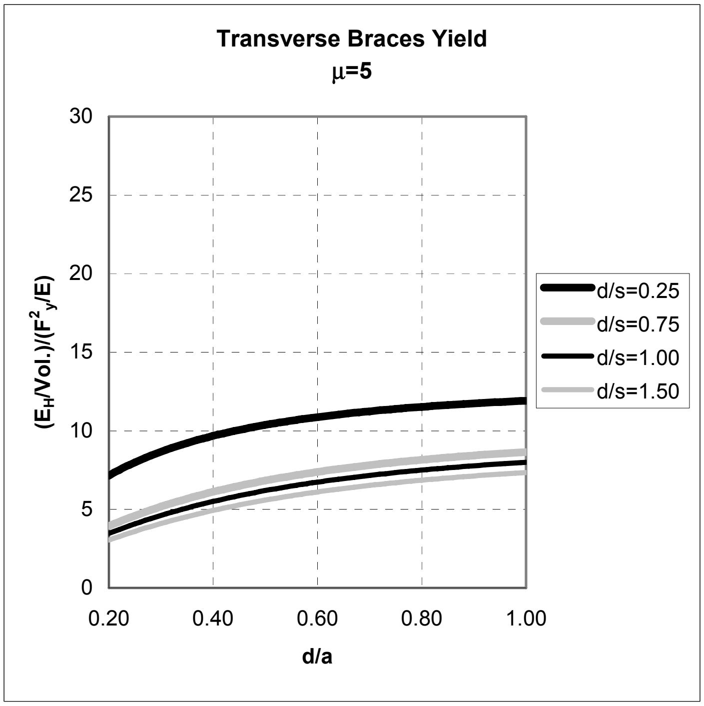

(a)

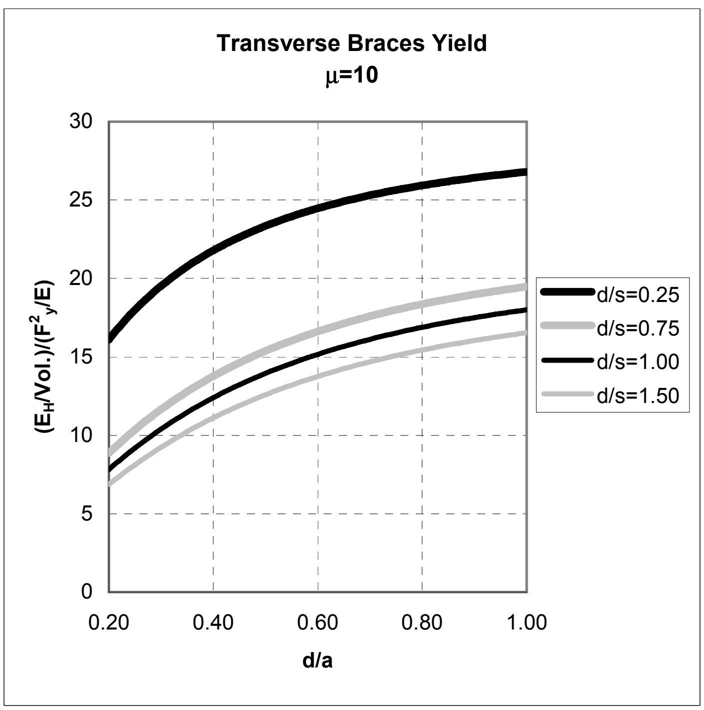

(b)

FIGURE 4-11 Volumetric Energy Dissipation versus End Diaphragm Geometric Ratios When Transverse Braces Yield: (a) For μ=5; (b) For μ=10

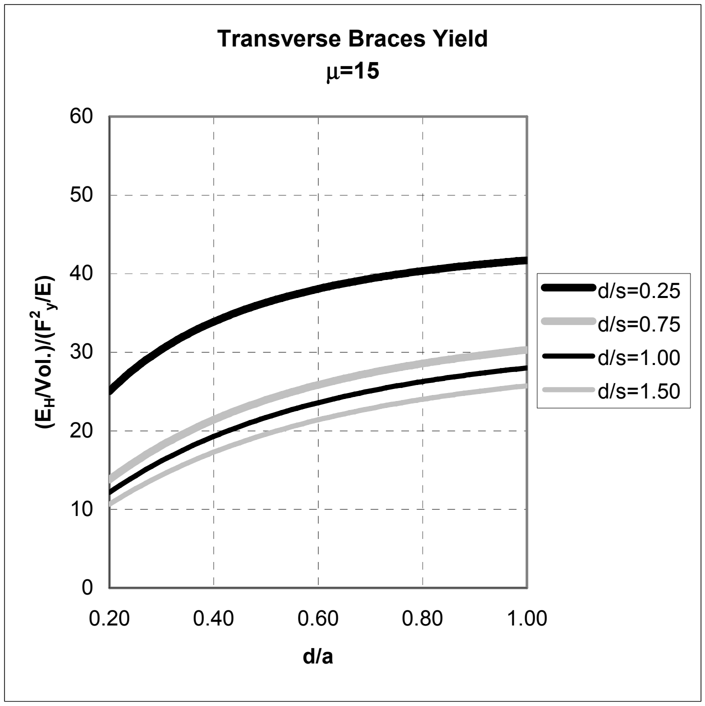

(c)

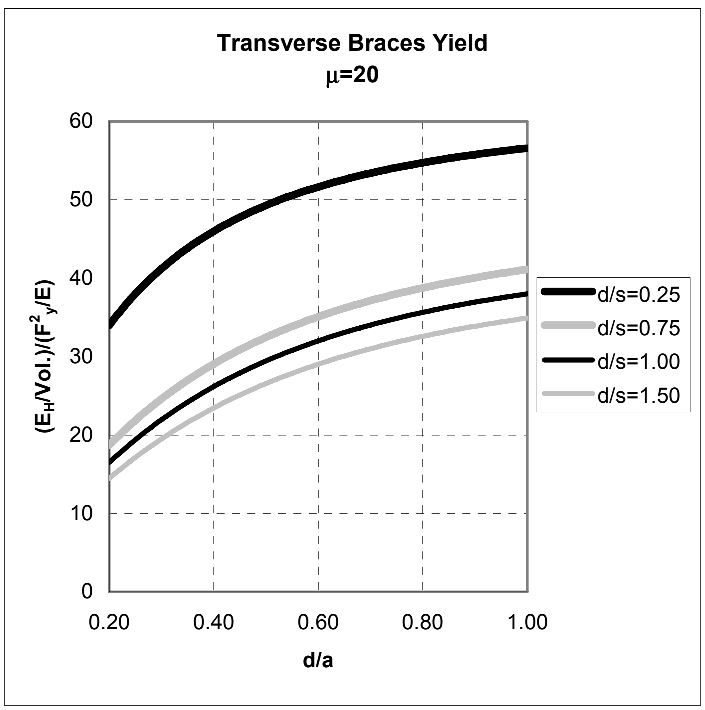

(d)

FIGURE 4-11 Volumetric Energy Dissipation versus End Diaphragm Geometric Ratios When Transverse Braces Yield (continued): (c) For μ=15; (d) For μ=20

4.2.4.1.2 Longitudinal Braces Yield

4.2.4.1.2.1 Transverse Response

When the longitudinal braces yield, using Eqs. (4-17), (4-18b), (4-19), and (4-20), base shear strength, lateral displacement, global displacement ductility, and the stiffness of the system in the transverse direction are reached as follows:

$$V_{yT} = \frac{2n_T}{\varepsilon\sqrt{1+(d/a)^2}}(F_y A) \tag{4-38}$$

$$\Delta_{yT} = \frac{n_T a(s^2+d^2)^{3/2}}{2s^2\varepsilon\sqrt{a^2+d^2}}\left(\frac{F_y}{E}\right) \tag{4-39a}$$

$$\frac{\Delta_{yT}}{dn_T} = \frac{\left[1+(d/s)^2\right]^{3/2}}{2\varepsilon(d/s)\sqrt{1+(d/a)^2}}\left(\frac{F_y}{E}\right) \tag{4-39b}$$

$$\mu_{GT} = 1 \tag{4-40}$$

$$K_T = \frac{4s^2}{(s^2+d^2)^{3/2}}(EA) \tag{4-41a}$$

$$K_T d = \frac{4(d/s)}{\left[1+(d/s)^2\right]^{3/2}}(EA) \tag{4-41b}$$

From Figures 4-12a and 4-12b, when longitudinal braces yield, nondimensional transverse base shear force is found to decrease as d/a ratio increases. To evaluate the variation of transverse drift with end diaphragm geometric ratios, similar curves are produced for grade 50 steel, as done before, and are given in Figures 4-13a through 4-13d. On these figures, there is a decrease in transverse drift as d/a ratio increases. The d/s ratio has an important impact on drift, since transverse drift varies significantly depending on d/a values. Also observed on the same figures, it is apparent that transverse drift, when P_1/P_2 is equal to 0.30 and 0.40, is comparatively larger than the drift when P_2/P_1 is equal to 0.30 and 0.40. Since Eq. (4-41b) is the same as Eq. (4-33b), the variation of transverse stiffness can be referred to Figure 4-7, keeping in mind that longitudinal braces yield.

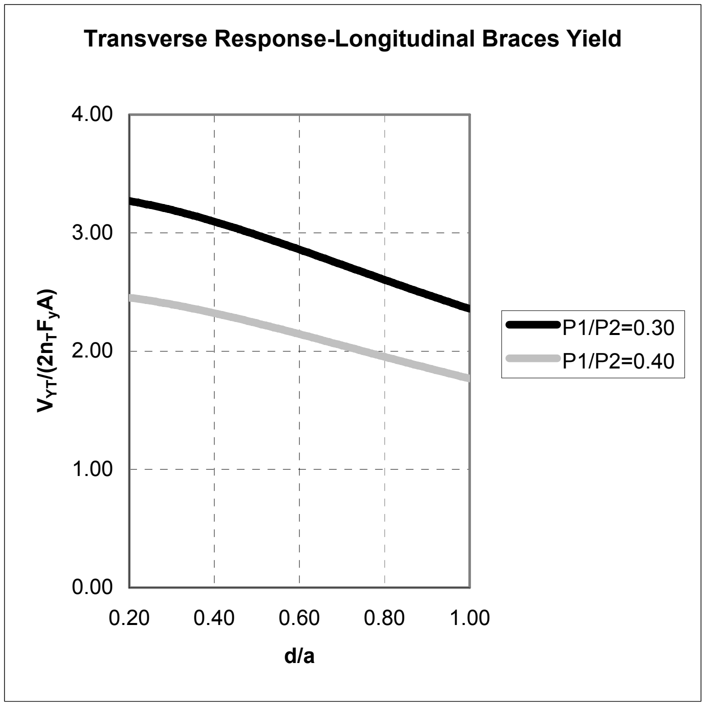

(a)

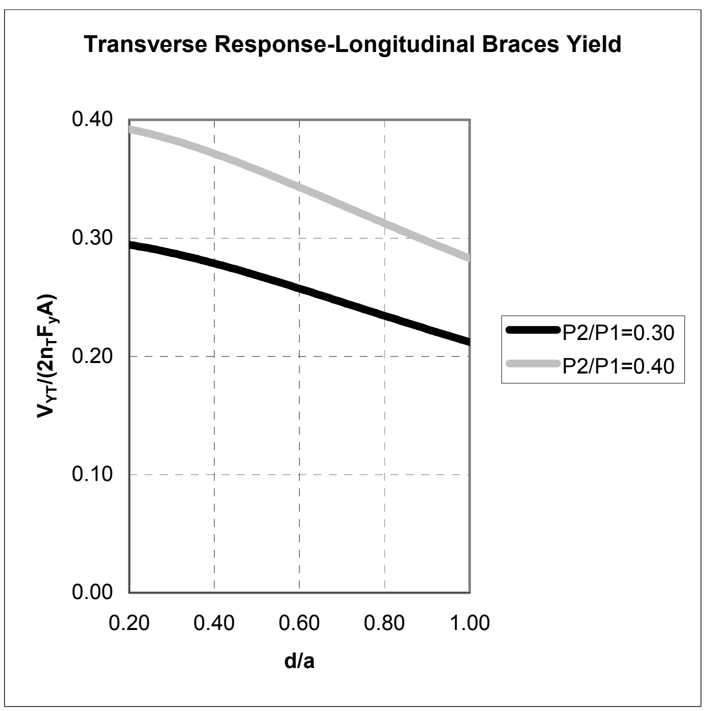

(b)

FIGURE 4-12 Nondimensional Transverse Base Shear versus d/a Ratio When Longitudinal Braces Yield: (a) For P_1/P_2=0.30 and 0.40; (b) For P_2/P_1=0.30 and 0.40

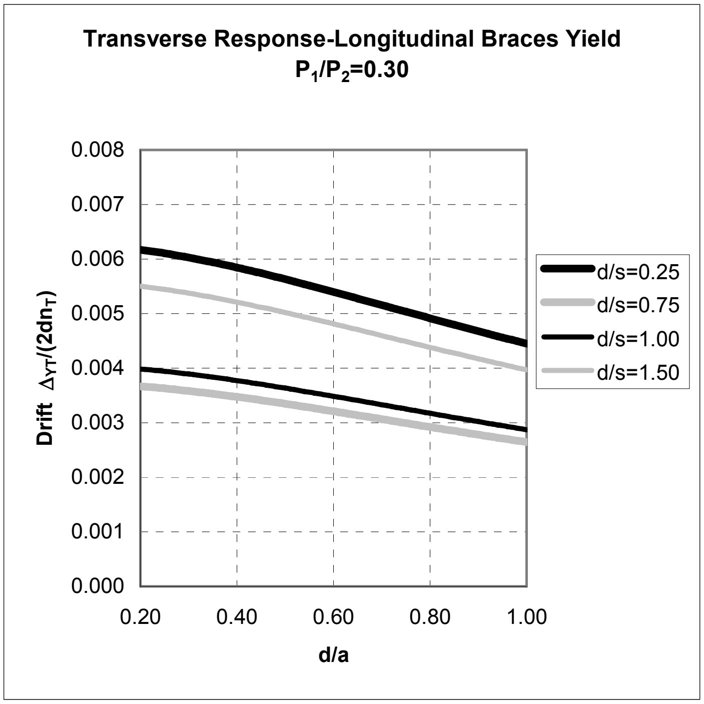

(a)

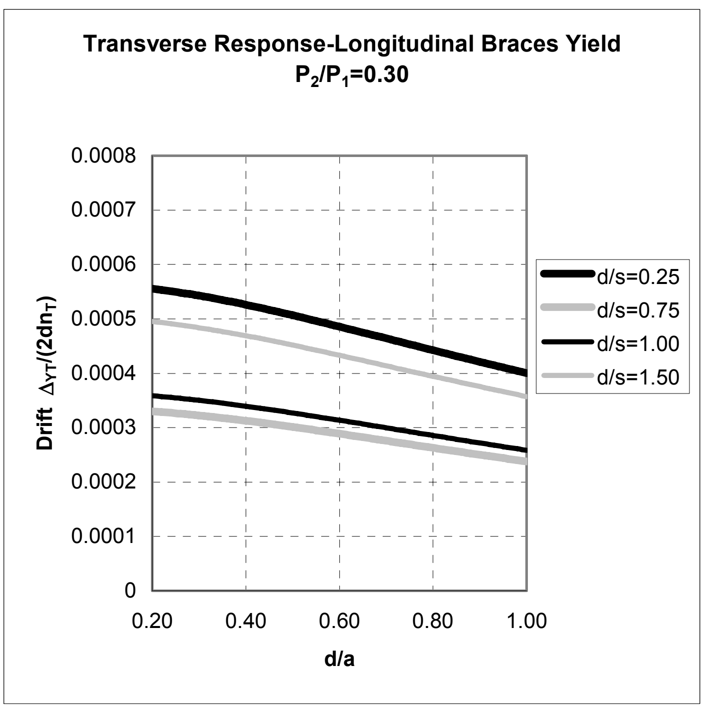

(b)

FIGURE 4-13 Transverse Drift versus d/a Ratio When Longitudinal Braces Yield: (a) For P_1/P_2=0.30; (b) For P_2/P_1=0.30

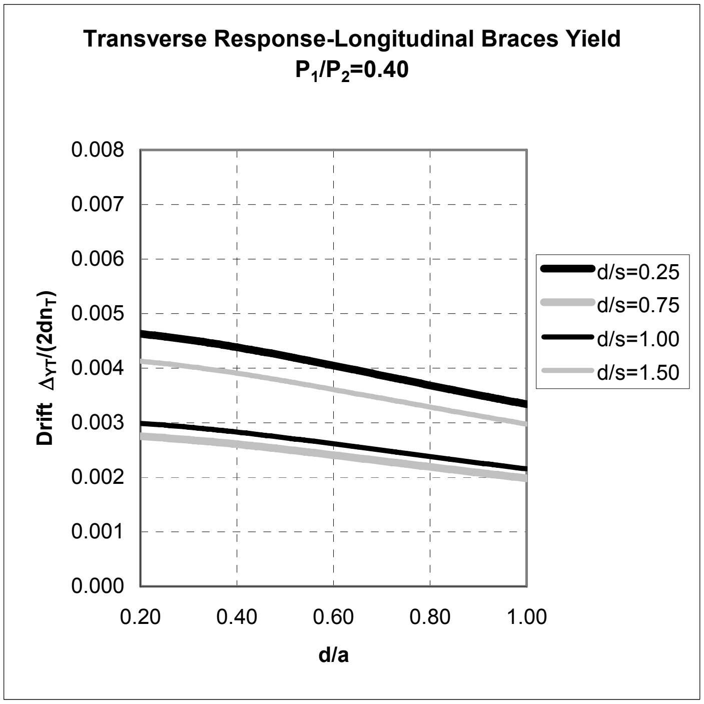

(c)

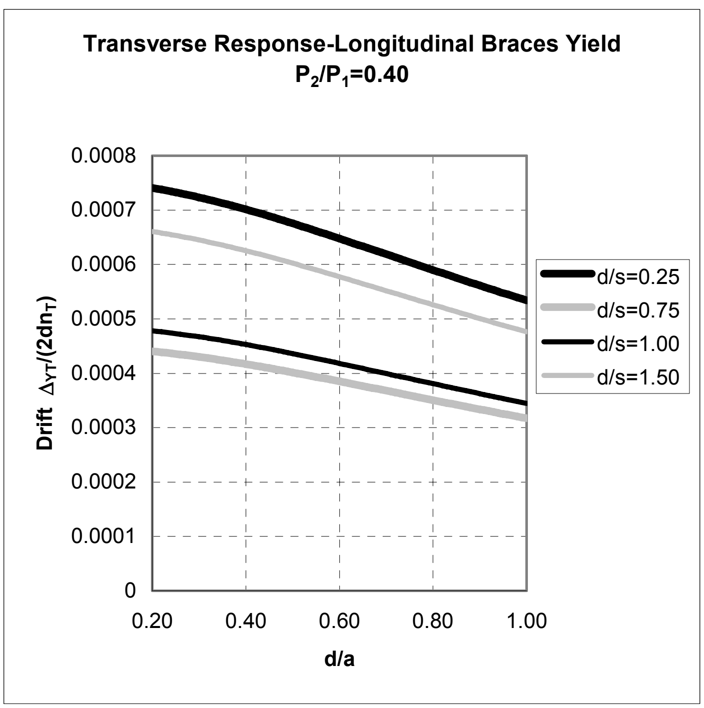

(d)

FIGURE 4-13 Transverse Drift versus d/a Ratio When Longitudinal Braces Yield (continued): (c) For P_1/P_2=0.40; (d) For P_2/P_1=0.40

4.2.4.1.2.2 Longitudinal Response

For the response in the longitudinal direction, the following relationships can be similarly developed using Eqs. (4-23), (4-24b), (4-25), and (4-26):

$$V_{yL} = \frac{2n_L}{\sqrt{1+(d/a)^2}}(F_y A) \tag{4-42}$$

$$\Delta_{yL} = \frac{n_L \mu (a^2 + d^2)}{2a}\left(\frac{F_y}{E}\right) \tag{4-43a}$$

$$\frac{\Delta_{yL}}{dn_L} = \frac{\mu\left[1+(d/a)^2\right]}{2(d/a)}\left(\frac{F_y}{E}\right) \tag{4-43b}$$

$$\mu_{GL} = \mu \tag{4-44}$$

$$K_L = \frac{4a^2}{(a^2+d^2)^{3/2}}(EA) \tag{4-45a}$$

$$K_L d = \frac{4(d/a)}{\left[1+(d/a)^2\right]^{3/2}}(EA) \tag{4-45b}$$

Figure 4-14 shows nondimensional longitudinal base shear strength versus d/a ratio. A decrease in the base shear is observed with increasing d/a ratio. As compared to the other cases, Eq. (4-43b) differs in that it depends on member ductility, μ. The resulting plots of longitudinal drift versus d/a ratio illustrate the impact of member ductility ratios between 5 through 20. Longitudinal drift decreases as d/a increases, and drift increases as the member ductility increases since larger ductilities cause larger drifts. Also seen in Figure 4-15, the rate of decrease in drift is slower for values of d/a=0.5 or larger, suggesting appropriate values between 0.5 and 1.0.

From Eq. (4-44), global system ductility in the longitudinal direction is equal to the member ductility and hysteretic energy is dissipated by the longitudinal braces only. Again Eq. (4-45b) is identical to Eq. (4-36b), and the variation of longitudinal stiffness would be identical to Figure 4-10, except that that longitudinal braces yield in this case.

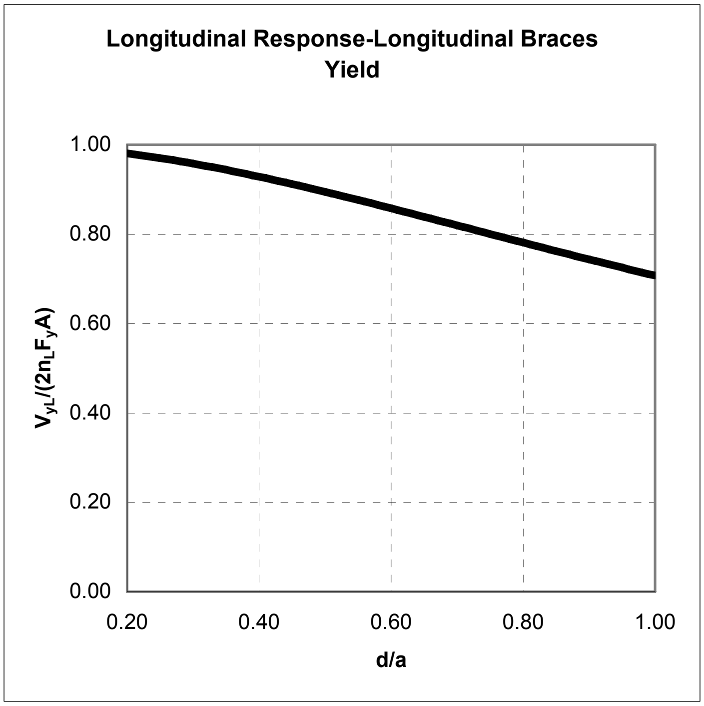

FIGURE 4-14 Nondimensional Longitudinal Base Shear Strength versus d/a Ratio When Longitudinal Braces Yield

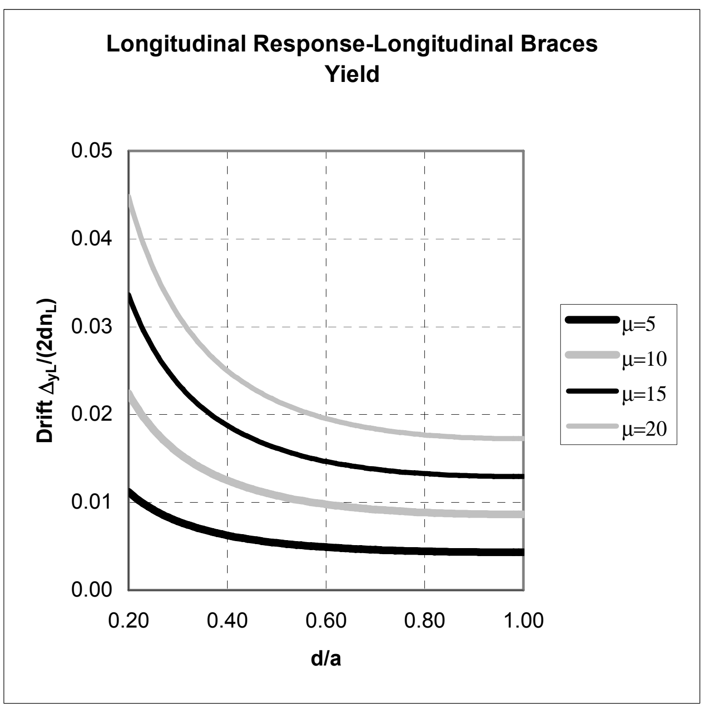

FIGURE 4-15 Longitudinal Drift versus d/a Ratio When Longitudinal Braces Yield

Hysteretic energy dissipation per volume is obtained using Eq. (4-22) and given below:

$$\frac{E_H}{Vol.} = \frac{4(\mu - 1)}{1 + \sqrt{\dfrac{s^2 + d^2}{a^2 + d^2}}} \left(\frac{F_y^2}{E} \right) \tag{4-46a}$$

$$\frac{E_H}{Vol.} = \frac{4(\mu - 1)}{1 + \dfrac{(d/a)}{(d/s)} \sqrt{\dfrac{1 + (d/s)^2}{1 + (d/a)^2}}} \left(\frac{F_y^2}{E} \right) \tag{4-46b}$$

Figures 4-16a through 4-16d demonstrate the variation of volumetric hysteretic energy dissipation with end diaphragm geometric ratios. As expected, dissipated energy decreases as d/a increases. More hysteretic energy is dissipated for larger member ductilities. Additionally, smaller d/s ratios result in lesser energy dissipation in the system.

Although these equations take simpler forms in several other special cases such as when $P_1=0$, $P_2\neq0$ (unidirectional loading in the transverse direction) and when $P_1\neq0$, $P_2=0$ (unidirectional loading in the longitudinal direction), those cases are not of interest in this work, since the objective was to investigate bidirectional effects.

4.2.4.2 Special Case 2- Skewed Bridges ($\varphi\neq0^o$) with Certain Geometric Ratios (d/a and d/s)

To investigate and quantify the impact of skewness on overall inelastic behavior of bridges having ductile diaphragms, fixed geometric ratios of end diaphragms are selected, and the skew angle is taken as a variable. This also allows to observe behavior as a function of the sequence of brace yielding. Code-defined combination rules are used to account for bidirectional earthquake effects.

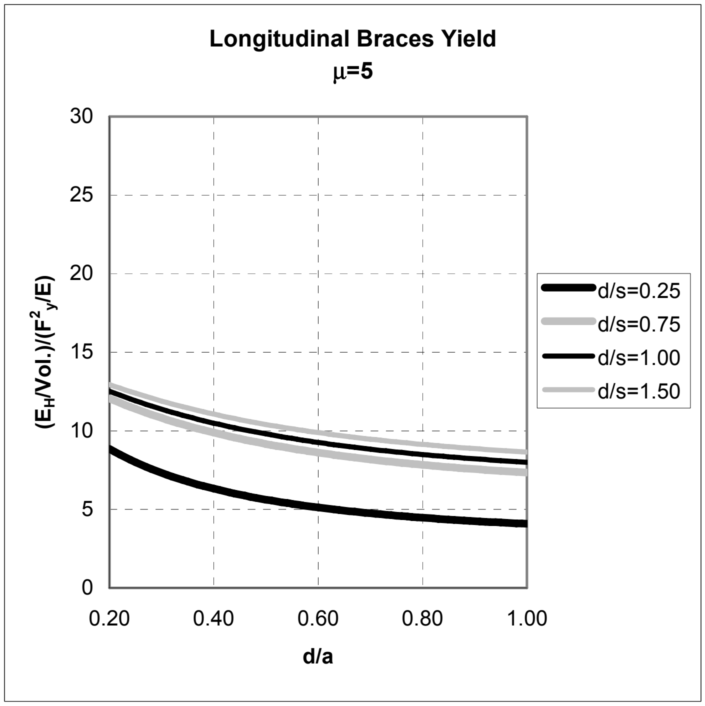

(a)

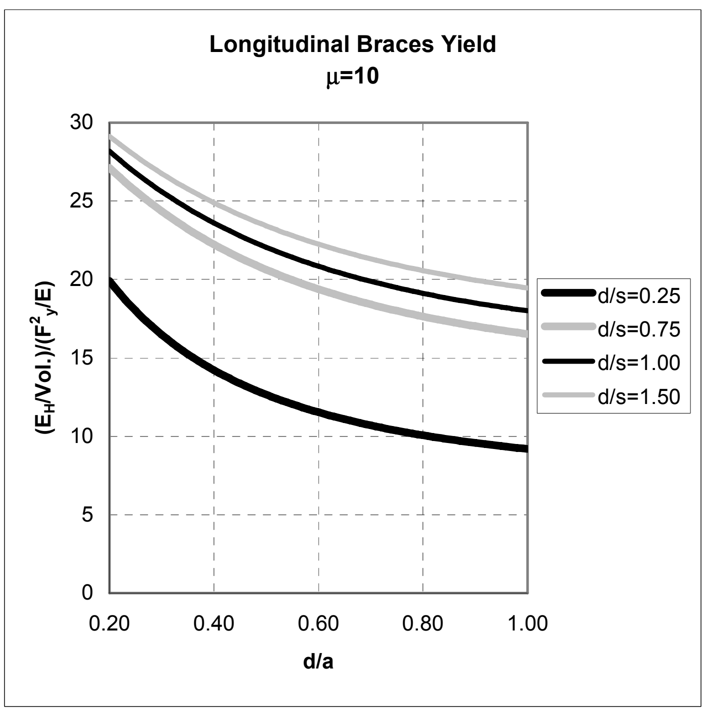

(b)

FIGURE 4-16 Volumetric Energy Dissipation versus End Diaphragm Geometric Ratios When Longitudinal Braces Yield: (a) For μ=5; (b) For μ=10

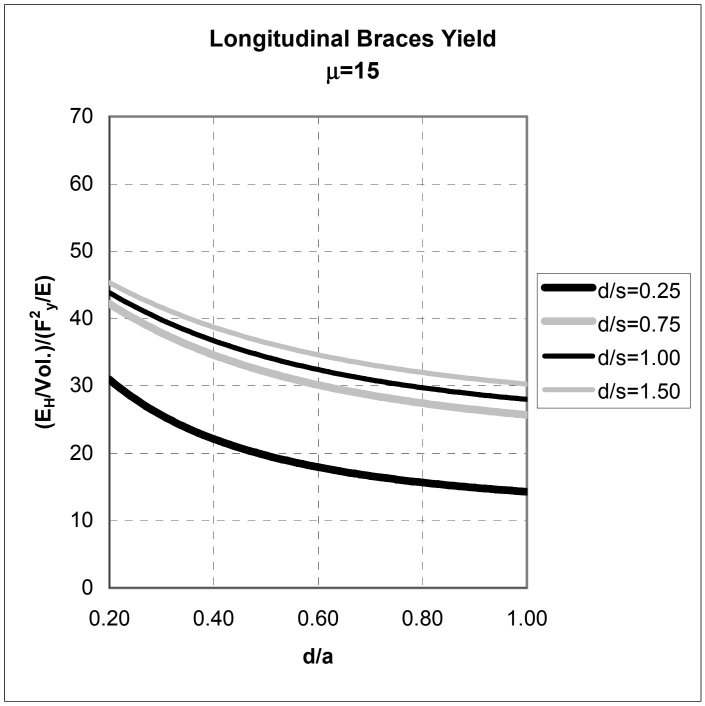

(c)

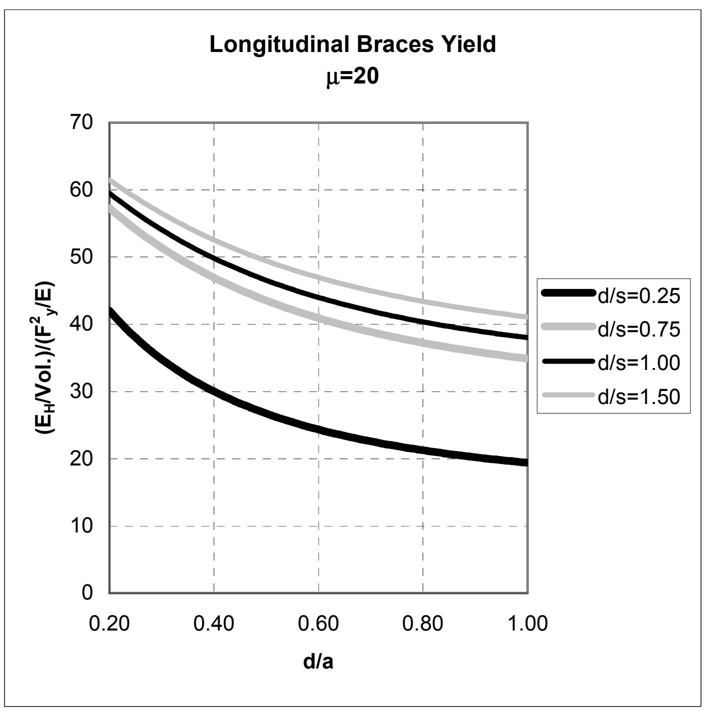

(d)

FIGURE 4-16 Volumetric Energy Dissipation versus End Diaphragm Geometric Ratios When Longitudinal Braces Yield (continued): (c) For μ=15; (d) For μ=20

In North America, practical numerical values for d/s fall in the range of 0.25, 0.50, 1.00, 1.25, and 1.50, covering most short and medium span slab-on-girder and deck-truss bridges. Also, d/a can be set equal to 0.20, 0.40, 0.60, 0.80, and 1.00.

The calculation of the ratio between the axial forces (before yielding) is necessary to determine the type of collapse mechanism. From Eqs. (4-2) and (4-3), for skewed bridges, this ratio can be obtained as follows:

$$\frac{C_L}{C_T} = \frac{T_L}{T_T} = \sqrt{\frac{1+(d/a)^2}{1+(d/s)^2}}\,(\varepsilon\cos\varphi - \sin\varphi) \qquad (4\text{-}47)$$

Eq. (4-47) includes two variables related to the bridge end diaphragm geometric properties, one for the generic bridge geometry (the skewness) and one accounting for the orthogonal earthquake effect. One of the end diaphragm variables can be taken as constant (say, for example, d/s=0.40 to be an average value as observed in many slab-on-girder bridges in North America), and then the variation of braces' forces ratio with respect to the skew angle can be investigated for different values of d/a and ε.

Figures 4-17 shows the variation of brace axial forces ratio with bridge geometry. The ratio of unbonded brace forces increases as the skew angle increases. For relatively small skew angles (say $\varphi \leq 25^{o}$), changes in d/a ratio have no significant effect on the force ratio.

This provides valuable information about the sensitivity of bridge end diaphragms geometry to bridge geometric relations and loading parameters.

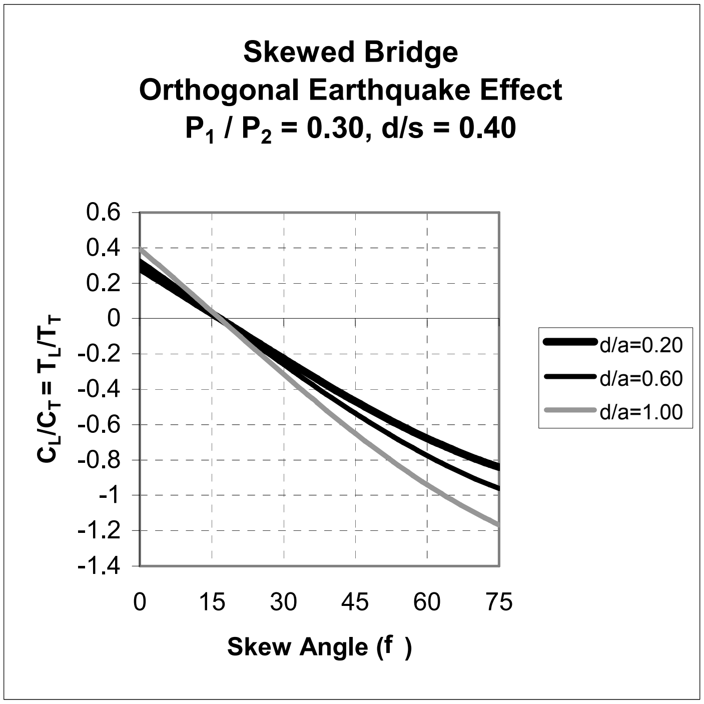

(a)

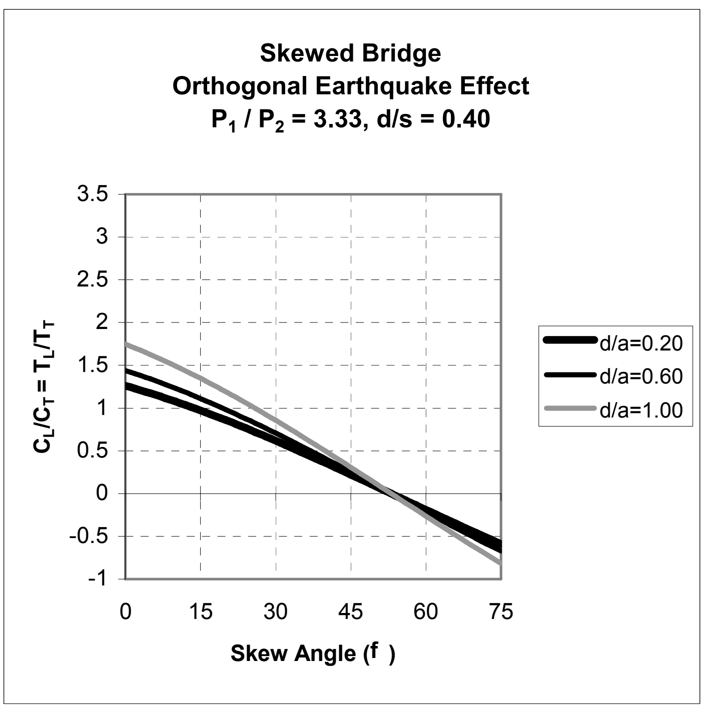

(b)

FIGURE 4-17 Variation of Brace Axial Forces Ratio with Bridge Geometric Relations: (a) For P_1/P_2=0.30; (b) For P_1/P_2=3.33

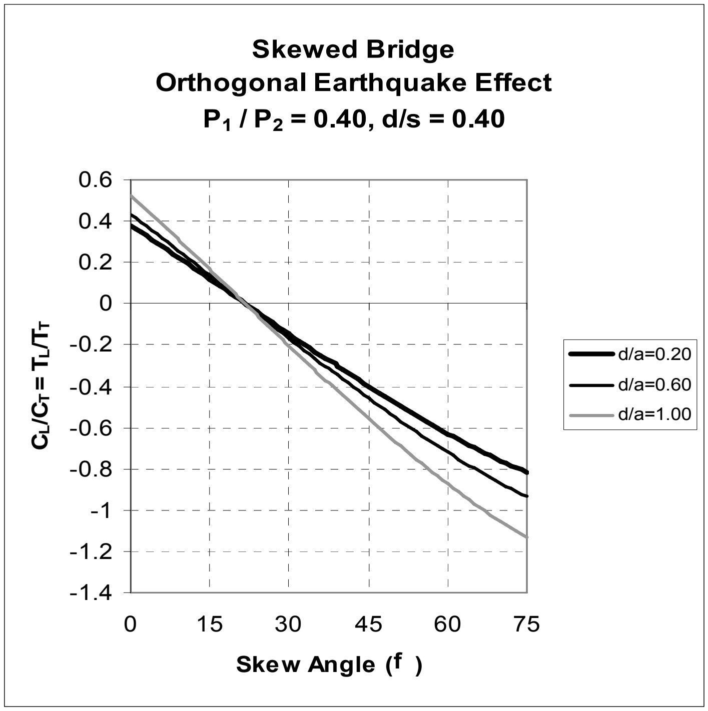

(c)

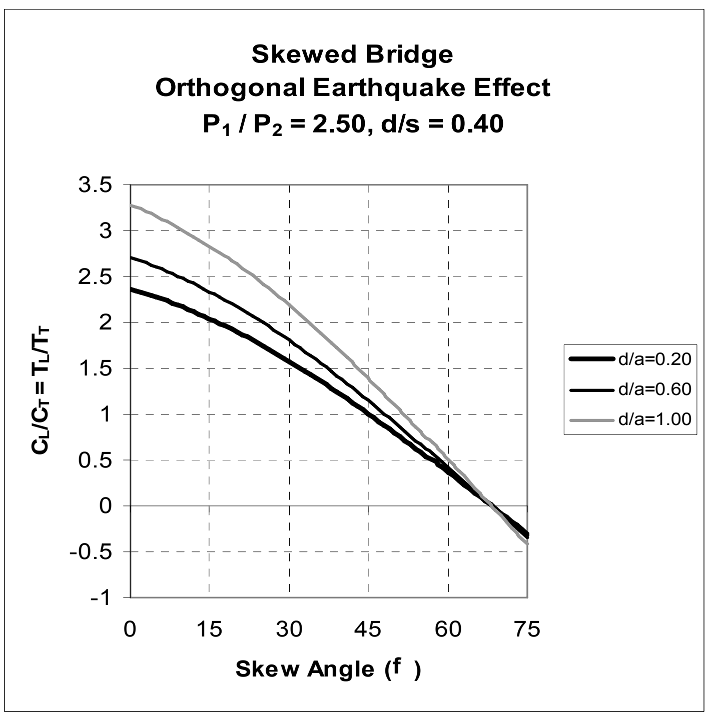

(d)

FIGURE 4-17 Variation of Brace Axial Forces Ratio with Bridge Geometric Relations (continued): (c) For P_1/P_2=0.40; (d) For P_1/P_2=2.50

4.2.4.3 Special Case 3- Bridges with a Certain Skew Angle

Likewise, the previously derived formulas in general forms can also be simplified for certain values of the skew angle, φ, (e.g. 15^o, 30^o, 45^o, and 60^o). Additionally, since the bridge codes specify certain load combinations under bidirectional earthquake effects (for example, P_1=0.30P_2 or P_2=0.30P_1 per the 30% rule), these rules can also be included in the special cases as necessary. Some of these cases are investigated as numerical examples in Section 6.

SECTION 5
CLOSED-FORM HYSTERETIC MODEL FOR RETROFIT SCHEME-2 UNDER BIDIRECTIONAL EARTHQUAKE EFFECTS

5.1 General Remarks

This section presents the development of analytical expressions that describe the behavior of bridges having Retrofit Scheme-2 implemented in end diaphragms. As done in the previous section, the SAP2000 analysis software is used to verify the analytically derived formulas. Again, special cases are considered to investigate the effect of certain parameters on the bi-directional seismic response of bridges. Modeling issues related to Retrofit Scheme-2 were addressed in Section 3. As indicated there, an ideal three dimensional truss system was used to represent the whole bridge superstructure for the purpose of analyzing the end diaphragm behavior. Again, a cyclic symmetric bilinear hysteretic model for unbonded braces is used in the analysis of bridge end diaphragms.

Section 5.2 describes the geometric properties, assumptions, method of analysis, and the derivation of formulas for Retrofit Scheme-2.

5.2 Bidirectional Pushover Analysis of Retrofit Scheme-2 (Floating Deck)

5.2.1 Geometric Relations

Figure 5-1 shows the selected configuration of unbonded braces for Retrofit Scheme-2, and the corresponding skew angle, skew girder spacing, and the depth of the girders. The following formulas take simpler forms in simple geometries (in case of non-skewed bridge for example).

Using Figure 5-1 and 5-2, theoretical brace lengths for long and short braces are respectively

$$LL = \sqrt{a^2 + s^2 + d^2 + 2as\sin\varphi} \qquad (5\text{-}1)$$

$$LS = \sqrt{a^2 + s^2 + d^2 - 2as\sin\varphi} \qquad (5\text{-}2)$$

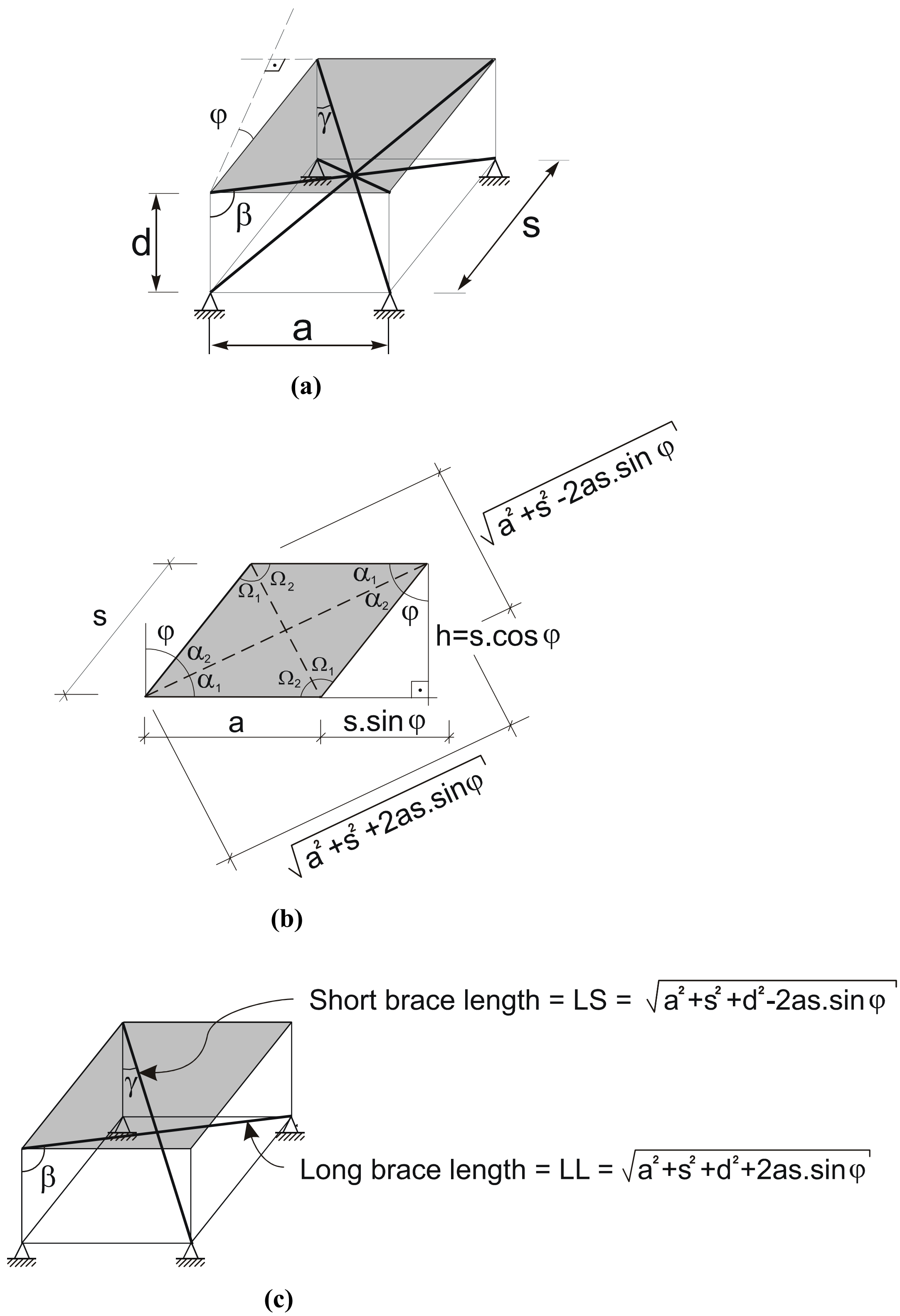

FIGURE 5-1 Geometric Properties for Retrofit Scheme-2:
(a) Idealized System (Axonometric View); (b) Plan View; (c) Braces' Lengths

From the same figures, other geometric relations can be obtained as follows:

$$\sin\Omega_1 = \frac{a\cos\varphi}{\sqrt{a^2 + s^2 - 2as\sin\varphi}} \tag{5-3}$$

$$\sin\Omega_2 = \frac{s\cos\varphi}{\sqrt{a^2 + s^2 - 2as\sin\varphi}} \tag{5-4}$$

$$\sin\alpha_1 = \frac{s\cos\varphi}{\sqrt{a^2 + s^2 + 2as\sin\varphi}} \tag{5-5}$$

$$\sin\alpha_2 = \frac{a\cos\varphi}{\sqrt{a^2 + s^2 + 2as\sin\varphi}} \tag{5-6}$$

$$\sin\beta = \sqrt{\frac{a^2 + s^2 + 2as\sin\varphi}{a^2 + s^2 + d^2 + 2as\sin\varphi}} \tag{5-7}$$

$$\sin\gamma = \sqrt{\frac{a^2 + s^2 - 2as\sin\varphi}{a^2 + s^2 + d^2 - 2as\sin\varphi}} \tag{5-8}$$

where α_1 , α_2 , Ω_1 , and Ω_2 are projection angles used to define the geometric properties of the idealized system.

5.2.2 Brace Axial Forces (Elastic Behavior)

Figure 5-2 (as explained previously) shows the idealized three dimensional truss system representing a bridge superstructure's end diaphragms, bidirectional loading and braces' axial forces under these effects. As was discussed for Retrofit Scheme-1, this model provides a valid representation of the actual retrofit for Retrofit Scheme-2. Many of the assumptions made in Section 4 are also applicable in this case. This truss system is composed of pin-connected unbonded braces with equal cross sectional area, A, and elastic modulus, E. The parameters β and γ are the angles between the unbonded braces and the vertical plane for the long and short braces respectively.

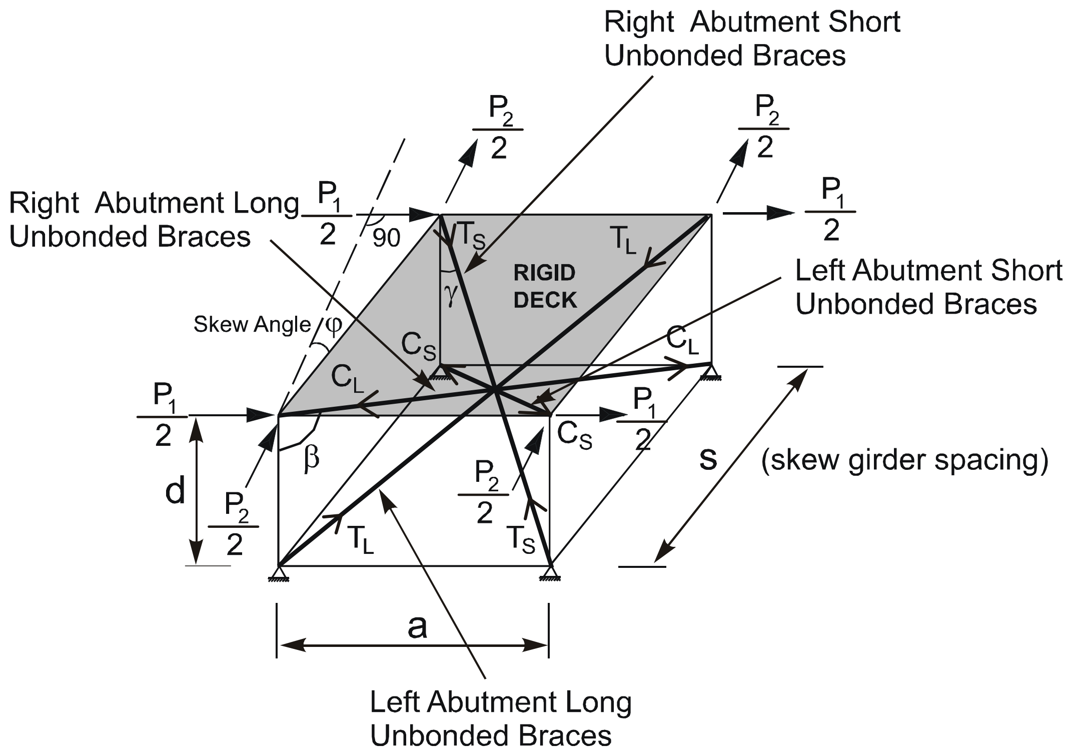

FIGURE 5-2 Bidirectional Loading and Brace Forces for Retrofit Scheme-2

Again, it is assumed that the skew angles, φ, at each end are equal. The value of "a" which is the horizontal longitudinal distance between connections of the unbonded braces at deck level and the abutment could be evaluated as a function of the girder spacing.

In a similar way to what was done in Section 4, equal proportions of the total lateral load in a given direction are applied at each corner of the deck. P_1 and P_2 are the lateral earthquake loads acting at the deck level on one diaphragm in the longitudinal and transverse directions respectively. The ratio of P_1/P_2 (or P_2/P_1) is kept constant in pushover analyses. The unbonded braces are assumed to be active only under earthquake loading and therefore do not carry any gravity loads.

The following summarizes the structural characteristics of the idealized system as functions of system geometrical properties.

To obtain load-displacement diagrams for the system considered, it is convenient to evaluate the ratio of short and long braces elastic forces using the geometrical and trigonometric relations of Figure 5-2. From the geometry of that figure, the long and short braces forces and their ratio are obtained as follows:

$$C_L = -T_L = \frac{LL}{2as\cos\varphi}\left[-s\cos\varphi P_1 + (-a + s\sin\varphi)P_2\right] \tag{5-9}$$

$$C_S = -T_S = \frac{LS}{2as\cos\varphi}\left[s\cos\varphi P_1 - (a + s\sin\varphi)P_2\right] \tag{5-10}$$

$$\frac{C_L}{C_S} = \frac{T_L}{T_S} = \left(\frac{LL}{LS}\right)\left[\frac{-s\cos\varphi P_1 + (-a + s\sin\varphi)P_2}{s\cos\varphi P_1 - (s\sin\varphi + a)P_2}\right] \tag{5-11a}$$

Here, C_S, T_S and C_L, T_L denote axial compression and tension forces in the short and longitudinal braces respectively. Note that Eq. (5-11a) gives always positive values. Taking $\varepsilon=P_1/P_2$ (the ratio of earthquake forces acting in each orthogonal direction) yields the following formula for elastic braces forces ratio:

$$\frac{C_L}{C_S} = \frac{T_L}{T_S} = \left(\frac{LL}{LS}\right)\left[\frac{-s\varepsilon\cos\varphi + (-a + s\sin\varphi)}{s\varepsilon\cos\varphi - (s\sin\varphi + a)}\right] \tag{5-11b}$$

As seen from Eqs. (5-9) through (5-11), axial forces produced in a brace vary depending on the system geometric dimensions. In the elastic range, shear forces in each longitudinal and transverse directions are $V_L=2P_1$ and $V_T=2P_2$. Typically, there are two possible plastic collapse mechanisms for this idealized end diaphragm system. The first mechanism occurs when the long braces yield first while the second one is reached when the short braces yield first. In some special loading and geometrical conditions, a combined mechanism in which all braces simultaneously yield at the same time is possible. Again, since the bridge behavior is bi-directional due to both bidirectional loading and the bridge geometry for each plastic collapse mechanism, both transverse and longitudinal responses are investigated separately. Figure 5-3 schematically shows the bidirectional response of Retrofit Scheme-2 up to specified limit state.

This response is numerically investigated and factors affecting this behavior are given in detail in Section 6, in Example-2.

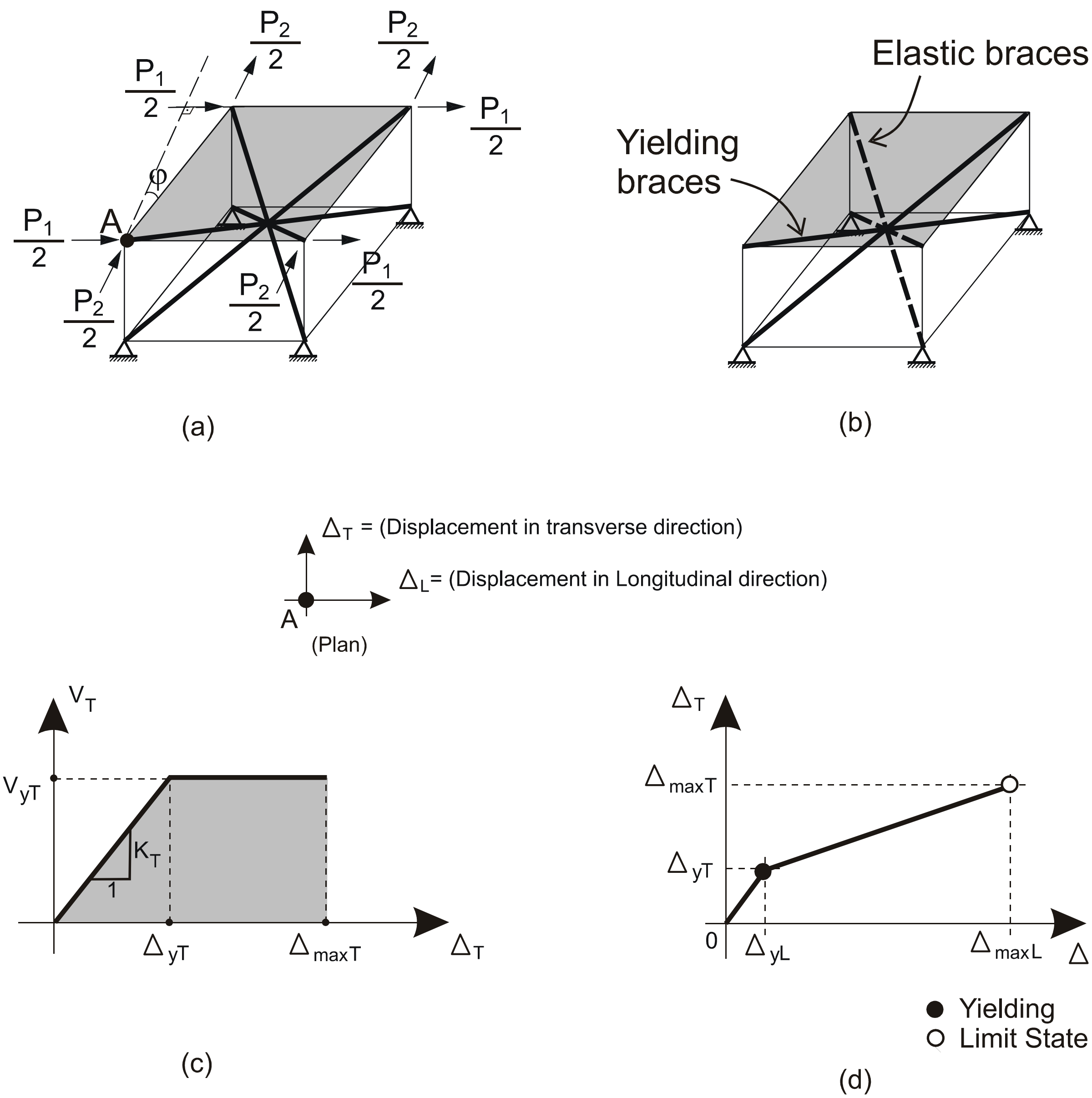

FIGURE 5-3 Bidirectional Response of Retrofit Scheme-2: (a) Idealized System and Loading; (b) Yielding and Non-yielding Unbonded Braces; (c) Base Shear versus Lateral Displacement in the Governing Direction; (d) Travel of Node A

5.2.3 Behavior When Short Braces Yield

When the value of axial forces for the short unbonded braces is greater than for the long braces, axial yielding in the short braces occurs. The type of collapse mode can be determined using Eq. (5-11b), which captures the relative magnitudes of braces axial forces.

Based on these explanations, the potential collapse modes can be defined as given below:

If $\frac{C_L}{C_S} = \frac{T_L}{T_S} > 1$ then long braces yield

If $\frac{C_L}{C_S} = \frac{T_L}{T_S} < 1$ then short braces yield

If $\frac{C_L}{C_S} = \frac{T_L}{T_S} = 1$ then all braces yield at the same time

Response in the Transverse Direction

To obtain the yield shear force in the transverse direction when short braces yield, the same procedure followed in Section 4 can be repeated. To do this, first, the elastic brace forces should be replaced with the axial yield forces in the yielding braces. Note that the other two longer braces remain elastic up to plastic collapse. For the three dimensional truss system considered, writing the equations of equilibrium in the transverse direction gives the yield base shear in this direction as follows:

$$V_{yT} = \left[\frac{4as\cos\varphi P_2}{LS[-s\cos\varphi P_1 + (s\sin\varphi + a)P_2]} \right](F_y A) \tag{5-12a}$$

or, alternatively, defining $\varepsilon = P_1/P_2$ which is the ratio of forces in both orthogonal directions gives the following:

$$V_{yT} = \left[\frac{4as\cos\varphi}{LS[s(\sin\varphi - \varepsilon\cos\varphi) + a)]} \right](F_y A) \tag{5-12b}$$

To obtain the corresponding yield drift in the transverse direction, virtual work can be used with unit loading applied at the joints where the displacement is to be determined. The load should be in the same direction as the specified displacement (i.e. in the transverse direction). Unbonded brace forces from unit loading can be obtained using Eqs. (5-9) and (5-10) during the analysis of displacements. Furthermore, with reference to Section 4, the axial member displacement ductility of the unbonded braces is again defined as μ. Using this procedure, the following generalized formula is obtained for the transverse displacement at a member ductility of μ:

$$\Delta_T = \left[\frac{LS^3(s\sin\varphi + a)\left[s(\varepsilon\cos\varphi - \sin\varphi) - a\right]\mu + LL^3\left[s(\varepsilon\cos\varphi - \sin\varphi) + a\right](s\sin\varphi - a)}{2asLS\cos\varphi\left[s(\varepsilon\cos\varphi - \sin\varphi) - a\right]}\right]\left(\frac{F_y}{E}\right)$$

(5-13a)

For the yield displacement, substituting μ=1 gives the following:

$$\Delta_{yT} = \left[\frac{LS^3(s\sin\varphi + a)[s(\varepsilon\cos\varphi - \sin\varphi) - a] + LL^3[s(\varepsilon\cos\varphi - \sin\varphi) + a](s\sin\varphi - a)}{2asLS\cos\varphi[s(\varepsilon\cos\varphi - \sin\varphi) - a]}\right]\left(\frac{F_y}{E}\right)$$

(5-13b)

It is useful to express the system global ductility (μ_{GT}) as a function of the member (brace) ductility (μ). This corresponds to the ratio of the maximum displacement to the yield displacement:

$$\mu_{GT} = \frac{\Delta_T(\mu = \mu_{target})}{\Delta_{yT}(\mu = 1)} \qquad (5\text{-}14a)$$

Inserting the relevant formulas for the maximum and yield displacements gives the global system ductility in the transverse direction as follows:

$$\mu_{GT} = \left[\frac{LS^3(s\sin\varphi + a)[s(\varepsilon\cos\varphi - \sin\varphi) - a]\mu + LL^3[s\ (\varepsilon\cos\varphi - \sin\varphi) + a](s\sin\varphi - a)}{LS^3(s\sin\varphi + a)[s(\varepsilon\cos\varphi - \sin\varphi) - a] + LL^3[s\ (\varepsilon\cos\varphi - \sin\varphi) + a](s\sin\varphi - a)}\right]$$

(5-14b)

The initial stiffness of the system in the transverse direction can be obtained from equations above, taking μ=1, as:

$$K_T = \frac{V_{yT}}{\Delta_{yT}} \tag{5-15a}$$

or

$$K_T = \left[\frac{8a^2 s^2 \cos^2 \varphi}{LS^3 (s\sin\varphi + a)[-s(\varepsilon\cos\varphi - \sin\varphi) + a] + LL^3[-s\ (\varepsilon\cos\varphi - \sin\varphi) - a](s\sin\varphi - a)} \right](EA)$$

(5-15b)

Response in the Longitudinal Direction

After mathematical derivations similar to those performed in the previous section, the following system characteristics are reached for response in the longitudinal direction.

The base shear in the longitudinal direction for short braces yielding is:

$$V_{yL} = \left[\frac{4\mathrm{as}\cos\varphi P_1}{\mathrm{LS}[\mathrm{s}\cos\varphi P_1 - (s\sin\varphi + a)\mathrm{P}_2]} \right](F_y A) \tag{5-16a}$$

or, again, defining $\varepsilon = P_1/P_2$:

$$V_{yL} = \left[\frac{4\mathrm{as}\ \varepsilon\cos\varphi}{\mathrm{LS}[\mathrm{s}(\varepsilon\cos\varphi - \sin\varphi)\ \text{-}\ \mathrm{a}]} \right](F_y A) \tag{5-16b}$$

The corresponding displacement in the longitudinal direction is :

$$\Delta_L = \left[\frac{LS^3[s(-\varepsilon\cos\varphi + \sin\varphi) + a]\mu + LL^3[s\ (\text{-}\varepsilon\cos\varphi + \sin\varphi) - a]}{2aLS[s\ (\varepsilon\cos\varphi - \sin\varphi) - a]} \right]\left(\frac{F_y}{E} \right)$$

(5-17)

The global ductility in the longitudinal direction is:

$$\mu_{GL} = \left[\frac{LS^3[s(-\varepsilon\cos\varphi + \sin\varphi) + a]\mu + LL^3[s\ (\text{-}\varepsilon\cos\varphi + \sin\varphi) - a]}{LS^3[s(-\varepsilon\cos\varphi + \sin\varphi) + a] + LL^3[s\ (\text{-}\varepsilon\cos\varphi + \sin\varphi) - a]} \right]$$

(5-18a)

The initial stiffness in the longitudinal direction is

$$K_L = \left[\frac{8a^2 s\varepsilon \cos\varphi}{LS^3[s(-\varepsilon\cos\varphi+\sin\varphi)+a]+LL^3\left[s(-\varepsilon\cos\varphi+\sin\varphi)-a\right]} \right](EA) \tag{5-18b}$$

Hysteretic Energy Dissipation

Hysteretic energy dissipated through a full cycle of displacement of the entire system up to the target ductility of the braces reaching this target should be equal to the energy dissipated by the yielding brace members. This value will be given in a form of volumetric energy dissipated as follows:

$$\frac{\sum E_H}{\text{Vol.}} = \frac{4n_S(\mu-1)\frac{F_y^2}{E}(LS)A}{n_S A(LS)+n_L A(LL)} = \frac{4(\mu-1)n_s LS}{n_S LS + n_L LL}\left(\frac{F_y^2}{E}\right) \tag{5-19}$$

where n_S and n_L denote the number of short and long braces respectively. Note that these numbers have been kept constant and equal to each other in this report.

5.2.4 Behavior when Long Braces Yield

Long braces yield when $C_L/C_S=T_L/T_S > 1$. This ratio is calculated using Eq. (5-11b). The inelastic behavior of the truss system is governed by yielding of the long unbonded braces, and the system plastically displaces until the maximum displacement demand is reached which is related to the member ductility demand. Again, an elastic-plastic inelastic behavior develops.

Since bidirectional response for the end diaphragm system is expected, responses in the transverse and longitudinal directions will be investigated respectively.

Response in the Transverse Direction

As was done for the previous case with short braces yielding to drive all relevant equations, but this time instead replacing the axial force values of long braces by their corresponding yield values, the following equations are obtained:

$$V_{yT} = \left[\frac{4\text{ascos}\varphi P_2}{\text{LL}[\text{s}\cos\varphi P_1 + (a - s\sin\varphi)P_2]} \right](\text{F}_\text{y}\text{A}) \tag{5-20a}$$

or

$$V_{yT} = \left[\frac{4\text{ascos}\varphi}{\text{LL}[\text{s}(\varepsilon\cos\varphi - \sin\varphi) + \text{a}]} \right](\text{F}_\text{y}\text{A}) \tag{5-20b}$$

And the transverse displacement for a member (unbonded brace) ductility of μ is :

$$\Delta_\text{T} = \left[\frac{\text{LL}^3(\text{-a} + \text{ssin}\varphi)[s(\varepsilon\cos\varphi - \sin\varphi) + a]\mu + LS^3[\text{s}(\varepsilon\cos\varphi - \sin\varphi) - a](s\sin\varphi + a)}{2\text{ascos}\varphi LL[s(-\varepsilon\cos\varphi + \sin\varphi) - a]} \right]\left(\frac{\text{F}_\text{y}}{\text{E}}\right) \tag{5-21a}$$

To obtain the yield displacement in the transverse direction, taking μ=1 gives the following:

$$\Delta_{yT} = \left[\frac{\text{LL}^3(\text{-a} + \text{ssin}\varphi)[s(\varepsilon\cos\varphi - \sin\varphi) + a] + LS^3[\text{s}(\varepsilon\cos\varphi - \sin\varphi) - a](s\sin\varphi + a)}{2\text{ascos}\varphi LL[s(-\varepsilon\cos\varphi + \sin\varphi) - a]} \right]\left(\frac{\text{F}_\text{y}}{\text{E}}\right) \tag{5-21b}$$

Global (system) versus local (member) ductility is :

$$\mu_{GT} = \left[\frac{\text{LL}^3(\text{-a} + \text{ssin}\varphi)[s(\varepsilon\cos\varphi - \sin\varphi) + a]\mu + LS^3[\text{s}(\varepsilon\cos\varphi - \sin\varphi) - a](s\sin\varphi + a)}{\text{LL}^3(\text{-a} + \text{ssin}\varphi)[s(\varepsilon\cos\varphi - \sin\varphi) + a] + LS^3[\text{s}(\varepsilon\cos\varphi - \sin\varphi) - a](s\sin\varphi + a)} \right] \tag{5-22}$$

Initial stiffness of the system is :

$$K_\text{T} = \left[\frac{8a^2 s^2 \cos^2\varphi}{\text{LL}^3(\text{-a} + \text{ssin}\varphi)[-s(\varepsilon\cos\varphi - \sin\varphi) - a] + LS^3[\text{-s}(\varepsilon\cos\varphi - \sin\varphi) + a](s\sin\varphi + a)} \right](\text{EA}) \tag{5-23}$$

As expected, the initial stiffness of the system in the transverse direction is the same as that for the short brace yielding case.

Response in the Longitudinal Direction

Following the same procedure, the longitudinal base shear at long brace yielding is :

$$V_{yL} = \left[\frac{4\text{ascos}\varphi P_1}{\text{LL}[\text{-scos}\varphi P_1 + (-a + s\sin\varphi)\text{P}_2]} \right](\text{F}_\text{y}\text{A}) \tag{5-24a}$$

Defining $\varepsilon = P_1/P_2$ and rearranging, Eq. (5-24a) becomes :

$$\mathrm{V_{yL}} = \left[\frac{4as\varepsilon\cos\varphi}{LL[s(-\varepsilon\cos\varphi + \sin\varphi)\text{-}a]} \right] (\mathrm{F_y A}) \tag{5-24b}$$

Similarly, displacement in the longitudinal direction is :

$$\Delta_{\mathrm{L}} = \left[\frac{\mathrm{LL}^3[s(\varepsilon\cos\varphi - \sin\varphi) + a]\mu + LS^3[\mathrm{s}(\varepsilon\cos\varphi - \sin\varphi) - a]}{2\mathrm{aLL}[s(\varepsilon\cos\varphi - \sin\varphi) + a]} \right] \left(\frac{\mathrm{F_y}}{\mathrm{E}} \right) \tag{5-25a}$$

The yield displacement can be obtained by using $\mu=1$ in Eq. (5-25) :

$$\Delta_{\mathrm{yL}} = \left[\frac{\mathrm{LL}^3[s(\varepsilon\cos\varphi - \sin\varphi) + a] + LS^3[\mathrm{s}(\varepsilon\cos\varphi - \sin\varphi) - a]}{2\mathrm{aLL}[s(\varepsilon\cos\varphi - \sin\varphi) + a]} \right] \left(\frac{\mathrm{F_y}}{\mathrm{E}} \right) \tag{5-25b}$$

The variation of global versus local ductility in the longitudinal direction can be determined from Eqs. (5-25a) and (5-25b) :

$$\mu_{\mathrm{GL}} = \left[\frac{\mathrm{LL}^3[s(\varepsilon\cos\varphi - \sin\varphi) + a]\mu + LS^3[\mathrm{s}(\varepsilon\cos\varphi - \sin\varphi) - a]}{\mathrm{LL}^3[s(\varepsilon\cos\varphi - \sin\varphi) + a] + LS^3[\mathrm{s}(\varepsilon\cos\varphi - \sin\varphi) - a]} \right] \tag{5-26}$$

Finally, the initial stiffness in the longitudinal direction can be obtained by using Eqs. (5-24b) and (5-25b). The system stiffness as a function of end diaphragm geometric properties and ratio of bidirectional loading is :

$$\mathrm{K_L} = \left[\frac{8a^2s\varepsilon\cos\varphi}{\mathrm{LL}^3[s(-\varepsilon\cos\varphi + \sin\varphi) - a] + LS^3[\mathrm{s}(\text{-}\varepsilon\cos\varphi + \sin\varphi) + a]} \right] (\mathrm{EA}) \tag{5-27}$$

Again, the initial stiffness of the system in the longitudinal direction is the same as for the case of short brace yielding. This is why the system behaves elastically up to the first yielding, and therefore the initial stiffnesses computed from different ways should be equal to each other.

Hysteretic Energy Dissipation

As before, hysteretic energy dissipated through a full cycle in the system should be equal to the energy dissipated by the yielding brace members. In case of longitudinal brace yielding, this value is :

$$\frac{\sum E_H}{\text{Vol.}} = \frac{4n_L(\mu-1)\frac{F_y^{\;2}}{E}(LL)A}{n_S A(LS) + n_L A(LL)} = \frac{4(\mu-1)n_L LL}{n_S LS + n_L LL}\left(\frac{F_y^2}{E}\right) \tag{5-28}$$

where n_S and n_L denote the total number of short and long braces respectively. Note that these numbers have been kept constant and equal to each other in this report.

5.2.5 Special Cases

The developed equations in this section, as before, take simpler forms for a variety of special cases that are encountered in bridge engineering practice. These are discussed below.

5.2.5.1 Special Case 1-Non-Skewed Bridges (φ=0°)

In the relavent equations substituting φ=0 that corresponds to non-skewed bridges, the following formulas are obtained:

Using the geometrical relations of the idealized system as illustrated in Figures 5-1 and 5-2, the brace lengths become equal to each other as given below:

$$LL = LS = \sqrt{a^2 + s^2 + d^2} \tag{5-29}$$

Similarly, the previously defined projection angles α_1 , α_2 , Ω_1 , and Ω_2 takes the following simple forms in non-skewed systems:

$$\sin\Omega_1 = \sin\alpha_2 = \frac{a}{\sqrt{a^2+s^2}} \tag{5-30}$$

$$\sin\Omega_2 = \sin\alpha_1 = \frac{s}{\sqrt{a^2+s^2}} \tag{5-31}$$

$$\sin\beta = \sin\gamma = \sqrt{\frac{a^2 + s^2}{a^2 + s^2 + d^2}} \tag{5-32}$$

which reveals that, $\Omega_1 = \alpha_2$, $\Omega_2 = \alpha_1$, and $\beta=\gamma$.

The ratio of elastic axial compression and tension forces in the unbonded braces are given below as a function of the ratio of bidirectional earthquake forces (ε) imposed on the system and the end diaphragm geometric properties. Note that since the brace lengths are equal to each other (there are no more long and short braces), the ratio of the elastic braces forces becomes the ratio of forces created in opposite diagonal directions. This ratio equals to:

$$\frac{C_S}{C_L} = \frac{T_S}{T_L} = \frac{a - s\varepsilon}{a + s\varepsilon} \tag{5-33a}$$

or, rewritting this equation in terms of the nondimensional properties of ε and s/a gives the following:

$$\frac{C_S}{C_L} = \frac{T_S}{T_L} = \frac{1 - \varepsilon\left(\frac{s}{a}\right)}{1 + \varepsilon\left(\frac{s}{a}\right)} \tag{5-33b}$$

Figure (5-4) shows the variation of axial forces ratio with bidirectional loading and s/a ratios. As before, the curves are generated for ε values of 0.30 and 0.40. The practical values of s/a ratio are set to 0.25, 0.50, 0.75, 1.00, 1.25, and 1.50 in this report.

Also in non-skewed bridges end diaphragm systems, since bidirectional response develops under bidirectional loading, the behavior will be investigated in the transverse and longitudinal directions.

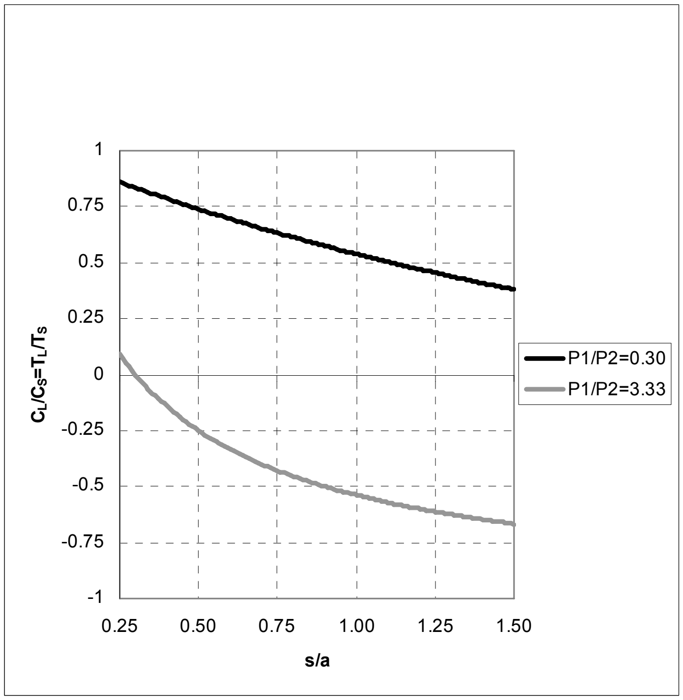

(a)

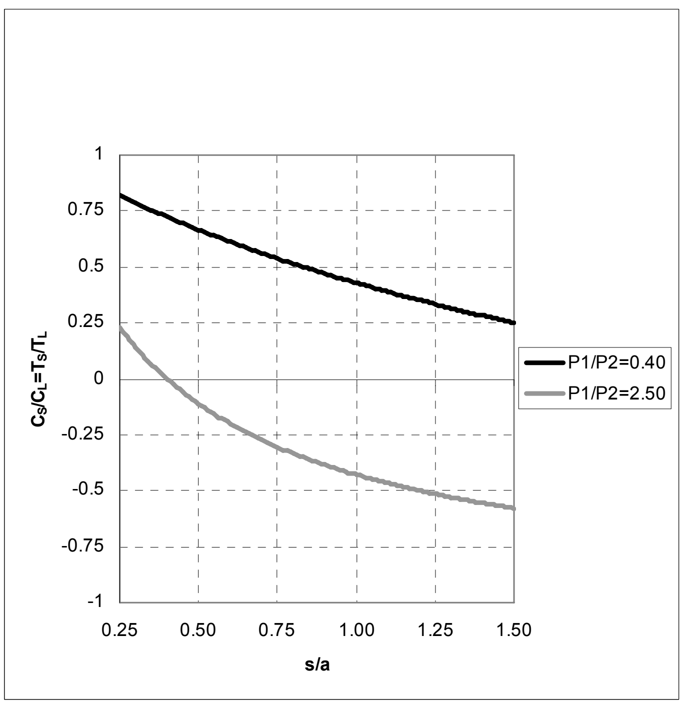

(b)

FIGURE 5-4 Variation of Brace Axial Forces Ratio with Bridge Geometric Relations: (a) For P_1/P_2=0.30 and P_1/P_2=3.33; (b) For P_1/P_2=0.40 and P_1/P_2=2.50

5.2.5.1.1 Short-Labeled Braces Yield

Although the lengths of the braces are equal to each other in non-skewed systems, for the sake of clarity, short-labeled and long-labeled braces in the skewed system as depicted in Figure 5-1 will be referred to in the following sections.

5.2.5.1.1.1 Transverse Response

After determining the yielding braces for a specified system geometry and loading ratio per Eq. (5-33a,b), the behavioral characteristics of the system such as base shear strength (V_{yT}), yield displacement (Δ_{yT}) and the corresponding drift (Δ_{yT}/d), global ductility demand (μ_{GT}), and the initial stiffness of the system (K_T) in the transverse direction are obtained using Eqs. (5-12) through (5-15), as follows:

The transverse base shear strength is:

$$V_{yT} = \left[\frac{4as}{LL(a - s\varepsilon)}\right](F_y A) \tag{5-34a}$$

or, by rearranging this equation using the nondimensional properties, the base shear strength in the transverse direction can also be expressed by:

$$V_{yT} = \left[\frac{4(s/a)}{\sqrt{1+(s/a)^2+(d/a)^2}\left[1-(s/a)\varepsilon\right]}\right](F_y A) \tag{5-34b}$$

The lateral drift (Δ_T/d), at a member ductility of μ, in the transverse direction is:

$$\frac{\Delta_T}{d} = \left[1+(s/a)^2+(d/a)^2\right]\frac{\left[(s/a)\varepsilon-1\right]\mu-\left[(s/a)\varepsilon+1\right]}{2(s/a)(d/a)\left[(s/a)\varepsilon-1\right]}\left(\frac{F_y}{E}\right) \tag{5-35}$$

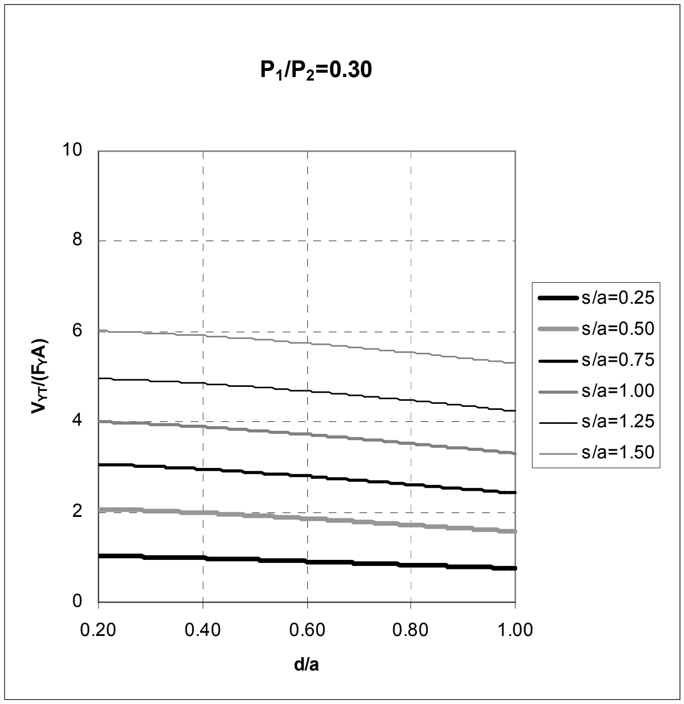

(a)

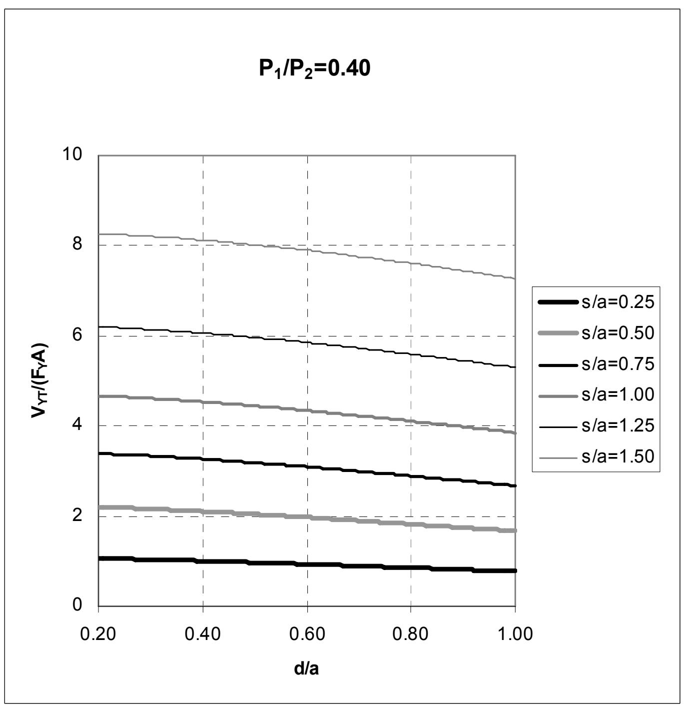

(b)

FIGURE 5-5 Nondimensional Transverse Base Shear Strength versus d/a Ratio When Short-Labeled Braces Yield: (a) For P_1/P_2=0.30; (b) For P_1/P_2=0.40

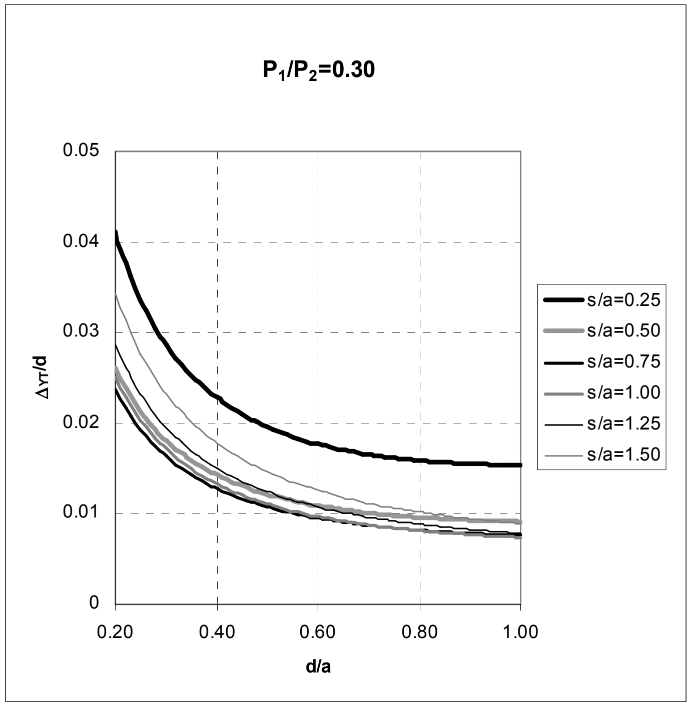

(a)

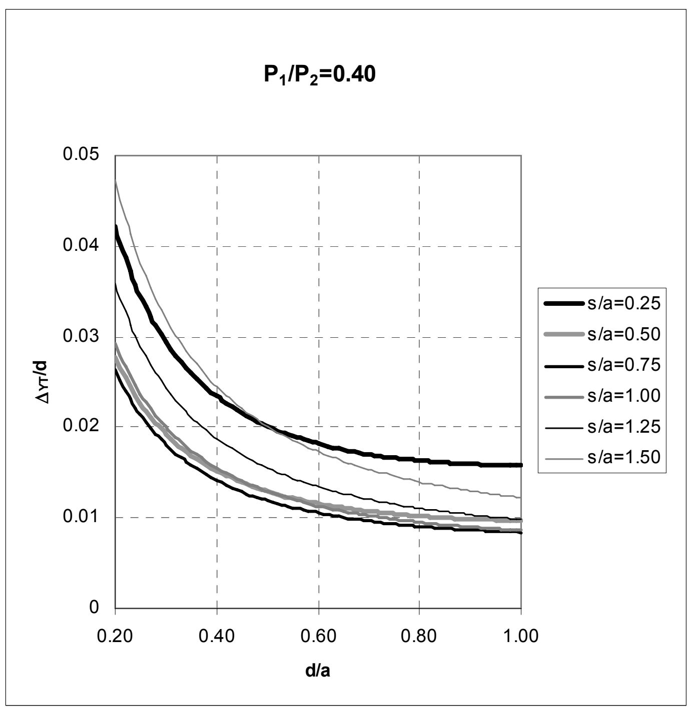

(b)

FIGURE 5-6 Transverse Drift versus d/a Ratio When Short- Labeled Braces Yield: (a) For P_1/P_2=0.30; (b) For P_1/P_2=0.40

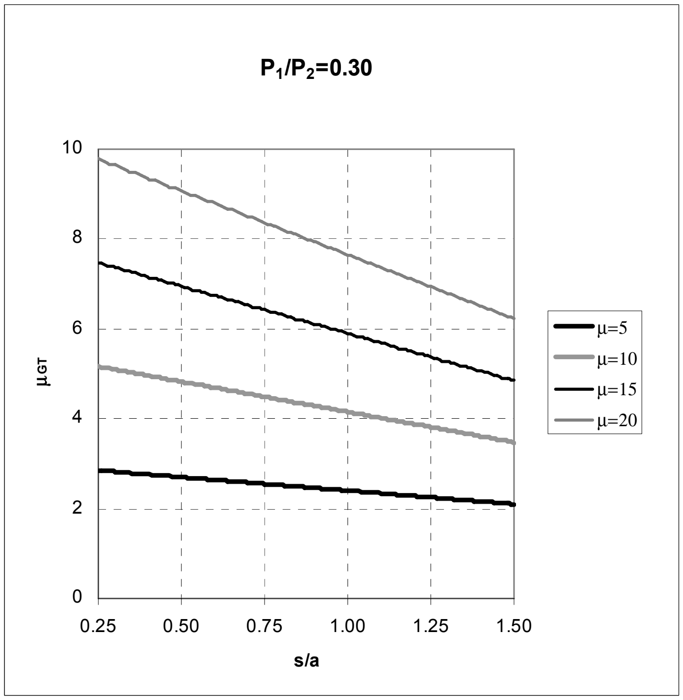

(a)

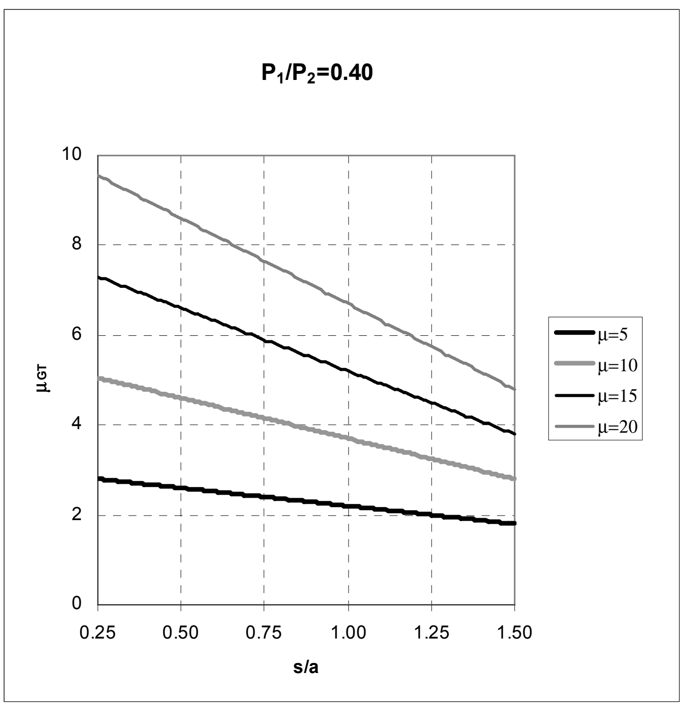

(b)

FIGURE 5-7 Global Transverse Ductility Ratio versus s/a Ratio and Local Ductility When Short- Labeled Braces Yield: (a) For P_1/P_2=0.30; (b) For P_1/P_2=0.40

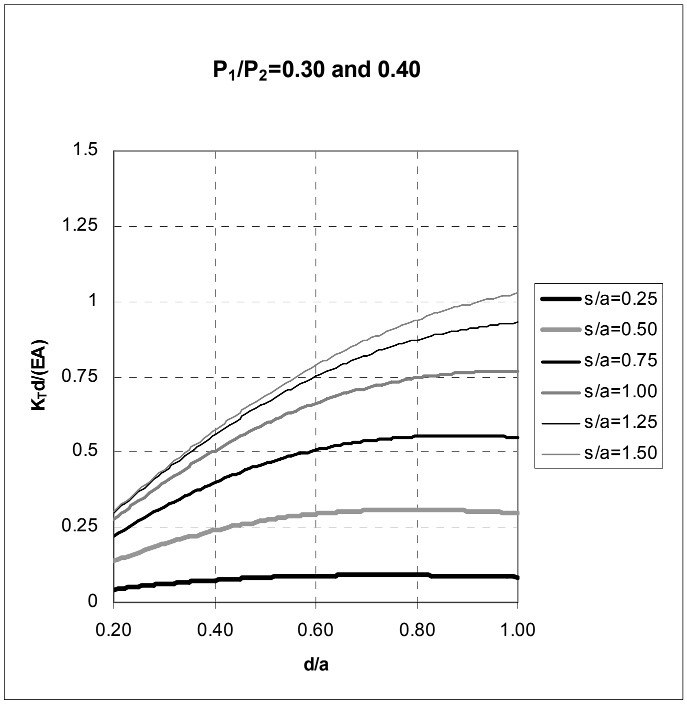

FIGURE 5-8 Nondimensional Transverse Stiffness versus d/a and s/a Ratios When Short- Labeled Braces Yield

and the corresponding drift at yield is obtained by substituting μ=1 in Eq. (5-35) as

$$\frac{\Delta_{yT}}{d} = \frac{\left[1+(s/a)^2+(d/a)^2\right]}{(s/a)(d/a)\left[1-(s/a)\varepsilon\right]}\left(\frac{F_y}{E}\right) \tag{5-36}$$

The global displacement ductility in the transverse direction (μ_{GT}) for the system is:

$$\mu_{GT} = \left[\frac{[1-(s/a)\varepsilon]\mu + [1+(s/a)\,\varepsilon]}{2}\right] \tag{5-37}$$

The initial stiffness of the system in the transverse direction can be obtained from equations above, taking μ=1, as:

$$K_T d = \left[\frac{4(s/a)^2 (d/a)}{\left[1 + (s/a)^2 + (d/a)^2\right]^{3/2}} \right] (EA)$$

(5-38)

5.2.5.1.1.2 Longitudinal Response

Similar equations can be obtained for the response in the longitudinal direction. The base shear strength in the longitudinal direction is:

$$V_{yL} = \left[\frac{4(s/a)\,\varepsilon}{\sqrt{1 + (s/a)^2 + (d/a)^2}\,[(s/a)\varepsilon - 1]} \right] (F_y A) \quad (5\text{-}39)$$

The lateral displacement in the longitudinal direction is given by

$$\frac{\Delta_L}{d} = \left[1 + (s/a)^2 + (d/a)^2\right] \frac{[1 - (s/a)\varepsilon]\mu - [1 + (s/a)\varepsilon]}{2(d/a)[(s/a)\varepsilon - 1]} \left(\frac{F_y}{E} \right) \quad (5\text{-}40)$$

and the longitudinal drift at brace yielding becomes

$$\frac{\Delta_{yL}}{d} = \frac{\left[1 + (s/a)^2 + (d/a)^2\right](s/a)\varepsilon}{(d/a)[1 - (s/a)\varepsilon]} \left(\frac{F_y}{E} \right) \quad (5\text{-}41)$$

The global ductility in the longitudinal direction can be derived as :

$$\mu_{GL} = \left[\frac{[(s/a)\varepsilon - 1]\mu + [(s/a)\varepsilon + 1]}{2(s/a)\varepsilon} \right] \quad (5\text{-}42)$$

The initial stiffness in the longitudinal direction can be found to be :

$$K_L d = \left[\frac{-4(d/a)}{\left[1 + (s/a)^2 + (d/a)^2\right]^{3/2}} \right] (EA) \quad (5\text{-}43)$$

Volumetric hysteretic energy dissipated through a full cycle of displacement can be rewritten as follows:

$$\frac{\sum E_H}{\text{Vol.}} = 2(\mu - 1)\left(\frac{F_y^2}{E} \right) \quad (5\text{-}44)$$

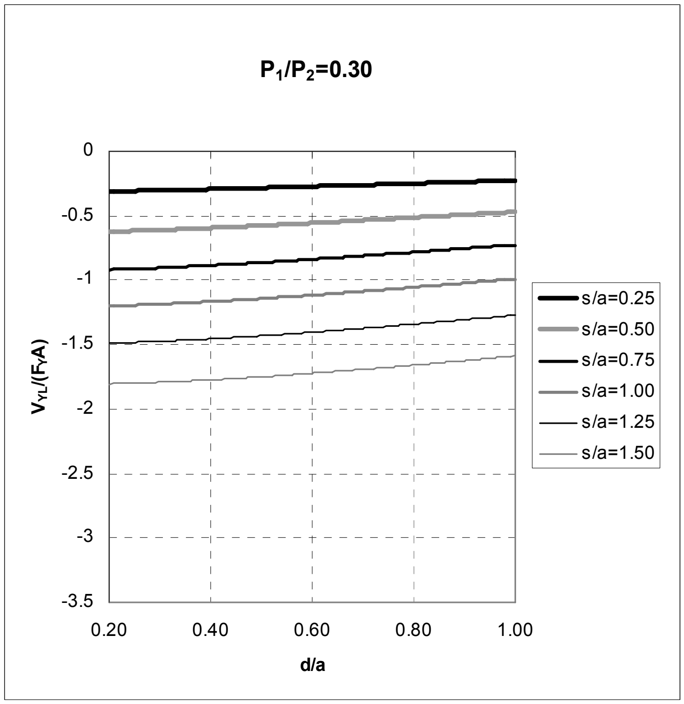

(a)

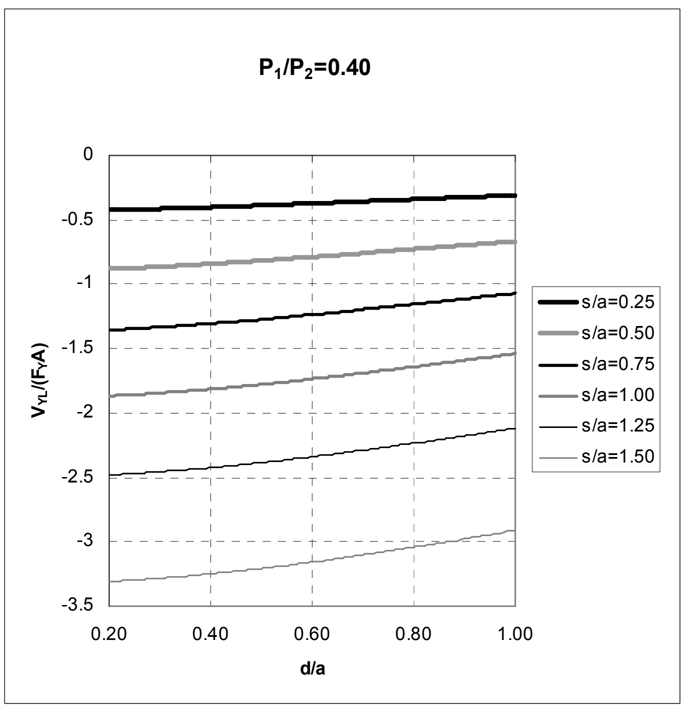

(b)

FIGURE 5-9 Nondimensional Longitudinal Base Shear Strength versus d/a Ratio When Short- Labeled Braces Yield: (a) For P_1/P_2=0.30; (b) For P_1/P_2=0.40

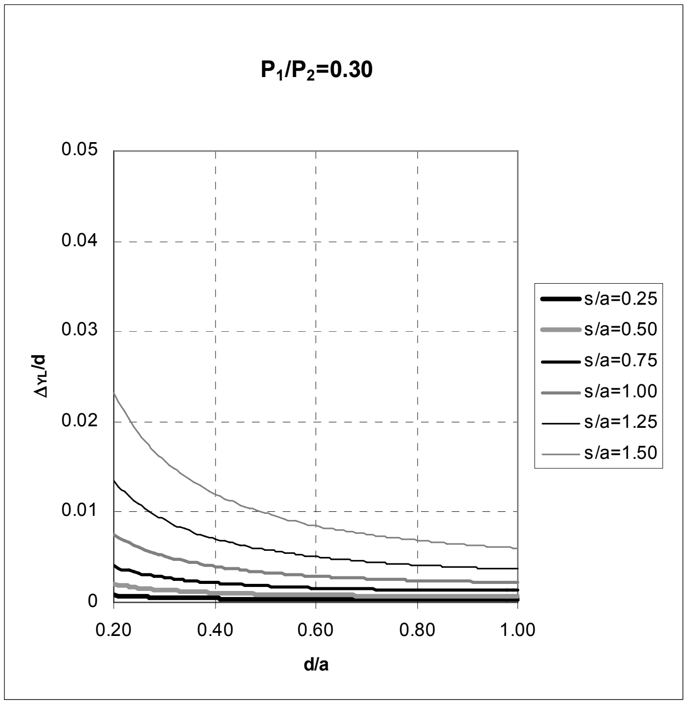

(a)

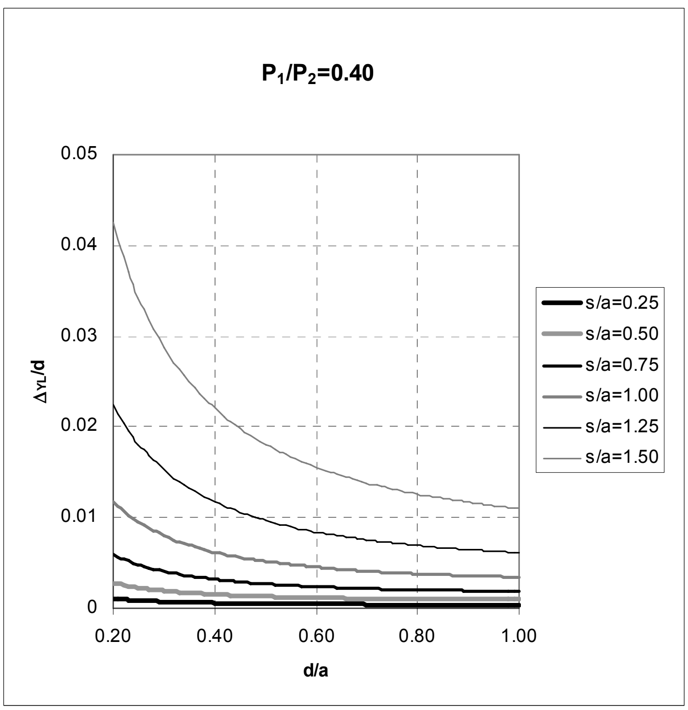

(b)

FIGURE 5-10 Longitudinal Drift versus d/a Ratio When Short- Labeled Braces Yield: (a) For P_1/P_2=0.30; (b) For P_1/P_2=0.40

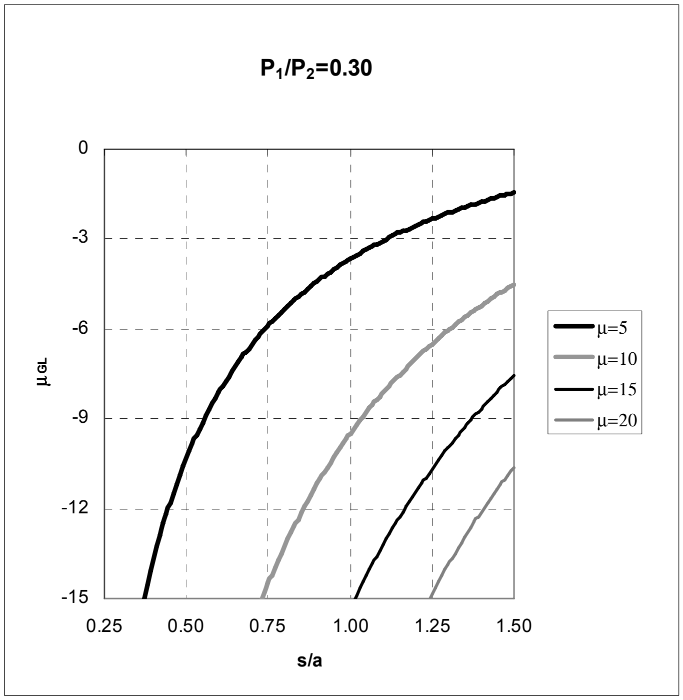

(a)

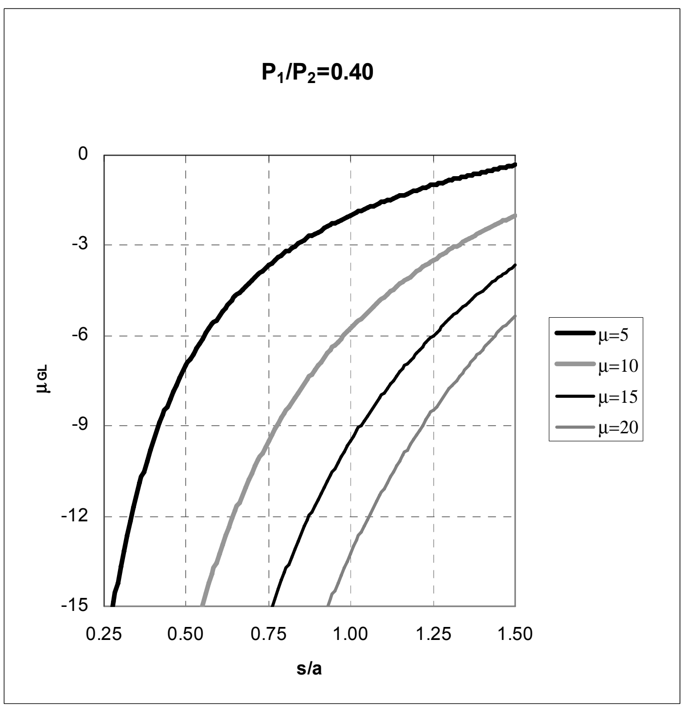

(b)

FIGURE 5-11 Global Longitudinal Ductility Ratio versus s/a Ratio and Local Ductility When Short- Labeled Braces Yield: (a) For P_1/P_2=0.30; (b) For P_1/P_2=0.40

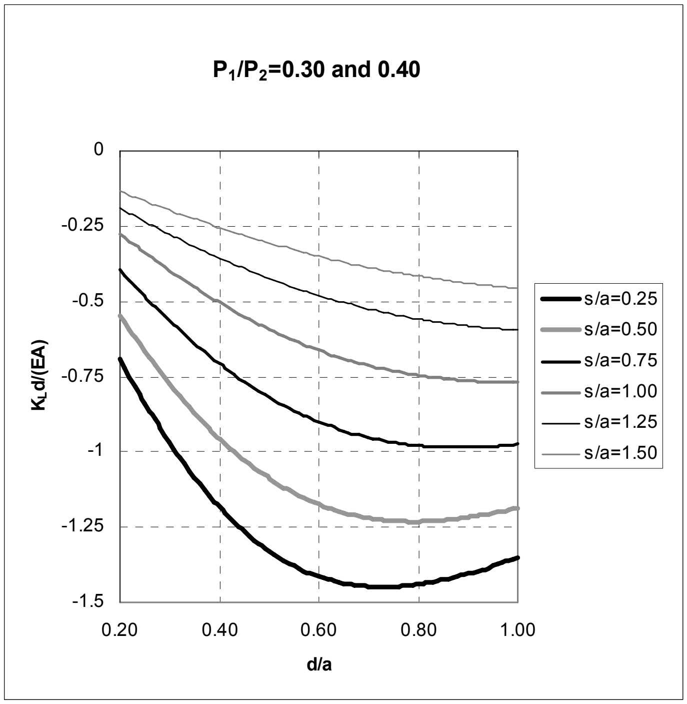

FIGURE 5-12 Nondimensional Longitudinal Stiffness versus d/a and s/a Ratios When Short- Labeled Braces Yield

5.2.5.1.2 Long-Labeled Braces Yield

Similar equations as obtained above can be reached when long-labeled braces yield.

5.2.5.1.2.1 Transverse Response

From Eq. (5-20a), the following is obtained:

$$V_{yT} = \left[\frac{4as}{LL(a+s\varepsilon)}\right](F_yA) \tag{5-45a}$$

The base shear strength in the transverse direction can be expressed using the nondimensional system geometric properties as:

$$V_{yT} = \left[\frac{4(s/a)}{\sqrt{1+(s/a)^2+(d/a)^2}\left[1+(s/a)\varepsilon\right]}\right](F_yA) \tag{5-45b}$$

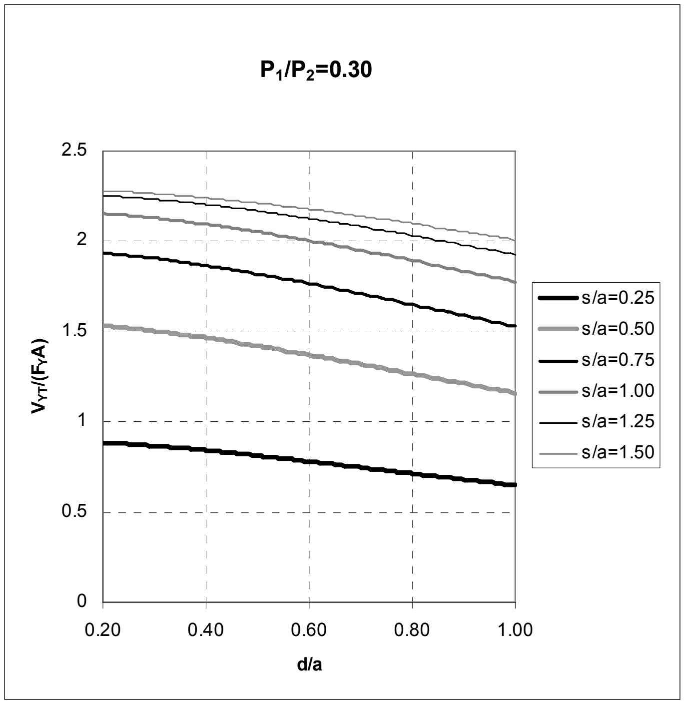

(a)

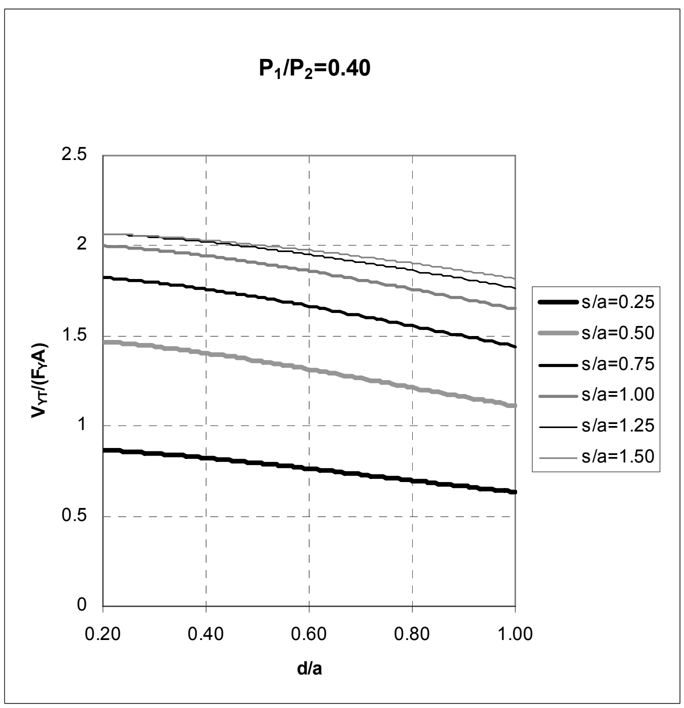

(b)

FIGURE 5-13 Nondimensional Transverse Base Shear Strength versus d/a Ratio When Long- Labeled Braces Yield: (a) For P_1/P_2=0.30; (b) For P_1/P_2=0.40

The lateral drift (Δ_T) in the transverse direction is

$$\frac{\Delta_T}{d} = \left[1 + (s/a)^2 + (d/a)^2\right]\frac{\left[(s/a)\varepsilon + 1\right]\mu - \left[(s/a)\varepsilon - 1\right]}{2(s/a)(d/a)\left[(s/a)\varepsilon + 1\right]}\left(\frac{F_y}{E}\right) \tag{5-46}$$

and the corresponding drift at yield is obtained by substituting μ=1 as

$$\frac{\Delta_{yT}}{d} = \frac{\left[1 + (s/a)^2 + (d/a)^2\right]}{(s/a)(d/a)\left[1 + (s/a)\varepsilon\right]}\left(\frac{F_y}{E}\right) \tag{5-47}$$

The global displacement ductility (μ_{GT}) of the system is

$$\mu_{GT} = \left[\frac{[1 + (s/a)\varepsilon]\mu + [1 - (s/a)\,\varepsilon]}{2}\right] \tag{5-48}$$

The initial stiffness of the system in the transverse direction can be written as :

$$K_T d = \left[\frac{4(s/a)^2(d/a)}{\left[1 + (s/a)^2 + (d/a)^2\right]^{3/2}}\right](EA) \tag{5-49}$$

5.2.5.1.2.2 Longitudinal Response

Similar equations can be obtained for the longitudinal direction.

The base shear strength in the longitudinal direction is:

$$V_{yL} = \left[\frac{-\,4(s/a)\,\varepsilon}{\sqrt{1 + (s/a)^2 + (d/a)^2}\,[(s/a)\varepsilon + 1]}\right](F_y A) \tag{5-50}$$

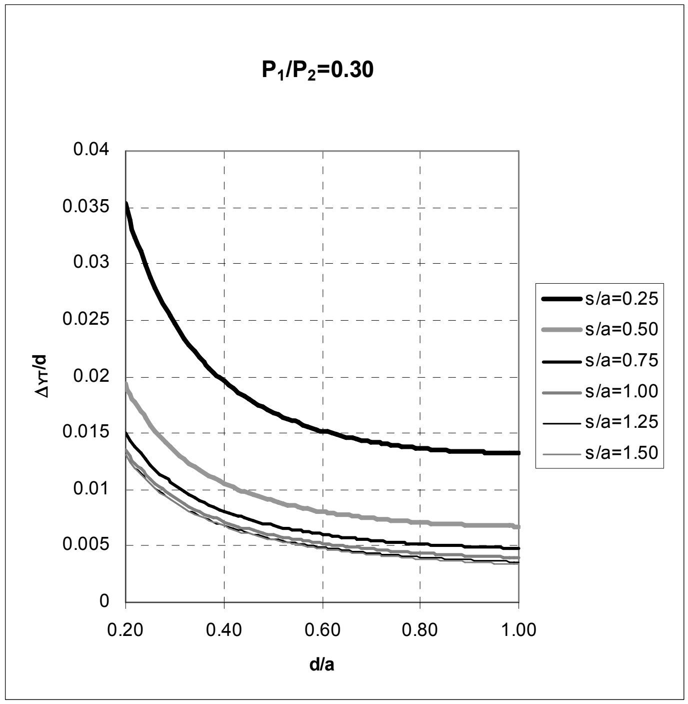

(a)

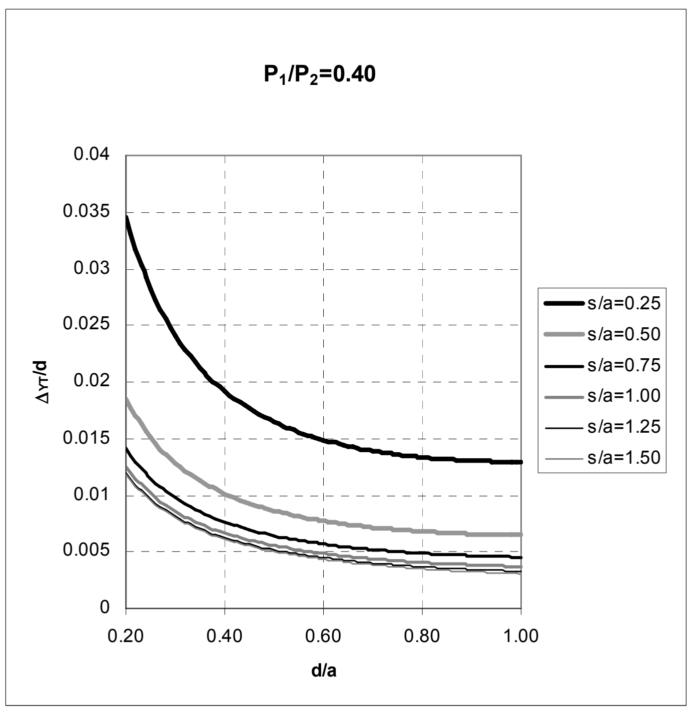

(b)

FIGURE 5-14 Transverse Drift versus d/a Ratio When Long- Labeled Braces Yield: (a) For P_1/P_2=0.30; (b) For P_1/P_2=0.40

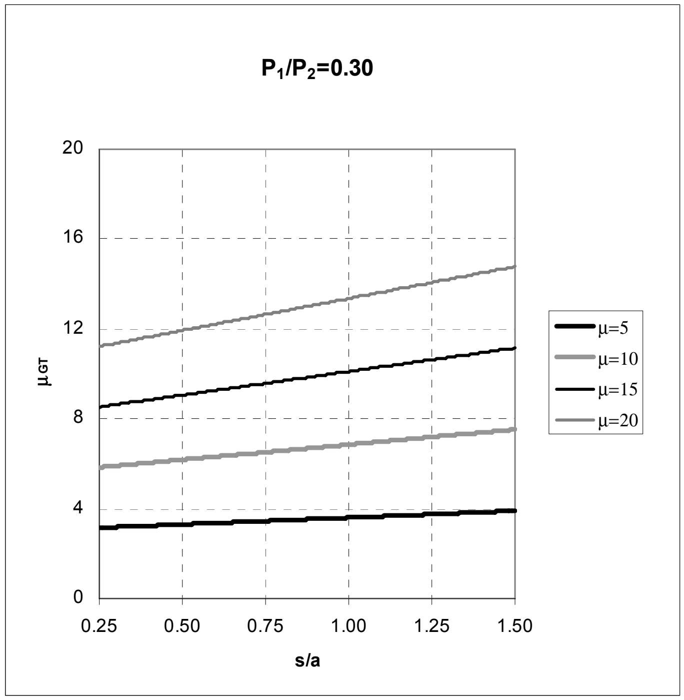

(a)

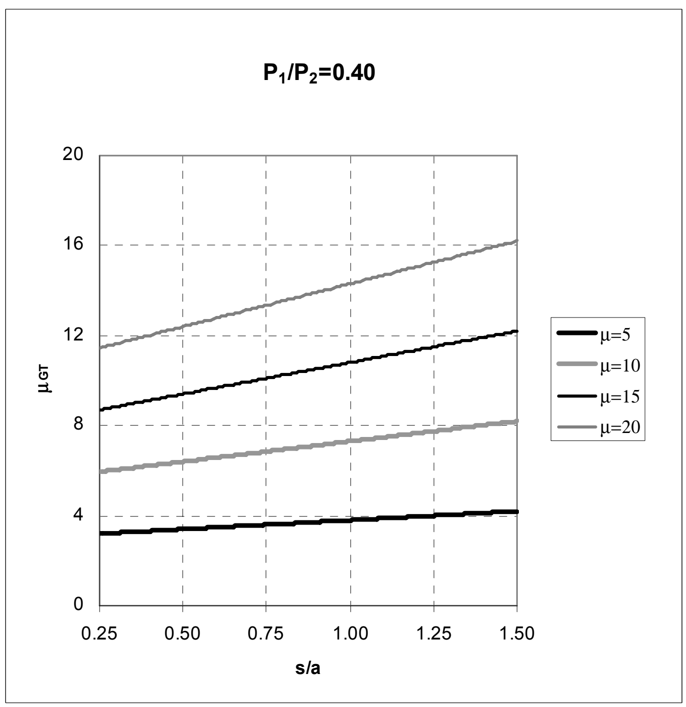

(b)

FIGURE 5-15 Global Transverse Ductility Ratio versus s/a Ratio and Local Ductility When Long-Labeled Braces Yield: (a) For P_1/P_2=0.30; (b) For P_1/P_2=0.40

The lateral displacement in the longitudinal direction is :

$$\frac{\Delta_L}{d} = \left[1+(s/a)^2+(d/a)^2\right]\frac{\left[1+(s/a)\varepsilon\right]\mu-\left[1-(s/a)\varepsilon\right]}{2(d/a)\left[(s/a)\varepsilon+1\right]}\left(\frac{F_y}{E}\right) \tag{5-51}$$

and the longitudinal drift at brace yielding is :

$$\frac{\Delta_{yL}}{d} = \frac{\left[1+(s/a)^2+(d/a)^2\right](s/a)\varepsilon}{(d/a)\left[1+(s/a)\varepsilon\right]}\left(\frac{F_y}{E}\right) \tag{5-52}$$

The global ductility in the longitudinal direction can be similarly derived as :

$$\mu_{GL} = \left[\frac{[(s/a)\varepsilon+1]\mu+[(s/a)\varepsilon-1]}{2(s/a)\varepsilon}\right] \tag{5-53}$$

The initial stiffness in the longitudinal direction becomes

$$K_L d = \left[\frac{-4(d/a)}{\left[1+(s/a)^2+(d/a)^2\right]^{3/2}}\right](EA) \tag{5-54}$$

Finally, volumetric hysteretic energy dissipated through a full cycle of displacement can be written as follows:

$$\frac{\sum E_H}{\text{Vol.}} = 2(\mu-1)\left(\frac{F_y^2}{E}\right) \tag{5-55}$$

For non-skewed bridges (φ=0º), in Retrofit Scheme-2 and when short-labeled braces yield, the base shear strength decreases as d/a increases for constant values of s/a and decreases as s/a decreases for constant values of d/a. Transverse drift (Δ_{yT}/d) decreases as d/a increases. For a constant value of d/a, the transverse drift decreases as s/a increases. Also, the change in drift is less for larger values of s/a ratios. Global transverse ductility (μ_{GT}) decreases as s/a increases. Expectedly, for constant values of s/a, the global ductility increases as the local (unbonded brace) ductility (μ) increases. Initial stiffness increases as d/a and s/a ratios increase. However, this increase is less after values of d/a=0.60. Similar behavioral tendency is observed in the longitudinal direction.

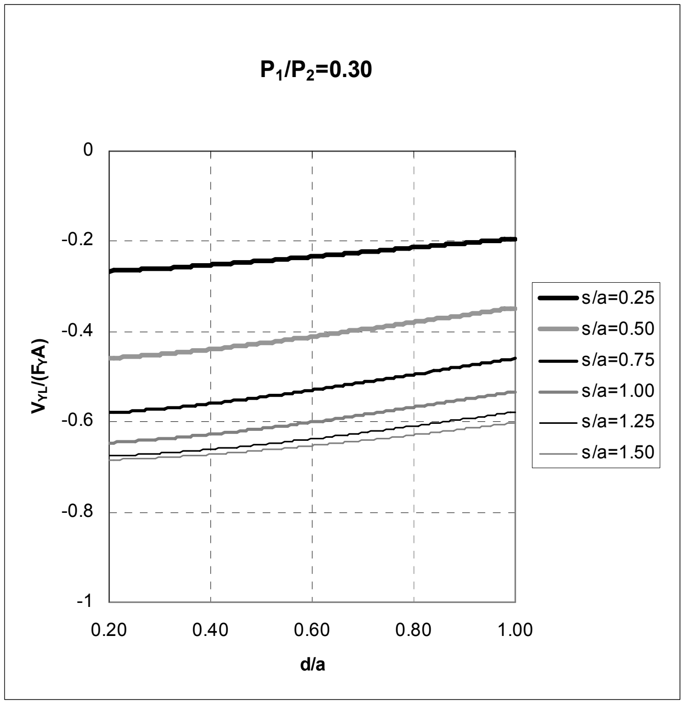

(a)

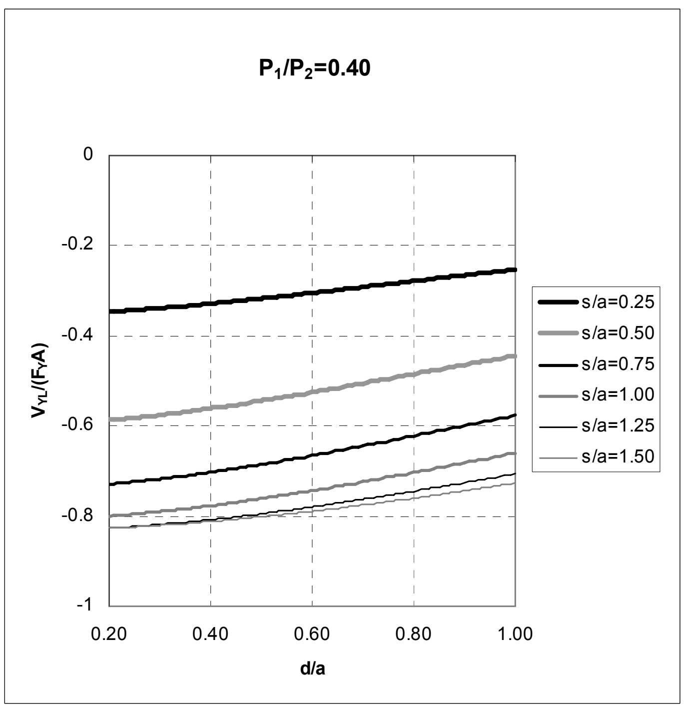

(b)

FIGURE 5-16 Nondimensional Longitudinal Base Shear Strength versus d/a Ratio When Long- Labeled Braces Yield: (a) For P_1/P_2=0.30; (b) For P_1/P_2=0.40

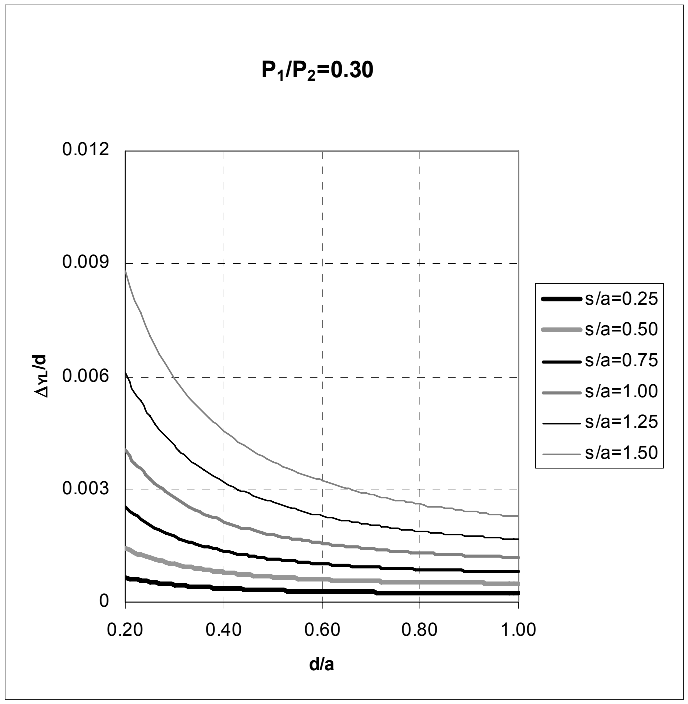

(a)

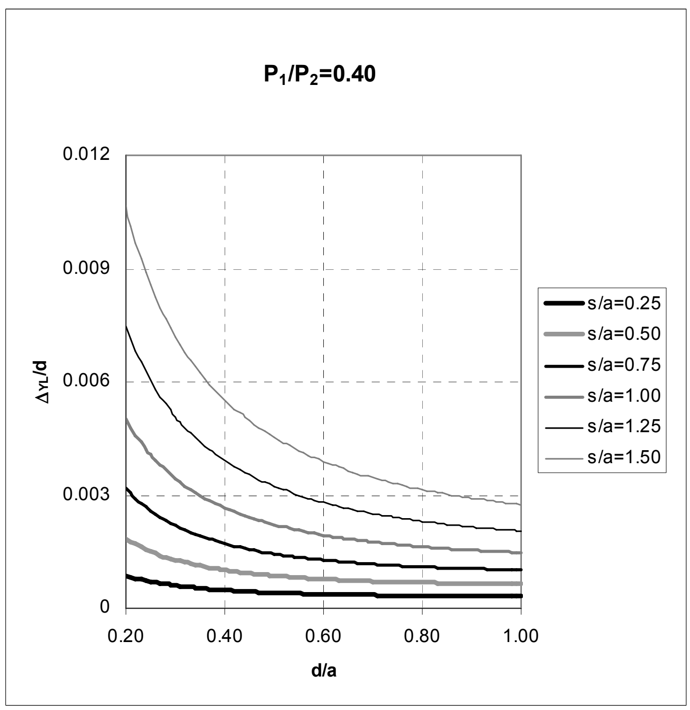

(b)

FIGURE 5-17 Longitudinal Drift versus d/a Ratio When Long- Labeled Braces Yield: (a) For P_1/P_2=0.30; (b) For P_1/P_2=0.40

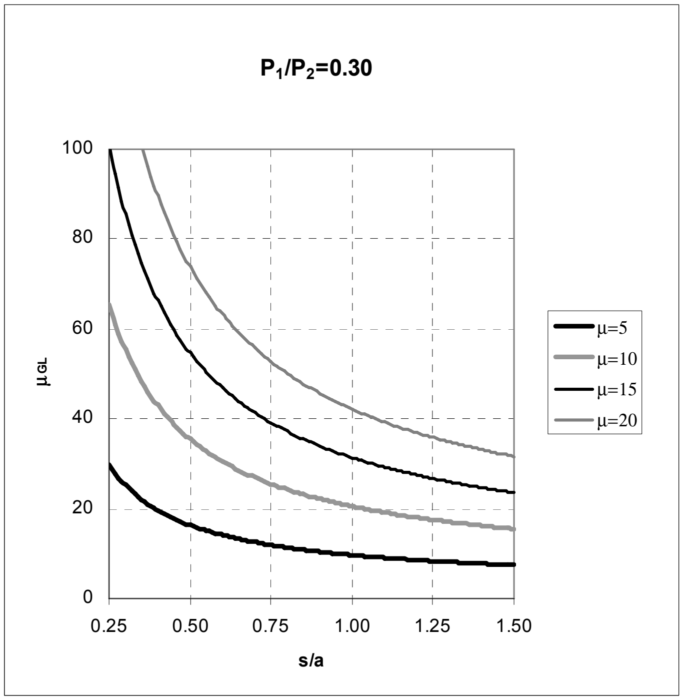

(a)

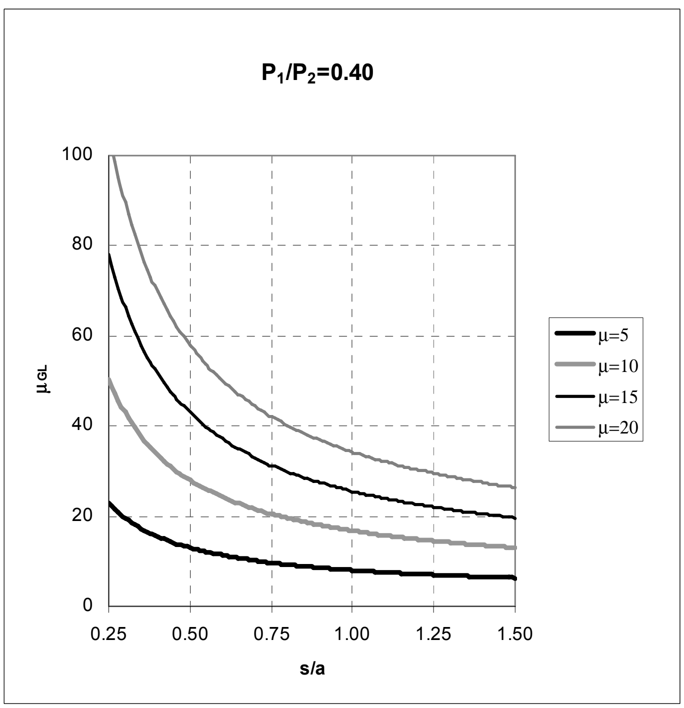

(b)

FIGURE 5-18 Global Longitudinal Ductility Ratio versus s/a Ratio and Local Ductility When Long- Labeled Braces Yield: (a) For P_1/P_2=0.30; (b) For P_1/P_2=0.40

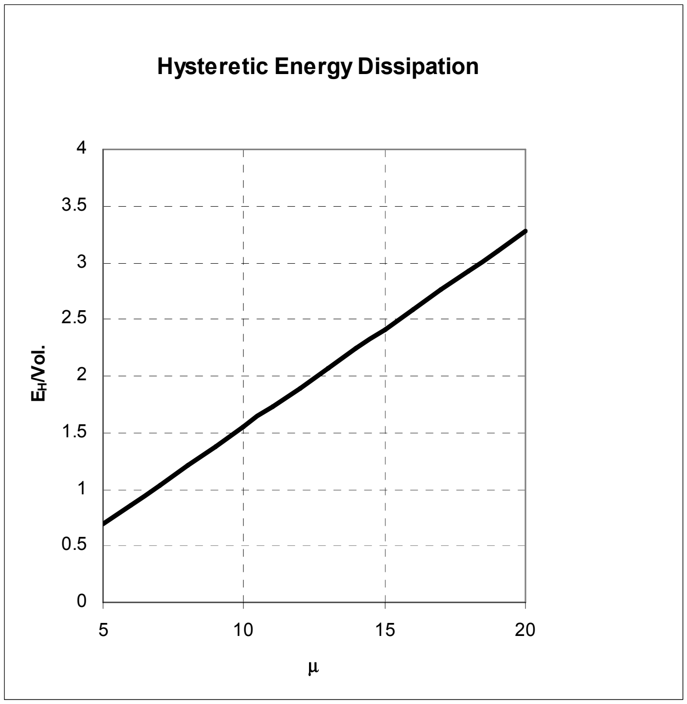

FIGURE 5-19 Variation of Volumetric Energy Dissipation versus Member (Unbonded Brace) Ductility

For non-skewed bridges ($\varphi=0^o$), in Retrofit Scheme-2 and when long-labeled braces yield, the tendency is the same as in the short-labeled brace yielding case, with an exception that global transverse ductility ratio (μ_{GT}) increases as s/a increases. Again, for constant values of s/a, the global ductility increases as the local (unbonded brace) ductility (μ) increases. Longitudinal base shear strength decreases as d/a increases. Longitudinal drift decreases as d/a increases and also decreases as s/a decreases. Global longitudinal ductility (μ_{GL}) decreases as s/a increases but increases as the local (unbonded brace) ductility (μ) increases. Hysteretic energy dissipation per volume increases as local ductility increases.

5.2.5.2 Special Case 2- Skewed Bridges ($\varphi\neq0^o$) with Certain Geometric Ratios (d/a and s/a)

The calculation of the ratio between the axial forces of long and short unbonded braces (before yielding) is necessary to determine the type of collapse mechanism. From Eqs. (5-9) to (5-11a,b), for skewed bridges in Retrofit Scheme 2, this ratio can be obtained as follows:

$$\frac{C_L}{C_S}=\frac{T_L}{T_S}=\sqrt{\frac{1+(s/a)^2+(d/a)^2+2(s/a)\sin\varphi}{1+(s/a)^2+(d/a)^2-2(s/a)\sin\varphi}}\;\frac{s/a(\sin\varphi-\varepsilon\cos\varphi)-1}{s/a(-\sin\varphi+\varepsilon\cos\varphi)-1} \tag{5-56}$$

Similarly, Eq. (5-56) includes four variables, namely s/a, d/a, φ and ε. As done before in case of Retrofit Scheme-1, one of the end diaphragm variables can be taken as s/a=0.50, 1.00, and 1,50 (possible average values as observed in many slab-on-girder bridges in North America), and then the variation of braces' forces ratio with respect to the skew angle can be investigated for different values of d/a and ε. Figure 5-20 shows the variation of brace axial forces ratio with bridge geometric relations.

The ratio of brace forces increases as the skew angle increases. As before, for small skew angles (say $\varphi\leq 25^\circ$), changes in d/a ratio have no significant effect on the force ratio in unbonded braces. For larger values of s/a, the effect of d/a ratio on the brace forces is negligible for practical skew angles. Note that the bidirectional loading ratio has an effect on the overall behavior.

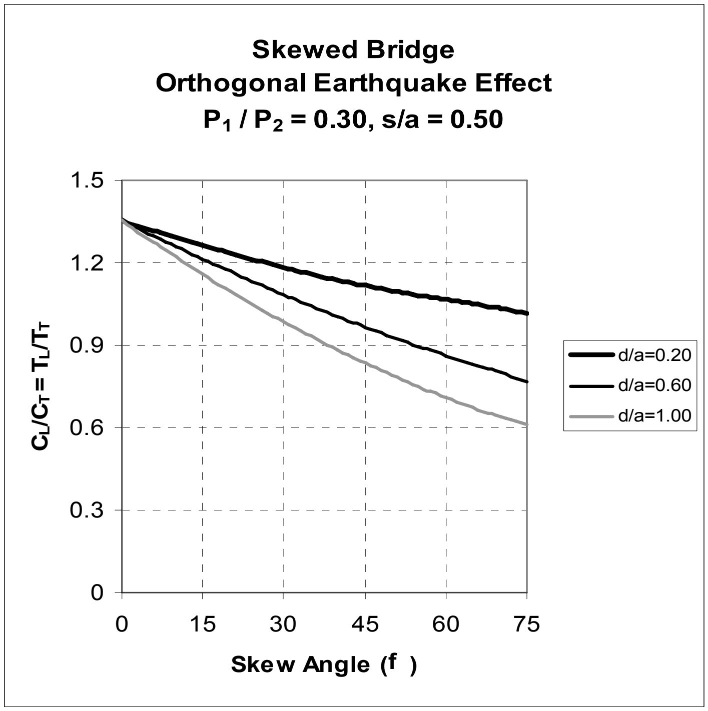

(a)

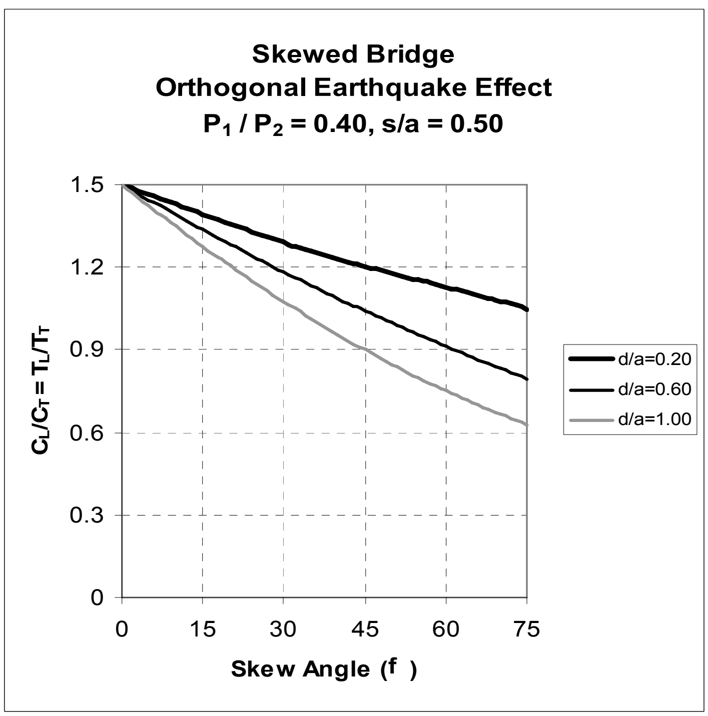

(b)

FIGURE 5-20 Variation of Brace Axial Forces Ratio with Bridge Skew Angle; (a) For P_1/P_2=0.30 and s/a=0.50; (b) For P_1/P_2=0.40 and s/a=0.50

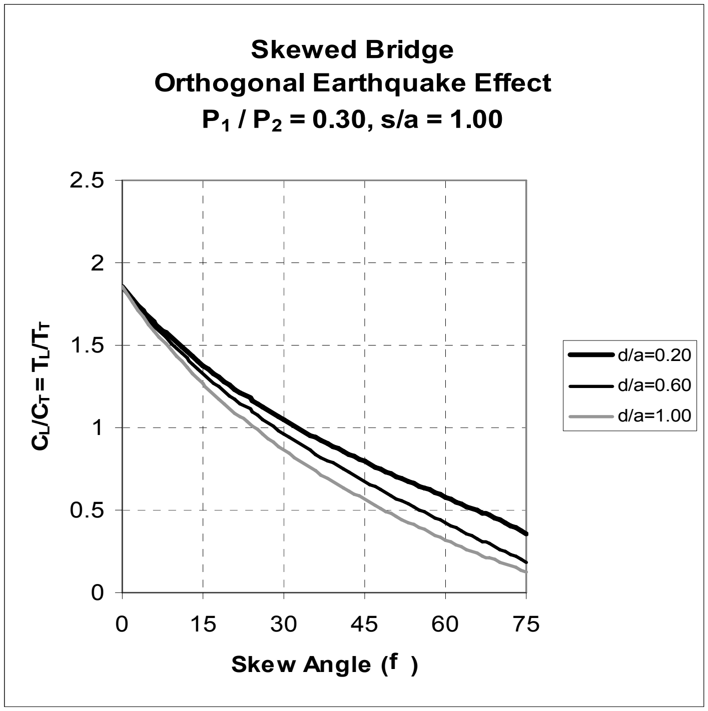

(c)

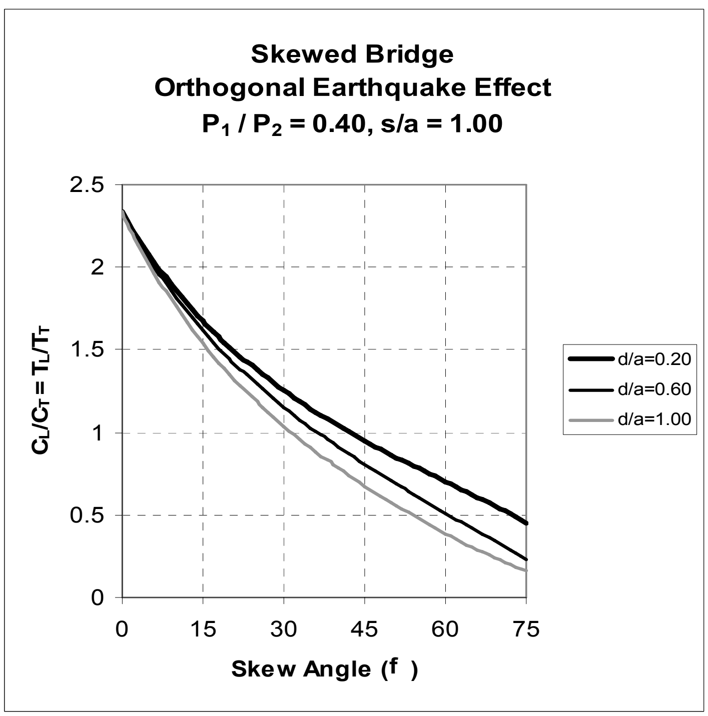

(d)

FIGURE 5-20 Variation of Brace Axial Forces Ratio with Bridge Skew Angle (continued); (c) For P_1/P_2=0.30 and s/a=1.00; (d) For P_1/P_2=0.40 and s/a=1.00

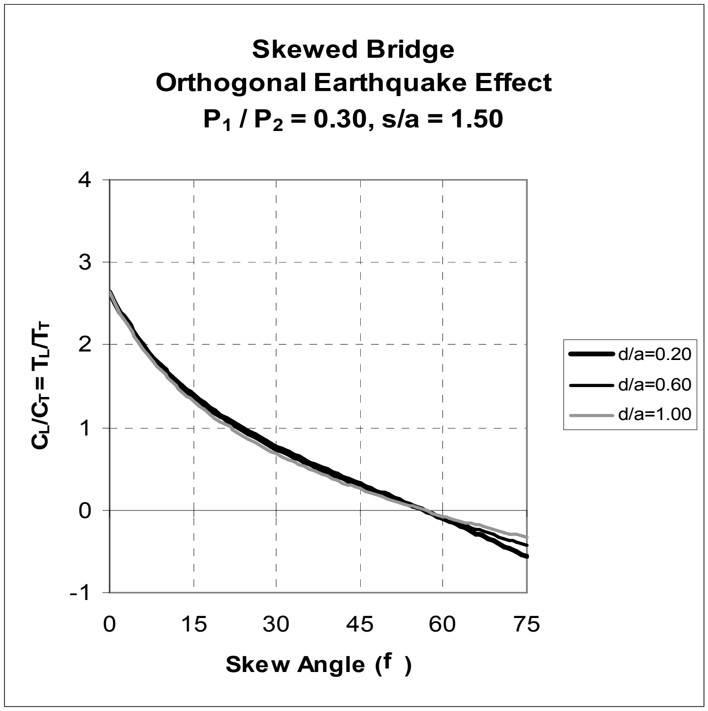

(e)

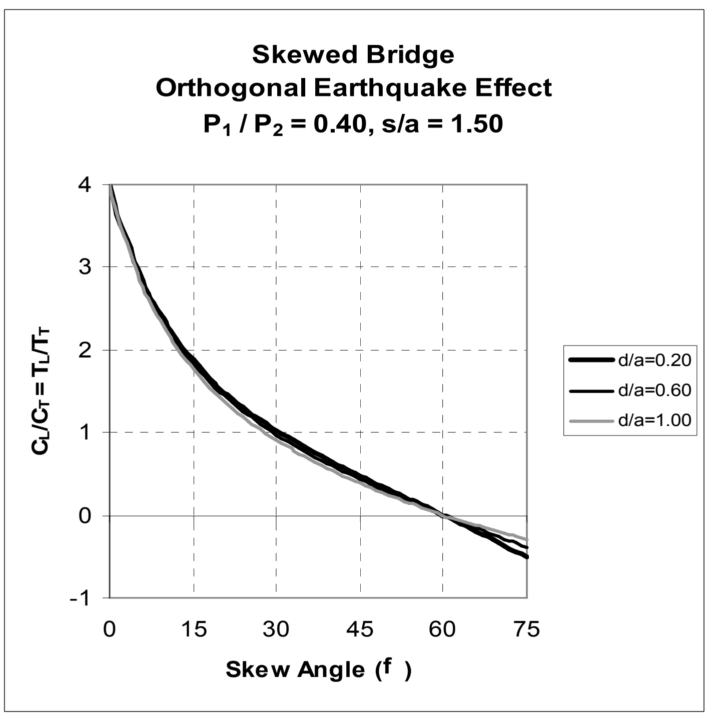

(f)

FIGURE 5-20 Variation of Brace Axial Forces Ratio with Bridge Skew Angle (continued); (e) For P_1/P_2=0.30 and s/a=1.50; (f) For P_1/P_2=0.40 and s/a=1.50

5.2.5.3 Special Case 3- Bridges with a Certain Skew Angle

Likewise, the previously derived formulas in general forms can also be simplified for certain values of the skew angle, φ, (e.g. 15^o, 30^o, 45^o, and 60^o). Also, for each skew angle, the bidirectional loading ratio can be taken as a variable. Some of these cases are investigated as numerical examples in Section 6.

5.3 Pushover Analysis of Retrofit Scheme-2 (Longitudinally Restrained Deck)

This section is devoted to the inelastic analysis of end diaphragms in Retrofit Scheme-2 when the bearings at one abutment are longitudinally restrained. This investigation is of importance for bridge superstructures with undamaged bearings. In this case, the idealized system becomes statically indeterminate since the number of unknowns (i.e. the axial forces of unbonded braces) exceeds the number of equilibrium equations. Compatibility and force displacement requirements are used to obtain these unknowns (or redundant unbonded braces axial forces). As done before, the principle of virtual work (or the unit load method) is used to evaluate lateral displacements in the system. Per the analysis procedure, external virtual unit load is applied in the direction of unknown top displacement (Figure 5-21).

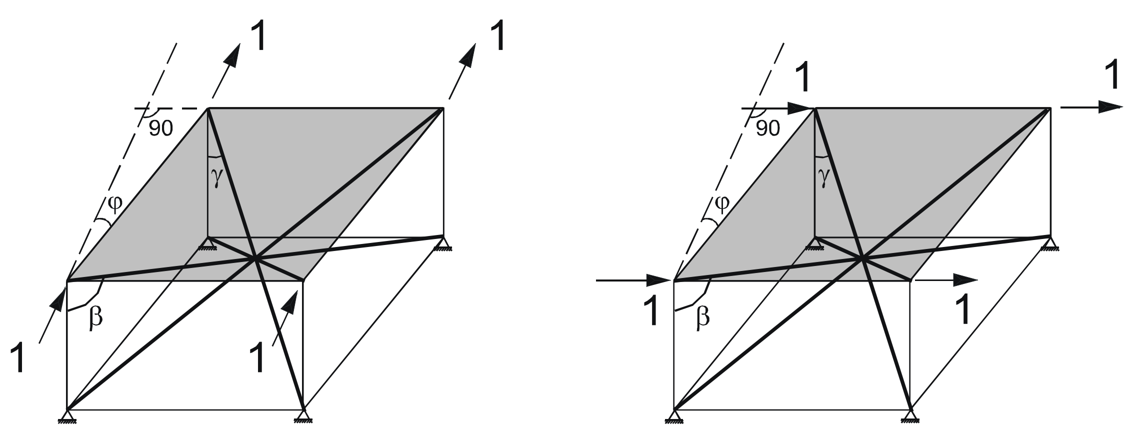

FIGURE 5-21 Typical Virtual Unit Loading

The procedure for analysis is summarized below:

- Place the virtual unit load in the direction where the desired displacement is needed.
- Calculate virtual internal forces in each unbonded brace.
- Determine the real internal forces caused only by the real loads acting on the system.
- Apply the equation of virtual work to determine the desired displacement by equating the work of external loads and the work of internal loads.

Once these forces have been determined, the remaining reactive forces on the system are obtained by satisfying the equilibrium requirements.

In longitudinally restrained deck systems, the limit state is reached when all braces (both short and long) yield progressively and the load-displacement curve becomes a tri-linear curve (Figure 5-22). Upon lateral loading in the transverse direction, the short and long unbonded braces yield at top displacements of Δ_{y1} and Δ_{y2} respectively. The corresponding base shear forces for these displacements are V_{y1} and V_{y2}. Since the braces have the same cross sectional areas, for a specified yield stress for steel, the axial yield strengths of the braces and the corresponding displacements are known which helps construct this tri-linear hysteretic curve as shown in Figure 5-22. The system unloads at a stiffness equals to the elastic (initial) stiffness. Fuller hysteretic loops and greater energy dissipation can be expected in longitudinally restrained deck systems since all braces yield and contribute to strength and energy dissipation.

Due to the geometric properties and loading, yielding first occurs in the short unbonded braces and the coordinates of the first yield point on the curve are obtained as:

$$V_{y1} = \frac{2s\cos\varphi(LL^3 + LS^3)}{LSLL^3}(F_y A) \tag{5-57}$$

$$\Delta_{y1} = \frac{LS^2}{s\cos\varphi}\left(\frac{F_y}{E}\right) \tag{5-58}$$

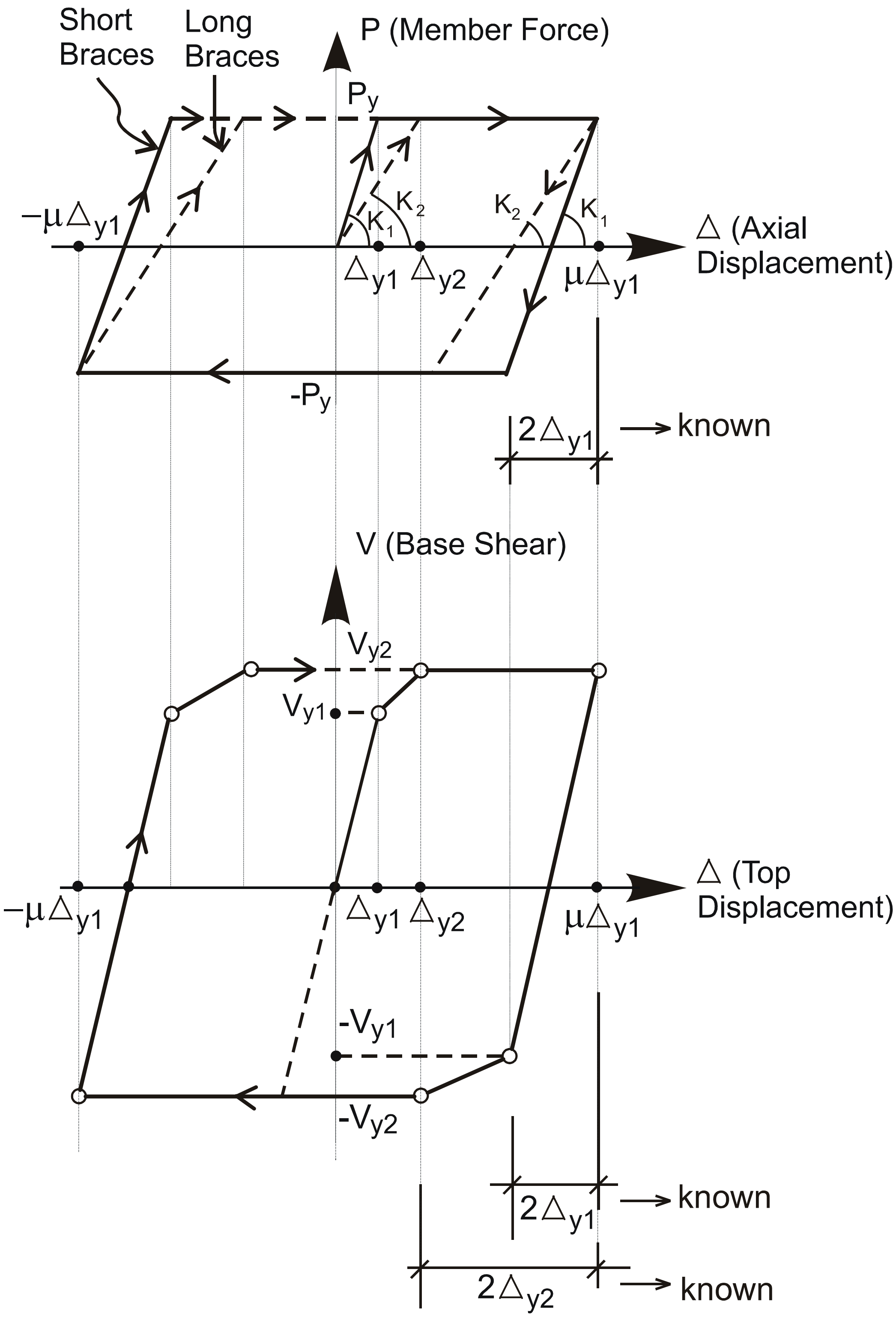

FIGURE 5-22 Tri-Linear Hysteretic Behavior of Retrofit Scheme-2 with Longitudinally Restrained Deck

Similarly, when the long braces yield, coordinates of the second point on that curve are :

$$V_{y2} = 2s\cos\varphi\left(\frac{LL + LS}{LSLL}\right)(F_y A) \tag{5-59}$$

$$\Delta_{y2} = \frac{LL^2}{s\cos\varphi}\left(\frac{F_y}{E}\right) \tag{5-60}$$

The initial transverse stiffness can be obtained using Eqs. (5-57) and (5-58) as follows:

$$K_T = \frac{2s^2\cos^2\varphi(LL^3 + LS^3)}{LL^3 LS^3}(EA) \tag{5-61}$$

The hysteretic curve has three geometrically different regions as shown in Figure 5-23a. These are depicted by E_{H1}, E_{H2} and E_{H3}. Total dissipated energy in an inelastic excursion (accounting for three regions) can be written as:

$$E_H = E_{H1} + E_{H2} + E_{H3} \tag{5-62}$$

Since the equations for both base shear and corresponding displacements have been developed above, dissipated energies can be obtained depending on system's material and geometric properties as well as the local ductility of each unbonded brace member.

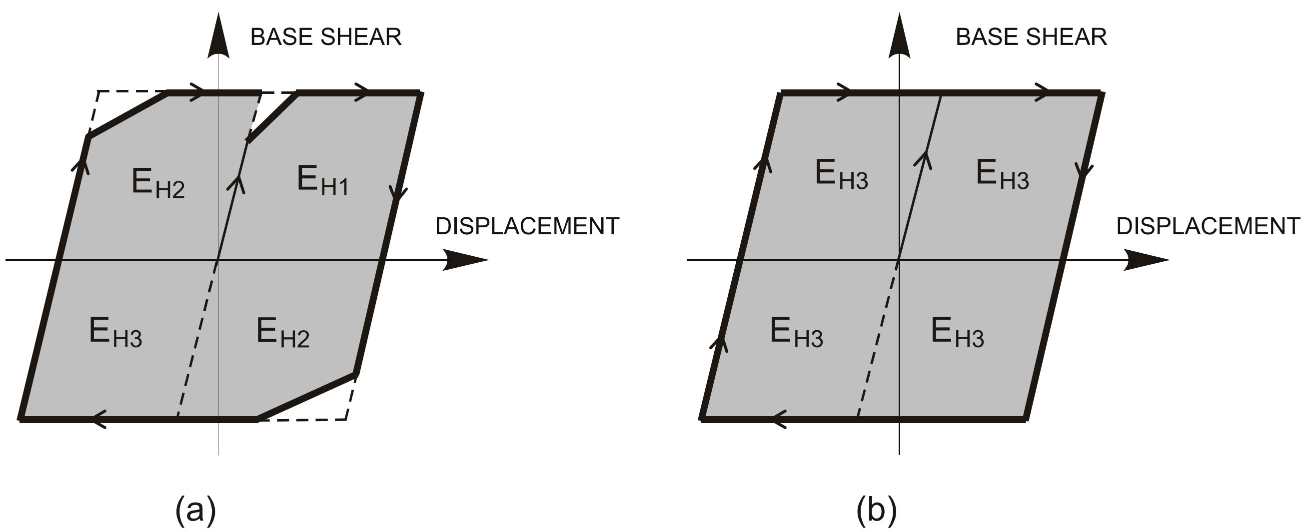

FIGURE 5-23 Dissipated Hysteretic Energy in Retrofit Scheme-2 with Longitudinally Restrained Deck: (a) Tri-Linear Model; (b) Bi-Linear Model (Ideal Hysteresis)

By this way, using Eqs.(5-57) through (5-62), Eq. (5-62) can be re-written as follows:

$$E_H = \frac{\left[6(LL^3+LS^3)(LL+LS)LS\right]\mu - \left[5LL^5+6LL^4LS+2LL^3LS^2+6LL^2LS^3+5LLLS^4\right]}{(LL^3+LS^3)LL}\left(\frac{F_y^{\,2}A}{E}\right) \tag{5-63}$$

Note that, for non-skewed bridges (i.e. φ=0º and LL=LS), all braces yield at the same displacement level and the dissipated energies in each region become equal (i.e. $E_{H1} = E_{H2} = E_{H3}$ as shown in Figure 5-23b). In this case, substituting LL=LS gives the total dissipated energy as

$$E_H = 12LL(\mu-1)\left(\frac{F_y^{\,2}A}{E}\right) \tag{5-64}$$

Eq. (5-63) can be further simplified for end diaphragm systems under repeated cyclic loadings. Four regions of the hysteretic curve (i.e. a full cycle) will be considered. Since the energy dissipation corresponding to E_{H1} occurs only once under severe cyclic displacements, this region can be assumed approximately equal to E_{H3}. Using this assumption, the total dissipated energy during a full cycle can be given by :

$$E_H \cong 2(E_{H2}+E_{H3}) \tag{5-65}$$

When the number of cycles increases, the error resulting from this simplification in computing the total dissipated energy would be negligible. The following simpler equation for the total energy is reached:

$$E_H \cong 8(LL+LS)\left[\frac{LS}{LL}\mu-1\right]\left(\frac{F_y^{\,2}A}{E}\right) \tag{5-66}$$

For ¼ cycle, the dissipated energy equals:

$$E_{H,1/4} \cong 2(LL+LS)\left[\frac{LS}{LL}\mu-1\right]\left(\frac{F_y^{\,2}A}{E}\right) \tag{5-67}$$

Energy dissipation efficiency with respect to an unpinched hysteretic curve shown in Figure 5-23b can also be evaluated. For this, $E_{H,\,1/4}$ and E_{H3} can be compared by setting up the ratio of $E_{H,\,1/4}$ / E_{H3}. After simplifications, this ratio gives the following :

$$\frac{E_{H,1/4}}{E_{H3}} = \frac{\left(\frac{LS}{LL}\right)\mu - 1}{\left(\frac{LS}{LL}\right)\mu - \left[\frac{(LL+LS)LSLL}{LL^3+LS^3}\right]} \tag{5-68}$$

This procedure is numerically investigated in an example in Section 6.

SECTION 6
NUMERICAL EXAMPLES

6.1 General

This section presents numerical examples related to the modeling issues and end diaphragms concepts presented in the previous sections. Both numerical results from SAP2000 and closed-form solutions that express the inelastic behavior of bridge end diaphragms are evaluated. Some special cases are considered (such as different bidirectional loading ratios, various end diaphragm geometries, and the two retrofit schemes) to illustrate the particular behavioral characteristics of different specific systems. The design intent is to obtain the most appropriate retrofit scheme for a given bridge superstructure. The numerical examples are provided to hopefully make such a comparison possible.

6.2 Examples

6.2.1 Example 1

In this example, six systems, namely S1 through S6, representing the bridge end diaphragms are selected to numerically show the impact of several structural parameters on the inelastic behavior of the systems considered. Special emphasis is placed on hysteretic energy dissipation. The numerical results of this example are useful to preliminary assess the effects of various unbonded bracing configurations on the seismic behavior of bridge end diaphragms. The descriptions of all six systems considered in this example are given below:

S1 is a non-skewed system (φ=0º) having single unbonded braces in only one direction (in the transverse, X, direction) at each end of the superstructure. This scheme corresponds to what has been done so far in the existing ductile retrofit concepts and can serve as one reference system. This system is effective only for unidirectional earthquake loading and does not provide strength in the longitudinal direction.

S2 is a non-skewed system (φ=0º) with a three dimensional unbonded braces configuration at each end of the bridge superstructure. Since the system is not skewed, both diagonal braces' lengths are equal in this case. Unlike S1, S2 provides strength to resist bidirectional loading.

Comparing the dissipated energies obtained from the analyses of S1 and S2 can provide preliminary insight into the structural behavior of systems having different bracing configurations (even though it is recognized that system S1 can be incomplete for the purpose of resisting bidirectional earthquake excitations in some cases).

S3 is a non-skewed system (φ=0º) with unbonded braces in two orthogonal directions. This system is expanding on the concept of S1 in that unbonded braces are located in the principal orthogonal directions (two braces in each direction in this case). Note that this system corresponds to Retrofit Scheme-1 illustrated in Figures 3-3 and 3-7 (i.e. one of the proposed retrofit schemes investigated analytically throughout this report). This system (as opposed to S1) can resist bidirectional earthquake loading.

S4 is a non-skewed system (φ=0º) with four equal length diagonal unbonded braces connecting the top and bottom corners of the cube. This system corresponds to the second proposed retrofit scheme (Retrofit Scheme-2) schematically illustrated in Figures 3-4 and 3-8. Comparison between S3 and S4 is key in this study to identify the most appropriate scheme that could be used for the seismic retrofit of bridge superstructures.

S5 is a skewed system (φ=45˚) having unbonded bracing configuration similar to that of Retrofit Scheme-1. S6 is a skewed system (φ=45˚) having unbonded bracing configuration similar to that of S4, except that because of the skew angle, the lengths of the unbonded braces are not equal to each other (thus “short” and “long” braces exist). This also corresponds to Retrofit Scheme-2 for skewed systems. Comparison between S5 and S6 is also important to assess the relative effectiveness of the two proposed unbonded bracing end diaphragm configurations on the inelastic behavior for skewed systems. Comparison between S3 and S5, as well as S4 and S6, is also worthwhile to illustrate how the presence of skew affects the results for both systems.

Figure 6-1 shows the selected six systems having various unbonded braces configurations described above. The geometrical dimensions of these systems are arbitrarily selected for simplicity and not intended to correspond to a specific bridge. For this purpose, a cube having a side length of 914.4mm (36”) is selected for the analyses. Both straight (non-skewed) and skewed

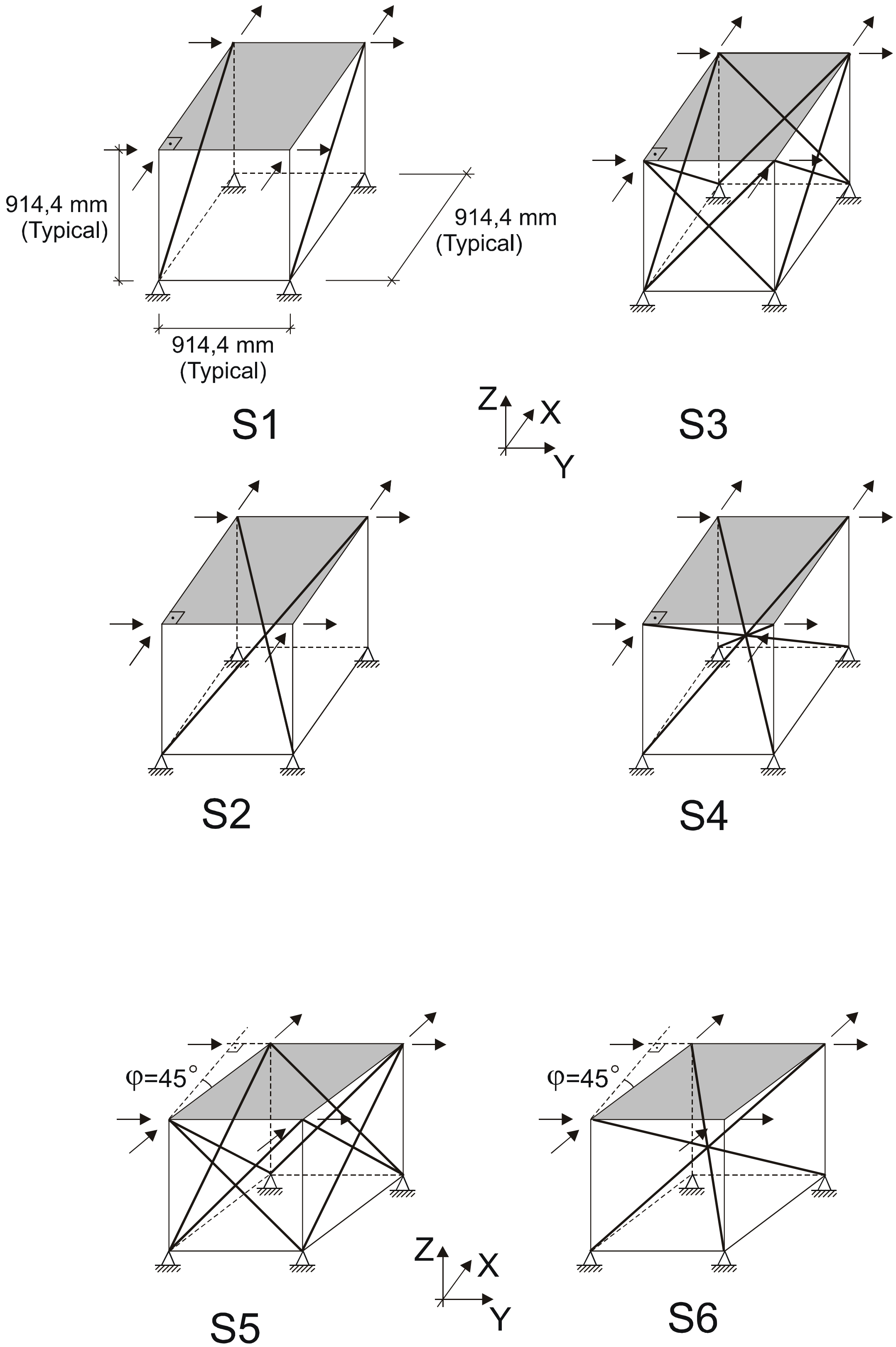

FIGURE 6-1 Selected Systems Representing Various End Diaphragm Bracing Configurations (For Table 6-1 and 6-2)

systems (with a skew angle of φ=45°) are taken into account. Again, both unidirectional and bidirectional loadings are considered to show the effect of bidirectional earthquake effects. All supports are taken as simple supports. In the analyses, the unbonded braces used are assumed to be pinned at their ends, and they are assumed to exhibit an axially yielding (elastic-plastic) hysteretic behavior with no strain hardening and with equal tension and compression capacities (i.e. T_y=C_y), although not quite the case in practice.

Figure 6-2 shows three skewed systems having various unbonded bracing configurations. They are conceptually all identical to S5, but with single braces in each plane (instead of two). These systems will exhibit identical structural behavior when all brace members have symmetric cyclic hysteretic characteristics (i.e. T_y=C_y).

In this example, it is further assumed that the unbonded braces have a target displacement ductility of μ=4, a yield point of F_y=345MPa (50 ksi), and a modulus of elasticity of E=200000MPa (29000 ksi). Other system properties are summarized in Tables 6-1 and 6-2.

Static unidirectional (in X or Y directions) and bidirectional (in X and Y directions, labeled X+Y in the Tables) pushover analyses are conducted using SAP2000. Note that X and Y indicate the transverse and longitudinal directions respectively. Using SAP2000 results and the formulas developed in the previous sections, the system parameters and responses of each system are summarized in Tables 6-1 and 6-2.

To compare the effectiveness of each system, similar systems are defined as having either braces with same cross sectional area (SA), braces with the same base shear strength in the governing direction (SBS), and braces with the same initial stiffness (SIS). For each case, results are typically presented for the base shear at yield (V_B) in the governing direction (X or Y in cases as depicted in the Tables), the corresponding yield displacement (Δ_y), the corresponding maximum displacement reached (Δ_{max}), hysteretic energy dissipated (E_H) at an assumed brace (or member) displacement ductility of μ=4, the corresponding volumetric energy dissipation (E_H/Vol.) which is the energy dissipated per unbonded brace material used, and the effectiveness ratio (with respect to an arbitrarily chosen reference system having similar properties) of each system in

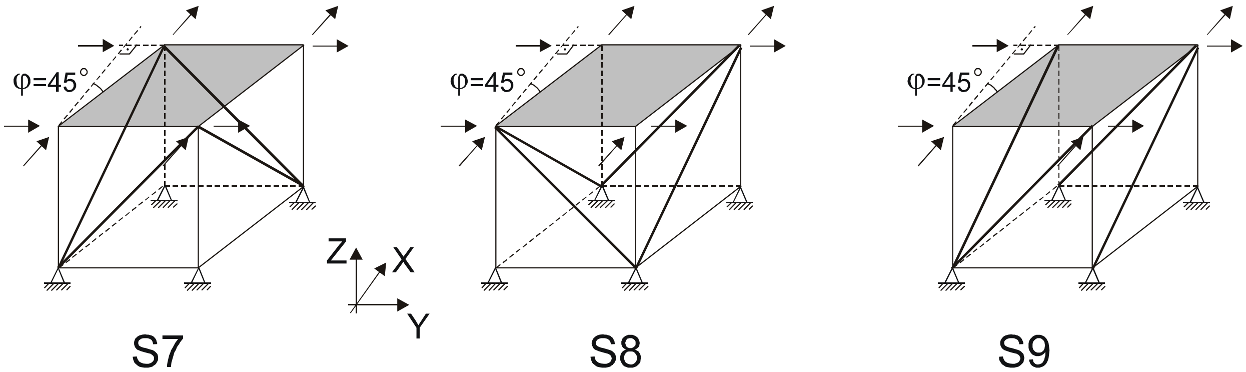

FIGURE 6-2 Various End Diaphragm Unbonded Bracing Configurations Showing Identical Behavior

terms of hysteretic energy dissipation. Note that E_H is calculated here using the area under ¼ of a complete hysteretic loop as illustrated in Tables 6-1 and 6-2.

The following observations can be made from Tables 6-1 and 6-2:

For non-skewed bridges (φ=0) *end diaphragm systems as represented by S1, S2, S3, and S4:*

- For unidirectional loading (in X direction) and braces having the same cross sectional area (SA), S3 has obviously twice the initial stiffness (K_E), base shear capacity (V_B), and total hysteretic energy dissipation (E_H) of S1 which is expected since S3 has twice the number of braces in a given transverse direction. These values become identical when S1 and S3 are normalized to the same base shear. Note that volumetric hysteretic energy dissipations (E_H/Vol.) are calculated using all braces, but that for uniaxial excitations, half of the braces are inactive for the case S3 (the unbonded braces in the longitudinal (Y) direction are not active and do not dissipate any energy).
- For braces having the same cross sectional area, comparing S1 and S2 subjected to unidirectional loading (in X direction), S2 has lower base shear capacity and initial stiffness, but greater yield and maximum displacements and total energy dissipation. As a result, the corresponding volumetric energy dissipation values are identical. Thus, their effectiveness is identical. For systems having the same initial stiffness, compared to S1,

S2 has greater base shear capacity, yield and maximum displacements, total energy dissipation, and required cross sectional area. However, since 126% more material is used in S2, the resulting volumetric energy dissipations are equal. Similarly, equal volumetric energy dissipation results are obtained for systems normalized by base shear.

- Under unidirectional loading and for the same cross sectional area, S4 has twice the initial stiffness, base shear capacity, and total hysteretic energy dissipation of S2, but the values of volumetric energy dissipation are equal since 100% more bracing material is used in S4. Note that yield and maximum displacements are also equal. For the cases of identical base shear and equal initial stiffness, identical volumetric energy dissipations are again obtained following a similar logic.
- Under unidirectional loading and for the same cross sectional area, compared to S4, S3 has greater initial stiffness and base shear capacity but lower total and volumetric hysteretic energy dissipations and yield and maximum displacement capacities. 63% more bracing material is used in S3 (i.e. shorter braces in S3, but more of them). For the same base shear, compared to S4, S3 has greater initial stiffness but lower required cross sectional area, yield and maximum displacements, total and volumetric hysteretic energy dissipation. In this case, 33% more bracing material is used in S3. For the same initial lateral stiffness in the direction of loading, compared to S3, S4 has greater base shear capacity, the yield and maximum displacements, and total and volumetric hysteretic energy dissipations. Compared to S3, S4 has also greater required cross sectional area. In this case, 12% more bracing material is used in S4. In all cases, the volumetric energy dissipation is always twice for S4 than S3. However, note that under unidirectional loading, when the volumetric ratios of hysteretic energy dissipation in S4 are greater than for S3, the braces in the orthogonal direction to the loading direction are inactive (unloaded) and do not dissipate any energy. It could be argued that a more fair comparison for the unidirectional loading case would discount these inactive unbonded braces. In such case, S3 and S4 would share identical values of E_H/Vol.
- For bidirectional and orthogonal loading, with the same intensity of loading in each direction (in X and Y directions, the loading ratio is ε=1.00), for the case in which all unbonded braces have the same cross sectional area, compared to S4, S3 has greater initial stiffness, base shear capacity, and total and volumetric hysteretic energy dissipations.

Note that 63% more bracing material is used in S3. For the same base shear capacity, compared to S4, S3 has greater yield and maximum displacements, total and volumetric energies but lower initial stiffness and required cross sectional area. In this case, 50% more bracing material is used in S4. However, note that in both cases, when brace ductility reaches a value of μ=4 (the premise of how the data in this table were derived) S4 consistently dissipated less total hysteretic energy (as a system) than S3, and less volumetric hysteretic energy (exactly half). This is probably partly a consequence of the fact that S4 has half fewer braces than S3 (4 versus 8). This is some what similar to the observation made comparing S2 and S4. Given that braces dissipate energy by axial elongation, the yield threshold is not sensibly affected by the number of braces (compare S2 to S4). Overall, for a given required design base shear in each direction, S3 achieves the same displacement demand performance than S4 (i.e. μ=4) with a lesser volume of material (while providing braces in an X configuration in both cases). The orthogonal brace configuration therefore seems to be more effective. On the other hand, S4 has the advantage over S3 (again for the case of same design base shear) to result in a more flexible ductile diaphragm, which can be advantageous when trying to implement the system in bridges having relatively flexible substructures in which the diaphragms need to reach a larger lateral displacement for the given ductility (see Alfawakhiri and Bruneau, 2000 and 2001). However, note that highly flexible (in transverse or longitudinal directions) unbonded bracing end diaphragm systems must also be checked to prevent the occurrence of excessive drift and deformations in other parts of the bridge superstructure (such as in deck truss bridges for example). In stiff substructures, it is implicit that both retrofit schemes can be used. Finally, the smaller braces that result from case S3 will develop smaller yield forces than those in S4, resulting in simple connections to superstructure and substructure (although using a larger number of unbonded braces is always possible to minimize this problem).

For skewed bridges (φ=45˚) *end diaphragm systems as represented by S5 and S6*:

- As stated above, S5 and S6 represent previously defined Retrofit Schemes 1 and 2 (with skew) respectively. From Table 6-2, under the loading in X direction and for the same cross sectional area, compared to S6, S5 has greater base shear strength, yield and maximum displacement demands as well as total and volumetric hysteretic energies, but lower initial stiffness. 68% more bracing material is used in S5. For the same base shear in the transverse direction, compared to S6, S5 has greater yield and maximum displacements, total and volumetric hysteretic energy dissipations, but lower initial stiffness and required cross sectional area. 11% more material is used in S5. For the same initial stiffness, all structural response characteristics are greater in S5 as compared to S6. In all cases, under the effect of transverse loading, the effectiveness ratios for S5 and S6 are 1,00 and 0,75 respectively.

- Under unidirectional loading in the longitudinal (Y) direction and for the same cross sectional area, compared to S6, S5 has greater base shear capacity, initial stiffness, and total hysteretic energy dissipation but lower yield and maximum displacements, and volumetric hysteretic energy dissipation. In this case, 68% more bracing material is used in S5. For the same base shear, compared to S6, S5 has greater initial stiffness but lower yield and maximum displacement demands, required cross sectional area, and total and volumetric hysteretic energy dissipations. 13% more material is used in S5. For the same initial stiffness in the longitudinal direction, all structural response characteristics are lower in S5 as compared to S6. 19% more bracing material is used in S6. In all cases, under the effect of longitudinal loading, the effectiveness ratios for S5 and S6 are 0,80 and 1,00 respectively. Note that the efficiency is reversed under the longitudinal and bidirectional loadings (compared to transverse loading) since the yielding braces change in S6 (when long braces yield in S6, the system dissipates more energy as compared to S5).
- Under two directional loading, it is appropriate to investigate the systems' response in each of the principal orthogonal direction. For the same cross sectional area and considering the transverse response in the transverse direction under bidirectional loading, compared to S6, S5 has greater base shear capacity, initial stiffness, and the yield and maximum displacement demands. In the longitudinal direction, since the axial forces of the braces in the longitudinal direction are zero, the system (S5) does not displace and no energy is dissipated for this particular case (i.e. for the selected bridge geometry and bidirectional loading ratio). The unbonded braces in the skew direction yield in this case (4 out of 8). The overall behavior is bidirectional in S6 (i.e. it displaces in both orthogonal

directions) and after the yielding of long braces, the system moves significantly in the longitudinal direction and reaches its maximum displacement. This typical behavior will be further illustrated in Example 2. From Table 6-2, the numerical values of the global displacement ductilities in both transverse and longitudinal directions are calculated as 2.34 and 4.84 respectively, keeping in mind that the unbonded braces used a member (local) displacement ductility of 4. As compared to S6, S5 has greater longitudinal base shear strength and total hysteretic energy dissipation but lower energy dissipated per brace volume. 68% more bracing material is used in S5. For the same base shear strength in the transverse direction, compared to S6, S5 has greater yield and maximum displacements but lower initial stiffness. Again, no response is obtained in the longitudinal direction in S5 as explained above. The behavior is also bidirectional in S6 and after the yielding of long braces, the system displaces in the longitudinal direction significantly (the global ductilities are the same as above). Compared to S6, S5 has lower required cross sectional area, total and volumetric hysteretic energy dissipations. 13% more material is used in S5 (8 braces in S5, 4 braces in S6). In all cases, effectiveness ratios for S5 and S6 are 0,80 and 1,00 respectively. Note that lower required cross sectional areas for the braces lead to lower axial yield forces and thus creates lower end connection forces which could be desirable in seismic design.

- A comparison between S3 and S5, as well as S4 and S6 is worthwhile to explore the impact of skewness on the inelastic behavior of ductile end diaphragms. From Tables 6-1 and 6-2, under unidirectional loading (X) and for the same cross sectional brace area, compared to S5 (skewed system), S3 (non-skewed system) has greater base shear strength and initial stiffness but lower yield and maximum displacement demands. The same statement is also valid when a comparison is made between S4 (non-skewed) and S6 (skewed). Total and volumetric energies are equal in S3 and S5 since similar braces (i.e. braces with equal cross sectional area and lengths) yield in both systems. However, since half of the braces in S6 do not yield, compared to S4 in which all braces yield and dissipate energy, the total and volumetric energy dissipation are less in S6. In bidirectional loading and for the same cross sectional area, compared to S5, S3 has greater base shear strength, initial stiffness, total and volumetric energies but lower yield and maximum displacement demands. Compared to S6, S4 has greater initial stiffness in the transverse and lower initial stiffness in the longitudinal directions. S4 has lower base shear strength in both directions since the axial forces in non-yielding braces vanish in S4 (due to the geometry and loading ratio for this particular case) and therefore their contribution to the base shear capacity is zero, resulting in a lesser base shear strength (See Section 5-2). S4 has lower yield displacement in both directions and greater maximum displacement demand in the transverse direction but lower maximum displacement demand in the longitudinal direction. In other words, Table 6-2 reveals that the global ductility demands (the ratio of maximum and yield displacements) of the skewed systems in both directions vary and may be different from each other. It is also concluded from that table that the global ductility demands in skewed bridges end diaphragms may exceed the local ductility demands placed on the unbonded bracing end diaphragms (For example, μ_G=4.84 for S6, SA, in the longitudinal direction). This behavior will be investigated in detail in Example 2. Note that, under bidirectional loading, since the behavioral characteristics for S3 an S4in both orthogonal directions are equal in non-skewed systems, the values are given for one direction only in Table 6-1. However, in skewed systems, the behavioral characteristics vary per direction under bidirectional loading.

In addition to these evaluations, other observations regarding the overall behavior of the selected systems are as follows:

- Under the selected boundary conditions for the idealized systems considered herein, in all cases (skewed or non-skewed), unbonded braces of the same geometric properties (i.e. same cross sectional area and geometric configuration) yield at the same displacement level since their axial forces are equal. In other words, base shear vs. lateral displacement curves are typically bilinear. When the yield level is reached, a group of similar braces yields simultaneously, maximum system strength is reached, and the structure displaces up to the maximum target displacement at Δ_{max} which depends on a predetermined displacement ductility for the braces. Simultaneous yielding of a group of unbonded braces is especially important to ensure a stable seismic behavior, enhance hysteretic energy dissipation capability, and minimizes the potential differences of local displacement demands in the braces. Note that no effort has been made to calculate actual ductility demands for the unbonded braces; instead a displacement ductility of μ=4 is assumed in this example.

- For some systems considered, some braces may not yield and remain elastic (or may unload depending on the loading ratio in the orthogonal directions and the skew angle of the bridge).

TABLE 6-1 Effect of Bracing Configuration on Hysteretic Energy Dissipation (Straight Bridges, φ=0º)

SYSTEM	INFO	V_B (kN)	K_E (kN/mm)	Δ_y (mm)	Δ_{max} (mm)	μ_G	A_g (mm²)	L_B (mm)	LOAD	E_H (kNmm)	Vol. (mm³)	E_H/Vol (10^{-3}) (kNmm/mm³)	Eff. Ratio
S1	SA	314,58	99,9	3,15	12,60	4,00	645,16	1293,11	X	2972,78	1668526	1,78	1,00
S2	SA	256,84	54,3	4,73	18,92	4,00	645,16	1583,69	X	3644,56	2043467	1,78	1,00
S3	SA	629,20	199,7	3,15	12,60	4,00	645,16	1293,11	X	5945,94	6674103	0,89	0,50
S4	SA	513,90	108,7	4,73	18,92	4,00	645,16	1583,69	X	7292,24	4086934	1,78	1,00
S1	SBS	177,93	56,5	3,15	12,60	4,00	364,90	1293,11	X	1681,44	943712	1,78	1,00
S2	SBS	177,93	37,6	4,73	18,92	4,00	446,97	1583,69	X	2524,83	1415724	1,78	1,00
S3	SBS	177,93	56,5	3,15	12,60	4,00	182,45	1293,11	X	1681,44	1887423	0,89	0,50
S4	SBS	177,93	37,6	4,73	18,92	4,00	223,35	1583,69	X	2524,83	1414869	1,78	1,00
S1	SIS	314,58	99,9	3,15	12,60	4,00	645,16	1293,11	X	2972,78	1668526	1,78	1,00
S2	SIS	472,93	99,9	4,73	18,92	4,00	1187,99	1583,69	X	6710,88	3762816	1,78	1,00
S3	SIS	629,20	199,7	3,15	12,60	4,00	645,16	1293,11	X	5945,94	6674103	0,89	0,50
S4	SIS	943,96	199,7	4,73	18,92	4,00	1184,51	1583,69	X	13394,79	7503587	1,78	1,00
S3	SA	629,20	199,7	3,15	12,60	4,00	645,16	1293,11	X+Y	11891,88	6674103	1,78	1,00
S4	SA	256,84	108,8	2,36	9,44	4,00	645,16	1583,69	X+Y	3636,85	4086934	0,89	0,50
S3	SBS	177,93	56,5	3,15	12,60	4,00	182,45	1293,11	X+Y	3362,88	1887423	1,78	1,00
S4	SBS	177,93	75,4	2,36	9,44	4,00	446,97	1583,69	X+Y	2519,49	2831448	0,89	0,50

SA : Same Cross Sectional Area
SBS : Same Base Shear in X Direction
SIS : Same Initial Stiffness in X Direction
V_B : Base Shear Strength in X Direction
K_E : Initial Stiffness in X Direction
Δ_y : Yield Displacement in X Direction
Δ_{max} : Maximum Displacement in X Direction
μ_G : Global Ductility Demand
A_g : Cross Sectional Area Brace of Each Unbonded Brace
L_B : Brace Length
E_H : Total Hysteretic Energy Dissipation in X and Y Directions
Vol. : Total Volume of Braces Used
Eff. Ratio : Ratio of Hysteretic Energy Diss. per Volume to Maximum One
X : Loading in X Direction
X+Y : Same Loading in Both Orthogonal Directions

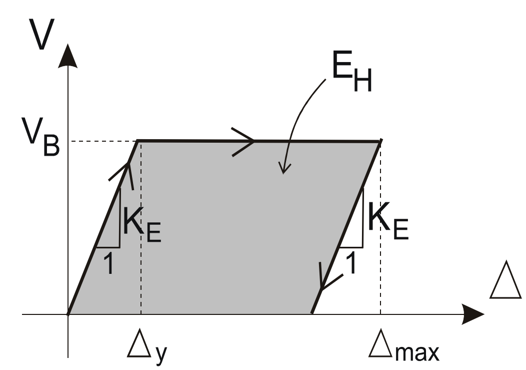

TABLE 6-2 Effect of Bracing Configuration on Hysteretic Energy Dissipation (Skewed Bridges, φ=45°)

SYSTEM	INFO		V_B (kN)	K_E (kN/mm)	Δ_y (mm)	Δ_{max} (mm)	μ_G	A_g (mm^2)	L_{BL} (mm)	L_{BS} (mm)	LOAD	E_H (kNmm)	Vol. (mm^3)	E_H/Vol (10^{-3}) (kNmm/mm^3)	Eff. Ratio
S5	SA	T	444,85	66,50	6,69	20,12	3,01	645,16	1293,11	NA	X	5974,34	6674103	0,89	1,00
S6	SA	T	292,65	85,32	3,43	12,51	3,65	645,16	1921,26	1151,38	X	2657,26	3964689	0,67	0,75
S5	SBS	T	125,81	18,81	6,69	20,12	3,01	182,45	1293,11	NA	X	1689,62	1887423	0,89	1,00
S6	SBS	T	125,81	36,68	3,43	12,51	3,65	277,42	1921,26	1151,38	X	1142,35	1704824	0,67	0,75
S5	SIS	T	444,85	66,50	6,69	20,12	3,01	645,16	1293,11	NA	X	5974,34	6674103	0,89	1,00
S6	SIS	T	228,28	66,50	3,43	12,51	3,65	503,22	1921,26	1151,38	X	2072,78	3092428	0,67	0,75
S5	SA	L	629,11	199,7	3,15	12,60	4,00	645,16	1293,11	NA	Y	5945,09	6674103	0,89	0,80
S6	SA	L	423,47	100,1	4,23	14,70	3,48	645,16	1921,26	1151,38	Y	4434,65	3964689	1,12	1,00
S5	SBS	L	177,93	56,5	3,15	12,60	4,00	182,45	1293,11	NA	Y	1683,47	1887423	0,89	0,80
S6	SBS	L	177,93	42,1	4,23	14,70	3,48	271,10	1921,26	1151,38	Y	1863,12	1665985	1,12	1,00
S5	SIS	L	629,11	199,7	3,15	12,60	4,00	645,16	1293,11	NA	Y	5945,09	6674103	0,89	0,80
S6	SIS	L	847,48	199,7	4,23	14,70	3,48	1291,22	1921,26	1151,38	Y	8874,96	7934908	1,12	1,00
S5	SA	T	444,85	99,7	4,46	17,88	4,00	645,16	1293,11	NA	X+Y	5969,89	6674103	0,89	0,80
		L	444,85	-	0	0	NA								
S6	SA	T	299,41	92,1	3,25	7,59	2,34	645,16	1921,26	1151,38	X+Y	4434,26	3964689	1,12	1,00
		L	299,41	109,7	2,73	13,20	4,84								
S5	SBS	T	125,81	28,2	4,46	17,88	4,00	182,50	1293,11	NA	X+Y	1688,24	1887941	0,89	0,80
		L	125,81	-	0	0	NA								
S6	SBS	T	125,81	38,7	3,25	7,59	2,34	271,10	1921,26	1151,38	X+Y	1863,10	1665962	1,12	1,00
		L	125,81	46,1	2,73	13,20	4,84								

SA : Same Cross Sectional Area
SBS : Same Base Shear (in X or Y Directions)
SIS : Same Initial Stiffness (in X or Y Directions)
V_B : Base Shear Strength (in X or Y Directions)
K_E : Initial Stiffness (in X or Y Directions)
Δ_y : Yield Displacement (in X or Y Directions)
Δ_{max} : Maximum Displacement (in X or Y Directions)
μ_G : Global Ductility Demand
A_g : Cross Sectional Area of Each Brace
L_{BL} : Long Brace Length
L_{BS} : Short Brace Length
E_H : Total Hysteretic Energy Dissipation in X and Y Directions
Vol. : Total Volume of Braces Used
Eff. Ratio : Ratio of Hysteretic Energy Diss. per Volume to Maximum One
X, Y : Loading in Transverse and Longitudinal Directions
X+Y : Same Loading in Both Orthogonal Directions
T, L : Transverse and Longitudinal Directions

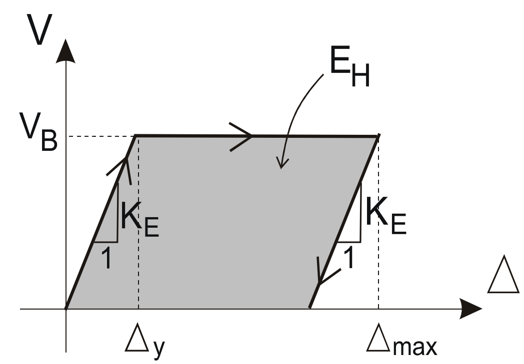

6.2.2 Example-2

Figure 6-3 shows an idealized end diaphragm system (for Retrofit Scheme-2) having a skew angle of φ=20.56°. This system is subjected to both unidirectional (Figure 6-3) and bidirectional (Figures 6-4 to 6-9) loading cases. The numerical values of the loads applied to the top nodes are identical at each node and correspond to code-specified values that would be obtained for earthquake excitation acting in the transverse and longitudinal directions. The system is designed to remain elastic under the loads shown on the system except for the unbonded braces. As assumed in the previous example, the maximum displacement ductility of μ=4 is taken as the target limit state for the unbonded braces, and similarly a yield point of F_y=345MPa (50 ksi), and a modulus of elasticity of E=200000MPa (29000 ksi) are considered as material characteristics for the braces. The cross sectional area for the braces is 645.16mm^2 (1"x1"), (i.e. only the "Same Area" case is considered in this example, contrary to the previous example). SAP2000 is used in the pushover analysis of these systems.

The purpose of this example is to illustrate the effect of various bidirectional loading combinations on the overall behavior of skewed end diaphragm systems. The same system is subjected to seven different bidirectional loading combinations (Loading Cases 1 through 7 as illustrated in Table 6-3), longitudinal to transverse loading ratios of 0.00, 0.10, -0.10, 0.30, 3.33 (i.e. 1/0.30), -3.33 (i.e. -1/0.30), and 0.50. For the same loading ratios, the effect of different loading directions (i.e. expressed by a negative ratio like –0.10) is also examined. Figures 6-3 through 6-9 show, for each system considered, the loads applied to each node, the yielding braces, the base shear force versus displacement in the governing directions for the yielding braces, and the bidirectional displacement travel of node A from the unloaded position to attainment of the specified limit state as a result of a pushover analysis. The plots of the transverse and longitudinal displacements of node A are useful to help understand system behavior. The results from this example investigating the effects of bidirectional loading and inelastic end diaphragm behavior are summarized in Table 6-3.

The following observations are possible from this numerical example:

- As discussed previously in Section 5.2, the system starts moving in different directions (transverse and longitudinal) due to the bidirectional loading and unsymmetrical system geometry (i.e. a skewed system). The ratio of the lateral displacements (i.e. transverse to longitudinal, Δ_T/Δ_L) differs after the braces yield (Figures 6-3d through 6-9d).
- The end diaphragm system's inelastic seismic behavior varies as a function of the loading ratios. The yielding sequence of unbonded braces, numerical values of base shear at yielding, displacements in both orthogonal directions, the ratios of the maximum to yield displacements (the displacement ductility), and local (unbonded brace) versus global (system) displacement ductility all vary significantly depending on the values and directions of the loads.
- For the systems considered, long and short braces do not yield simultaneously due to the uneven distribution of brace axial forces. Depending on the geometric properties of the system and the loading case, some braces (long or short) may remain elastic and thus do not dissipate energy throughout the entire loading history.
- Comparing the same systems under the same magnitude loading but with positive and negative loading ratios (the systems given in Figures 6-4 and 6-5 for example) can be useful to assess the behavioral differences of the systems. As depicted in Table 6-3, this system is subjected to bidirectional loading combinations of 0.10 (Loading Case 2) and -0.10 (Loading Case 3) respectively. In both loading cases, while the short unbonded braces yield, the other long braces remain elastic until the system reaches its specified limit state. For Loading Case 2, compared to Loading Case 3, the system has 19.50% greater base shear capacity and 211.80% greater ductility ratio in the longitudinal direction but 9.9% lower ductility ratio in the transverse direction. As seen in Figure 6-4d, the longitudinal displacement changes its sign (or direction) after yielding since the contribution of the yielding (short) braces to the transverse and longitudinal stiffnesses vanishes and thus the system moves towards the opposite (negative) longitudinal direction.
- Comparing systems under bidirectional loads with different principal acting directions (100% in transverse + 30% longitudinal and 30% transverse + 100% longitudinal for example, as the cases illustrated in Figures 6-6 and 6-7), the following can be observed: In both cases (i.e. Loading Cases 4 and 5), the same long braces yield in the system. The

distinctive feature of the behavior is that the governing direction of movement is in the transverse direction for Loading Case 4, and the longitudinal direction for Loading Case 5. In fact, as evidenced from Figures 6-6d and 6-7d and Table 6-3, the ratios of transverse to longitudinal yield displacements (Δ_{yT}/Δ_{yL}) in both loading cases are 1.89 and 0.08 respectively, showing that the governing response direction is the transverse direction. However, after yielding, the ratios of maximum transverse to maximum longitudinal displacements ($\Delta_{maxT}/\Delta_{maxL}$) are 0.59 and 0.29 at the specified limit state, revealing that the governing response direction has changed into the longitudinal direction in Loading Case 4, but unchanged in Loading Case 5.

- Significant reasons for the observed differences in system behavior can be partly explained by the following: Even though loading is applied in the transverse and unidirectional transverse directions, response is coupled by the skewed orientation of one set of braces. For example, even for Loading Case 1 in which only unidirectional loading is applied in the transverse direction, it can be seen that the system displaces in both the transverse and longitudinal directions simultaneously. This bidirectional response happens as a result of the longitudinal and transverse resultant of axial forces developed in the short and long unbonded braces of the 3D skewed truss system. Note that after yielding, the sum of resultants changes, and the system moves in a different combination of transverse and longitudinal directions up to the specified limit state (in this case, a ductility limit). In this particular case, the governing response direction is generally in the loading direction, but as shown in other Load Cases, the displacement path varies significantly depending on the magnitude of the longitudinal to transverse loads. For example, comparing Load Cases 1, 2, and 3, on can observe that the presence of a positive longitudinal load equal to only 10% of the magnitude of the transverse load results in the system moving in the positive longitudinal and transverse directions until the short braces yields. Comparing Loading Cases 1 and 2, it is seen that this positive longitudinal equal to 10% of the transverse loading actually reduces the magnitude of the longitudinal displacement. After yielding, since the short braces stop contributing to the stiffness, the system starts to move in the positive transverse but negative longitudinal directions simultaneously. Note that compared to the results for Loading Case 1, greater and lower magnitude of transverse and longitudinal displacements respectively are obtained in Loading Case 2 at the specified limit state. In Loading Case 3, compared to Loading Case 1, a negative longitudinal loading equal to 10% of the transverse loading (in addition to it) results in an increase in the longitudinal displacement but a decrease in the transverse direction. In all three loadings cases, the same (short) braces yield.

- Another systematic comparison can be made between the overall behavior of systems subjected to Loading Cases 4, 5, and 6. Finding for these three cases are similar to those for the loading combinations, except that a 30% companion loading has been used instead of the 10% used in Loading Cases 1, 2, and 3. Note that while the yielding braces are the long braces in Loading Case 4 (100% and 30%) and Loading Case 5 (30% and 100%), it is the short braces that yield under Loading Case 6 (100% and –30%). Furthermore, although the (Δ_{yT}/Δ_{yL}) ratios are positive both in Loading Cases 4 and 5, this ratio takes a negative value in Loading Case 6 since the system moves in the negative transverse direction.
- As a general observation made from Figures 6-3 through 6-9 and Table 6-3, the base shear strength is highly dependent on the loading combination assumed; the ratio of minimum base shear (Loading Case 5) to maximum one (Loading Case 4) is 0.61. This could be important in an end diaphragm system designed with a strength based approach. While the unbonded braces of the designed system may reach their prescribed yield values (both strength and displacements) under a loading case (e.g. 100% + 30% as shown in Loading Case 5), they may be elastic and dissipate no energy in another loading combination (e.g. 30% + 100% as shown in Loading Case 4). Comparing the obtained other values (presented in Table 6-3) for Loading Cases 1, 2, 4, and 7 that correspond to the loading ratios of 0.00, 0.10, 0.30, and 0.50 respectively, reveals that the inelastic behavior is very sensitive to these loading ratios.

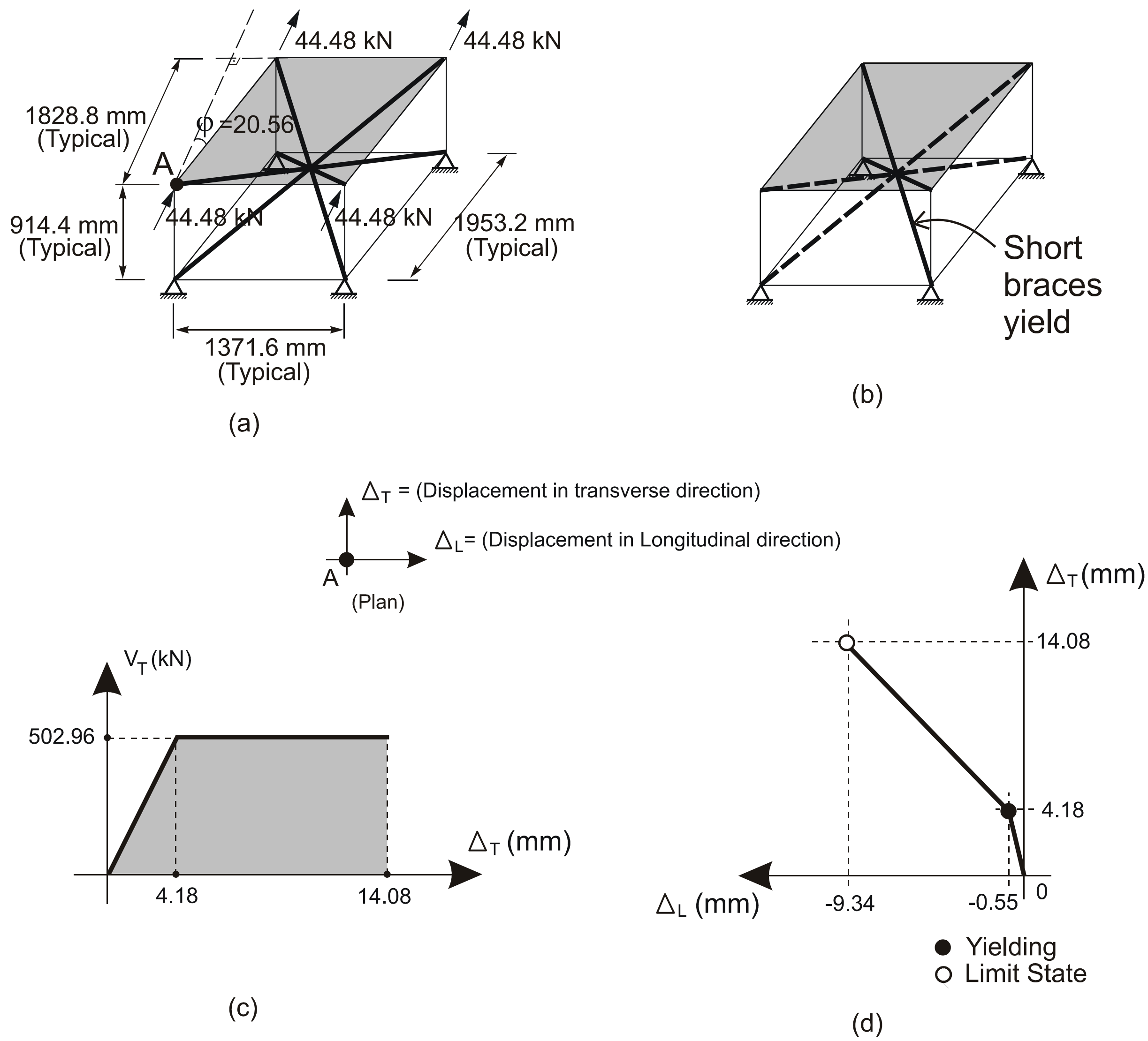

FIGURE 6-3 End Diaphragm Scheme-2 with Skew Under Transverse Loading (Unidirectional Loading): (a) System Geometry and 100% Loading in Transverse Direction; (b) Yielding Unbonded Braces; (c) Transverse Base Shear Versus Displacement Diagram; (d) Bidirectional Travel of Node A from Unloaded Position up to Specified Limit State

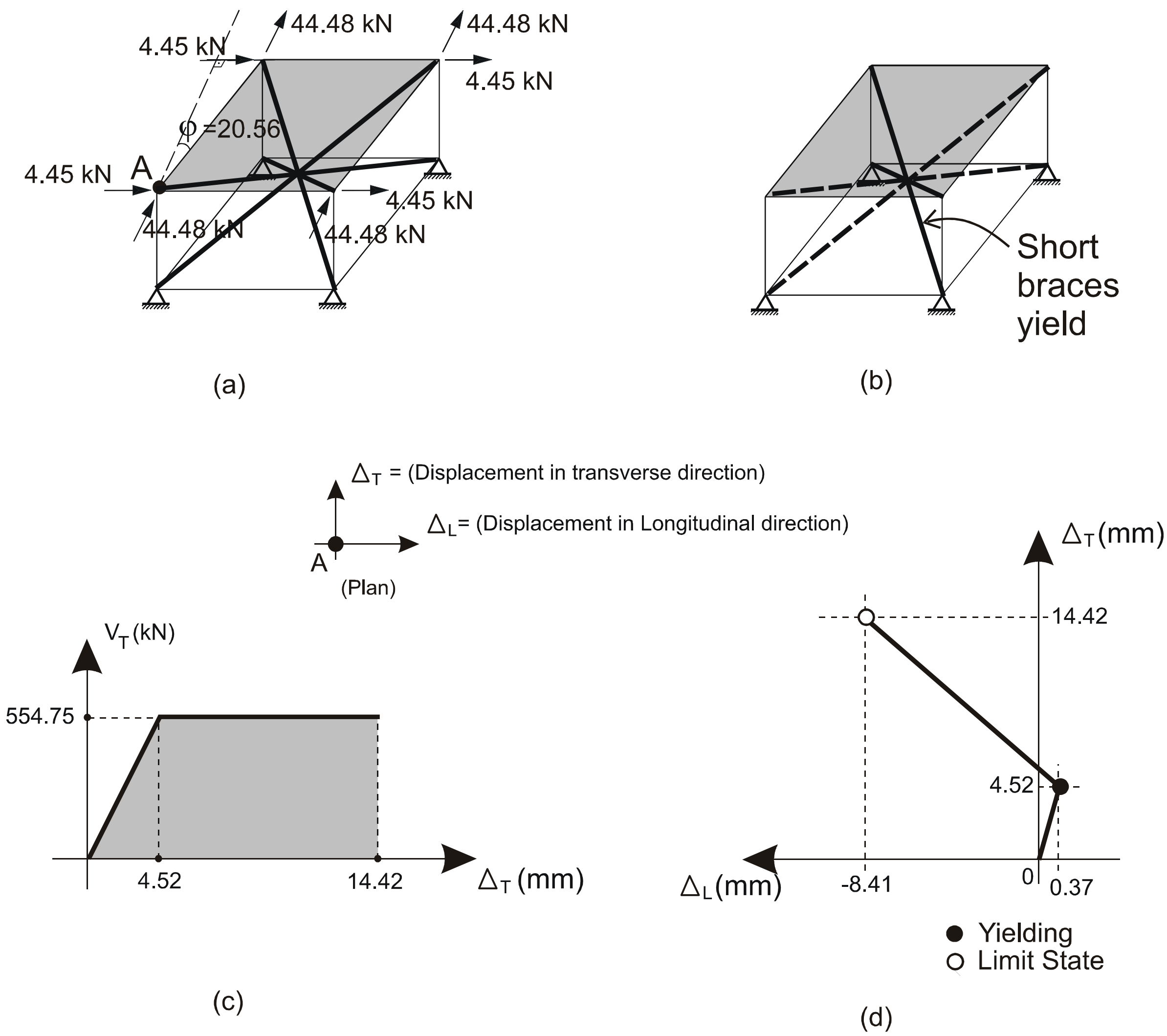

FIGURE 6-4 End Diaphragm Scheme-2 with Skew Under Bidirectional Loading (a) 100% Loading in Transverse and 10% in Longitudinal Directions (b) Yielding Unbonded Braces; (c) Transverse Base Shear Versus Displacement Diagram; (d) Bidirectional Travel of Node A from Unloaded Position up to Specified Limit State

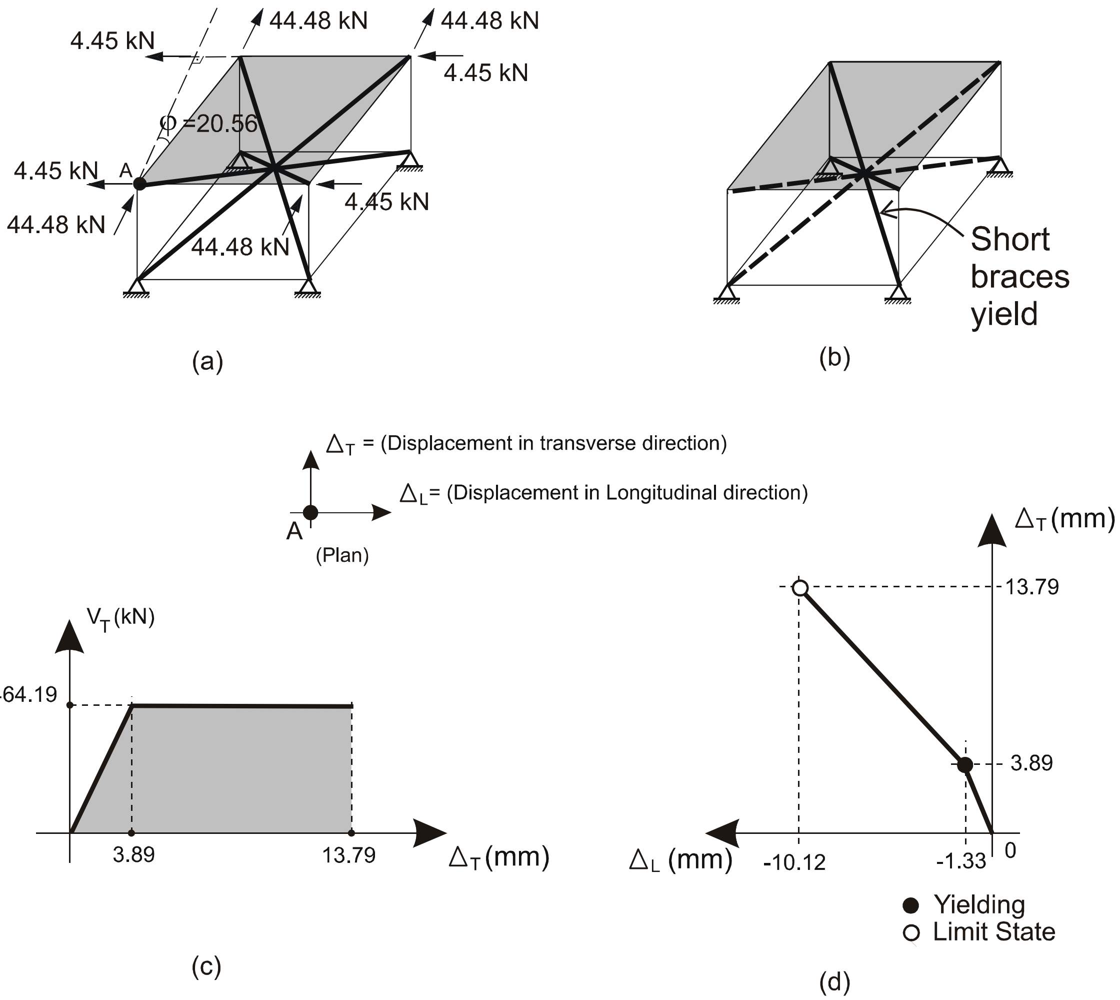

FIGURE 6-5 End Diaphragm Scheme-2 with Skew Under Bidirectional Loading
(a) 100% Loading in Transverse and -10% in Longitudinal Directions (b) Yielding Unbonded Braces; (c) Transverse Base Shear Versus Displacement Diagram;
(d) Bidirectional Travel of Node A from Unloaded Position up to Specified Limit State

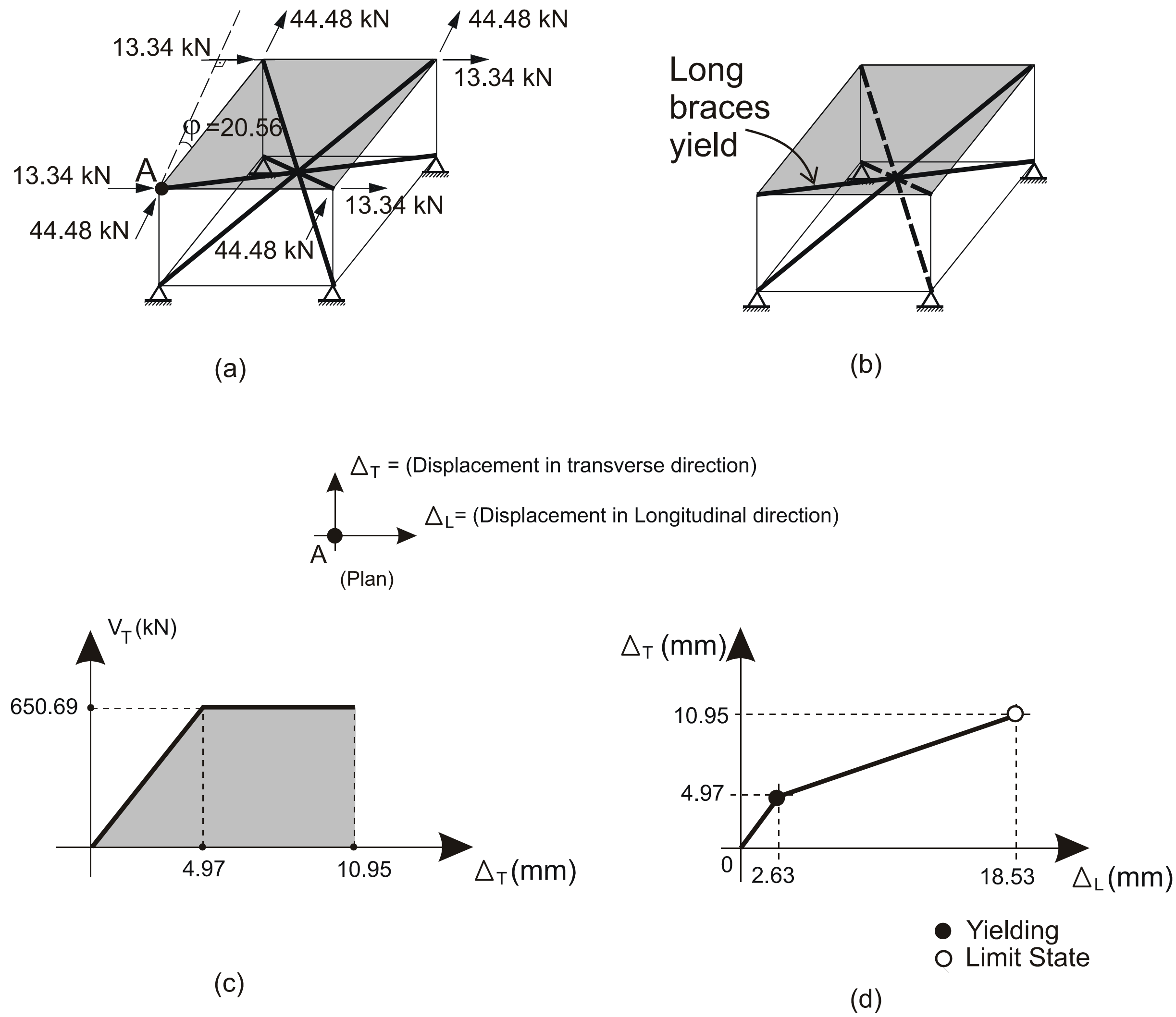

FIGURE 6-6 End Diaphragm Scheme-2 with Skew Under Bidirectional Loading
(a) 100% Loading in Transverse and 30% in Longitudinal Directions (b) Yielding Unbonded Braces; (c) Transverse Base Shear Versus Displacement Diagram;
(d) Bidirectional Travel of Node A from Unloaded Position up to Specified Limit State

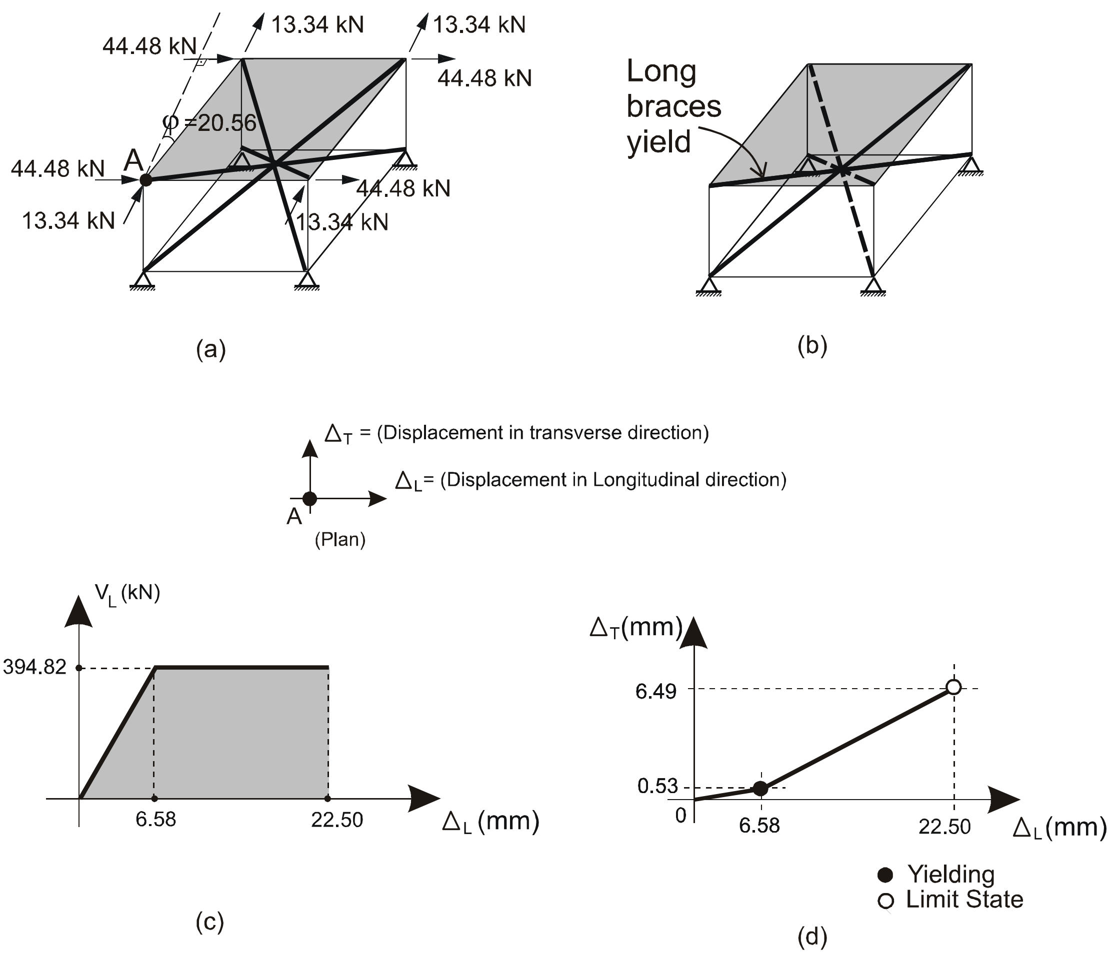

FIGURE 6-7 End Diaphragm Scheme-2 with Skew Under Bidirectional Loading
(a) 30% Loading in Transverse and 100% in Longitudinal Directions (b) Yielding Unbonded Braces; (c) Longitudinal Base Shear Versus Displacement Diagram;
(d) Bidirectional Travel of Node A from Unloaded Position up to Specified Limit State

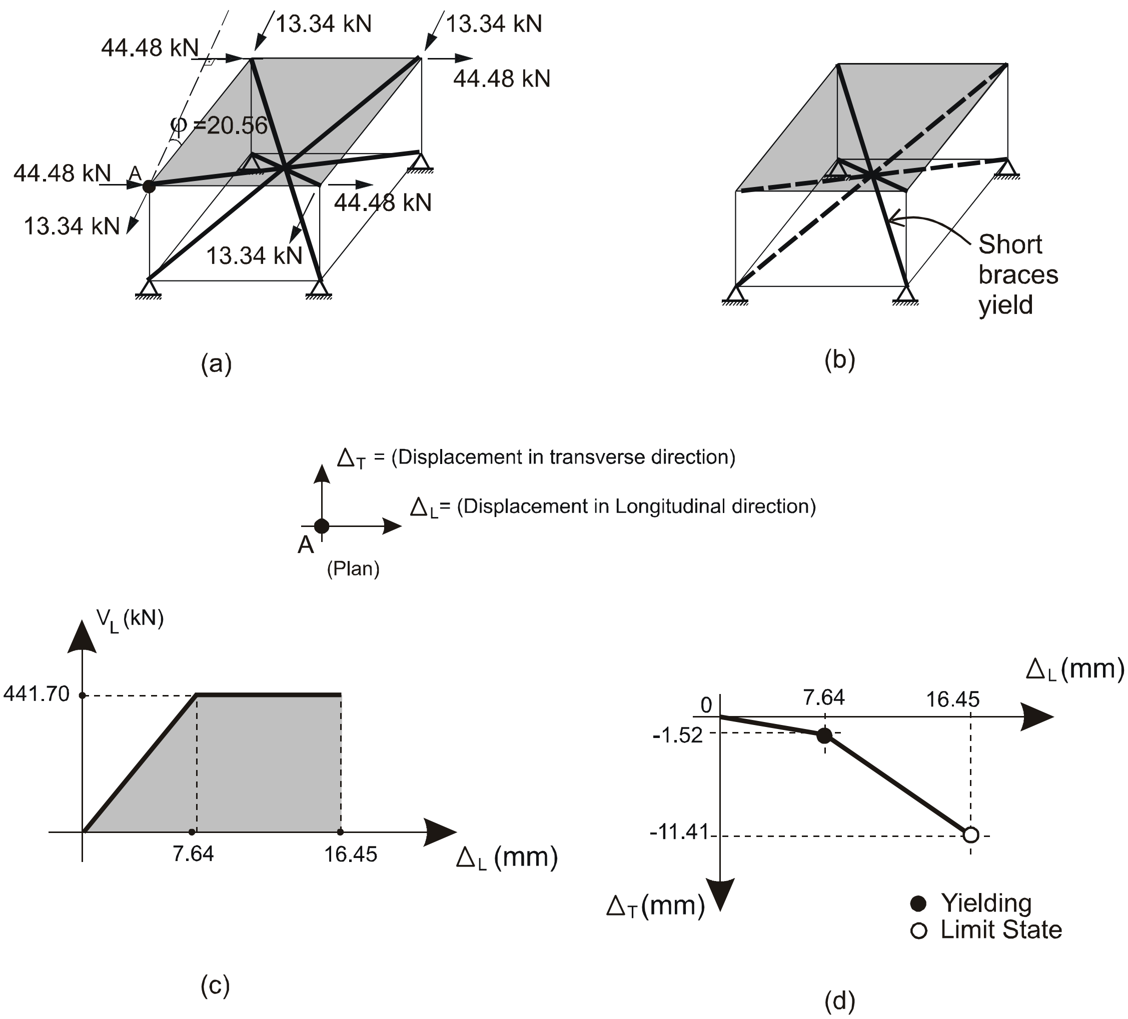

FIGURE 6-8 End Diaphragm Scheme-2 with Skew Under Bidirectional Loading
(a) -30% Loading in Transverse and 100% in Longitudinal Directions (b) Yielding Unbonded Braces; (c) Longitudinal Base Shear Versus Displacement Diagram;
(d) Bidirectional Travel of Node A from Unloaded Position up to Specified Limit State

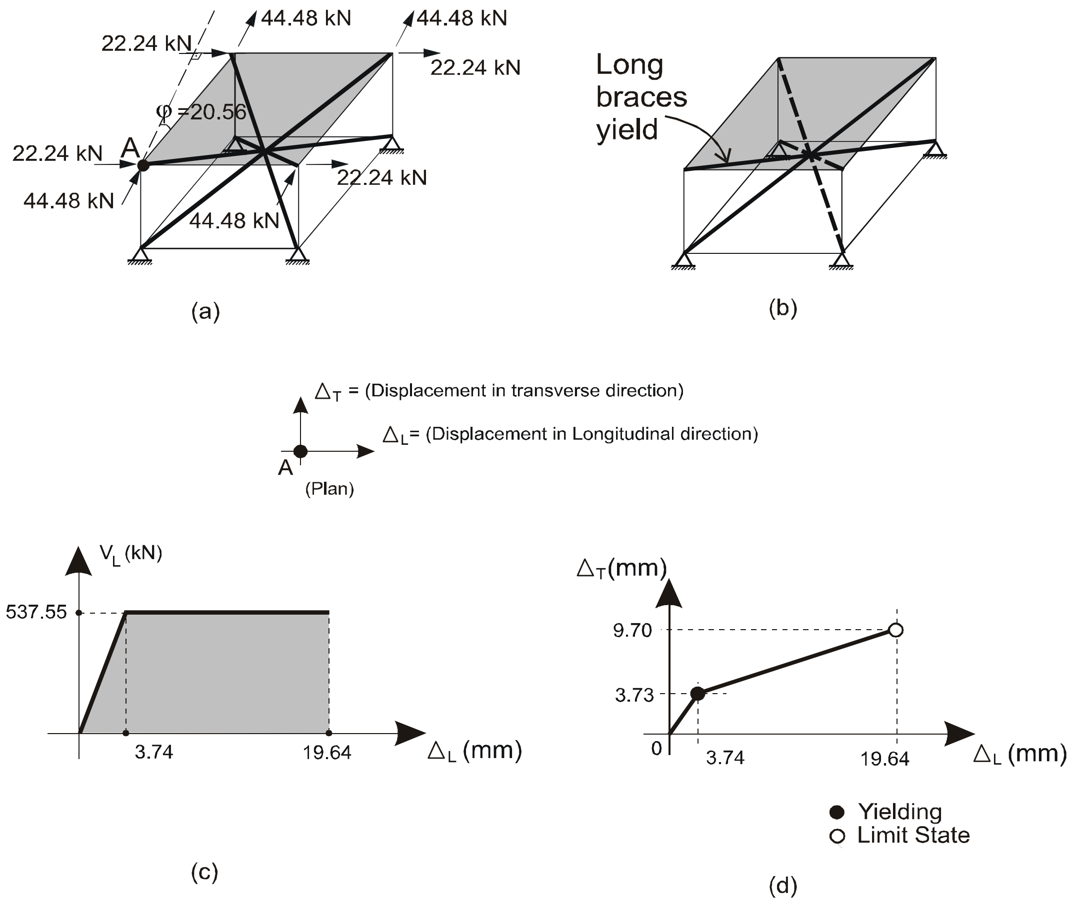

FIGURE 6-9 End Diaphragm Scheme-2 with Skew Under Bidirectional Loading
(a) 100% Loading in Transverse and 50% in Longitudinal Directions (b) Yielding Unbonded Braces; (c) Longitudinal Base Shear Versus Displacement Diagram;
(d) Bidirectional Travel of Node A from Unloaded Position up to Specified Limit State

TABLE 6-3 Effect of Bidirectional Loading Ratio on Inelastic End Diaphragm Behavior: Summary of Results

System (Plan View)	Loading Cases	Yielding Braces	V_{max} (in yielding direction)	Δ_{yT} (mm)	Δ_{yL} (mm)	Δ_{maxT} (mm)	Δ_{maxL} (mm)	$\Delta_{maxT}/\Delta_{yT}$	$\Delta_{maxL}/\Delta_{yL}$	Remarks
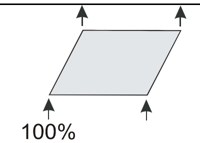	1	Short	502.96	4.18	-0.55	14.08	-9.34	3.37	16.98	-
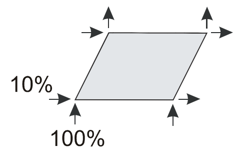	2	Short	554.75	4.52	0.37	14.42	-8.41	3.19	23.73	Long. drift changed direction
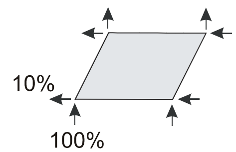	3	Short	464.19	3.89	-1.33	13.79	-10.12	3.54	7.61	-
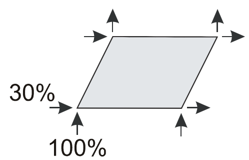	4	Long	650.69	4.97	2.63	10.95	18.53	2.20	7.05	Response direction changed after yielding
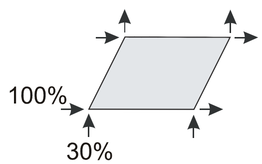	5	Long	394.82	0.53	6.58	6.49	22.50	12.25	3.42	-
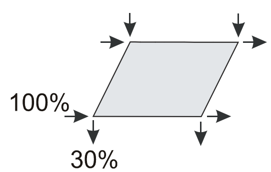	6	Short	441.70	-1.52	7.64	-11.41	16.45	7.51	2.16	Sequence of yielding in braces changed
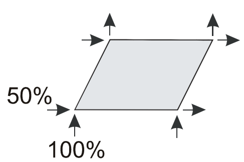	7	Long	537.55	3.73	3.74	9.70	19.64	2.60	5.25	-

6.2.3 Example-3

The purpose of this example is to investigate inelastic displacement demands in both types of ductile end diaphragms considered as they relate to a selected design spectrum. For this purpose, the systems previously considered (with equal brace area and equal base shear) are used as the starting point for design. Pushover analysis is conducted on the systems to determine their strength-deformation characteristics. The spectral displacement demand corresponding to those systems is compared to the target ductility demand of 4, and strength of the ductile diaphragm is changed iteratively until the target ductility is reached (i.e. $\Delta_{max}=4\Delta_y=S_d$). This approach is effectively a displacement based design.

Systems S3 and S4 (both with no skew, i.e. $\varphi=0$) in Example-1, which could also represent Retrofit Schemes 1 and 2 as discussed in Sections 4 and 5 respectively, are investigated. For simplicity, the analysis is carried out in the transverse (Y) direction only (i.e. unidirectional loading case). The design spectra proposed by Newmark and Hall (1982) were considered for this example since this procedure specifies simplified spectral amplification factors to estimate the spectral ordinates (S_a, S_v, and S_d) of a SDOF system having a fundamental period of T. For systems having damping ratios of 2 and 5%, spectral amplification factors for acceleration are 4.3 and 2.6 respectively. Because maximum displacements of elastic systems and similar period yielding (or inelastic) systems are roughly equal, no response modification factor is used in determining the seismic drifts.

To compare the relative seismic 'effectiveness' of systems S3 and S4 previously investigated in 6.2.1 as Example-1, seismic displacement in the transverse direction is used as one of the key parameters for this purpose. Assuming Systems S3 and S4 are in an area where the expected maximum ground acceleration is a_{max}=0.10g, the spectral accelerations are obtained as 0.43 and 0.26 for damping ratios of 2 and 5% respectively. Again, a total weight of W=1779.2 kN (400 K) and a mass of m=0.181 kNs^2/mm are assumed for each system. Systems with the same unbonded brace cross sectional area of 1"x1" (SA) and the same base shear of 177.93kN (SBS) are used to start the iterative design process. Figure 6-10 shows the resulting base shear versus top displacement curves from the pushover analyses for this initial step of the design process (as well as for the final design). Note that the values shown in Figure 6-10 are from Table 6-1.

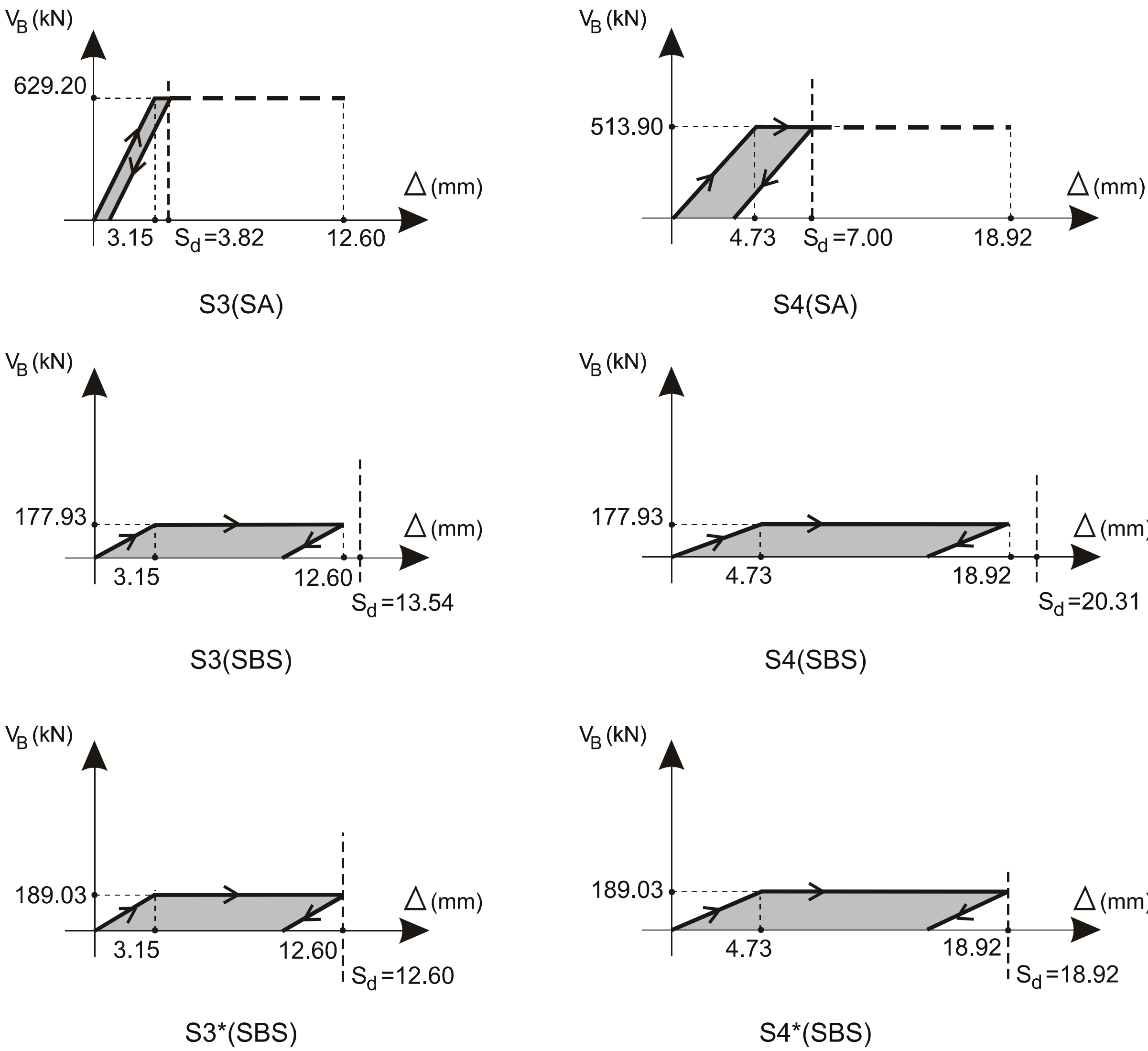

FIGURE 6-10 Base Shear versus Displacement Curves and Comparison with Displacement Demand

Properties of these two systems are summarized in Table 6.4, namely the base shear strength, the yield displacement, initial stiffness, and fundamental period (T), as well as response properties such as spectral displacement (or maximum displacement demand, S_d) and other normalized response characteristics such as the ratios of S_d/Δ_y, $S_d/(4\Delta_y)$ and the dissipated energies for the systems. S_d/Δ_y and $S_d/(4\Delta_y)$ indicate the ratios of seismic drift demand to the yield drift and to the target drift respectively assuming a brace member ductility of μ=4.

For the initial step of design, the systems having the same cross sectional unbonded brace area (S3 (SA) and S4 (SA)) are able to reach the spectral displacement demands. S3 (SBS) and S4 (SBS), on the other hand, which are the systems having the same base shear capacity of 177.93 kN cannot reach this drift demand. Table 6-4 reveals that the initial stiffness for S3 (SA) is 83.7% greater than for S4 (SA) due to its geometric properties, resulting in a 26.2% shorter period. Similarly, the initial stiffness for S3 (SBS) is 50.3% greater than for S4 (SBS), resulting in an 18.3% shorter period. The seismic drift demand exceeds the target drift in both S3 (SBS) and S4 (SBS). At this point, it was decided to perform the iteration process from the equal base shear perspective since in final outcome both systems are not expected to have the same unbonded brace area.

S3*and S4*, given in the last row of Figure 6-10 and in Table 6-4, are the final design outcome. Note that, in that table, S3** and S4** are the same end diaphragm systems, but their effectiveness ratios are calculated using only the yielding braces volumes. Likewise, S3*** and S4*** are again the same end diaphragm systems, but their dissipated energies are calculated at the same displacement demand, namely that corresponding to the S_d of S3 (i.e. S_d=12.60mm). Again, effectiveness ratios of these systems are calculated by only using the yielding braces volumes.

TABLE 6-4 System Characteristics of Straight Bridges Using Spectral Amplification Factors

System	Info	A_g (mm^2)	V_B	K_E (kN/mm)	m (kNs^2/mm)	T (s)	ω (1/s)	S_d (mm)	Δ_y (mm)	$4\Delta_y$ (mm)	S_d/Δ_y	$S_d/4\Delta_y$	E_H (kNmm)	Vol. (mm^3)	E_H/Vol. (10^{-4}) ($kNmm/mm^3$)	Eff. Ratio
S3	SA	645,16	629.20	199.7	0.181	0.189	33.24	3.82	3.15	12.60	1.21	0.30	421.6	6674103	0.6	0.21
S4	SA	645,16	513.90	108.7	0.181	0.256	24.54	7.00	4.73	18.92	1.48	0.37	1166.6	4086934	2.9	1.00
S3	SBS	182,45	177.93	56.5	0.181	0.356	17.65	13.54	3.15	12.60	4.30	1.08	1681.4	1887423	8.9	0.50
S4	SBS	223,35	177.93	37.6	0.181	0.436	14.41	20.31	4.73	18.92	4.30	1.08	2524.8	1414869	17.8	1.00
S3*	SBS	196.06	189.03	60.7	0.181	0.343	18.32	12.60	3.15	12.60	4.00	1.00	1786.3	2028291	8.8	0.50
S4*	SBS	240.00	189.03	40.4	0.181	0.421	14.94	18.92	4.73	18.92	4.00	1.00	2682.3	1520435	17.6	1.00
S3**	SBS	196.06	189.03	60.7	0.181	0.343	18.32	12.60	3.15	12.60	4.00	1.00	1786.3	1014146	17.6	1.00
S4**	SBS	240.00	189.03	40.4	0.181	0.421	14.94	18.92	4.73	18.92	4.00	1.00	2682.3	1520435	17.6	1.00
S3***	SBS	196.06	189.03	60.7	0.181	0.343	18.32	12.60	3.15	12.60	4.00	1.00	1786.3	1014146	17.6	1.00
S4***	SBS	240.00	189.03	40.4	0.181	0.421	14.94	18.92	4.73	18.92	4.00	1.00	1487.7	1520435	9.8	0.56

* These values correspond to the systems designed for $\Delta_{max}=S_d$

** These values correspond to the systems designed for $\Delta_{max}=S_{d.}$ Effectiveness ratios are calculated by using the yielding braces' volumes only.

*** These values correspond to the systems designed for $\Delta_{max}=S_{d..}$ Dissipated energies are calculated at the same displacement demand of S3. Effectiveness ratios are calculated by using the yielding braces' volumes only.

As shown in Table 6-4, for the same base shear strength, dissipated energies and the corresponding effectiveness ratios take different values depending on the performance criteria. For example, for S3* and S4* where Δ_{max} is equal to S_d, the effectiveness ratio for S3* is half of S4* since half of the braces do not yield in this loading condition. However, when the volumes of the yielding braces are taken in the calculations, the effectiveness of both systems is equal. Further, when dissipated energies are calculated at the same displacement demand of S3 (S_d=12.60mm), the effectiveness ratios of S3*** and S4*** are 1.00 and 0.56 respectively. For the same base shear strength, calculating dissipated energies at the same displacement level and considering the yielding braces only as braces volumes reveal that Retrofit Scheme 1 (S3) is superior over Retrofit Scheme 2 (S4) and may exhibit better seismic response.

Note that the above example was done for an arbitrary level of peak ground acceleration, namely a_{max}=0.10g. However, the approach is linearly scalable. Figures 6-11 and 6-12 show the variation of seismic drift demand/yield drift and seismic drift demand/target drift ratios to design peak ground acceleration up to a_{max}=0.40g for damping ratios of 2 and 5%. A linear relationship is observed on these figures both for designs of the same unbonded brace cross sectional area and the same base shear strength.

As expected, structural damping has an impact on the drift demand of end diaphragms. This could be of importance in the selection of end connection types of unbonded braces in bridge end diaphragms (bolted or welded). However, for a given value of structural damping, all systems designed for the same base shear exhibit the same drift demand/yield drift (S_d/Δ_y) and drift demand/target drift ($S_d/4\Delta_y$) ratios. Normally, these ratios for the selected systems increase as the peak ground acceleration increases.

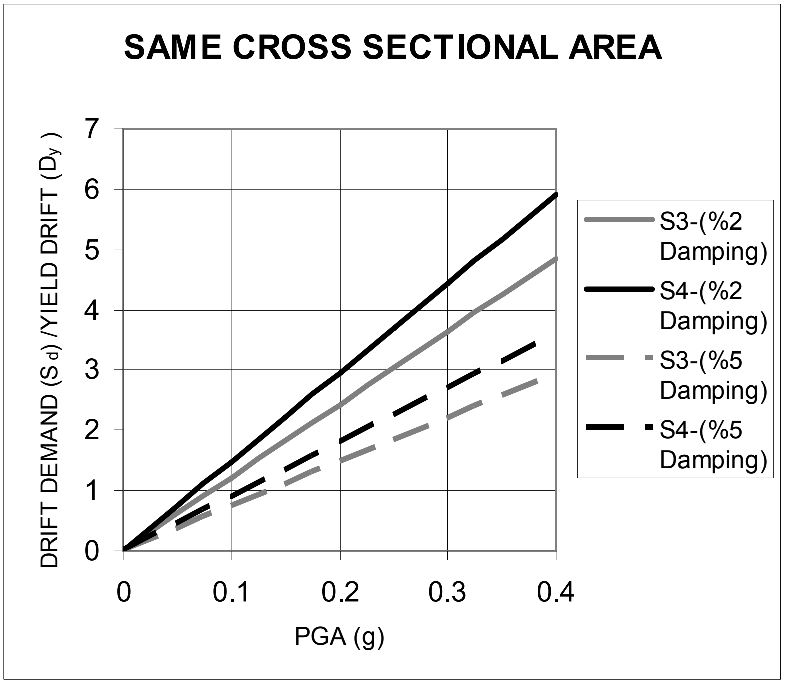

(a)

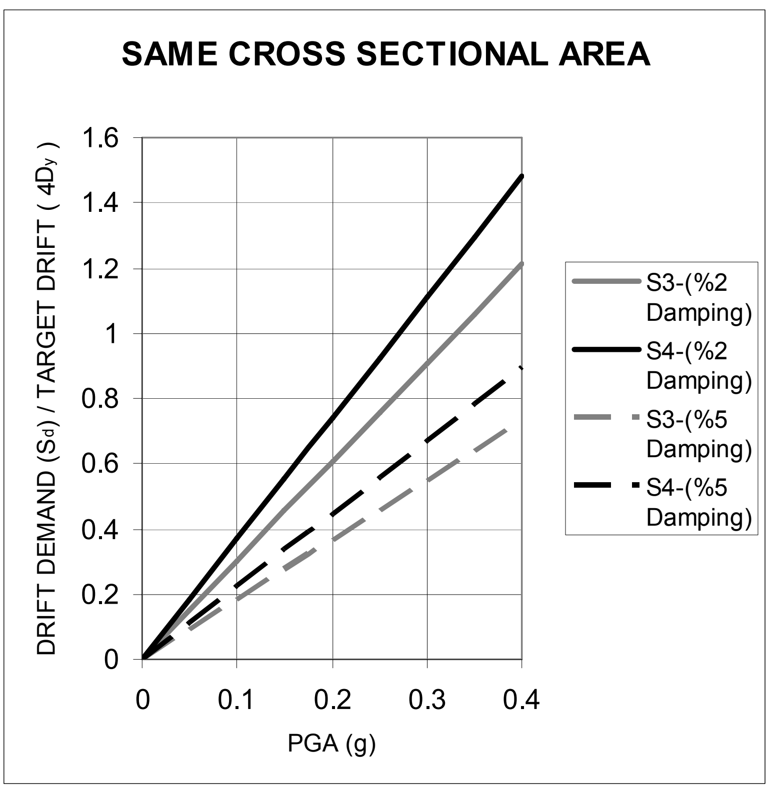

(b)

FIGURE 6-11 Variation of Drift Properties with Peak Ground Acceleration (PGA) for Same Unbonded Brace Cross Sectional Area (SA)

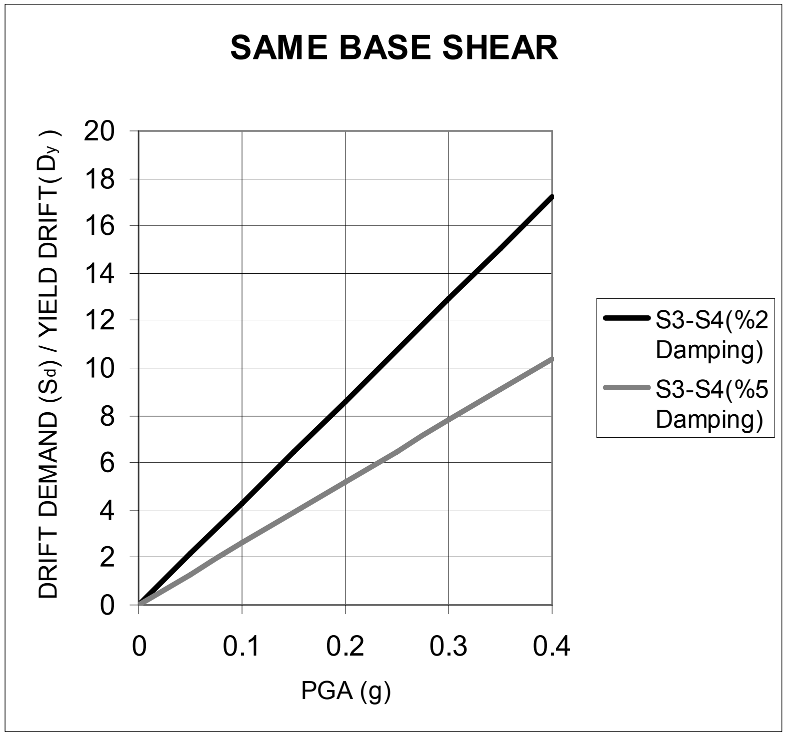

(a)

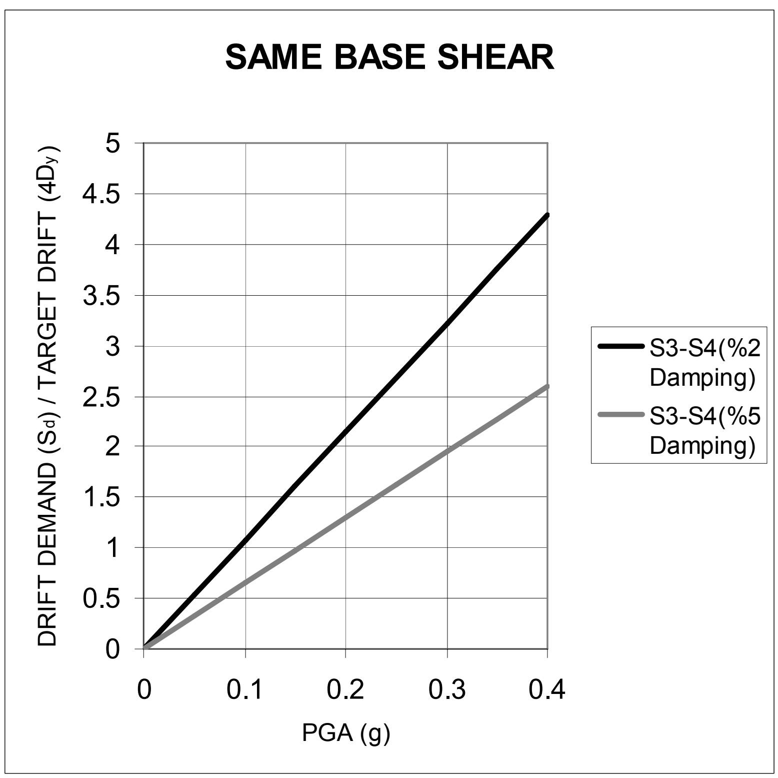

(b)

FIGURE 6-12 Variation of Drift Properties with Peak Ground Acceleration (PGA) for Same Base Shear Capacity (SBS)

6.2.4 Example-4

As shown in Section 5.3, the longitudinally restrained deck is used here to illustrate the inelastic behavior of the end diaphragm system and the resulting dissipated energy. For this purpose, the system illustrated in Figure 6.3 (Retrofit Scheme 2 with skew and subjected to unidirectional loading) is considered (although with a different boundary conditions). All geometric and material properties are kept unchanged. Following the procedure described in Section 5.3, the resulting tri-linear hysteretic curve is shown in Figure 6-13. To construct this curve, axial yield strengths of the unbonded braces and corresponding yield displacements were determined.

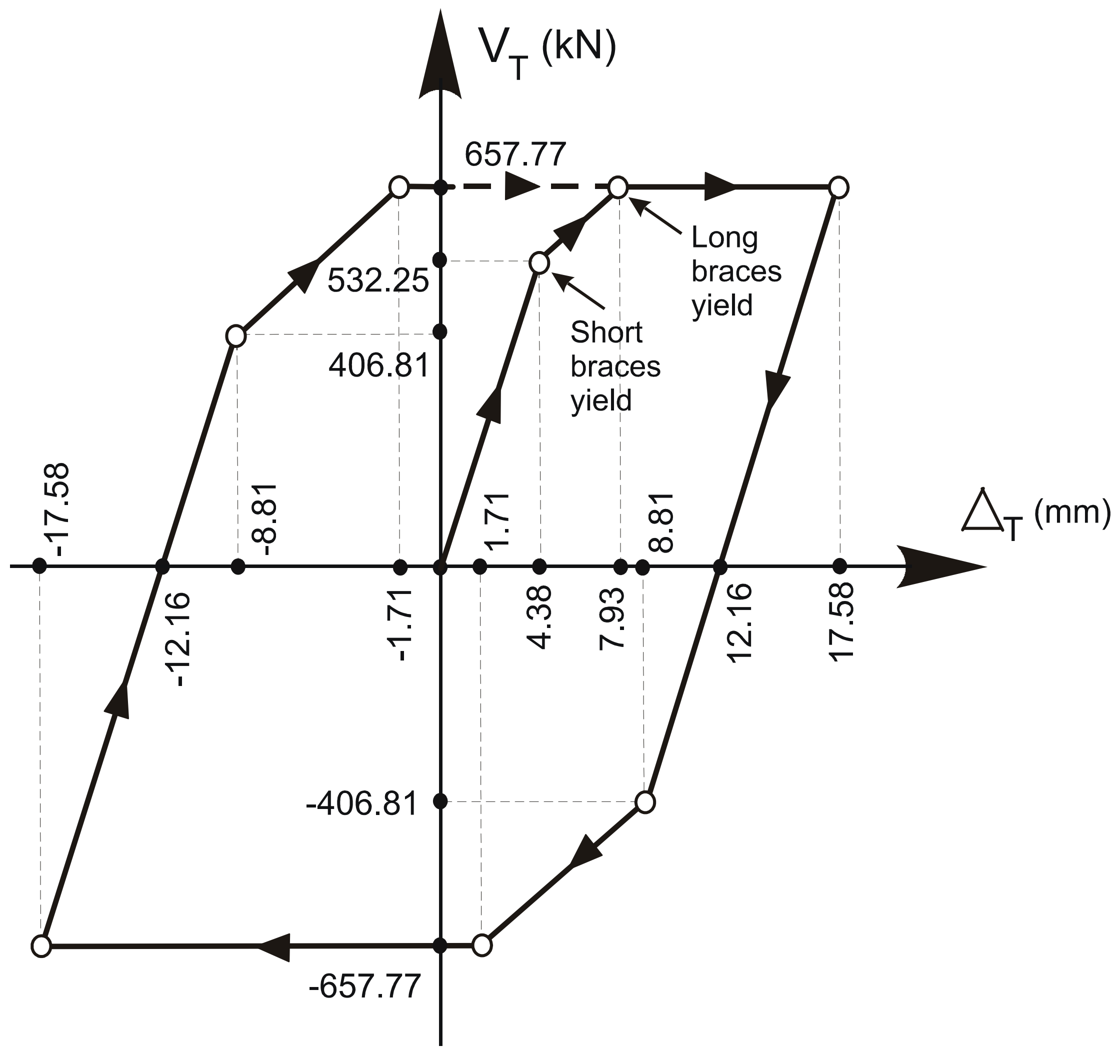

FIGURE 6-13 Tri-Linear Hysteretic Behavior of Skewed End Diaphragm System with Longitudinally Restrained Deck (Transverse Loading)

Since cross sectional areas of the unbonded braces are the same, the volume of material used is the same. Comparing the base shear capacities and dissipated energies at the same displacement level can be useful for seismic performance evaluation. Note that local ductilities of the unbonded braces are also kept unchanged (μ=4).

The following can be observed: As discussed in Section 5-3, while only the short braces yield in the floating deck systems given in Figure 6-3 (the long braces remain elastic), both short (LS=2156.6mm) and long (LL=2900.6mm) braces progressively yield in case of longitudinally restrained bridge superstructures. This results in 30.8% greater base shear capacity. At the same displacement level of 14.08mm which correspond to target member ductility for the floating deck system, the dissipated energy for the longitudinally restrained deck (E_H=20884.62kNmm) is 4.7% greater than for the floating deck system (E_H=19917.22kNmm). The relative increase in the dissipated energy could be seen as less than expected. Note that, as expected, there is no change in the initial stiffness.

Also, as discussed in Section 5-3, energy dissipation efficiency with respect to the ideal hysteretic curve (full loop) can be a useful indicator. For the present example, this ratio is approximately obtained from Eq.(5-68) as follows :

$$\frac{E_{H,1/4}}{E_{H3}} = \frac{\left(\frac{2156.6}{2900.6}\right)4.00 - 1}{\left(\frac{2156.6}{2900.6}\right)4.00 - \left[\frac{(2156.6 + 2900.6)x2156.6x2900.6}{2156.6^3 + 2900.6^3}\right]} = 0.960$$

where $E_{H,1/4}$ and E_{H3} are the hysteretic energies per ¼ cycles defined previously. From the hysteresis curve given in Figure 6-13, this ratio is 0.967.

SECTION 7
SUMMARY AND CONCLUSIONS

7.1 Summary

Two ductile end diaphragms configurations incorporating unbonded braces have been developed and analytically investigated for the seismic retrofit of bridge superstructures (labeled Retrofit Scheme-1 and Retrofit Scheme-2). Both bidirectional earthquake effects and generic bridge geometrical properties (including skewness) were considered in the analysis. Unbonded braces were used for their advantages over other ductile retrofit solutions for bridges ductile diaphragms (such as shear panel systems (SPS), steel triangular plate added damping and stiffness devices (TADAS), or eccentrically braced end diaphragms (EBF)). Unbonded braces provide stable and full hysteretic behavior (both in compression and tension).

Closed form solutions to the proposed retrofit schemes have been developed for practical design purposes. Simple idealized models were used for analytical investigation based on the knowledge that seismic demand in bridge superstructure concentrates at the end diaphragms. Boundary conditions of floating deck and longitudinally restrained deck were considered. Unbonded braces were assumed to have idealized elastic-plastic bilinear force-displacement relationships. A design objective of maximum hysteretic energy dissipation at a prescribed ductility level was used to compare the efficiency of various bracing configurations.

Both general and special cases were considered. Many diagrams for both retrofit schemes were obtained to evaluate the effect of several parameters (both material and geometrical) on the inelastic behavior of ductile end diaphragm systems. Special cases include non-skewed (straight) bridges ($\varphi=0^o$), skewed bridges ($\varphi\neq0^o$) with certain geometric ratios, and bridges with variable skew angles. Four numerical examples covering many special cases were presented.

7.2 Conclusions

The major conclusions reached from this analytical study are as follows:

1. Unbonded braces can be used to provide an effective ductile end diaphragm concept as ductile fuses in existing bridges. Some shortcomings of the known ductile end diaphragm concepts have been resolved using the selected bidirectional bracing configurations (Retrofit Scheme-1 and Retrofit Scheme-2). As such, since both transverse and longitudinal effects can be resisted by these members, and because of their ease of construction, the proposed retrofit schemes are promising and seem viable compared to the alternatives commonly used in bridge seismic retrofit (or design) applications.
2. Both non-skewed and skewed bridge superstructures can be retrofitted to dissipate seismic energy using the retrofit schemes proposed here.
3. The hysteretic behavior of bridge end diaphragms depends on bidirectional earthquake effects, the boundary conditions of girders, and the skew angle. As such, the governing response direction may be altered in case of severe skew angles. Special cases presented in this report help understand the impact of structural parameters on the inelastic behavior of bridge end-diaphragms with unbonded brace end diaphragms.
4. For non-skewed bridges ($\varphi=0^{o}$), in Retrofit Scheme-1 and when transverse braces yield, the base shear strength is observed to decrease as the d/s ratio increases. Transverse drift (Δ_{yT}/d) reaches a minimum value at d/s = 1. The nondimensional transverse stiffness (K_T) is maximum at d/s=0.707. The reduction in drift is relatively less after d/s=0.5. This suggests that an appropriate value for d/s could be between 0.5 and 1.0. In the longitudinal direction, for a constant d/s, the longitudinal drift (Δ_{yL}/d) becomes minimum at d/a=0.707. Since the variation in drift after d/a=0.5 is relatively insignificant, optimal d/a ratios can also be selected between 0.5 and 1.0. Dissipated hysteretic energy increases as d/a increases for constant values of d/s, but decreases as d/s increases for constant values of d/a. However, the decrease in energy dissipation is relatively less for larger values of d/s. Hysteretic energy increases (logically) as member (unbonded brace) ductility increases. The effect of bidirectional loading ratio (30% or 40%) is obvious and suggests that greater seismic drifts are obtained under greater P_1/P_2 ratios but smaller drifts are obtained under smaller P_2/P_1 ratios in the longitudinal direction.
5. For non-skewed bridges ($\varphi=0^{o}$), in Retrofit Scheme-1 and when longitudinal braces yield, the nondimensional base shear strength decreases as d/a ratio and P_1/P_2 and increase. The

transverse drift decreases as d/a increases. In the longitudinal direction, a decrease in the base shear is observed with increasing d/a ratio. Longitudinal drift decreases as d/a increases and drift increases as the unbonded brace ductility increases. The rate of decrease in the longitudinal drift is slower for values of d/a=0.5 or larger, suggesting suitable values between 0.5 and 1.0. Dissipated energy decreases as d/a increases. More hysteretic energy is dissipated for larger member ductilities. Smaller d/s ratios result in lesser energy dissipation.

6. For skewed ($\varphi \neq 0^{o}$) bridges in Retrofit Scheme-1, the ratio of brace forces increases as the skew angle increases. For small skew angles ($\varphi \leq 25^{o}$), changes in d/a ratio have no significant effect on the force ratio in unbonded braces.
7. For non-skewed bridges ($\varphi = 0^{o}$), in Retrofit Scheme-2 and when short-labeled braces yield, the base shear strength decreases as d/a increases for constant values of s/a and decreases as s/a decreases for constant values of d/a. Transverse drift (Δ_{yT}/d) decreases as d/a increases. For a constant value of d/a, the transverse drift decreases as s/a increases. Also, the change in drift is less for larger values of s/a ratios. Global transverse ductility (μ_{GT}) decreases as s/a increases. For constant values of s/a, the global ductility increases as the local (unbonded brace) ductility (μ) increases. Initial stiffness increases as d/a and s/a ratios increase. However, this increase is less after values of d/a=0.60. Similar behavioral tendency is observed in the longitudinal direction.
8. For non-skewed bridges ($\varphi = 0^{o}$), in Retrofit Scheme-2 and when long-labeled braces yield, the tendency is the same as in the short-labeled brace yielding case, with the exception that global transverse ductility ratio (μ_{GT}) increases as s/a increases. Trends observed for longitudinal base shear strength,longitudinal drift, and global longitudinal ductility (μ_{GL}) are the same as observed for transverse values in the preceeding case.
9. For skewed ($\varphi \neq 0^{o}$) bridges in Retrofit Scheme-2, the ratio of brace forces increases as the skew angle increases. As in Retrofit Scheme 1, for small skew angles ($\varphi \leq 25^{o}$), changes in d/a ratio have no significant effect on the force ratio in unbonded braces. For larger values of s/a, the effect of d/a ratio on the brace forces is negligible for practical skew angles. Note that the bidirectional loading ratio has an effect on the overall behavior.

From the numerical examples in Section 6, the followings can be drawn:

1. For non-skewed systems and under unidirectional loading, for a given required design base shear, Retrofit Scheme-1 achieves the same displacement demand than Retrofit Scheme-2 with a lesser volume of material. The orthogonal brace configuration therefore seems to be more effective. On the other hand, Retrofit Scheme-2 has the advantage over Retrofit Scheme-1 to result in a more flexible ductile diaphragm. Smaller braces that result from Retrofit Scheme-1 will develop smaller yield forces than those in Retrofit Scheme-2, resulting in simpler connections to superstructure and substructure.
2. Under transverse loading, for severely skewed systems (with φ=45º for example), compared to Retrofit Scheme-2, higher effectiveness ratios are obtained for Retrofit Scheme-1. The efficiency is reversed under the longitudinal and bidirectional loadings. A further comparison between skewed and non-skewed systems reveals that non-skewed systems have greater base shear strength and initial stiffness but lower yield and maximum displacement demands.
3. In skewed systems in Retrofit Scheme-2, the system starts moving in different directions due to bidirectional loading and system geometry. The inelastic behavior varies as a function of the loading ratio and is sensitive to loading ratios (both percent values and principle acting directions). The base shear strength depends on the loading combination assumed. This could be important in an end diaphragm system designed with a strength based approach. The governing response direction may also change upon yielding. The global ductility demands in skewed bridges end diaphragms may exceed the local ductility demands placed on the unbonded braces.
4. In longitudinally restrained deck systems, greater base shear capacity and hysteretic energy dissipation can be obtained due to the yielding of all (both short and long) braces.

7.3 Recommendations for Future Research

Two possible types of unbonded bracing configurations in bridges end diaphragms have been developed and analytically investigated. These seismic mitigation measures showed promise for use in new bridges superstructures or as a retrofitting technique in old bridges. As an extension of this work, an experimental study on shake table can be useful to observe the inelastic behavior of ductile end diaphragms with unbonded braces in steel skewed bridges. Comparing results and behavioral observations from the present analytical and future experimental studies would be worthwhile.

Some of the assumptions made in this report could be eliminated in future analytical work. For example, diaphragms having unbonded braces of unequal area (if determined to be necessary or practical in some cases), and bridges having unequal skew angles at both abutments, could be investigated. Although all lateral deformations are taken by the end diaphragm system in regular bridges, there is still need for thorough analytical work to determine the bounds of this assumption in skewed bridges. Also, it is worth considering if the ductile end diaphragms concept could be used in curved bridge superstructures.

Detailing issues could also be of interest in these retrofit schemes. Especially, a suitable connection location on the deck should be investigated for the new unbonded braces. As shown in Figure 7-1, these braces can be supported by either the existing cross bracing (that may need some modifications) or a newly placed transverse beam or frame specially designed for elastically transmitting the unbonded braces forces.

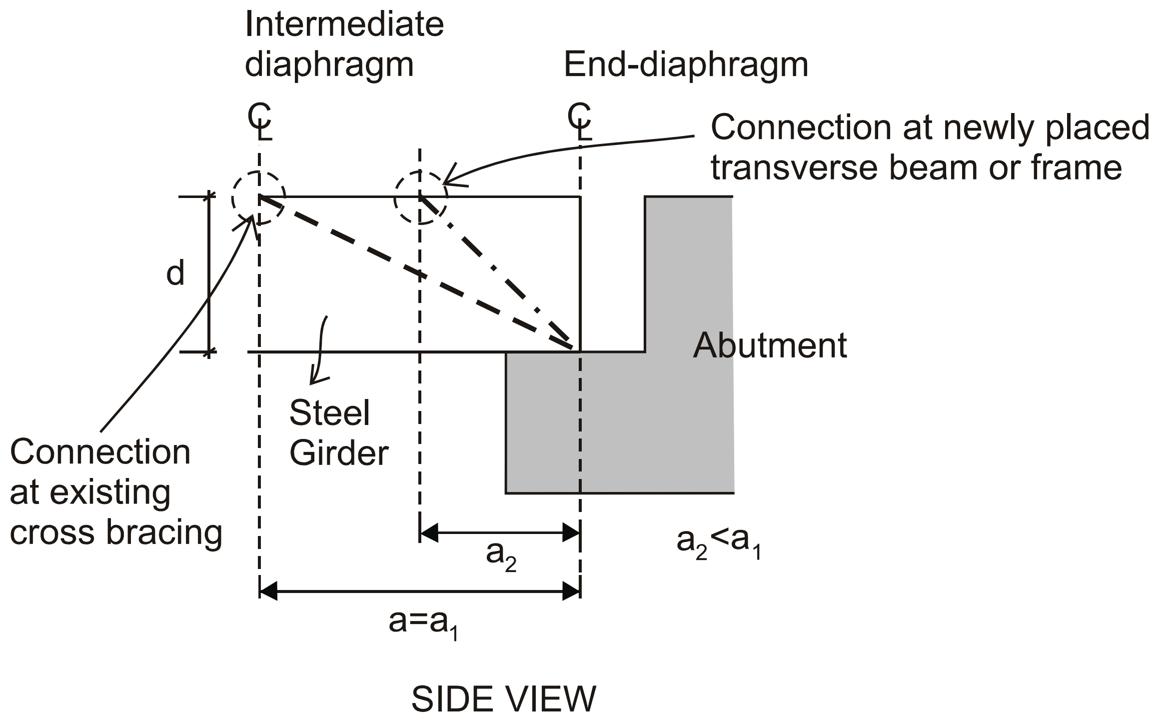

FIGURE 7-1 Connection of Unbonded Braces to Bridge Deck

It would also be of interest to determine the best layout of cross and end diaphragm bracings to use in skewed bridges. Some possible orientations are as illustrated in Figure 7-2. This may require the use of refined finite element models and pushover analysis.

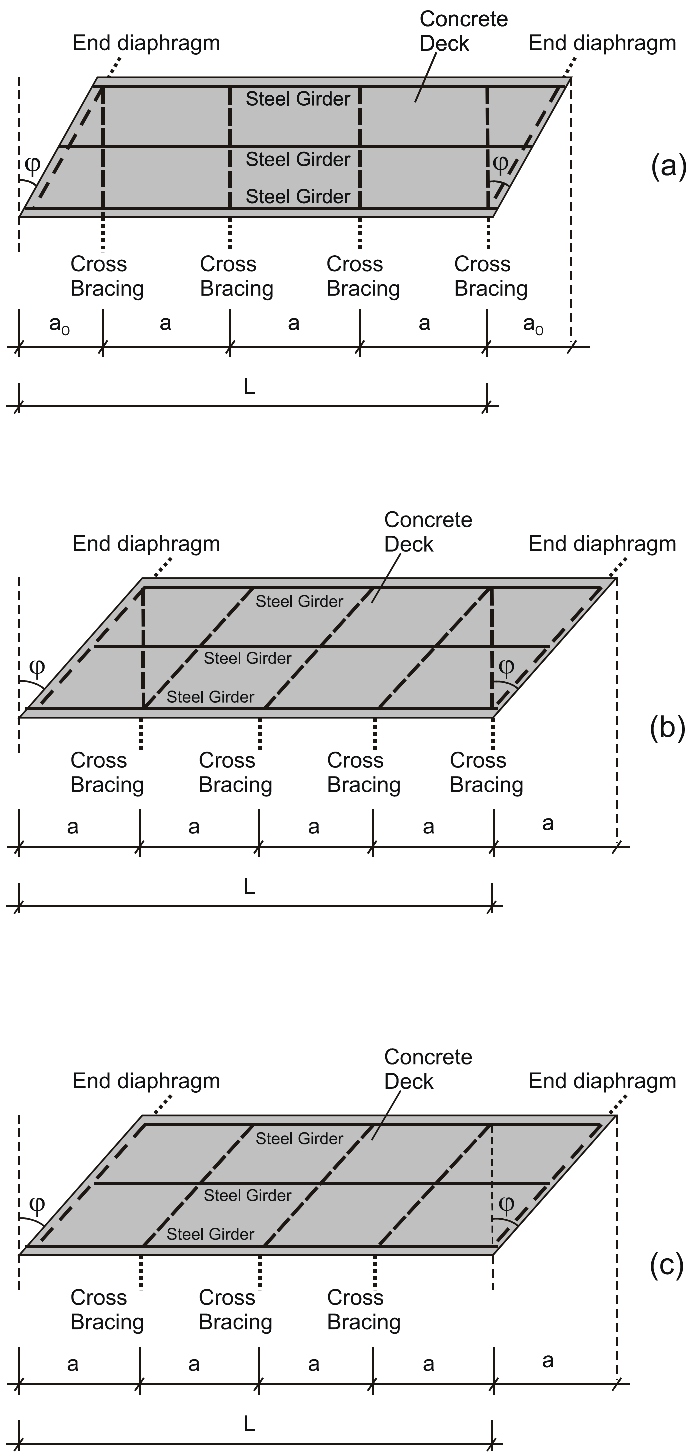

FIGURE 7-2 End and Cross Bracing Orientations in Skewed Bridge Decks

SECTION 8
REFERENCES

AASHTO (2002) "Standard Specifications for Highway Bridges", American Association of State Highway and Transportation Officials, Washington, D.C.

AISI (1995) "Short-Span Steel Bridges- Plans" American Iron and Steel Institute, Washington, D.C.

Alfawakhiri, F. and Bruneau, M. (2000) "Flexibility of Superstructures and Supports in the Seismic Analysis of Simple Bridges", Journal of Earthquake Engineering and Structural Dynamics, Vol.29, No.5, pp.711-729.

Alfawakhiri, F. and Bruneau, M. (2001) "Local versus Global Ductility Demands in Simple Bridges", Journal of Structural Engineering, ASCE, Vol.127, No.5, pp.554-560.

ATC-32 (1996) "Improved Seismic Design Criteria for California Bridges: Provisional Recommendations", Applied Technology Council, California-Washington, D.C.

Black, C., Makris, N. and Aiken, I. (2002) "Component Testing, Stability Analysis and Characterization of Buckling-Restrained Unbonded Braces", PEER Report 2002/08, Pacific Earthquake Engineering Research Center, University of California, Berkeley.

Bruneau, M., Wilson, J.C. and Tremblay, R. (1996) "Performance of Steel Bridges during the 1995 Hyogo-ken Nanbu (Kobe, Japan) Earthquake", Canadian Journal of Civil Engineering, Vol.23, pp.678-713.

Bruneau, M., Uang, C.M. and Whittaker, A. (1998) "Ductile Design of Steel Structures", McGraw-Hill, NY.

Bruneau, M., Sarraf, M., Zahrai, S.M. and Alfawakhiri, F. (2002) “Displacement-Based Energy Dissipation Systems for Steel Bridges Diaphragms”, Journal of Constructional Steel Research, Vol.58, No.5-8, pp.801-817.

Carden, L.P., Itani, A.M. and Buckle, I.G. (2003) “An Experimental Study into the Distribution of Earthquake Forces in Steel Plate Girder Bridges”, Pacific Conference on Earthquake Engineering, Paper No.60.

Carden, L.P., Itani, A.M. and Buckle, I.G. (2006a) “Seismic Performance of Steel Girder Bridges with Ductile Cross Frames Using Single Angle X Braces”, Journal of Structural Engineering, ASCE, Vol.132, No.3, pp.329-337.

Carden, L.P., Itani, A.M. and Buckle, I.G. (2006b) “Seismic Performance of Steel Girder Bridges with Ductile Cross Frames Using Buckling-Restrained Braces”, Journal of Structural Engineering, ASCE, Vol.132, No.3, pp.338-345.

Chen, S.S. (2003) Personal Communication, University at Buffalo, SUNY, Department of Civil, Structural&Environmental Engineering, Buffalo, NY.

Clark, P., Aiken, I., Kasai, K., Ko., E., and Kimura, I. (1999) “Design Procedures for Buildings Incorporating Hysteretic Damping Devices”, Structural Engineers Association of California (SEAC), Proceedings of 68th Annual Convention, Santa Barbara, CA, October.

CSI (1998) “SAP2000 Integrated Finite Element Analysis and Design of Structures- Detailed Tutorial Including Pushover Analysis”, Computers and Structures, Inc., Berkeley, California.

FHWA-SA-97-017 (1997) “Seismic Bridge Design Applications-Part I and II”, NHI Course No. 13063.

Itani, A.M. (2003) Personal Communication, University of Nevada, Reno, Department of Civil&Environmental Engineering, Reno, NV.

Itani, A.M., Bruneau, M., Carden, L. and Buckle, I.G. (2004) "Seismic Behavior of Steel Girder Bridge Superstructures", Journal of Bridge Engineering-Special Edition on Steel Bridges, Vol.9, No.3, pp.243-249.

JRA (1996) "Design Specifications of Highway Bridges- Part V-Seismic Design", Japan Road Association, Tokyo, Japan.

Kanaji, H., Kitazawa, M. and Suzuki, N. (2003) "Seismic Retrofit Strategy using Damage Control Design Concept and the Response Reduction Effect for a Long-Span Truss Bridge", 19th US-Japan Bridge Engineering Workshop, Panel on Wind and Seismic Effects, UJNR, October 27-29, Tsukuba Science City, Japan.

Kanaji, H., Hamada, N., Ishibashi, T., Amako, M. and Oryu, T. (2005) "Design and Performance Tests of Buckling Restrained Braces for Seismic Retrofit of a Long-Span Bridge", 21th US-Japan Bridge Engineering Workshop, Panel on Wind and Seismic Effects, UJNR, October 3-5, Tsukuba, Japan.

MCEER/ATC-49 (2003) "Recommended LRFD Guidelines for the Seismic Design of Highway Bridges-Part I: Specifications", Applied Technology Council/Multidisciplinary Center for Earthquake Engineering Research Joint Venture, Buffalo, N.Y.

Pekcan, G., Mander, J. and Chen, S.S. (2000) "Seismic Retrofit of End-Sway Frames of Deck-Truss Bridges with a Supplemental Tendon System: Experimental and Analytical Investigation", Technical Report, MCEER-00-0004, Multidisciplinary Center for Earthquake Engineering Research, Buffalo, N.Y.

Priestly, M.J.N, Seible, F. and Calvi, G.M. (1996) "Seismic Design and Retrofit of Bridges", John Wiley & Sons, Inc., N.Y.

Ramberger, G. (2002) "Structural Bearings and Expansion Joints for Bridges", Structural Engineering Documents, International Association for Bridge and Structural Engineering (IABSE), Zurich, Switzerland.

Sabelli, R., Mahin, S. and Chang, C. (2003) "Seismic Demands on Steel Braced Frame Buildings with Buckling-Restrained Braces", Engineering Structures Journal, Vol.25, No.5, pp.655-666.

Sarraf, M. and Bruneau, M. (1998a) "Ductile Seismic Retrofit of Steel Deck-Truss Bridges. I: Strategy and Modeling", Journal of Structural Engineering, ASCE, Vol.124, No.11, pp.1253-1262.

Sarraf, M. and Bruneau, M. (1998b) "Ductile Seismic Retrofit of Steel Deck-Truss Bridges. II: Design Applications", Journal of Structural Engineering, ASCE, Vol.124, No.11, pp.1263-1271.

Sarraf, M. and Bruneau, M. (2002) "Seismic Performance of a Ductile Retrofitted Deck-Truss Bridge", 7th National Conference on Earthquake Engineering, Boston, July, on CD-ROM.

Sarraf, M. and Bruneau, M. (2004) "Performance Tests of Innovative Ductile Steel Seismically Retrofitted Deck-Truss Bridges", 13th World Conference on Earthquake Engineering, Vancouver, Canada, August, CD-ROM, Paper # 1803.

Yashinsky, M., Karshenas, M.J. (2003) "Fundamentals of Seismic Protection for Bridges", Earthquake Engineering Research Institute (EERI), Monograph Series MNO-9.

Zahrai, S.M. and Bruneau, M. (1998) “Impact of Diaphragms on Seismic Response of Straight Slab-on-Girder Steel Bridges”, Journal of Structural Engineering, ASCE, Vol.124, No.8, pp.938-947.

Zahrai, S.M. and Bruneau, M. (1999a) “Ductile End-Diaphragms for Seismic Retrofit of Slab-on-Girder Steel Bridges”, Journal of Structural Engineering, ASCE, Vol.125, No.1, pp.71-80.

Zahrai, S.M. and Bruneau, M. (1999b) “Cyclic Testing of Ductile End-Diaphragms for Slab-on-Girder Steel Bridges”, Journal of Structural Engineering, ASCE, Vol.125, No.9, pp.987-996.

MCEER Technical Reports

MCEER publishes technical reports on a variety of subjects written by authors funded through MCEER. These reports are available from both MCEER Publications and the National Technical Information Service (NTIS). Requests for reports should be directed to MCEER Publications, MCEER, University at Buffalo, State University of New York, Red Jacket Quadrangle, Buffalo, New York 14261. Reports can also be requested through NTIS, 5285 Port Royal Road, Springfield, Virginia 22161. NTIS accession numbers are shown in parenthesis, if available.

NCEER-87-0001 "First-Year Program in Research, Education and Technology Transfer," 3/5/87, (PB88-134275, A04, MF-A01).

NCEER-87-0002 "Experimental Evaluation of Instantaneous Optimal Algorithms for Structural Control," by R.C. Lin, T.T. Soong and A.M. Reinhorn, 4/20/87, (PB88-134341, A04, MF-A01).

NCEER-87-0003 "Experimentation Using the Earthquake Simulation Facilities at University at Buffalo," by A.M. Reinhorn and R.L. Ketter, to be published.

NCEER-87-0004 "The System Characteristics and Performance of a Shaking Table," by J.S. Hwang, K.C. Chang and G.C. Lee, 6/1/87, (PB88-134259, A03, MF-A01). This report is available only through NTIS (see address given above).

NCEER-87-0005 "A Finite Element Formulation for Nonlinear Viscoplastic Material Using a Q Model," by O. Gyebi and G. Dasgupta, 11/2/87, (PB88-213764, A08, MF-A01).

NCEER-87-0006 "Symbolic Manipulation Program (SMP) - Algebraic Codes for Two and Three Dimensional Finite Element Formulations," by X. Lee and G. Dasgupta, 11/9/87, (PB88-218522, A05, MF-A01).

NCEER-87-0007 "Instantaneous Optimal Control Laws for Tall Buildings Under Seismic Excitations," by J.N. Yang, A. Akbarpour and P. Ghaemmaghami, 6/10/87, (PB88-134333, A06, MF-A01). This report is only available through NTIS (see address given above).

NCEER-87-0008 "IDARC: Inelastic Damage Analysis of Reinforced Concrete Frame - Shear-Wall Structures," by Y.J. Park, A.M. Reinhorn and S.K. Kunnath, 7/20/87, (PB88-134325, A09, MF-A01). This report is only available through NTIS (see address given above).

NCEER-87-0009 "Liquefaction Potential for New York State: A Preliminary Report on Sites in Manhattan and Buffalo," by M. Budhu, V. Vijayakumar, R.F. Giese and L. Baumgras, 8/31/87, (PB88-163704, A03, MF-A01). This report is available only through NTIS (see address given above).

NCEER-87-0010 "Vertical and Torsional Vibration of Foundations in Inhomogeneous Media," by A.S. Veletsos and K.W. Dotson, 6/1/87, (PB88-134291, A03, MF-A01). This report is only available through NTIS (see address given above).

NCEER-87-0011 "Seismic Probabilistic Risk Assessment and Seismic Margins Studies for Nuclear Power Plants," by Howard H.M. Hwang, 6/15/87, (PB88-134267, A03, MF-A01). This report is only available through NTIS (see address given above).

NCEER-87-0012 "Parametric Studies of Frequency Response of Secondary Systems Under Ground-Acceleration Excitations," by Y. Yong and Y.K. Lin, 6/10/87, (PB88-134309, A03, MF-A01). This report is only available through NTIS (see address given above).

NCEER-87-0013 "Frequency Response of Secondary Systems Under Seismic Excitation," by J.A. HoLung, J. Cai and Y.K. Lin, 7/31/87, (PB88-134317, A05, MF-A01). This report is only available through NTIS (see address given above).

NCEER-87-0014 "Modelling Earthquake Ground Motions in Seismically Active Regions Using Parametric Time Series Methods," by G.W. Ellis and A.S. Cakmak, 8/25/87, (PB88-134283, A08, MF-A01). This report is only available through NTIS (see address given above).

NCEER-87-0015 "Detection and Assessment of Seismic Structural Damage," by E. DiPasquale and A.S. Cakmak, 8/25/87, (PB88-163712, A05, MF-A01). This report is only available through NTIS (see address given above).

NCEER-87-0016 "Pipeline Experiment at Parkfield, California," by J. Isenberg and E. Richardson, 9/15/87, (PB88-163720, A03, MF-A01). This report is available only through NTIS (see address given above).

NCEER-87-0017 "Digital Simulation of Seismic Ground Motion," by M. Shinozuka, G. Deodatis and T. Harada, 8/31/87, (PB88-155197, A04, MF-A01). This report is available only through NTIS (see address given above).

NCEER-87-0018 "Practical Considerations for Structural Control: System Uncertainty, System Time Delay and Truncation of Small Control Forces," J.N. Yang and A. Akbarpour, 8/10/87, (PB88-163738, A08, MF-A01). This report is only available through NTIS (see address given above).

NCEER-87-0019 "Modal Analysis of Nonclassically Damped Structural Systems Using Canonical Transformation," by J.N. Yang, S. Sarkani and F.X. Long, 9/27/87, (PB88-187851, A04, MF-A01).

NCEER-87-0020 "A Nonstationary Solution in Random Vibration Theory," by J.R. Red-Horse and P.D. Spanos, 11/3/87, (PB88-163746, A03, MF-A01).

NCEER-87-0021 "Horizontal Impedances for Radially Inhomogeneous Viscoelastic Soil Layers," by A.S. Veletsos and K.W. Dotson, 10/15/87, (PB88-150859, A04, MF-A01).

NCEER-87-0022 "Seismic Damage Assessment of Reinforced Concrete Members," by Y.S. Chung, C. Meyer and M. Shinozuka, 10/9/87, (PB88-150867, A05, MF-A01). This report is available only through NTIS (see address given above).

NCEER-87-0023 "Active Structural Control in Civil Engineering," by T.T. Soong, 11/11/87, (PB88-187778, A03, MF-A01).

NCEER-87-0024 "Vertical and Torsional Impedances for Radially Inhomogeneous Viscoelastic Soil Layers," by K.W. Dotson and A.S. Veletsos, 12/87, (PB88-187786, A03, MF-A01).

NCEER-87-0025 "Proceedings from the Symposium on Seismic Hazards, Ground Motions, Soil-Liquefaction and Engineering Practice in Eastern North America," October 20-22, 1987, edited by K.H. Jacob, 12/87, (PB88-188115, A23, MF-A01). This report is available only through NTIS (see address given above).

NCEER-87-0026 "Report on the Whittier-Narrows, California, Earthquake of October 1, 1987," by J. Pantelic and A. Reinhorn, 11/87, (PB88-187752, A03, MF-A01). This report is available only through NTIS (see address given above).

NCEER-87-0027 "Design of a Modular Program for Transient Nonlinear Analysis of Large 3-D Building Structures," by S. Srivastav and J.F. Abel, 12/30/87, (PB88-187950, A05, MF-A01). This report is only available through NTIS (see address given above).

NCEER-87-0028 "Second-Year Program in Research, Education and Technology Transfer," 3/8/88, (PB88-219480, A04, MF-A01).

NCEER-88-0001 "Workshop on Seismic Computer Analysis and Design of Buildings With Interactive Graphics," by W. McGuire, J.F. Abel and C.H. Conley, 1/18/88, (PB88-187760, A03, MF-A01). This report is only available through NTIS (see address given above).

NCEER-88-0002 "Optimal Control of Nonlinear Flexible Structures," by J.N. Yang, F.X. Long and D. Wong, 1/22/88, (PB88-213772, A06, MF-A01).

NCEER-88-0003 "Substructuring Techniques in the Time Domain for Primary-Secondary Structural Systems," by G.D. Manolis and G. Juhn, 2/10/88, (PB88-213780, A04, MF-A01).

NCEER-88-0004 "Iterative Seismic Analysis of Primary-Secondary Systems," by A. Singhal, L.D. Lutes and P.D. Spanos, 2/23/88, (PB88-213798, A04, MF-A01).

NCEER-88-0005 "Stochastic Finite Element Expansion for Random Media," by P.D. Spanos and R. Ghanem, 3/14/88, (PB88-213806, A03, MF-A01).

NCEER-88-0006 "Combining Structural Optimization and Structural Control," by F.Y. Cheng and C.P. Pantelides, 1/10/88, (PB88-213814, A05, MF-A01).

NCEER-88-0007 "Seismic Performance Assessment of Code-Designed Structures," by H.H-M. Hwang, J-W. Jaw and H-J. Shau, 3/20/88, (PB88-219423, A04, MF-A01). This report is only available through NTIS (see address given above).

NCEER-88-0008 "Reliability Analysis of Code-Designed Structures Under Natural Hazards," by H.H-M. Hwang, H. Ushiba and M. Shinozuka, 2/29/88, (PB88-229471, A07, MF-A01). This report is only available through NTIS (see address given above).

NCEER-88-0009 "Seismic Fragility Analysis of Shear Wall Structures," by J-W Jaw and H.H-M. Hwang, 4/30/88, (PB89-102867, A04, MF-A01).

NCEER-88-0010 "Base Isolation of a Multi-Story Building Under a Harmonic Ground Motion - A Comparison of Performances of Various Systems," by F-G Fan, G. Ahmadi and I.G. Tadjbakhsh, 5/18/88, (PB89-122238, A06, MF-A01). This report is only available through NTIS (see address given above).

NCEER-88-0011 "Seismic Floor Response Spectra for a Combined System by Green's Functions," by F.M. Lavelle, L.A. Bergman and P.D. Spanos, 5/1/88, (PB89-102875, A03, MF-A01).

NCEER-88-0012 "A New Solution Technique for Randomly Excited Hysteretic Structures," by G.Q. Cai and Y.K. Lin, 5/16/88, (PB89-102883, A03, MF-A01).

NCEER-88-0013 "A Study of Radiation Damping and Soil-Structure Interaction Effects in the Centrifuge," by K. Weissman, supervised by J.H. Prevost, 5/24/88, (PB89-144703, A06, MF-A01).

NCEER-88-0014 "Parameter Identification and Implementation of a Kinematic Plasticity Model for Frictional Soils," by J.H. Prevost and D.V. Griffiths, to be published.

NCEER-88-0015 "Two- and Three- Dimensional Dynamic Finite Element Analyses of the Long Valley Dam," by D.V. Griffiths and J.H. Prevost, 6/17/88, (PB89-144711, A04, MF-A01).

NCEER-88-0016 "Damage Assessment of Reinforced Concrete Structures in Eastern United States," by A.M. Reinhorn, M.J. Seidel, S.K. Kunnath and Y.J. Park, 6/15/88, (PB89-122220, A04, MF-A01). This report is only available through NTIS (see address given above).

NCEER-88-0017 "Dynamic Compliance of Vertically Loaded Strip Foundations in Multilayered Viscoelastic Soils," by S. Ahmad and A.S.M. Israil, 6/17/88, (PB89-102891, A04, MF-A01).

NCEER-88-0018 "An Experimental Study of Seismic Structural Response With Added Viscoelastic Dampers," by R.C. Lin, Z. Liang, T.T. Soong and R.H. Zhang, 6/30/88, (PB89-122212, A05, MF-A01). This report is available only through NTIS (see address given above).

NCEER-88-0019 "Experimental Investigation of Primary - Secondary System Interaction," by G.D. Manolis, G. Juhn and A.M. Reinhorn, 5/27/88, (PB89-122204, A04, MF-A01).

NCEER-88-0020 "A Response Spectrum Approach For Analysis of Nonclassically Damped Structures," by J.N. Yang, S. Sarkani and F.X. Long, 4/22/88, (PB89-102909, A04, MF-A01).

NCEER-88-0021 "Seismic Interaction of Structures and Soils: Stochastic Approach," by A.S. Veletsos and A.M. Prasad, 7/21/88, (PB89-122196, A04, MF-A01). This report is only available through NTIS (see address given above).

NCEER-88-0022 "Identification of the Serviceability Limit State and Detection of Seismic Structural Damage," by E. DiPasquale and A.S. Cakmak, 6/15/88, (PB89-122188, A05, MF-A01). This report is available only through NTIS (see address given above).

NCEER-88-0023 "Multi-Hazard Risk Analysis: Case of a Simple Offshore Structure," by B.K. Bhartia and E.H. Vanmarcke, 7/21/88, (PB89-145213, A05, MF-A01).

NCEER-88-0024 "Automated Seismic Design of Reinforced Concrete Buildings," by Y.S. Chung, C. Meyer and M. Shinozuka, 7/5/88, (PB89-122170, A06, MF-A01). This report is available only through NTIS (see address given above).

NCEER-88-0025 "Experimental Study of Active Control of MDOF Structures Under Seismic Excitations," by L.L. Chung, R.C. Lin, T.T. Soong and A.M. Reinhorn, 7/10/88, (PB89-122600, A04, MF-A01).

NCEER-88-0026 "Earthquake Simulation Tests of a Low-Rise Metal Structure," by J.S. Hwang, K.C. Chang, G.C. Lee and R.L. Ketter, 8/1/88, (PB89-102917, A04, MF-A01).

NCEER-88-0027 "Systems Study of Urban Response and Reconstruction Due to Catastrophic Earthquakes," by F. Kozin and H.K. Zhou, 9/22/88, (PB90-162348, A04, MF-A01).

NCEER-88-0028 "Seismic Fragility Analysis of Plane Frame Structures," by H.H-M. Hwang and Y.K. Low, 7/31/88, (PB89-131445, A06, MF-A01).

NCEER-88-0029 "Response Analysis of Stochastic Structures," by A. Kardara, C. Bucher and M. Shinozuka, 9/22/88, (PB89-174429, A04, MF-A01).

NCEER-88-0030 "Nonnormal Accelerations Due to Yielding in a Primary Structure," by D.C.K. Chen and L.D. Lutes, 9/19/88, (PB89-131437, A04, MF-A01).

NCEER-88-0031 "Design Approaches for Soil-Structure Interaction," by A.S. Veletsos, A.M. Prasad and Y. Tang, 12/30/88, (PB89-174437, A03, MF-A01). This report is available only through NTIS (see address given above).

NCEER-88-0032 "A Re-evaluation of Design Spectra for Seismic Damage Control," by C.J. Turkstra and A.G. Tallin, 11/7/88, (PB89-145221, A05, MF-A01).

NCEER-88-0033 "The Behavior and Design of Noncontact Lap Splices Subjected to Repeated Inelastic Tensile Loading," by V.E. Sagan, P. Gergely and R.N. White, 12/8/88, (PB89-163737, A08, MF-A01).

NCEER-88-0034 "Seismic Response of Pile Foundations," by S.M. Mamoon, P.K. Banerjee and S. Ahmad, 11/1/88, (PB89-145239, A04, MF-A01).

NCEER-88-0035 "Modeling of R/C Building Structures With Flexible Floor Diaphragms (IDARC2)," by A.M. Reinhorn, S.K. Kunnath and N. Panahshahi, 9/7/88, (PB89-207153, A07, MF-A01).

NCEER-88-0036 "Solution of the Dam-Reservoir Interaction Problem Using a Combination of FEM, BEM with Particular Integrals, Modal Analysis, and Substructuring," by C-S. Tsai, G.C. Lee and R.L. Ketter, 12/31/88, (PB89-207146, A04, MF-A01).

NCEER-88-0037 "Optimal Placement of Actuators for Structural Control," by F.Y. Cheng and C.P. Pantelides, 8/15/88, (PB89-162846, A05, MF-A01).

NCEER-88-0038 "Teflon Bearings in Aseismic Base Isolation: Experimental Studies and Mathematical Modeling," by A. Mokha, M.C. Constantinou and A.M. Reinhorn, 12/5/88, (PB89-218457, A10, MF-A01). This report is available only through NTIS (see address given above).

NCEER-88-0039 "Seismic Behavior of Flat Slab High-Rise Buildings in the New York City Area," by P. Weidlinger and M. Ettouney, 10/15/88, (PB90-145681, A04, MF-A01).

NCEER-88-0040 "Evaluation of the Earthquake Resistance of Existing Buildings in New York City," by P. Weidlinger and M. Ettouney, 10/15/88, to be published.

NCEER-88-0041 "Small-Scale Modeling Techniques for Reinforced Concrete Structures Subjected to Seismic Loads," by W. Kim, A. El-Attar and R.N. White, 11/22/88, (PB89-189625, A05, MF-A01).

NCEER-88-0042 "Modeling Strong Ground Motion from Multiple Event Earthquakes," by G.W. Ellis and A.S. Cakmak, 10/15/88, (PB89-174445, A03, MF-A01).

NCEER-88-0043 "Nonstationary Models of Seismic Ground Acceleration," by M. Grigoriu, S.E. Ruiz and E. Rosenblueth, 7/15/88, (PB89-189617, A04, MF-A01).

NCEER-88-0044 "SARCF User's Guide: Seismic Analysis of Reinforced Concrete Frames," by Y.S. Chung, C. Meyer and M. Shinozuka, 11/9/88, (PB89-174452, A08, MF-A01).

NCEER-88-0045 "First Expert Panel Meeting on Disaster Research and Planning," edited by J. Pantelic and J. Stoyle, 9/15/88, (PB89-174460, A05, MF-A01).

NCEER-88-0046 "Preliminary Studies of the Effect of Degrading Infill Walls on the Nonlinear Seismic Response of Steel Frames," by C.Z. Chrysostomou, P. Gergely and J.F. Abel, 12/19/88, (PB89-208383, A05, MF-A01).

NCEER-88-0047 "Reinforced Concrete Frame Component Testing Facility - Design, Construction, Instrumentation and Operation," by S.P. Pessiki, C. Conley, T. Bond, P. Gergely and R.N. White, 12/16/88, (PB89-174478, A04, MF-A01).

NCEER-89-0001 "Effects of Protective Cushion and Soil Compliancy on the Response of Equipment Within a Seismically Excited Building," by J.A. HoLung, 2/16/89, (PB89-207179, A04, MF-A01).

NCEER-89-0002 "Statistical Evaluation of Response Modification Factors for Reinforced Concrete Structures," by H.H-M. Hwang and J-W. Jaw, 2/17/89, (PB89-207187, A05, MF-A01).

NCEER-89-0003 "Hysteretic Columns Under Random Excitation," by G-Q. Cai and Y.K. Lin, 1/9/89, (PB89-196513, A03, MF-A01).

NCEER-89-0004 "Experimental Study of `Elephant Foot Bulge' Instability of Thin-Walled Metal Tanks," by Z-H. Jia and R.L. Ketter, 2/22/89, (PB89-207195, A03, MF-A01).

NCEER-89-0005 "Experiment on Performance of Buried Pipelines Across San Andreas Fault," by J. Isenberg, E. Richardson and T.D. O'Rourke, 3/10/89, (PB89-218440, A04, MF-A01). This report is available only through NTIS (see address given above).

NCEER-89-0006 "A Knowledge-Based Approach to Structural Design of Earthquake-Resistant Buildings," by M. Subramani, P. Gergely, C.H. Conley, J.F. Abel and A.H. Zaghw, 1/15/89, (PB89-218465, A06, MF-A01).

NCEER-89-0007 "Liquefaction Hazards and Their Effects on Buried Pipelines," by T.D. O'Rourke and P.A. Lane, 2/1/89, (PB89-218481, A09, MF-A01).

NCEER-89-0008 "Fundamentals of System Identification in Structural Dynamics," by H. Imai, C-B. Yun, O. Maruyama and M. Shinozuka, 1/26/89, (PB89-207211, A04, MF-A01).

NCEER-89-0009 "Effects of the 1985 Michoacan Earthquake on Water Systems and Other Buried Lifelines in Mexico," by A.G. Ayala and M.J. O'Rourke, 3/8/89, (PB89-207229, A06, MF-A01).

NCEER-89-R010 "NCEER Bibliography of Earthquake Education Materials," by K.E.K. Ross, Second Revision, 9/1/89, (PB90-125352, A05, MF-A01). This report is replaced by NCEER-92-0018.

NCEER-89-0011 "Inelastic Three-Dimensional Response Analysis of Reinforced Concrete Building Structures (IDARC-3D), Part I - Modeling," by S.K. Kunnath and A.M. Reinhorn, 4/17/89, (PB90-114612, A07, MF-A01). This report is available only through NTIS (see address given above).

NCEER-89-0012 "Recommended Modifications to ATC-14," by C.D. Poland and J.O. Malley, 4/12/89, (PB90-108648, A15, MF-A01).

NCEER-89-0013 "Repair and Strengthening of Beam-to-Column Connections Subjected to Earthquake Loading," by M. Corazao and A.J. Durrani, 2/28/89, (PB90-109885, A06, MF-A01).

NCEER-89-0014 "Program EXKAL2 for Identification of Structural Dynamic Systems," by O. Maruyama, C-B. Yun, M. Hoshiya and M. Shinozuka, 5/19/89, (PB90-109877, A09, MF-A01).

NCEER-89-0015 "Response of Frames With Bolted Semi-Rigid Connections, Part I - Experimental Study and Analytical Predictions," by P.J. DiCorso, A.M. Reinhorn, J.R. Dickerson, J.B. Radziminski and W.L. Harper, 6/1/89, to be published.

NCEER-89-0016 "ARMA Monte Carlo Simulation in Probabilistic Structural Analysis," by P.D. Spanos and M.P. Mignolet, 7/10/89, (PB90-109893, A03, MF-A01).

NCEER-89-P017 "Preliminary Proceedings from the Conference on Disaster Preparedness - The Place of Earthquake Education in Our Schools," Edited by K.E.K. Ross, 6/23/89, (PB90-108606, A03, MF-A01).

NCEER-89-0017 "Proceedings from the Conference on Disaster Preparedness - The Place of Earthquake Education in Our Schools," Edited by K.E.K. Ross, 12/31/89, (PB90-207895, A012, MF-A02). This report is available only through NTIS (see address given above).

NCEER-89-0018 "Multidimensional Models of Hysteretic Material Behavior for Vibration Analysis of Shape Memory Energy Absorbing Devices, by E.J. Graesser and F.A. Cozzarelli, 6/7/89, (PB90-164146, A04, MF-A01).

NCEER-89-0019 "Nonlinear Dynamic Analysis of Three-Dimensional Base Isolated Structures (3D-BASIS)," by S. Nagarajaiah, A.M. Reinhorn and M.C. Constantinou, 8/3/89, (PB90-161936, A06, MF-A01). This report has been replaced by NCEER-93-0011.

NCEER-89-0020 "Structural Control Considering Time-Rate of Control Forces and Control Rate Constraints," by F.Y. Cheng and C.P. Pantelides, 8/3/89, (PB90-120445, A04, MF-A01).

NCEER-89-0021 "Subsurface Conditions of Memphis and Shelby County," by K.W. Ng, T-S. Chang and H-H.M. Hwang, 7/26/89, (PB90-120437, A03, MF-A01).

NCEER-89-0022 "Seismic Wave Propagation Effects on Straight Jointed Buried Pipelines," by K. Elhmadi and M.J. O'Rourke, 8/24/89, (PB90-162322, A10, MF-A02).

NCEER-89-0023 "Workshop on Serviceability Analysis of Water Delivery Systems," edited by M. Grigoriu, 3/6/89, (PB90-127424, A03, MF-A01).

NCEER-89-0024 "Shaking Table Study of a 1/5 Scale Steel Frame Composed of Tapered Members," by K.C. Chang, J.S. Hwang and G.C. Lee, 9/18/89, (PB90-160169, A04, MF-A01).

NCEER-89-0025 "DYNA1D: A Computer Program for Nonlinear Seismic Site Response Analysis - Technical Documentation," by Jean H. Prevost, 9/14/89, (PB90-161944, A07, MF-A01). This report is available only through NTIS (see address given above).

NCEER-89-0026 "1:4 Scale Model Studies of Active Tendon Systems and Active Mass Dampers for Aseismic Protection," by A.M. Reinhorn, T.T. Soong, R.C. Lin, Y.P. Yang, Y. Fukao, H. Abe and M. Nakai, 9/15/89, (PB90-173246, A10, MF-A02). This report is available only through NTIS (see address given above).

NCEER-89-0027 "Scattering of Waves by Inclusions in a Nonhomogeneous Elastic Half Space Solved by Boundary Element Methods," by P.K. Hadley, A. Askar and A.S. Cakmak, 6/15/89, (PB90-145699, A07, MF-A01).

NCEER-89-0028 "Statistical Evaluation of Deflection Amplification Factors for Reinforced Concrete Structures," by H.H.M. Hwang, J-W. Jaw and A.L. Ch'ng, 8/31/89, (PB90-164633, A05, MF-A01).

NCEER-89-0029 "Bedrock Accelerations in Memphis Area Due to Large New Madrid Earthquakes," by H.H.M. Hwang, C.H.S. Chen and G. Yu, 11/7/89, (PB90-162330, A04, MF-A01).

NCEER-89-0030 "Seismic Behavior and Response Sensitivity of Secondary Structural Systems," by Y.Q. Chen and T.T. Soong, 10/23/89, (PB90-164658, A08, MF-A01).

NCEER-89-0031 "Random Vibration and Reliability Analysis of Primary-Secondary Structural Systems," by Y. Ibrahim, M. Grigoriu and T.T. Soong, 11/10/89, (PB90-161951, A04, MF-A01).

NCEER-89-0032 "Proceedings from the Second U.S. - Japan Workshop on Liquefaction, Large Ground Deformation and Their Effects on Lifelines, September 26-29, 1989," Edited by T.D. O'Rourke and M. Hamada, 12/1/89, (PB90-209388, A22, MF-A03).

NCEER-89-0033 "Deterministic Model for Seismic Damage Evaluation of Reinforced Concrete Structures," by J.M. Bracci, A.M. Reinhorn, J.B. Mander and S.K. Kunnath, 9/27/89, (PB91-108803, A06, MF-A01).

NCEER-89-0034 "On the Relation Between Local and Global Damage Indices," by E. DiPasquale and A.S. Cakmak, 8/15/89, (PB90-173865, A05, MF-A01).

NCEER-89-0035 "Cyclic Undrained Behavior of Nonplastic and Low Plasticity Silts," by A.J. Walker and H.E. Stewart, 7/26/89, (PB90-183518, A10, MF-A01).

NCEER-89-0036 "Liquefaction Potential of Surficial Deposits in the City of Buffalo, New York," by M. Budhu, R. Giese and L. Baumgrass, 1/17/89, (PB90-208455, A04, MF-A01).

NCEER-89-0037 "A Deterministic Assessment of Effects of Ground Motion Incoherence," by A.S. Veletsos and Y. Tang, 7/15/89, (PB90-164294, A03, MF-A01).

NCEER-89-0038 "Workshop on Ground Motion Parameters for Seismic Hazard Mapping," July 17-18, 1989, edited by R.V. Whitman, 12/1/89, (PB90-173923, A04, MF-A01).

NCEER-89-0039 "Seismic Effects on Elevated Transit Lines of the New York City Transit Authority," by C.J. Costantino, C.A. Miller and E. Heymsfield, 12/26/89, (PB90-207887, A06, MF-A01).

NCEER-89-0040 "Centrifugal Modeling of Dynamic Soil-Structure Interaction," by K. Weissman, Supervised by J.H. Prevost, 5/10/89, (PB90-207879, A07, MF-A01).

NCEER-89-0041 "Linearized Identification of Buildings With Cores for Seismic Vulnerability Assessment," by I-K. Ho and A.E. Aktan, 11/1/89, (PB90-251943, A07, MF-A01).

NCEER-90-0001 "Geotechnical and Lifeline Aspects of the October 17, 1989 Loma Prieta Earthquake in San Francisco," by T.D. O'Rourke, H.E. Stewart, F.T. Blackburn and T.S. Dickerman, 1/90, (PB90-208596, A05, MF-A01).

NCEER-90-0002 "Nonnormal Secondary Response Due to Yielding in a Primary Structure," by D.C.K. Chen and L.D. Lutes, 2/28/90, (PB90-251976, A07, MF-A01).

NCEER-90-0003 "Earthquake Education Materials for Grades K-12," by K.E.K. Ross, 4/16/90, (PB91-251984, A05, MF-A05). This report has been replaced by NCEER-92-0018.

NCEER-90-0004 "Catalog of Strong Motion Stations in Eastern North America," by R.W. Busby, 4/3/90, (PB90-251984, A05, MF-A01).

NCEER-90-0005 "NCEER Strong-Motion Data Base: A User Manual for the GeoBase Release (Version 1.0 for the Sun3)," by P. Friberg and K. Jacob, 3/31/90 (PB90-258062, A04, MF-A01).

NCEER-90-0006 "Seismic Hazard Along a Crude Oil Pipeline in the Event of an 1811-1812 Type New Madrid Earthquake," by H.H.M. Hwang and C-H.S. Chen, 4/16/90, (PB90-258054, A04, MF-A01).

NCEER-90-0007 "Site-Specific Response Spectra for Memphis Sheahan Pumping Station," by H.H.M. Hwang and C.S. Lee, 5/15/90, (PB91-108811, A05, MF-A01).

NCEER-90-0008 "Pilot Study on Seismic Vulnerability of Crude Oil Transmission Systems," by T. Ariman, R. Dobry, M. Grigoriu, F. Kozin, M. O'Rourke, T. O'Rourke and M. Shinozuka, 5/25/90, (PB91-108837, A06, MF-A01).

NCEER-90-0009 "A Program to Generate Site Dependent Time Histories: EQGEN," by G.W. Ellis, M. Srinivasan and A.S. Cakmak, 1/30/90, (PB91-108829, A04, MF-A01).

NCEER-90-0010 "Active Isolation for Seismic Protection of Operating Rooms," by M.E. Talbott, Supervised by M. Shinozuka, 6/8/9, (PB91-110205, A05, MF-A01).

NCEER-90-0011 "Program LINEARID for Identification of Linear Structural Dynamic Systems," by C-B. Yun and M. Shinozuka, 6/25/90, (PB91-110312, A08, MF-A01).

NCEER-90-0012 "Two-Dimensional Two-Phase Elasto-Plastic Seismic Response of Earth Dams," by A.N. Yiagos, Supervised by J.H. Prevost, 6/20/90, (PB91-110197, A13, MF-A02).

NCEER-90-0013 "Secondary Systems in Base-Isolated Structures: Experimental Investigation, Stochastic Response and Stochastic Sensitivity," by G.D. Manolis, G. Juhn, M.C. Constantinou and A.M. Reinhorn, 7/1/90, (PB91-110320, A08, MF-A01).

NCEER-90-0014 "Seismic Behavior of Lightly-Reinforced Concrete Column and Beam-Column Joint Details," by S.P. Pessiki, C.H. Conley, P. Gergely and R.N. White, 8/22/90, (PB91-108795, A11, MF-A02).

NCEER-90-0015 "Two Hybrid Control Systems for Building Structures Under Strong Earthquakes," by J.N. Yang and A. Danielians, 6/29/90, (PB91-125393, A04, MF-A01).

NCEER-90-0016 "Instantaneous Optimal Control with Acceleration and Velocity Feedback," by J.N. Yang and Z. Li, 6/29/90, (PB91-125401, A03, MF-A01).

NCEER-90-0017 "Reconnaissance Report on the Northern Iran Earthquake of June 21, 1990," by M. Mehrain, 10/4/90, (PB91-125377, A03, MF-A01).

NCEER-90-0018 "Evaluation of Liquefaction Potential in Memphis and Shelby County," by T.S. Chang, P.S. Tang, C.S. Lee and H. Hwang, 8/10/90, (PB91-125427, A09, MF-A01).

NCEER-90-0019 "Experimental and Analytical Study of a Combined Sliding Disc Bearing and Helical Steel Spring Isolation System," by M.C. Constantinou, A.S. Mokha and A.M. Reinhorn, 10/4/90, (PB91-125385, A06, MF-A01). This report is available only through NTIS (see address given above).

NCEER-90-0020 "Experimental Study and Analytical Prediction of Earthquake Response of a Sliding Isolation System with a Spherical Surface," by A.S. Mokha, M.C. Constantinou and A.M. Reinhorn, 10/11/90, (PB91-125419, A05, MF-A01).

NCEER-90-0021 "Dynamic Interaction Factors for Floating Pile Groups," by G. Gazetas, K. Fan, A. Kaynia and E. Kausel, 9/10/90, (PB91-170381, A05, MF-A01).

NCEER-90-0022 "Evaluation of Seismic Damage Indices for Reinforced Concrete Structures," by S. Rodriguez-Gomez and A.S. Cakmak, 9/30/90, PB91-171322, A06, MF-A01).

NCEER-90-0023 "Study of Site Response at a Selected Memphis Site," by H. Desai, S. Ahmad, E.S. Gazetas and M.R. Oh, 10/11/90, (PB91-196857, A03, MF-A01).

NCEER-90-0024 "A User's Guide to Strongmo: Version 1.0 of NCEER's Strong-Motion Data Access Tool for PCs and Terminals," by P.A. Friberg and C.A.T. Susch, 11/15/90, (PB91-171272, A03, MF-A01).

NCEER-90-0025 "A Three-Dimensional Analytical Study of Spatial Variability of Seismic Ground Motions," by L-L. Hong and A.H.-S. Ang, 10/30/90, (PB91-170399, A09, MF-A01).

NCEER-90-0026 "MUMOID User's Guide - A Program for the Identification of Modal Parameters," by S. Rodriguez-Gomez and E. DiPasquale, 9/30/90, (PB91-171298, A04, MF-A01).

NCEER-90-0027 "SARCF-II User's Guide - Seismic Analysis of Reinforced Concrete Frames," by S. Rodriguez-Gomez, Y.S. Chung and C. Meyer, 9/30/90, (PB91-171280, A05, MF-A01).

NCEER-90-0028 "Viscous Dampers: Testing, Modeling and Application in Vibration and Seismic Isolation," by N. Makris and M.C. Constantinou, 12/20/90 (PB91-190561, A06, MF-A01).

NCEER-90-0029 "Soil Effects on Earthquake Ground Motions in the Memphis Area," by H. Hwang, C.S. Lee, K.W. Ng and T.S. Chang, 8/2/90, (PB91-190751, A05, MF-A01).

NCEER-91-0001 "Proceedings from the Third Japan-U.S. Workshop on Earthquake Resistant Design of Lifeline Facilities and Countermeasures for Soil Liquefaction, December 17-19, 1990," edited by T.D. O'Rourke and M. Hamada, 2/1/91, (PB91-179259, A99, MF-A04).

NCEER-91-0002 "Physical Space Solutions of Non-Proportionally Damped Systems," by M. Tong, Z. Liang and G.C. Lee, 1/15/91, (PB91-179242, A04, MF-A01).

NCEER-91-0003 "Seismic Response of Single Piles and Pile Groups," by K. Fan and G. Gazetas, 1/10/91, (PB92-174994, A04, MF-A01).

NCEER-91-0004 "Damping of Structures: Part 1 - Theory of Complex Damping," by Z. Liang and G. Lee, 10/10/91, (PB92-197235, A12, MF-A03).

NCEER-91-0005 "3D-BASIS - Nonlinear Dynamic Analysis of Three Dimensional Base Isolated Structures: Part II," by S. Nagarajaiah, A.M. Reinhorn and M.C. Constantinou, 2/28/91, (PB91-190553, A07, MF-A01). This report has been replaced by NCEER-93-0011.

NCEER-91-0006 "A Multidimensional Hysteretic Model for Plasticity Deforming Metals in Energy Absorbing Devices," by E.J. Graesser and F.A. Cozzarelli, 4/9/91, (PB92-108364, A04, MF-A01).

NCEER-91-0007 "A Framework for Customizable Knowledge-Based Expert Systems with an Application to a KBES for Evaluating the Seismic Resistance of Existing Buildings," by E.G. Ibarra-Anaya and S.J. Fenves, 4/9/91, (PB91-210930, A08, MF-A01).

NCEER-91-0008 "Nonlinear Analysis of Steel Frames with Semi-Rigid Connections Using the Capacity Spectrum Method," by G.G. Deierlein, S-H. Hsieh, Y-J. Shen and J.F. Abel, 7/2/91, (PB92-113828, A05, MF-A01).

NCEER-91-0009 "Earthquake Education Materials for Grades K-12," by K.E.K. Ross, 4/30/91, (PB91-212142, A06, MF-A01). This report has been replaced by NCEER-92-0018.

NCEER-91-0010 "Phase Wave Velocities and Displacement Phase Differences in a Harmonically Oscillating Pile," by N. Makris and G. Gazetas, 7/8/91, (PB92-108356, A04, MF-A01).

NCEER-91-0011 "Dynamic Characteristics of a Full-Size Five-Story Steel Structure and a 2/5 Scale Model," by K.C. Chang, G.C. Yao, G.C. Lee, D.S. Hao and Y.C. Yeh," 7/2/91, (PB93-116648, A06, MF-A02).

NCEER-91-0012 "Seismic Response of a 2/5 Scale Steel Structure with Added Viscoelastic Dampers," by K.C. Chang, T.T. Soong, S-T. Oh and M.L. Lai, 5/17/91, (PB92-110816, A05, MF-A01).

NCEER-91-0013 "Earthquake Response of Retaining Walls; Full-Scale Testing and Computational Modeling," by S. Alampalli and A-W.M. Elgamal, 6/20/91, to be published.

NCEER-91-0014 "3D-BASIS-M: Nonlinear Dynamic Analysis of Multiple Building Base Isolated Structures," by P.C. Tsopelas, S. Nagarajaiah, M.C. Constantinou and A.M. Reinhorn, 5/28/91, (PB92-113885, A09, MF-A02).

NCEER-91-0015 "Evaluation of SEAOC Design Requirements for Sliding Isolated Structures," by D. Theodossiou and M.C. Constantinou, 6/10/91, (PB92-114602, A11, MF-A03).

NCEER-91-0016 "Closed-Loop Modal Testing of a 27-Story Reinforced Concrete Flat Plate-Core Building," by H.R. Somaprasad, T. Toksoy, H. Yoshiyuki and A.E. Aktan, 7/15/91, (PB92-129980, A07, MF-A02).

NCEER-91-0017 "Shake Table Test of a 1/6 Scale Two-Story Lightly Reinforced Concrete Building," by A.G. El-Attar, R.N. White and P. Gergely, 2/28/91, (PB92-222447, A06, MF-A02).

NCEER-91-0018 "Shake Table Test of a 1/8 Scale Three-Story Lightly Reinforced Concrete Building," by A.G. El-Attar, R.N. White and P. Gergely, 2/28/91, (PB93-116630, A08, MF-A02).

NCEER-91-0019 "Transfer Functions for Rigid Rectangular Foundations," by A.S. Veletsos, A.M. Prasad and W.H. Wu, 7/31/91, to be published.

NCEER-91-0020 "Hybrid Control of Seismic-Excited Nonlinear and Inelastic Structural Systems," by J.N. Yang, Z. Li and A. Danielians, 8/1/91, (PB92-143171, A06, MF-A02).

NCEER-91-0021 "The NCEER-91 Earthquake Catalog: Improved Intensity-Based Magnitudes and Recurrence Relations for U.S. Earthquakes East of New Madrid," by L. Seeber and J.G. Armbruster, 8/28/91, (PB92-176742, A06, MF-A02).

NCEER-91-0022 "Proceedings from the Implementation of Earthquake Planning and Education in Schools: The Need for Change - The Roles of the Changemakers," by K.E.K. Ross and F. Winslow, 7/23/91, (PB92-129998, A12, MF-A03).

NCEER-91-0023 "A Study of Reliability-Based Criteria for Seismic Design of Reinforced Concrete Frame Buildings," by H.H.M. Hwang and H-M. Hsu, 8/10/91, (PB92-140235, A09, MF-A02).

NCEER-91-0024 "Experimental Verification of a Number of Structural System Identification Algorithms," by R.G. Ghanem, H. Gavin and M. Shinozuka, 9/18/91, (PB92-176577, A18, MF-A04).

NCEER-91-0025 "Probabilistic Evaluation of Liquefaction Potential," by H.H.M. Hwang and C.S. Lee," 11/25/91, (PB92-143429, A05, MF-A01).

NCEER-91-0026 "Instantaneous Optimal Control for Linear, Nonlinear and Hysteretic Structures - Stable Controllers," by J.N. Yang and Z. Li, 11/15/91, (PB92-163807, A04, MF-A01).

NCEER-91-0027 "Experimental and Theoretical Study of a Sliding Isolation System for Bridges," by M.C. Constantinou, A. Kartoum, A.M. Reinhorn and P. Bradford, 11/15/91, (PB92-176973, A10, MF-A03).

NCEER-92-0001 "Case Studies of Liquefaction and Lifeline Performance During Past Earthquakes, Volume 1: Japanese Case Studies," Edited by M. Hamada and T. O'Rourke, 2/17/92, (PB92-197243, A18, MF-A04).

NCEER-92-0002 "Case Studies of Liquefaction and Lifeline Performance During Past Earthquakes, Volume 2: United States Case Studies," Edited by T. O'Rourke and M. Hamada, 2/17/92, (PB92-197250, A20, MF-A04).

NCEER-92-0003 "Issues in Earthquake Education," Edited by K. Ross, 2/3/92, (PB92-222389, A07, MF-A02).

NCEER-92-0004 "Proceedings from the First U.S. - Japan Workshop on Earthquake Protective Systems for Bridges," Edited by I.G. Buckle, 2/4/92, (PB94-142239, A99, MF-A06).

NCEER-92-0005 "Seismic Ground Motion from a Haskell-Type Source in a Multiple-Layered Half-Space," A.P. Theoharis, G. Deodatis and M. Shinozuka, 1/2/92, to be published.

NCEER-92-0006 "Proceedings from the Site Effects Workshop," Edited by R. Whitman, 2/29/92, (PB92-197201, A04, MF-A01).

NCEER-92-0007 "Engineering Evaluation of Permanent Ground Deformations Due to Seismically-Induced Liquefaction," by M.H. Baziar, R. Dobry and A-W.M. Elgamal, 3/24/92, (PB92-222421, A13, MF-A03).

NCEER-92-0008 "A Procedure for the Seismic Evaluation of Buildings in the Central and Eastern United States," by C.D. Poland and J.O. Malley, 4/2/92, (PB92-222439, A20, MF-A04).

NCEER-92-0009 "Experimental and Analytical Study of a Hybrid Isolation System Using Friction Controllable Sliding Bearings," by M.Q. Feng, S. Fujii and M. Shinozuka, 5/15/92, (PB93-150282, A06, MF-A02).

NCEER-92-0010 "Seismic Resistance of Slab-Column Connections in Existing Non-Ductile Flat-Plate Buildings," by A.J. Durrani and Y. Du, 5/18/92, (PB93-116812, A06, MF-A02).

NCEER-92-0011 "The Hysteretic and Dynamic Behavior of Brick Masonry Walls Upgraded by Ferrocement Coatings Under Cyclic Loading and Strong Simulated Ground Motion," by H. Lee and S.P. Prawel, 5/11/92, to be published.

NCEER-92-0012 "Study of Wire Rope Systems for Seismic Protection of Equipment in Buildings," by G.F. Demetriades, M.C. Constantinou and A.M. Reinhorn, 5/20/92, (PB93-116655, A08, MF-A02).

NCEER-92-0013 "Shape Memory Structural Dampers: Material Properties, Design and Seismic Testing," by P.R. Witting and F.A. Cozzarelli, 5/26/92, (PB93-116663, A05, MF-A01).

NCEER-92-0014 "Longitudinal Permanent Ground Deformation Effects on Buried Continuous Pipelines," by M.J. O'Rourke, and C. Nordberg, 6/15/92, (PB93-116671, A08, MF-A02).

NCEER-92-0015 "A Simulation Method for Stationary Gaussian Random Functions Based on the Sampling Theorem," by M. Grigoriu and S. Balopoulou, 6/11/92, (PB93-127496, A05, MF-A01).

NCEER-92-0016 "Gravity-Load-Designed Reinforced Concrete Buildings: Seismic Evaluation of Existing Construction and Detailing Strategies for Improved Seismic Resistance," by G.W. Hoffmann, S.K. Kunnath, A.M. Reinhorn and J.B. Mander, 7/15/92, (PB94-142007, A08, MF-A02).

NCEER-92-0017 "Observations on Water System and Pipeline Performance in the Limón Area of Costa Rica Due to the April 22, 1991 Earthquake," by M. O'Rourke and D. Ballantyne, 6/30/92, (PB93-126811, A06, MF-A02).

NCEER-92-0018 "Fourth Edition of Earthquake Education Materials for Grades K-12," Edited by K.E.K. Ross, 8/10/92, (PB93-114023, A07, MF-A02).

NCEER-92-0019 "Proceedings from the Fourth Japan-U.S. Workshop on Earthquake Resistant Design of Lifeline Facilities and Countermeasures for Soil Liquefaction," Edited by M. Hamada and T.D. O'Rourke, 8/12/92, (PB93-163939, A99, MF-E11).

NCEER-92-0020 "Active Bracing System: A Full Scale Implementation of Active Control," by A.M. Reinhorn, T.T. Soong, R.C. Lin, M.A. Riley, Y.P. Wang, S. Aizawa and M. Higashino, 8/14/92, (PB93-127512, A06, MF-A02).

NCEER-92-0021 "Empirical Analysis of Horizontal Ground Displacement Generated by Liquefaction-Induced Lateral Spreads," by S.F. Bartlett and T.L. Youd, 8/17/92, (PB93-188241, A06, MF-A02).

NCEER-92-0022 "IDARC Version 3.0: Inelastic Damage Analysis of Reinforced Concrete Structures," by S.K. Kunnath, A.M. Reinhorn and R.F. Lobo, 8/31/92, (PB93-227502, A07, MF-A02).

NCEER-92-0023 "A Semi-Empirical Analysis of Strong-Motion Peaks in Terms of Seismic Source, Propagation Path and Local Site Conditions, by M. Kamiyama, M.J. O'Rourke and R. Flores-Berrones, 9/9/92, (PB93-150266, A08, MF-A02).

NCEER-92-0024 "Seismic Behavior of Reinforced Concrete Frame Structures with Nonductile Details, Part I: Summary of Experimental Findings of Full Scale Beam-Column Joint Tests," by A. Beres, R.N. White and P. Gergely, 9/30/92, (PB93-227783, A05, MF-A01).

NCEER-92-0025 "Experimental Results of Repaired and Retrofitted Beam-Column Joint Tests in Lightly Reinforced Concrete Frame Buildings," by A. Beres, S. El-Borgi, R.N. White and P. Gergely, 10/29/92, (PB93-227791, A05, MF-A01).

NCEER-92-0026 "A Generalization of Optimal Control Theory: Linear and Nonlinear Structures," by J.N. Yang, Z. Li and S. Vongchavalitkul, 11/2/92, (PB93-188621, A05, MF-A01).

NCEER-92-0027 "Seismic Resistance of Reinforced Concrete Frame Structures Designed Only for Gravity Loads: Part I - Design and Properties of a One-Third Scale Model Structure," by J.M. Bracci, A.M. Reinhorn and J.B. Mander, 12/1/92, (PB94-104502, A08, MF-A02).

NCEER-92-0028 "Seismic Resistance of Reinforced Concrete Frame Structures Designed Only for Gravity Loads: Part II - Experimental Performance of Subassemblages," by L.E. Aycardi, J.B. Mander and A.M. Reinhorn, 12/1/92, (PB94-104510, A08, MF-A02).

NCEER-92-0029 "Seismic Resistance of Reinforced Concrete Frame Structures Designed Only for Gravity Loads: Part III - Experimental Performance and Analytical Study of a Structural Model," by J.M. Bracci, A.M. Reinhorn and J.B. Mander, 12/1/92, (PB93-227528, A09, MF-A01).

NCEER-92-0030 "Evaluation of Seismic Retrofit of Reinforced Concrete Frame Structures: Part I - Experimental Performance of Retrofitted Subassemblages," by D. Choudhuri, J.B. Mander and A.M. Reinhorn, 12/8/92, (PB93-198307, A07, MF-A02).

NCEER-92-0031 "Evaluation of Seismic Retrofit of Reinforced Concrete Frame Structures: Part II - Experimental Performance and Analytical Study of a Retrofitted Structural Model," by J.M. Bracci, A.M. Reinhorn and J.B. Mander, 12/8/92, (PB93-198315, A09, MF-A03).

NCEER-92-0032 "Experimental and Analytical Investigation of Seismic Response of Structures with Supplemental Fluid Viscous Dampers," by M.C. Constantinou and M.D. Symans, 12/21/92, (PB93-191435, A10, MF-A03). This report is available only through NTIS (see address given above).

NCEER-92-0033 "Reconnaissance Report on the Cairo, Egypt Earthquake of October 12, 1992," by M. Khater, 12/23/92, (PB93-188621, A03, MF-A01).

NCEER-92-0034 "Low-Level Dynamic Characteristics of Four Tall Flat-Plate Buildings in New York City," by H. Gavin, S. Yuan, J. Grossman, E. Pekelis and K. Jacob, 12/28/92, (PB93-188217, A07, MF-A02).

NCEER-93-0001 "An Experimental Study on the Seismic Performance of Brick-Infilled Steel Frames With and Without Retrofit," by J.B. Mander, B. Nair, K. Wojtkowski and J. Ma, 1/29/93, (PB93-227510, A07, MF-A02).

NCEER-93-0002 "Social Accounting for Disaster Preparedness and Recovery Planning," by S. Cole, E. Pantoja and V. Razak, 2/22/93, (PB94-142114, A12, MF-A03).

NCEER-93-0003 "Assessment of 1991 NEHRP Provisions for Nonstructural Components and Recommended Revisions," by T.T. Soong, G. Chen, Z. Wu, R-H. Zhang and M. Grigoriu, 3/1/93, (PB93-188639, A06, MF-A02).

NCEER-93-0004 "Evaluation of Static and Response Spectrum Analysis Procedures of SEAOC/UBC for Seismic Isolated Structures," by C.W. Winters and M.C. Constantinou, 3/23/93, (PB93-198299, A10, MF-A03).

NCEER-93-0005 "Earthquakes in the Northeast - Are We Ignoring the Hazard? A Workshop on Earthquake Science and Safety for Educators," edited by K.E.K. Ross, 4/2/93, (PB94-103066, A09, MF-A02).

NCEER-93-0006 "Inelastic Response of Reinforced Concrete Structures with Viscoelastic Braces," by R.F. Lobo, J.M. Bracci, K.L. Shen, A.M. Reinhorn and T.T. Soong, 4/5/93, (PB93-227486, A05, MF-A02).

NCEER-93-0007 "Seismic Testing of Installation Methods for Computers and Data Processing Equipment," by K. Kosar, T.T. Soong, K.L. Shen, J.A. HoLung and Y.K. Lin, 4/12/93, (PB93-198299, A07, MF-A02).

NCEER-93-0008 "Retrofit of Reinforced Concrete Frames Using Added Dampers," by A. Reinhorn, M. Constantinou and C. Li, to be published.

NCEER-93-0009 "Seismic Behavior and Design Guidelines for Steel Frame Structures with Added Viscoelastic Dampers," by K.C. Chang, M.L. Lai, T.T. Soong, D.S. Hao and Y.C. Yeh, 5/1/93, (PB94-141959, A07, MF-A02).

NCEER-93-0010 "Seismic Performance of Shear-Critical Reinforced Concrete Bridge Piers," by J.B. Mander, S.M. Waheed, M.T.A. Chaudhary and S.S. Chen, 5/12/93, (PB93-227494, A08, MF-A02).

NCEER-93-0011 "3D-BASIS-TABS: Computer Program for Nonlinear Dynamic Analysis of Three Dimensional Base Isolated Structures," by S. Nagarajaiah, C. Li, A.M. Reinhorn and M.C. Constantinou, 8/2/93, (PB94-141819, A09, MF-A02).

NCEER-93-0012 "Effects of Hydrocarbon Spills from an Oil Pipeline Break on Ground Water," by O.J. Helweg and H.H.M. Hwang, 8/3/93, (PB94-141942, A06, MF-A02).

NCEER-93-0013 "Simplified Procedures for Seismic Design of Nonstructural Components and Assessment of Current Code Provisions," by M.P. Singh, L.E. Suarez, E.E. Matheu and G.O. Maldonado, 8/4/93, (PB94-141827, A09, MF-A02).

NCEER-93-0014 "An Energy Approach to Seismic Analysis and Design of Secondary Systems," by G. Chen and T.T. Soong, 8/6/93, (PB94-142767, A11, MF-A03).

NCEER-93-0015 "Proceedings from School Sites: Becoming Prepared for Earthquakes - Commemorating the Third Anniversary of the Loma Prieta Earthquake," Edited by F.E. Winslow and K.E.K. Ross, 8/16/93, (PB94-154275, A16, MF-A02).

NCEER-93-0016 "Reconnaissance Report of Damage to Historic Monuments in Cairo, Egypt Following the October 12, 1992 Dahshur Earthquake," by D. Sykora, D. Look, G. Croci, E. Karaesmen and E. Karaesmen, 8/19/93, (PB94-142221, A08, MF-A02).

NCEER-93-0017 "The Island of Guam Earthquake of August 8, 1993," by S.W. Swan and S.K. Harris, 9/30/93, (PB94-141843, A04, MF-A01).

NCEER-93-0018 "Engineering Aspects of the October 12, 1992 Egyptian Earthquake," by A.W. Elgamal, M. Amer, K. Adalier and A. Abul-Fadl, 10/7/93, (PB94-141983, A05, MF-A01).

NCEER-93-0019 "Development of an Earthquake Motion Simulator and its Application in Dynamic Centrifuge Testing," by I. Krstelj, Supervised by J.H. Prevost, 10/23/93, (PB94-181773, A-10, MF-A03).

NCEER-93-0020 "NCEER-Taisei Corporation Research Program on Sliding Seismic Isolation Systems for Bridges: Experimental and Analytical Study of a Friction Pendulum System (FPS)," by M.C. Constantinou, P. Tsopelas, Y-S. Kim and S. Okamoto, 11/1/93, (PB94-142775, A08, MF-A02).

NCEER-93-0021 "Finite Element Modeling of Elastomeric Seismic Isolation Bearings," by L.J. Billings, Supervised by R. Shepherd, 11/8/93, to be published.

NCEER-93-0022 "Seismic Vulnerability of Equipment in Critical Facilities: Life-Safety and Operational Consequences," by K. Porter, G.S. Johnson, M.M. Zadeh, C. Scawthorn and S. Eder, 11/24/93, (PB94-181765, A16, MF-A03).

NCEER-93-0023 "Hokkaido Nansei-oki, Japan Earthquake of July 12, 1993, by P.I. Yanev and C.R. Scawthorn, 12/23/93, (PB94-181500, A07, MF-A01).

NCEER-94-0001 "An Evaluation of Seismic Serviceability of Water Supply Networks with Application to the San Francisco Auxiliary Water Supply System," by I. Markov, Supervised by M. Grigoriu and T. O'Rourke, 1/21/94, (PB94-204013, A07, MF-A02).

NCEER-94-0002 "NCEER-Taisei Corporation Research Program on Sliding Seismic Isolation Systems for Bridges: Experimental and Analytical Study of Systems Consisting of Sliding Bearings, Rubber Restoring Force Devices and Fluid Dampers," Volumes I and II, by P. Tsopelas, S. Okamoto, M.C. Constantinou, D. Ozaki and S. Fujii, 2/4/94, (PB94-181740, A09, MF-A02 and PB94-181757, A12, MF-A03).

NCEER-94-0003 "A Markov Model for Local and Global Damage Indices in Seismic Analysis," by S. Rahman and M. Grigoriu, 2/18/94, (PB94-206000, A12, MF-A03).

NCEER-94-0004 "Proceedings from the NCEER Workshop on Seismic Response of Masonry Infills," edited by D.P. Abrams, 3/1/94, (PB94-180783, A07, MF-A02).

NCEER-94-0005 "The Northridge, California Earthquake of January 17, 1994: General Reconnaissance Report," edited by J.D. Goltz, 3/11/94, (PB94-193943, A10, MF-A03).

NCEER-94-0006 "Seismic Energy Based Fatigue Damage Analysis of Bridge Columns: Part I - Evaluation of Seismic Capacity," by G.A. Chang and J.B. Mander, 3/14/94, (PB94-219185, A11, MF-A03).

NCEER-94-0007 "Seismic Isolation of Multi-Story Frame Structures Using Spherical Sliding Isolation Systems," by T.M. Al-Hussaini, V.A. Zayas and M.C. Constantinou, 3/17/94, (PB94-193745, A09, MF-A02).

NCEER-94-0008 "The Northridge, California Earthquake of January 17, 1994: Performance of Highway Bridges," edited by I.G. Buckle, 3/24/94, (PB94-193851, A06, MF-A02).

NCEER-94-0009 "Proceedings of the Third U.S.-Japan Workshop on Earthquake Protective Systems for Bridges," edited by I.G. Buckle and I. Friedland, 3/31/94, (PB94-195815, A99, MF-A06).

NCEER-94-0010 "3D-BASIS-ME: Computer Program for Nonlinear Dynamic Analysis of Seismically Isolated Single and Multiple Structures and Liquid Storage Tanks," by P.C. Tsopelas, M.C. Constantinou and A.M. Reinhorn, 4/12/94, (PB94-204922, A09, MF-A02).

NCEER-94-0011 "The Northridge, California Earthquake of January 17, 1994: Performance of Gas Transmission Pipelines," by T.D. O'Rourke and M.C. Palmer, 5/16/94, (PB94-204989, A05, MF-A01).

NCEER-94-0012 "Feasibility Study of Replacement Procedures and Earthquake Performance Related to Gas Transmission Pipelines," by T.D. O'Rourke and M.C. Palmer, 5/25/94, (PB94-206638, A09, MF-A02).

NCEER-94-0013 "Seismic Energy Based Fatigue Damage Analysis of Bridge Columns: Part II - Evaluation of Seismic Demand," by G.A. Chang and J.B. Mander, 6/1/94, (PB95-18106, A08, MF-A02).

NCEER-94-0014 "NCEER-Taisei Corporation Research Program on Sliding Seismic Isolation Systems for Bridges: Experimental and Analytical Study of a System Consisting of Sliding Bearings and Fluid Restoring Force/Damping Devices," by P. Tsopelas and M.C. Constantinou, 6/13/94, (PB94-219144, A10, MF-A03).

NCEER-94-0015 "Generation of Hazard-Consistent Fragility Curves for Seismic Loss Estimation Studies," by H. Hwang and J-R. Huo, 6/14/94, (PB95-181996, A09, MF-A02).

NCEER-94-0016 "Seismic Study of Building Frames with Added Energy-Absorbing Devices," by W.S. Pong, C.S. Tsai and G.C. Lee, 6/20/94, (PB94-219136, A10, A03).

NCEER-94-0017 "Sliding Mode Control for Seismic-Excited Linear and Nonlinear Civil Engineering Structures," by J. Yang, J. Wu, A. Agrawal and Z. Li, 6/21/94, (PB95-138483, A06, MF-A02).

NCEER-94-0018 "3D-BASIS-TABS Version 2.0: Computer Program for Nonlinear Dynamic Analysis of Three Dimensional Base Isolated Structures," by A.M. Reinhorn, S. Nagarajaiah, M.C. Constantinou, P. Tsopelas and R. Li, 6/22/94, (PB95-182176, A08, MF-A02).

NCEER-94-0019 "Proceedings of the International Workshop on Civil Infrastructure Systems: Application of Intelligent Systems and Advanced Materials on Bridge Systems," Edited by G.C. Lee and K.C. Chang, 7/18/94, (PB95-252474, A20, MF-A04).

NCEER-94-0020 "Study of Seismic Isolation Systems for Computer Floors," by V. Lambrou and M.C. Constantinou, 7/19/94, (PB95-138533, A10, MF-A03).

NCEER-94-0021 "Proceedings of the U.S.-Italian Workshop on Guidelines for Seismic Evaluation and Rehabilitation of Unreinforced Masonry Buildings," Edited by D.P. Abrams and G.M. Calvi, 7/20/94, (PB95-138749, A13, MF-A03).

NCEER-94-0022 "NCEER-Taisei Corporation Research Program on Sliding Seismic Isolation Systems for Bridges: Experimental and Analytical Study of a System Consisting of Lubricated PTFE Sliding Bearings and Mild Steel Dampers," by P. Tsopelas and M.C. Constantinou, 7/22/94, (PB95-182184, A08, MF-A02).

NCEER-94-0023 "Development of Reliability-Based Design Criteria for Buildings Under Seismic Load," by Y.K. Wen, H. Hwang and M. Shinozuka, 8/1/94, (PB95-211934, A08, MF-A02).

NCEER-94-0024 "Experimental Verification of Acceleration Feedback Control Strategies for an Active Tendon System," by S.J. Dyke, B.F. Spencer, Jr., P. Quast, M.K. Sain, D.C. Kaspari, Jr. and T.T. Soong, 8/29/94, (PB95-212320, A05, MF-A01).

NCEER-94-0025 "Seismic Retrofitting Manual for Highway Bridges," Edited by I.G. Buckle and I.F. Friedland, published by the Federal Highway Administration (PB95-212676, A15, MF-A03).

NCEER-94-0026 "Proceedings from the Fifth U.S.-Japan Workshop on Earthquake Resistant Design of Lifeline Facilities and Countermeasures Against Soil Liquefaction," Edited by T.D. O'Rourke and M. Hamada, 11/7/94, (PB95-220802, A99, MF-E08).

NCEER-95-0001 "Experimental and Analytical Investigation of Seismic Retrofit of Structures with Supplemental Damping: Part 1 - Fluid Viscous Damping Devices," by A.M. Reinhorn, C. Li and M.C. Constantinou, 1/3/95, (PB95-266599, A09, MF-A02).

NCEER-95-0002 "Experimental and Analytical Study of Low-Cycle Fatigue Behavior of Semi-Rigid Top-And-Seat Angle Connections," by G. Pekcan, J.B. Mander and S.S. Chen, 1/5/95, (PB95-220042, A07, MF-A02).

NCEER-95-0003 "NCEER-ATC Joint Study on Fragility of Buildings," by T. Anagnos, C. Rojahn and A.S. Kiremidjian, 1/20/95, (PB95-220026, A06, MF-A02).

NCEER-95-0004 "Nonlinear Control Algorithms for Peak Response Reduction," by Z. Wu, T.T. Soong, V. Gattulli and R.C. Lin, 2/16/95, (PB95-220349, A05, MF-A01).

NCEER-95-0005 "Pipeline Replacement Feasibility Study: A Methodology for Minimizing Seismic and Corrosion Risks to Underground Natural Gas Pipelines," by R.T. Eguchi, H.A. Seligson and D.G. Honegger, 3/2/95, (PB95-252326, A06, MF-A02).

NCEER-95-0006 "Evaluation of Seismic Performance of an 11-Story Frame Building During the 1994 Northridge Earthquake," by F. Naeim, R. DiSulio, K. Benuska, A. Reinhorn and C. Li, to be published.

NCEER-95-0007 "Prioritization of Bridges for Seismic Retrofitting," by N. Basöz and A.S. Kiremidjian, 4/24/95, (PB95-252300, A08, MF-A02).

NCEER-95-0008 "Method for Developing Motion Damage Relationships for Reinforced Concrete Frames," by A. Singhal and A.S. Kiremidjian, 5/11/95, (PB95-266607, A06, MF-A02).

NCEER-95-0009 "Experimental and Analytical Investigation of Seismic Retrofit of Structures with Supplemental Damping: Part II - Friction Devices," by C. Li and A.M. Reinhorn, 7/6/95, (PB96-128087, A11, MF-A03).

NCEER-95-0010 "Experimental Performance and Analytical Study of a Non-Ductile Reinforced Concrete Frame Structure Retrofitted with Elastomeric Spring Dampers," by G. Pekcan, J.B. Mander and S.S. Chen, 7/14/95, (PB96-137161, A08, MF-A02).

NCEER-95-0011 "Development and Experimental Study of Semi-Active Fluid Damping Devices for Seismic Protection of Structures," by M.D. Symans and M.C. Constantinou, 8/3/95, (PB96-136940, A23, MF-A04).

NCEER-95-0012 "Real-Time Structural Parameter Modification (RSPM): Development of Innervated Structures," by Z. Liang, M. Tong and G.C. Lee, 4/11/95, (PB96-137153, A06, MF-A01).

NCEER-95-0013 "Experimental and Analytical Investigation of Seismic Retrofit of Structures with Supplemental Damping: Part III - Viscous Damping Walls," by A.M. Reinhorn and C. Li, 10/1/95, (PB96-176409, A11, MF-A03).

NCEER-95-0014 "Seismic Fragility Analysis of Equipment and Structures in a Memphis Electric Substation," by J-R. Huo and H.H.M. Hwang, 8/10/95, (PB96-128087, A09, MF-A02).

NCEER-95-0015 "The Hanshin-Awaji Earthquake of January 17, 1995: Performance of Lifelines," Edited by M. Shinozuka, 11/3/95, (PB96-176383, A15, MF-A03).

NCEER-95-0016 "Highway Culvert Performance During Earthquakes," by T.L. Youd and C.J. Beckman, available as NCEER-96-0015.

NCEER-95-0017 "The Hanshin-Awaji Earthquake of January 17, 1995: Performance of Highway Bridges," Edited by I.G. Buckle, 12/1/95, to be published.

NCEER-95-0018 "Modeling of Masonry Infill Panels for Structural Analysis," by A.M. Reinhorn, A. Madan, R.E. Valles, Y. Reichmann and J.B. Mander, 12/8/95, (PB97-110886, MF-A01, A06).

NCEER-95-0019 "Optimal Polynomial Control for Linear and Nonlinear Structures," by A.K. Agrawal and J.N. Yang, 12/11/95, (PB96-168737, A07, MF-A02).

NCEER-95-0020 "Retrofit of Non-Ductile Reinforced Concrete Frames Using Friction Dampers," by R.S. Rao, P. Gergely and R.N. White, 12/22/95, (PB97-133508, A10, MF-A02).

NCEER-95-0021 "Parametric Results for Seismic Response of Pile-Supported Bridge Bents," by G. Mylonakis, A. Nikolaou and G. Gazetas, 12/22/95, (PB97-100242, A12, MF-A03).

NCEER-95-0022 "Kinematic Bending Moments in Seismically Stressed Piles," by A. Nikolaou, G. Mylonakis and G. Gazetas, 12/23/95, (PB97-113914, MF-A03, A13).

NCEER-96-0001 "Dynamic Response of Unreinforced Masonry Buildings with Flexible Diaphragms," by A.C. Costley and D.P. Abrams," 10/10/96, (PB97-133573, MF-A03, A15).

NCEER-96-0002 "State of the Art Review: Foundations and Retaining Structures," by I. Po Lam, to be published.

NCEER-96-0003 "Ductility of Rectangular Reinforced Concrete Bridge Columns with Moderate Confinement," by N. Wehbe, M. Saiidi, D. Sanders and B. Douglas, 11/7/96, (PB97-133557, A06, MF-A02).

NCEER-96-0004 "Proceedings of the Long-Span Bridge Seismic Research Workshop," edited by I.G. Buckle and I.M. Friedland, to be published.

NCEER-96-0005 "Establish Representative Pier Types for Comprehensive Study: Eastern United States," by J. Kulicki and Z. Prucz, 5/28/96, (PB98-119217, A07, MF-A02).

NCEER-96-0006 "Establish Representative Pier Types for Comprehensive Study: Western United States," by R. Imbsen, R.A. Schamber and T.A. Osterkamp, 5/28/96, (PB98-118607, A07, MF-A02).

NCEER-96-0007 "Nonlinear Control Techniques for Dynamical Systems with Uncertain Parameters," by R.G. Ghanem and M.I. Bujakov, 5/27/96, (PB97-100259, A17, MF-A03).

NCEER-96-0008 "Seismic Evaluation of a 30-Year Old Non-Ductile Highway Bridge Pier and Its Retrofit," by J.B. Mander, B. Mahmoodzadegan, S. Bhadra and S.S. Chen, 5/31/96, (PB97-110902, MF-A03, A10).

NCEER-96-0009 "Seismic Performance of a Model Reinforced Concrete Bridge Pier Before and After Retrofit," by J.B. Mander, J.H. Kim and C.A. Ligozio, 5/31/96, (PB97-110910, MF-A02, A10).

NCEER-96-0010 "IDARC2D Version 4.0: A Computer Program for the Inelastic Damage Analysis of Buildings," by R.E. Valles, A.M. Reinhorn, S.K. Kunnath, C. Li and A. Madan, 6/3/96, (PB97-100234, A17, MF-A03).

NCEER-96-0011 "Estimation of the Economic Impact of Multiple Lifeline Disruption: Memphis Light, Gas and Water Division Case Study," by S.E. Chang, H.A. Seligson and R.T. Eguchi, 8/16/96, (PB97-133490, A11, MF-A03).

NCEER-96-0012 "Proceedings from the Sixth Japan-U.S. Workshop on Earthquake Resistant Design of Lifeline Facilities and Countermeasures Against Soil Liquefaction, Edited by M. Hamada and T. O'Rourke, 9/11/96, (PB97-133581, A99, MF-A06).

NCEER-96-0013 "Chemical Hazards, Mitigation and Preparedness in Areas of High Seismic Risk: A Methodology for Estimating the Risk of Post-Earthquake Hazardous Materials Release," by H.A. Seligson, R.T. Eguchi, K.J. Tierney and K. Richmond, 11/7/96, (PB97-133565, MF-A02, A08).

NCEER-96-0014 "Response of Steel Bridge Bearings to Reversed Cyclic Loading," by J.B. Mander, D-K. Kim, S.S. Chen and G.J. Premus, 11/13/96, (PB97-140735, A12, MF-A03).

NCEER-96-0015 "Highway Culvert Performance During Past Earthquakes," by T.L. Youd and C.J. Beckman, 11/25/96, (PB97-133532, A06, MF-A01).

NCEER-97-0001 "Evaluation, Prevention and Mitigation of Pounding Effects in Building Structures," by R.E. Valles and A.M. Reinhorn, 2/20/97, (PB97-159552, A14, MF-A03).

NCEER-97-0002 "Seismic Design Criteria for Bridges and Other Highway Structures," by C. Rojahn, R. Mayes, D.G. Anderson, J. Clark, J.H. Hom, R.V. Nutt and M.J. O'Rourke, 4/30/97, (PB97-194658, A06, MF-A03).

NCEER-97-0003 "Proceedings of the U.S.-Italian Workshop on Seismic Evaluation and Retrofit," Edited by D.P. Abrams and G.M. Calvi, 3/19/97, (PB97-194666, A13, MF-A03).

NCEER-97-0004 "Investigation of Seismic Response of Buildings with Linear and Nonlinear Fluid Viscous Dampers," by A.A. Seleemah and M.C. Constantinou, 5/21/97, (PB98-109002, A15, MF-A03).

NCEER-97-0005 "Proceedings of the Workshop on Earthquake Engineering Frontiers in Transportation Facilities," edited by G.C. Lee and I.M. Friedland, 8/29/97, (PB98-128911, A25, MR-A04).

NCEER-97-0006 "Cumulative Seismic Damage of Reinforced Concrete Bridge Piers," by S.K. Kunnath, A. El-Bahy, A. Taylor and W. Stone, 9/2/97, (PB98-108814, A11, MF-A03).

NCEER-97-0007 "Structural Details to Accommodate Seismic Movements of Highway Bridges and Retaining Walls," by R.A. Imbsen, R.A. Schamber, E. Thorkildsen, A. Kartoum, B.T. Martin, T.N. Rosser and J.M. Kulicki, 9/3/97, (PB98-108996, A09, MF-A02).

NCEER-97-0008 "A Method for Earthquake Motion-Damage Relationships with Application to Reinforced Concrete Frames," by A. Singhal and A.S. Kiremidjian, 9/10/97, (PB98-108988, A13, MF-A03).

NCEER-97-0009 "Seismic Analysis and Design of Bridge Abutments Considering Sliding and Rotation," by K. Fishman and R. Richards, Jr., 9/15/97, (PB98-108897, A06, MF-A02).

NCEER-97-0010 "Proceedings of the FHWA/NCEER Workshop on the National Representation of Seismic Ground Motion for New and Existing Highway Facilities," edited by I.M. Friedland, M.S. Power and R.L. Mayes, 9/22/97, (PB98-128903, A21, MF-A04).

NCEER-97-0011 "Seismic Analysis for Design or Retrofit of Gravity Bridge Abutments," by K.L. Fishman, R. Richards, Jr. and R.C. Divito, 10/2/97, (PB98-128937, A08, MF-A02).

NCEER-97-0012 "Evaluation of Simplified Methods of Analysis for Yielding Structures," by P. Tsopelas, M.C. Constantinou, C.A. Kircher and A.S. Whittaker, 10/31/97, (PB98-128929, A10, MF-A03).

NCEER-97-0013 "Seismic Design of Bridge Columns Based on Control and Repairability of Damage," by C-T. Cheng and J.B. Mander, 12/8/97, (PB98-144249, A11, MF-A03).

NCEER-97-0014 "Seismic Resistance of Bridge Piers Based on Damage Avoidance Design," by J.B. Mander and C-T. Cheng, 12/10/97, (PB98-144223, A09, MF-A02).

NCEER-97-0015 “Seismic Response of Nominally Symmetric Systems with Strength Uncertainty,” by S. Balopoulou and M. Grigoriu, 12/23/97, (PB98-153422, A11, MF-A03).

NCEER-97-0016 “Evaluation of Seismic Retrofit Methods for Reinforced Concrete Bridge Columns,” by T.J. Wipf, F.W. Klaiber and F.M. Russo, 12/28/97, (PB98-144215, A12, MF-A03).

NCEER-97-0017 “Seismic Fragility of Existing Conventional Reinforced Concrete Highway Bridges,” by C.L. Mullen and A.S. Cakmak, 12/30/97, (PB98-153406, A08, MF-A02).

NCEER-97-0018 “Loss Asssessment of Memphis Buildings,” edited by D.P. Abrams and M. Shinozuka, 12/31/97, (PB98-144231, A13, MF-A03).

NCEER-97-0019 “Seismic Evaluation of Frames with Infill Walls Using Quasi-static Experiments,” by K.M. Mosalam, R.N. White and P. Gergely, 12/31/97, (PB98-153455, A07, MF-A02).

NCEER-97-0020 “Seismic Evaluation of Frames with Infill Walls Using Pseudo-dynamic Experiments,” by K.M. Mosalam, R.N. White and P. Gergely, 12/31/97, (PB98-153430, A07, MF-A02).

NCEER-97-0021 “Computational Strategies for Frames with Infill Walls: Discrete and Smeared Crack Analyses and Seismic Fragility,” by K.M. Mosalam, R.N. White and P. Gergely, 12/31/97, (PB98-153414, A10, MF-A02).

NCEER-97-0022 “Proceedings of the NCEER Workshop on Evaluation of Liquefaction Resistance of Soils,” edited by T.L. Youd and I.M. Idriss, 12/31/97, (PB98-155617, A15, MF-A03).

MCEER-98-0001 “Extraction of Nonlinear Hysteretic Properties of Seismically Isolated Bridges from Quick-Release Field Tests,” by Q. Chen, B.M. Douglas, E.M. Maragakis and I.G. Buckle, 5/26/98, (PB99-118838, A06, MF-A01).

MCEER-98-0002 “Methodologies for Evaluating the Importance of Highway Bridges,” by A. Thomas, S. Eshenaur and J. Kulicki, 5/29/98, (PB99-118846, A10, MF-A02).

MCEER-98-0003 “Capacity Design of Bridge Piers and the Analysis of Overstrength,” by J.B. Mander, A. Dutta and P. Goel, 6/1/98, (PB99-118853, A09, MF-A02).

MCEER-98-0004 "Evaluation of Bridge Damage Data from the Loma Prieta and Northridge, California Earthquakes," by N. Basoz and A. Kiremidjian, 6/2/98, (PB99-118861, A15, MF-A03).

MCEER-98-0005 "Screening Guide for Rapid Assessment of Liquefaction Hazard at Highway Bridge Sites," by T. L. Youd, 6/16/98, (PB99-118879, A06, not available on microfiche).

MCEER-98-0006 "Structural Steel and Steel/Concrete Interface Details for Bridges," by P. Ritchie, N. Kauhl and J. Kulicki, 7/13/98, (PB99-118945, A06, MF-A01).

MCEER-98-0007 "Capacity Design and Fatigue Analysis of Confined Concrete Columns," by A. Dutta and J.B. Mander, 7/14/98, (PB99-118960, A14, MF-A03).

MCEER-98-0008 "Proceedings of the Workshop on Performance Criteria for Telecommunication Services Under Earthquake Conditions," edited by A.J. Schiff, 7/15/98, (PB99-118952, A08, MF-A02).

MCEER-98-0009 "Fatigue Analysis of Unconfined Concrete Columns," by J.B. Mander, A. Dutta and J.H. Kim, 9/12/98, (PB99-123655, A10, MF-A02).

MCEER-98-0010 "Centrifuge Modeling of Cyclic Lateral Response of Pile-Cap Systems and Seat-Type Abutments in Dry Sands," by A.D. Gadre and R. Dobry, 10/2/98, (PB99-123606, A13, MF-A03).

MCEER-98-0011 "IDARC-BRIDGE: A Computational Platform for Seismic Damage Assessment of Bridge Structures," by A.M. Reinhorn, V. Simeonov, G. Mylonakis and Y. Reichman, 10/2/98, (PB99-162919, A15, MF-A03).

MCEER-98-0012 "Experimental Investigation of the Dynamic Response of Two Bridges Before and After Retrofitting with Elastomeric Bearings," by D.A. Wendichansky, S.S. Chen and J.B. Mander, 10/2/98, (PB99-162927, A15, MF-A03).

MCEER-98-0013 "Design Procedures for Hinge Restrainers and Hinge Sear Width for Multiple-Frame Bridges," by R. Des Roches and G.L. Fenves, 11/3/98, (PB99-140477, A13, MF-A03).

MCEER-98-0014 "Response Modification Factors for Seismically Isolated Bridges," by M.C. Constantinou and J.K. Quarshie, 11/3/98, (PB99-140485, A14, MF-A03).

MCEER-98-0015 "Proceedings of the U.S.-Italy Workshop on Seismic Protective Systems for Bridges," edited by I.M. Friedland and M.C. Constantinou, 11/3/98, (PB2000-101711, A22, MF-A04).

MCEER-98-0016 "Appropriate Seismic Reliability for Critical Equipment Systems: Recommendations Based on Regional Analysis of Financial and Life Loss," by K. Porter, C. Scawthorn, C. Taylor and N. Blais, 11/10/98, (PB99-157265, A08, MF-A02).

MCEER-98-0017 "Proceedings of the U.S. Japan Joint Seminar on Civil Infrastructure Systems Research," edited by M. Shinozuka and A. Rose, 11/12/98, (PB99-156713, A16, MF-A03).

MCEER-98-0018 "Modeling of Pile Footings and Drilled Shafts for Seismic Design," by I. PoLam, M. Kapuskar and D. Chaudhuri, 12/21/98, (PB99-157257, A09, MF-A02).

MCEER-99-0001 "Seismic Evaluation of a Masonry Infilled Reinforced Concrete Frame by Pseudodynamic Testing," by S.G. Buonopane and R.N. White, 2/16/99, (PB99-162851, A09, MF-A02).

MCEER-99-0002 "Response History Analysis of Structures with Seismic Isolation and Energy Dissipation Systems: Verification Examples for Program SAP2000," by J. Scheller and M.C. Constantinou, 2/22/99, (PB99-162869, A08, MF-A02).

MCEER-99-0003 "Experimental Study on the Seismic Design and Retrofit of Bridge Columns Including Axial Load Effects," by A. Dutta, T. Kokorina and J.B. Mander, 2/22/99, (PB99-162877, A09, MF-A02).

MCEER-99-0004 "Experimental Study of Bridge Elastomeric and Other Isolation and Energy Dissipation Systems with Emphasis on Uplift Prevention and High Velocity Near-source Seismic Excitation," by A. Kasalanati and M. C. Constantinou, 2/26/99, (PB99-162885, A12, MF-A03).

MCEER-99-0005 "Truss Modeling of Reinforced Concrete Shear-flexure Behavior," by J.H. Kim and J.B. Mander, 3/8/99, (PB99-163693, A12, MF-A03).

MCEER-99-0006 "Experimental Investigation and Computational Modeling of Seismic Response of a 1:4 Scale Model Steel Structure with a Load Balancing Supplemental Damping System," by G. Pekcan, J.B. Mander and S.S. Chen, 4/2/99, (PB99-162893, A11, MF-A03).

MCEER-99-0007 "Effect of Vertical Ground Motions on the Structural Response of Highway Bridges," by M.R. Button, C.J. Cronin and R.L. Mayes, 4/10/99, (PB2000-101411, A10, MF-A03).

MCEER-99-0008 "Seismic Reliability Assessment of Critical Facilities: A Handbook, Supporting Documentation, and Model Code Provisions," by G.S. Johnson, R.E. Sheppard, M.D. Quilici, S.J. Eder and C.R. Scawthorn, 4/12/99, (PB2000-101701, A18, MF-A04).

MCEER-99-0009 "Impact Assessment of Selected MCEER Highway Project Research on the Seismic Design of Highway Structures," by C. Rojahn, R. Mayes, D.G. Anderson, J.H. Clark, D'Appolonia Engineering, S. Gloyd and R.V. Nutt, 4/14/99, (PB99-162901, A10, MF-A02).

MCEER-99-0010 "Site Factors and Site Categories in Seismic Codes," by R. Dobry, R. Ramos and M.S. Power, 7/19/99, (PB2000-101705, A08, MF-A02).

MCEER-99-0011 "Restrainer Design Procedures for Multi-Span Simply-Supported Bridges," by M.J. Randall, M. Saiidi, E. Maragakis and T. Isakovic, 7/20/99, (PB2000-101702, A10, MF-A02).

MCEER-99-0012 "Property Modification Factors for Seismic Isolation Bearings," by M.C. Constantinou, P. Tsopelas, A. Kasalanati and E. Wolff, 7/20/99, (PB2000-103387, A11, MF-A03).

MCEER-99-0013 "Critical Seismic Issues for Existing Steel Bridges," by P. Ritchie, N. Kauhl and J. Kulicki, 7/20/99, (PB2000-101697, A09, MF-A02).

MCEER-99-0014 "Nonstructural Damage Database," by A. Kao, T.T. Soong and A. Vender, 7/24/99, (PB2000-101407, A06, MF-A01).

MCEER-99-0015 "Guide to Remedial Measures for Liquefaction Mitigation at Existing Highway Bridge Sites," by H.G. Cooke and J. K. Mitchell, 7/26/99, (PB2000-101703, A11, MF-A03).

MCEER-99-0016 "Proceedings of the MCEER Workshop on Ground Motion Methodologies for the Eastern United States," edited by N. Abrahamson and A. Becker, 8/11/99, (PB2000-103385, A07, MF-A02).

MCEER-99-0017 "Quindío, Colombia Earthquake of January 25, 1999: Reconnaissance Report," by A.P. Asfura and P.J. Flores, 10/4/99, (PB2000-106893, A06, MF-A01).

MCEER-99-0018 "Hysteretic Models for Cyclic Behavior of Deteriorating Inelastic Structures," by M.V. Sivaselvan and A.M. Reinhorn, 11/5/99, (PB2000-103386, A08, MF-A02).

MCEER-99-0019 "Proceedings of the 7th U.S.- Japan Workshop on Earthquake Resistant Design of Lifeline Facilities and Countermeasures Against Soil Liquefaction," edited by T.D. O'Rourke, J.P. Bardet and M. Hamada, 11/19/99, (PB2000-103354, A99, MF-A06).

MCEER-99-0020 "Development of Measurement Capability for Micro-Vibration Evaluations with Application to Chip Fabrication Facilities," by G.C. Lee, Z. Liang, J.W. Song, J.D. Shen and W.C. Liu, 12/1/99, (PB2000-105993, A08, MF-A02).

MCEER-99-0021 "Design and Retrofit Methodology for Building Structures with Supplemental Energy Dissipating Systems," by G. Pekcan, J.B. Mander and S.S. Chen, 12/31/99, (PB2000-105994, A11, MF-A03).

MCEER-00-0001 "The Marmara, Turkey Earthquake of August 17, 1999: Reconnaissance Report," edited by C. Scawthorn; with major contributions by M. Bruneau, R. Eguchi, T. Holzer, G. Johnson, J. Mander, J. Mitchell, W. Mitchell, A. Papageorgiou, C. Scaethorn, and G. Webb, 3/23/00, (PB2000-106200, A11, MF-A03).

MCEER-00-0002 "Proceedings of the MCEER Workshop for Seismic Hazard Mitigation of Health Care Facilities," edited by G.C. Lee, M. Ettouney, M. Grigoriu, J. Hauer and J. Nigg, 3/29/00, (PB2000-106892, A08, MF-A02).

MCEER-00-0003 "The Chi-Chi, Taiwan Earthquake of September 21, 1999: Reconnaissance Report," edited by G.C. Lee and C.H. Loh, with major contributions by G.C. Lee, M. Bruneau, I.G. Buckle, S.E. Chang, P.J. Flores, T.D. O'Rourke, M. Shinozuka, T.T. Soong, C-H. Loh, K-C. Chang, Z-J. Chen, J-S. Hwang, M-L. Lin, G-Y. Liu, K-C. Tsai, G.C. Yao and C-L. Yen, 4/30/00, (PB2001-100980, A10, MF-A02).

MCEER-00-0004 "Seismic Retrofit of End-Sway Frames of Steel Deck-Truss Bridges with a Supplemental Tendon System: Experimental and Analytical Investigation," by G. Pekcan, J.B. Mander and S.S. Chen, 7/1/00, (PB2001-100982, A10, MF-A02).

MCEER-00-0005 "Sliding Fragility of Unrestrained Equipment in Critical Facilities," by W.H. Chong and T.T. Soong, 7/5/00, (PB2001-100983, A08, MF-A02).

MCEER-00-0006 "Seismic Response of Reinforced Concrete Bridge Pier Walls in the Weak Direction," by N. Abo-Shadi, M. Saiidi and D. Sanders, 7/17/00, (PB2001-100981, A17, MF-A03).

MCEER-00-0007 "Low-Cycle Fatigue Behavior of Longitudinal Reinforcement in Reinforced Concrete Bridge Columns," by J. Brown and S.K. Kunnath, 7/23/00, (PB2001-104392, A08, MF-A02).

MCEER-00-0008 "Soil Structure Interaction of Bridges for Seismic Analysis," I. PoLam and H. Law, 9/25/00, (PB2001-105397, A08, MF-A02).

MCEER-00-0009 "Proceedings of the First MCEER Workshop on Mitigation of Earthquake Disaster by Advanced Technologies (MEDAT-1), edited by M. Shinozuka, D.J. Inman and T.D. O'Rourke, 11/10/00, (PB2001-105399, A14, MF-A03).

MCEER-00-0010 "Development and Evaluation of Simplified Procedures for Analysis and Design of Buildings with Passive Energy Dissipation Systems," by O.M. Ramirez, M.C. Constantinou, C.A. Kircher, A.S. Whittaker, M.W. Johnson, J.D. Gomez and C. Chrysostomou, 11/16/01, (PB2001-105523, A23, MF-A04).

MCEER-00-0011 "Dynamic Soil-Foundation-Structure Interaction Analyses of Large Caissons," by C-Y. Chang, C-M. Mok, Z-L. Wang, R. Settgast, F. Waggoner, M.A. Ketchum, H.M. Gonnermann and C-C. Chin, 12/30/00, (PB2001-104373, A07, MF-A02).

MCEER-00-0012 "Experimental Evaluation of Seismic Performance of Bridge Restrainers," by A.G. Vlassis, E.M. Maragakis and M. Saiid Saiidi, 12/30/00, (PB2001-104354, A09, MF-A02).

MCEER-00-0013 "Effect of Spatial Variation of Ground Motion on Highway Structures," by M. Shinozuka, V. Saxena and G. Deodatis, 12/31/00, (PB2001-108755, A13, MF-A03).

MCEER-00-0014 "A Risk-Based Methodology for Assessing the Seismic Performance of Highway Systems," by S.D. Werner, C.E. Taylor, J.E. Moore, II, J.S. Walton and S. Cho, 12/31/00, (PB2001-108756, A14, MF-A03).

MCEER-01-0001 “Experimental Investigation of P-Delta Effects to Collapse During Earthquakes,” by D. Vian and M. Bruneau, 6/25/01, (PB2002-100534, A17, MF-A03).

MCEER-01-0002 “Proceedings of the Second MCEER Workshop on Mitigation of Earthquake Disaster by Advanced Technologies (MEDAT-2),” edited by M. Bruneau and D.J. Inman, 7/23/01, (PB2002-100434, A16, MF-A03).

MCEER-01-0003 “Sensitivity Analysis of Dynamic Systems Subjected to Seismic Loads,” by C. Roth and M. Grigoriu, 9/18/01, (PB2003-100884, A12, MF-A03).

MCEER-01-0004 “Overcoming Obstacles to Implementing Earthquake Hazard Mitigation Policies: Stage 1 Report,” by D.J. Alesch and W.J. Petak, 12/17/01, (PB2002-107949, A07, MF-A02).

MCEER-01-0005 “Updating Real-Time Earthquake Loss Estimates: Methods, Problems and Insights,” by C.E. Taylor, S.E. Chang and R.T. Eguchi, 12/17/01, (PB2002-107948, A05, MF-A01).

MCEER-01-0006 "Experimental Investigation and Retrofit of Steel Pile Foundations and Pile Bents Under Cyclic Lateral Loadings," by A. Shama, J. Mander, B. Blabac and S. Chen, 12/31/01, (PB2002-107950, A13, MF-A03).

MCEER-02-0001 "Assessment of Performance of Bolu Viaduct in the 1999 Duzce Earthquake in Turkey" by P.C. Roussis, M.C. Constantinou, M. Erdik, E. Durukal and M. Dicleli, 5/8/02, (PB2003-100883, A08, MF-A02).

MCEER-02-0002 "Seismic Behavior of Rail Counterweight Systems of Elevators in Buildings," by M.P. Singh, Rildova and L.E. Suarez, 5/27/02. (PB2003-100882, A11, MF-A03).

MCEER-02-0003 "Development of Analysis and Design Procedures for Spread Footings," by G. Mylonakis, G. Gazetas, S. Nikolaou and A. Chauncey, 10/02/02, (PB2004-101636, A13, MF-A03, CD-A13).

MCEER-02-0004 "Bare-Earth Algorithms for Use with SAR and LIDAR Digital Elevation Models," by C.K. Huyck, R.T. Eguchi and B. Houshmand, 10/16/02, (PB2004-101637, A07, CD-A07).

MCEER-02-0005 "Review of Energy Dissipation of Compression Members in Concentrically Braced Frames," by K.Lee and M. Bruneau, 10/18/02, (PB2004-101638, A10, CD-A10).

MCEER-03-0001 "Experimental Investigation of Light-Gauge Steel Plate Shear Walls for the Seismic Retrofit of Buildings" by J. Berman and M. Bruneau, 5/2/03, (PB2004-101622, A10, MF-A03, CD-A10).

MCEER-03-0002 "Statistical Analysis of Fragility Curves," by M. Shinozuka, M.Q. Feng, H. Kim, T. Uzawa and T. Ueda, 6/16/03, (PB2004-101849, A09, CD-A09).

MCEER-03-0003 "Proceedings of the Eighth U.S.-Japan Workshop on Earthquake Resistant Design f Lifeline Facilities and Countermeasures Against Liquefaction," edited by M. Hamada, J.P. Bardet and T.D. O'Rourke, 6/30/03, (PB2004-104386, A99, CD-A99).

MCEER-03-0004 "Proceedings of the PRC-US Workshop on Seismic Analysis and Design of Special Bridges," edited by L.C. Fan and G.C. Lee, 7/15/03, (PB2004-104387, A14, CD-A14).

MCEER-03-0005 "Urban Disaster Recovery: A Framework and Simulation Model," by S.B. Miles and S.E. Chang, 7/25/03, (PB2004-104388, A07, CD-A07).

MCEER-03-0006 "Behavior of Underground Piping Joints Due to Static and Dynamic Loading," by R.D. Meis, M. Maragakis and R. Siddharthan, 11/17/03, (PB2005-102194, A13, MF-A03, CD-A00).

MCEER-03-0007 "Seismic Vulnerability of Timber Bridges and Timber Substructures," by A.A. Shama, J.B. Mander, I.M. Friedland and D.R. Allicock, 12/15/03.

MCEER-04-0001 "Experimental Study of Seismic Isolation Systems with Emphasis on Secondary System Response and Verification of Accuracy of Dynamic Response History Analysis Methods," by E. Wolff and M. Constantinou, 1/16/04 (PB2005-102195, A99, MF-E08, CD-A00).

MCEER-04-0002 "Tension, Compression and Cyclic Testing of Engineered Cementitious Composite Materials," by K. Kesner and S.L. Billington, 3/1/04, (PB2005-102196, A08, CD-A08).

MCEER-04-0003 "Cyclic Testing of Braces Laterally Restrained by Steel Studs to Enhance Performance During Earthquakes," by O.C. Celik, J.W. Berman and M. Bruneau, 3/16/04, (PB2005-102197, A13, MF-A03, CD-A00).

MCEER-04-0004 "Methodologies for Post Earthquake Building Damage Detection Using SAR and Optical Remote Sensing: Application to the August 17, 1999 Marmara, Turkey Earthquake," by C.K. Huyck, B.J. Adams, S. Cho, R.T. Eguchi, B. Mansouri and B. Houshmand, 6/15/04, (PB2005-104888, A10, CD-A00).

MCEER-04-0005 "Nonlinear Structural Analysis Towards Collapse Simulation: A Dynamical Systems Approach," by M.V. Sivaselvan and A.M. Reinhorn, 6/16/04, (PB2005-104889, A11, MF-A03, CD-A00).

MCEER-04-0006 "Proceedings of the Second PRC-US Workshop on Seismic Analysis and Design of Special Bridges," edited by G.C. Lee and L.C. Fan, 6/25/04, (PB2005-104890, A16, CD-A00).

MCEER-04-0007 "Seismic Vulnerability Evaluation of Axially Loaded Steel Built-up Laced Members," by K. Lee and M. Bruneau, 6/30/04, (PB2005-104891, A16, CD-A00).

MCEER-04-0008 "Evaluation of Accuracy of Simplified Methods of Analysis and Design of Buildings with Damping Systems for Near-Fault and for Soft-Soil Seismic Motions," by E.A. Pavlou and M.C. Constantinou, 8/16/04, (PB2005-104892, A08, MF-A02, CD-A00).

MCEER-04-0009 "Assessment of Geotechnical Issues in Acute Care Facilities in California," by M. Lew, T.D. O'Rourke, R. Dobry and M. Koch, 9/15/04, (PB2005-104893, A08, CD-A00).

MCEER-04-0010 "Scissor-Jack-Damper Energy Dissipation System," by A.N. Sigaher-Boyle and M.C. Constantinou, 12/1/04 (PB2005-108221).

MCEER-04-0011 "Seismic Retrofit of Bridge Steel Truss Piers Using a Controlled Rocking Approach," by M. Pollino and M. Bruneau, 12/20/04 (PB2006-105795).

MCEER-05-0001 "Experimental and Analytical Studies of Structures Seismically Isolated with an Uplift-Restraint Isolation System," by P.C. Roussis and M.C. Constantinou, 1/10/05 (PB2005-108222).

MCEER-05-0002 "A Versatile Experimentation Model for Study of Structures Near Collapse Applied to Seismic Evaluation of Irregular Structures," by D. Kusumastuti, A.M. Reinhorn and A. Rutenberg, 3/31/05 (PB2006-101523).

MCEER-05-0003 "Proceedings of the Third PRC-US Workshop on Seismic Analysis and Design of Special Bridges," edited by L.C. Fan and G.C. Lee, 4/20/05, (PB2006-105796).

MCEER-05-0004 "Approaches for the Seismic Retrofit of Braced Steel Bridge Piers and Proof-of-Concept Testing of an Eccentrically Braced Frame with Tubular Link," by J.W. Berman and M. Bruneau, 4/21/05 (PB2006-101524).

MCEER-05-0005 "Simulation of Strong Ground Motions for Seismic Fragility Evaluation of Nonstructural Components in Hospitals," by A. Wanitkorkul and A. Filiatrault, 5/26/05 (PB2006-500027).

MCEER-05-0006 "Seismic Safety in California Hospitals: Assessing an Attempt to Accelerate the Replacement or Seismic Retrofit of Older Hospital Facilities," by D.J. Alesch, L.A. Arendt and W.J. Petak, 6/6/05 (PB2006-105794).

MCEER-05-0007 "Development of Seismic Strengthening and Retrofit Strategies for Critical Facilities Using Engineered Cementitious Composite Materials," by K. Kesner and S.L. Billington, 8/29/05 (PB2006-111701).

MCEER-05-0008 "Experimental and Analytical Studies of Base Isolation Systems for Seismic Protection of Power Transformers," by N. Murota, M.Q. Feng and G-Y. Liu, 9/30/05 (PB2006-111702).

MCEER-05-0009 "3D-BASIS-ME-MB: Computer Program for Nonlinear Dynamic Analysis of Seismically Isolated Structures," by P.C. Tsopelas, P.C. Roussis, M.C. Constantinou, R. Buchanan and A.M. Reinhorn, 10/3/05 (PB2006-111703).

MCEER-05-0010 "Steel Plate Shear Walls for Seismic Design and Retrofit of Building Structures," by D. Vian and M. Bruneau, 12/15/05 (PB2006-111704).

MCEER-05-0011 "The Performance-Based Design Paradigm," by M.J. Astrella and A. Whittaker, 12/15/05 (PB2006-111705).

MCEER-06-0001 "Seismic Fragility of Suspended Ceiling Systems," H. Badillo-Almaraz, A.S. Whittaker, A.M. Reinhorn and G.P. Cimellaro, 2/4/06 (PB2006-111706).

MCEER-06-0002 "Multi-Dimensional Fragility of Structures," by G.P. Cimellaro, A.M. Reinhorn and M. Bruneau, 3/1/06 (PB2007-106974, A09, MF-A02, CD A00).

MCEER-06-0003 "Built-Up Shear Links as Energy Dissipators for Seismic Protection of Bridges," by P. Dusicka, A.M. Itani and I.G. Buckle, 3/15/06 (PB2006-111708).

MCEER-06-0004 "Analytical Investigation of the Structural Fuse Concept," by R.E. Vargas and M. Bruneau, 3/16/06 (PB2006-111709).

MCEER-06-0005 "Experimental Investigation of the Structural Fuse Concept," by R.E. Vargas and M. Bruneau, 3/17/06 (PB2006-111710).

MCEER-06-0006 "Further Development of Tubular Eccentrically Braced Frame Links for the Seismic Retrofit of Braced Steel Truss Bridge Piers," by J.W. Berman and M. Bruneau, 3/27/06 (PB2007-105147).

MCEER-06-0007 "REDARS Validation Report," by S. Cho, C.K. Huyck, S. Ghosh and R.T. Eguchi, 8/8/06 (PB2007-106983).

MCEER-06-0008 "Review of Current NDE Technologies for Post-Earthquake Assessment of Retrofitted Bridge Columns," by J.W. Song, Z. Liang and G.C. Lee, 8/21/06 06 (PB2007-106984).

MCEER-06-0009 "Liquefaction Remediation in Silty Soils Using Dynamic Compaction and Stone Columns," by S. Thevanayagam, G.R. Martin, R. Nashed, T. Shenthan, T. Kanagalingam and N. Ecemis, 8/28/06 06 (PB2007-106985).

MCEER-06-0010 "Conceptual Design and Experimental Investigation of Polymer Matrix Composite Infill Panels for Seismic Retrofitting," by W. Jung, M. Chiewanichakorn and A.J. Aref, 9/21/06 (PB2007-106986).

MCEER-06-0011 "A Study of the Coupled Horizontal-Vertical Behavior of Elastomeric and Lead-Rubber Seismic Isolation Bearings," by G.P. Warn and A.S. Whittaker, 9/22/06 (PB2007-108679).

MCEER-06-0012 "Proceedings of the Fourth PRC-US Workshop on Seismic Analysis and Design of Special Bridges: Advancing Bridge Technologies in Research, Design, Construction and Preservation," Edited by L.C. Fan, G.C. Lee and L. Ziang, 10/12/06.

MCEER-06-0013 "Cyclic Response and Low Cycle Fatigue Characteristics of Plate Steels," by P. Dusicka, A.M. Itani and I.G. Buckle, 11/1/06 06 (PB2007-106987).

MCEER-06-0014 "Proceedings of the Second US-Taiwan Bridge Engineering Workshop," edited by W.P. Yen, J. Shen, J-Y. Chen and M. Wang, 11/15/06.

MCEER-06-0015 "User Manual and Technical Documentation for the REDARS™ Import Wizard," by S. Cho, S. Ghosh, C.K. Huyck and S.D. Werner, 11/30/06.

MCEER-06-0016 "Hazard Mitigation Strategy and Monitoring Technologies for Urban and Infrastructure Public Buildings: Proceedings of the China-US Workshops," edited by X.Y. Zhou, A.L. Zhang, G.C. Lee and M. Tong, 12/12/06.

MCEER-07-0001 "Static and Kinetic Coefficients of Friction for Rigid Blocks," by C. Kafali, S. Fathali, M. Grigoriu and A.S. Whittaker, 3/20/07.

MCEER-07-0002 "Hazard Mitigation Investment Decision Making: Organizational Response to Legislative Mandate," by L.A. Arendt, D.J. Alesch and W.J. Petak, 4/9/07.

MCEER-07-0003 "Seismic Behavior of Bidirectional-Resistant Ductile End Diaphragms with Unbonded Braces in Straight or Skewed Steel Bridges," by O. Celik and M. Bruneau, 4/11/07.

MCEER
EARTHQUAKE ENGINEERING TO EXTREME EVENTS
University at Buffalo, The State University of New York
Red Jacket Quadrangle ▪ Buffalo, New York 14261
Phone: (716) 645-3391 ▪ Fax: (716) 645-3399
E-mail: *mceer@buffalo.edu* ▪ WWW Site *http://mceer.buffalo.edu*
University at Buffalo *The State University of New York*

ISSN 1520-295X